

https://dspace.org/

Anastrozole when used as a superovulator, may alter key focal adhesion proteins associated with receptivity of uterine epithelial cells during implantation in the rat: a potential therapeutic clue in assisted reproductive technologies

Mwakikunga, Anthony Raphael.

2015
http://hdl.handle.net/10539/21599

Downloaded from a DSpace repository. https://dspace.org/

ANASTROZOLE WHEN USED AS A SUPEROVULATOR, MAY ALTER KEY FOCAL ADHESION PROTEINS ASSOCIATED WITH RECEPTIVITY OF UTERINE EPITHELIAL CELLS DURING IMPLANTATION IN THE RAT: A POTENTIAL THERAPEUTIC CLUE IN ASSISTED REPRODUCTIVE TECHNOLOGIES

by

Anthony Raphael Mwakikunga

FACULTY OF HEALTH SCIENCES

A thesis submitted to the Faculty of Health Sciences,

University of the Witwatersrand, Johannesburg, in fulfillment of the

requirements for the degree of

Doctor of Philosophy

July, 2015

DECLARATION

I, Anthony Raphael Mwakikunga, declare that this thesis is my own work. It is being submitted for the degree of Doctor of Philosophy in the University of the Witwatersrand, Johannesburg. It has not been submitted before for any degree or examination at this or any other university.

.....

.....day of....., 2015

DEDICATION

This work has been dedicated to my wife, Gertrude and my children for their support, and to my parents for their guidance because their attitudes, values, hopes and dreams became a part of me.

PUBLICATIONS AND PRESENTATIONS ARISING FROM THIS STUDY

Mwakikunga, A. & Hosie, M. (2015) Anastrozole is a dose specific superovulator and favors implantation in rats: a prospective study. *Cell and Tissue Research*. DOI 10.1007/s00441-015-2180-1.

Mwakikunga, A., Adefolaju, A & Hosie, M. (2015) Focal adhesion proteins vinculin and integrin β5 dynamics during early pregnancy in rats: Anastrozole favors their normal distribution. *Histochemistry and Cell Biology*. (submitted but it is not accepted as yet).

Mwakikunga, A., Adefolaju, A & Hosie, M. (2015) Focal adhesion proteins, paxillin and FAK, reorganization during early pregnancy in rat uterine epithelial cells: Anastrozole favors implantation. *Journal of Morphology*. (submitted but it is not accepted as yet).

Conference presentations:

Microscopy Society of Southern Africa, 3rd - 6th December, 2013, Pretoria, South Africa - poster presentation.

Anastrozole is a dose specific superovulator and favors implantation in rats: A prospective study

Health Science Faculty Research Day, University of the Witwatersrand, Johannesburg, South Africa, August 2014 - poster presentation.

Anastrozole is a dose specific superovulator and favors implantation in rats: A prospective study

Health Science Faculty Research Day, University of the Witwatersrand, Johannesburg, South Africa, August 2014 - poster presentation.

Focal adhesion proteins vinculin and integrin β5 dynamics during early pregnancy in rats: Anastrozole does not hamper their normal distribution

ABSTRACT

Introduction: Anastrozole is clinically effective in ovulation induction, but it has not been well researched. There is need for a new superovulator to replace clomiphene citrate, which is unsuitable for use in some women especially those with polycystic ovarian syndrome and additionally has low pregnancy rates. The aim of this study was to determine the optimal dose for anastrozole as a superovulator and ascertain its effects on implantation in Wistar rats; also to determine its effects on uterine morphology during early pregnancy using light microscopy and scanning electron microscopy (SEM). In order to further determine the effectiveness of anastrozole as a superovulator and compare it with chlomiphene citrate (CC) in similar situations, the study was designed to determine the effects of the these drugs on the expression of the selected focal adhesion proteins vinculin, integrin β5, paxillin and focal adhesion kinase (FAK) in the surface uterine luminal epithelial cells of Wistar rats during early pregnancy.

Methods: The project was divided into two parts. Part one was a preliminary dose response study of anastrozole, where the aim was to determine the optimal dose of anastrozole that could give the highest number of implantation sites upon administration in the Wistar rats. Therefore, only day 6 pregnant rats were used in the preliminary study because the investigators were only interested in the number of blastocysts implanted with different anastrozole dose regimes. A one way ANOVA followed by a Tukey-Kramer HSD was used to compare the number of implantation sites between treatment groups. Differences were considered statistically significant when $p < 0.05$ (JMP10). The optimal dose of anastrozole (15mg/kg) determined from this study was used in the second part of the project, and this part

included both day 1 and day 6 pregnant rats. The second part of the project (main study) employed scanning electron microscopy (SEM), immunofluorescence and confocal microscopy and quantitative real time polymerase chain reaction (qPCR) techniques to determine the ultrastructure of the surface uterine epithelium during early pregnancy; and to determine the expression levels and localization of focal adhesion proteins vinculin, integrin β5, paxillin and FAK in the rat uterine epithelial cells and blastocysts during implantation *in vivo*. High resolution SEM was used to compare and analyze the uterine surface ultrastructure between treatments. The parameters measured were microvilli density, microvilli length, microvilli surface beads, uterine surface folding, large surface protrusions, surface glycocalyx, membrane pores, cell apices, cell borders and small secretions. The micrographs were scored by two researchers using a random blinded method and then analyzed using a one way ANOVA followed by a Tukey-Kramer HSD. For the immunofluorescence experiments, the chosen focal adhesion protein expression levels and localization in the confocal images were scored using a scoring method modified from previous studies (Englund *et al.,* 2001). JMP10 software (SAS Institute, Cary, NC, USA) was used for the statistical comparisons of means of focal adhesion protein expression of vinculin, integrin β5, paxillin and FAK among treatment groups using a one way ANOVA followed by a Tukey-Kramer *post hoc* analysis. Differences were considered statistically significant when $p < 0.05$. The RT-PCR comparative C_T method ($2^{-\Delta\Delta CT}$ method) was used to determine the gene expression fold change relative to the control following drug treatment regimes. The data were first normalized using the three reference genes β-actin, 18S rRNA and Lactate dehydrogenase A.

Results: A significant increase of implantation sites is seen in the 15mg/kg anastrozole treated rats, 16.6 ± 0.8 (mean ± SE) (Appendix G) in comparison to control group, 7.8 ± 0.8 ($p <$

0.0001) (Appendix G). Day 6 pregnant rats treated with 15mg/kg anastrozole show short irregular microvilli on the luminal epithelium similar to the control ($p>0.05$) (Appendix G). Pinopods are mostly noted in, but not limited to anastrozole treated rats at day 6 of pregnancy.

With regard to gene and protein expression, focal adhesion proteins vinculin and integrin β5 are co-localized at the base of the uterine epithelium at day 1 of pregnancy whereas at day 6, they disassemble from the basal focal adhesions and co-localize and significantly increase their expression apically ($p<0.0001$) (Appendix G). Moreover, there is a significant difference in the protein expression levels of vinculin and integrin β5 in uterine luminal epithelial cells between untreated (control) and chlomiphene citrate (CC) treated rats ($p<0.0001$) (Appendix G), anastrozole and chlomiphene citrate (CC) treated rats at both day 1 and day 6 ($p<0.0001$) (Appendix G). Although there is no significant difference in the expression levels of vinculin and integrin β5 in uterine luminal epithelial cells between untreated and anastrozole treated rats at day 1 and day 6 ($p>0.05$) (Appendix G), the means for vinculin and integrin β5 expression are higher in the anastrozole treated groups suggesting that anastrozole seems to enhance their expression in order to perhaps assist in the implantation process of the embryo.

The immunofluorescence findings agree with the vinculin and integrin β5 gene expression experiments in which at day 6 of pregnancy vinculin and integrin β5 gene expression are significantly up-regulated in uterine luminal epithelial cell in the anastrozole treated group relative to the calibrator sample ($p<0.0001$) (Appendix G). However, vinculin and integrin β5 gene expression is down-regulated with chlomiphene citrate (CC) treatment at day 6 in uterine luminal epithelial cells relative to the calibrator sample.

Similarly, with the paxillin and FAK gene and protein expression, paxillin is localized in focal adhesions at the base of the uterine epithelial cells at day 1 of pregnancy whereas at day 6, paxillin disassembles from the basal focal adhesions and localizes and significantly increases its expression apically ($p<0.0001$) (Appendix G). FAK is faintly expressed at the basal aspect of the uterine epithelial cells while moderately expressed at the cell-to-cell contact at day 1 in all groups from where it disassembles and relocates apically and becomes significantly more intensely expressed at day 6 of pregnancy in uterine luminal epithelial cells of untreated and anastrozole treated rats ($p<0.0001$) (Appendix G). Although paxillin is localized apically at day 6, its expression is significantly down-regulated with CC treatment ($p<0.0001$) (Appendix G) suggesting its possible interference with the implantation process. Paxillin and FAK do not co-localize in focal adhesions at the base of the epithelium at day 1, but they co-localize and significantly increase their expression apically at day 6 ($p<0.0001$) (Appendix G) suggesting that they play a role in the implantation process.

With regard to the paxillin and FAK gene expression experiments, at day 1 of pregnancy, paxillin and FAK gene expression in uterine luminal epithelial cells is fairly similar in the anastrozole treated rats relative to the calibrator sample (day 1 untreated rats) suggesting that anastrozole does not disrupt their expression in preparation for the implantation process. Paxillin and FAK gene expression in uterine luminal epithelial cells is slightly down-regulated in the CC treated group when compared to the calibrator sample. At day 6 of pregnancy, paxillin and FAK gene expression in uterine luminal epithelial cells is significantly up-regulated in the anastrozole treated group relative to the calibrator ($p<0.0001$) (Appendix G). On the other hand, paxillin is down-regulated with chlomiphene citrate (CC) treatment in uterine luminal epithelial cells at day 6 relative to the calibrator sample. Interestingly,

chlomiphene citrate (CC) seems not to down-regulate FAK gene expression in uterine luminal epithelial cells at day 6 when compared to the calibrator sample.

In conclusion, the evidence for increased implantation sites in the Wistar rats treated with the 15mg/kg anastrozole in this study suggests that this particular dose superovulates and favors implantation in this species. It also confirms earlier studies that suggest higher anastrozole doses for ovulation induction. It is also important to note that anastrozole is a competitive inhibitor of aromatase in the conversion of androgens to estrogens (E_2); therefore, the 15mg/kg anastrozole dose, which is so effective in causing ovulation, may allow just enough of the intermediates and E_2 to be present with regard to the hormone profiles for ovulation and successful implantation of the embryo. The advantage of anastrozole therapy over chlomiphene citrate (CC) may be the lower E_2/P ratio and increased levels of FSH and LH. Therefore, measuring parameters such as the intermediates, estrogens and androgens in future studies may be of use in determining hormonal profiles for implantation. The surface uterine epithelial morphology further demonstrates that anastrozole is implantation friendly. The observed success of anastrozole in inducing ovulation and achieving pregnancy in the Wistar rats is provocative and warrants further research. The immunofluorescence and gene expression findings of the focal adhesions proteins vinculin, integrin β5, paxillin and FAK, which are uterine receptivity markers have also strongly demonstrated that anastrozole is implantation friendly. In summary, these findings make anastrozole a potential substitute oral ovulatory drug, which has proven superiority to chlomiphene citrate (CC) that could be used without the risk of hyperstimulation and with minimal monitoring and thus may emerge as the new first-line treatment for anovulatory or ovulatory infertility.

ACKNOWLEDGEMENTS

I am grateful to the management of the College of Medicine, University of Malawi and the Government of Norway for the financial assistance and Professor Margot Hosie's research grant from the National Research Foundation (NRF) to do this work. Thanks to my supervisor, Professor Margot Hosie for her untiring support and guidance in the supervision of this work.

I sincerely thank the staff of the Central Animal Unit of the University of the Witwatersrand for their assistance in animal handling training, drug administration and ethical issues.

I also thank the staff of microscopy and microanalysis units of the University of the Witwatersrand and University of Pretoria for their guidance in sputter coating tissues and using their scanning electron microscopes.

Special thanks to fellow graduate students and friends for moral support during the study period. In particular, I am grateful to Deran, Benga, Karren, Kutlwano, Monica, Mrs Ali, Alison, Glynis and Pam for their great support and kindness. Thanks to the staff of the School of Anatomical Sciences for their technical and administrative assistance.

I also thank the staff in the Internal Medicine Department, University of the Witwatersrand, for their assistance in providing technical support for my PCR work.

A big thank you to the management and staff of Newcastle University Medicine Malaysia for their support while finishing up this work and not forgetting Dr George and Prof Margot Hosie for their kindness and untiring support.

My sincere gratitude is to my wonderful wife, Gertrude Mwakikunga, and children for their love and moral support. Finally, I thank God, the Almighty, to make all this possible.

TABLE OF CONTENTS

DECLARATION ii

DEDICATION iii

PUBLICATIONS AND PRESENTATIONS ARISING FROM THIS STUDY iv

ABSTRACT vi

ACKNOWLEDGEMENTS xi

LIST OF TABLES xxiii

APPENDIX E xxiv

APPENDIX F xxiv

APPENDIX G xxiv

ABBREVIATIONS xxx

1 CHAPTER ONE: INTRODUCTION 1

1.1 Background 1

1.1.1 Assisted reproductive technologies (ART) and their importance 1

1.1.2 Superovulation 2

1.1.2.1 Gonadotropins 2

1.1.2.2 Clomiphene citrate 3

1.1.2.3 Aromatase inhibitors and their mechanism of action 7

1.1.2.3.1 Biosynthesis of steroid hormones 7

1.1.2.3.2 Aromatase 14

1.1.2.3.3 Aromatase involvement in disease 18

1.1.2.3.4 Structure of human aromatase 19

1.1.2.3.5 Aromatase inhibitors 23

1.1.2.3.6 Chemistry of anastrozole 30

1.1.2.3.7 Aromatase inhibitor mechanism of action 31
1.1.3 Reproduction and early pregnancy 33
1.1.3.1 Anatomy of the rat uterus 33
1.1.3.2 Estrous cycle of female rats and vaginal cytology 35
1.1.3.3 Uterine receptivity and blastocyst implantation 38
1.1.4 The cytoskeleton and focal adhesion dynamics 40
1.2 Problem statement 44
1.3 Aim and specific objectives 46
2 CHAPTER TWO: MATERIALS AND METHODS 48
2.1 Animals 48
2.2 Rationale for the doses 49
2.3 Drug preparation and administration 50
2.4 Treatment regimes for the dose response study 50
2.5 Tissue preparation 51
2.6 Animals for the main study (SEM, confocal microscopy and qPCR) 52
2.6.1 Scanning Electron Microscopy (SEM) 52
2.6.1.1 Data analysis for the dose response study and SEM study 53
2.6.2 Immunofluorescence and confocal microscopy 55
2.6.2.1 Tissue processing and sectioning 55
2.6.2.2 Immunofluorescence 55
2.6.3 Hematoxylin and Eosin (H&E) staining 57
2.6.4 Real time quantitative polymerase chain reaction (qPCR) 58
2.6.4.1 RNA extraction 59
2.6.4.2 RNA assessment: Nanodrop method 59
2.6.4.3 Genomic DNA removal from RNA preparations 60
2.6.4.4 Designing Primers 60
2.6.4.5 Complimentary DNA (cDNA) synthesis 63
2.6.4.6 Real-time quantitative polymerase chain reaction (qPCR) 63
2.6.4.7 PCR product gel electrophoresis 65

2.6.4.8 SYBR green qPCR data analysis 65

3 CHAPTER THREE: RESULTS 67

3.1 Preliminary dose response study of anastrozole 67

3.1.1 Optimal anastrozole dose 68

3.1.2 Implantation sites 69

3.2 Scanning Electron Microscopy (SEM) 70

3.2.1 Microvilli density (MD), microvilli surface beads (MSB), large surface protrusions (LSP) and membrane pores (MP) 71

3.2.2 Microvilli length (ML) 75

3.2.3 Uterine surface folding (SF) 77

3.2.4 Cell apices (CA) 81

3.2.5 Cell borders (CB) 84

3.2.6 Surface glycocalyx (SG) 85

3.2.7 Epithelial gland opening (EGO) 87

3.2.8 Small secretions (SS) 88

3.3 Immunofluorescence for the focal adhesion protein vinculin, integrin β5, paxillin and focal adhesion kinase (FAK) in luminal surface uterine epithelial cells of day 1 and day 6 of pregnancy in rats 94

3.3.1 Vinculin and integrin β5 95

3.3.2 Paxillin and FAK 104

3.4 Hematoxylin and eosin (H&E) staining 113

3.5 Real-time quantitative polymerase chain reaction (qPCR) of gene expression of vinculin, integrin β5, paxillin and FAK in the uterine epithelial cells from day 1 and day 6 pregnant rats 115

3.5.1 Relative quantification (RQ) analysis of vinculin and integrin β5 gene expression in the uterine epithelial cells from day 1 and day 6 pregnant rats 116

3.5.2 Relative quantification (RQ) analysis of paxillin and FAK gene expression in the uterine epithelial cells from day 1 and day 6 pregnant rats 120

4 CHAPTER FOUR: DISCUSSION AND CONCLUSIONS 124

4.1 Introduction and general structure 124

4.2 Anastrozole dose response study 125

4.3 Uterine surface ultrastructure 127

4.4 Focal adhesion protein dynamics in rat uterus 134

4.4.1 Gene and protein expression of vinculin and integrin β5 135

4.4.2 Gene and protein expression paxillin and FAK 140

4.5 Hematoxylin and eosin (H&E) staining 148

4.6 Conclusions and recommendations 150

5 REFERENCES 154

6 APPENDIX A: SOLUTIONS AND RECIPES FOR VAGINAL SMEAR, DRUG PREPARATION AND SACRIFICE 172

6.1 Vaginal smear method of staining 172

6.2 Normal saline (0.9%) 172

6.3 Toluidine blue 173

6.4 Vehicle for all drugs 173

6.5 Four anastrozole dose regimes for the preliminary dose response study: 173

6.6 Chlomiphene citrate 174

6.7 Anaesthesia: Anaket-Chanazine 174

6.8 Euthanasia: Euthapent solution 174

6.9 1% Pontamine sky blue 175

7 APPENDIX B: SOLUTIONS AND RECIPES FOR SCANNING ELECTRON MICROSCOPY (SEM) 176

7.1 The principle of the scanning electron microscopy and the rationale for using it in thecurrent study 176

7.2 0.1M Phosphate buffer (NaPO4), pH 7.4 177

7.3 2.5% Gluteraldehyde 177

7.4 1% Osmium tetroxide 177
7.5 1% Thiosemicarbizide 178
7.6 Hexamethyldisilazane (HMDS) 178
7.7 Graded alcohol solutions 178

8 APPENDIX C: SOLUTIONS AND RECIPES FOR IMMUNOFLUORESCENCE AND CONFOCAL MICROSCOPY 179

8.1 The principle of immunofluorescence and confocal microscopy and its rationale 179
8.2 10% Buffered formalin (2l) 181
8.3 Gelatin-coating solution 182
8.4 Phosphate buffered saline (PBS) pH 7.4 182
8.5 Peroxidase quenching solution 182
8.6 Permeabilized buffer 182
8.7 Blocking solution 182
8.8 Rabbit polyclonal anti-Integrin β5 in blocking solution (1:100) 183
8.9 Mouse monoclonal anti-Vinculin in blocking solution (1:100) 183
8.10 Mouse monoclonal anti-Paxillin in blocking solution (1:100) 183
8.11 Rabbit monoclonal anti-FAK in blocking solution (1:100) 183
8.12 Goat F(ab') 2 polyclonal secondary antibody to Rabbit IgG (TRITC) pre-adsorbed 183
8.13 Goat F(ab') 2 polyclonal secondary antibody to Mouse IgG (FITC) pre-adsorbed 184
8.14 DAPI (4',6-diamidino-2-phenylindole) 184

9 APPENDIX D: REAL TIME QUANTITATIVE POLYMERASE CHAIN REACTION (QPCR) 186

9.1 The principle of qPCR and the rationale for using it in the study 186
9.2 RNA extraction method 187
9.3 Complimentary DNA (cDNA) synthesis 188
9.4 Melt curves of the PCR products 189

9.5 Gel electrophoresis of genes of interest and reference genes 192

9.6 Comparative CT Method (2-ΔΔCT Method) for calculating fold change in gene expression 193

10 APPENDIX E: REAGENTS/CHEMICALS AND DRUGS 195

11 APPENDIX F: EQUIPMENT AND KITS USED 197

12 APPENDIX G: STATISTICAL ANALYSES 198

12.1 STATISTICAL ANALYSIS FOR THE DOSE RESPONSE STUDY 198

12.2 STATISTICAL ANALYSES FOR SCANNING ELECTRON MICROSCOPY 200

12.2.1 Microvilli density 200

12.2.2 Microvilli length 202

12.2.3 Microvilli surface beads 204

12.2.4 Large surface protrusions 206

12.2.5 Uterine surface folding 208

12.2.6 Surface glycocalyx 210

12.2.7 Membrane pores 212

12.2.8 Small secretions 214

12.2.9 Epithelial gland openings 216

12.2.10 Cell apices 218

12.2.11 Cell borbers 220

12.3 STATISTICAL ANALYSES FOR IMMUNOFLUORESCENCE 222

12.3.1 Vinculin protein expression in uterine epithelial cells of day 1 and day 6 pregnant rats 222

12.3.2 Integrin β5 protein expression in uterine epithelial cells of day 1 and day 6 pregnant rats 224

12.3.3 Paxillin protein expression in uterine epithelial cells of day 1 and day 6 pregnant rats 226

12.3.4 FAK protein expression in uterine epithelial cells of day 1 and day 6 pregnant rats 228

12.3.5 Vinculin epithelial domain localization in uterine epithelial cells 230

12.3.6 Integrin β5 epithelial domain localization in uterine epithelial cells 232

12.3.7 Paxillin epithelial domain localization in uterine epithelial cells 234

12.3.8 FAK epithelial domain localization in uterine epithelial cells 236

12.4 STATISTICAL ANALYSIS FOR REAL-TIME qPCR 238
12.4.1 Vinculin gene expression in uterine epithelial cells of day 1 and day 6 pregnant rats 238
12.4.2 Integrin β5 gene expression in uterine epithelial cells of day 1 and day 6 pregnant rats 241
12.4.3 Paxillin gene expression in uterine epithelial cells of day 1 and day 6 pregnant rats 243
12.4.4 FAK gene expression in uterine epithelial cells of day 1 and day 6 pregnant rats 245

13 APPENDIX H: NON-IMMUNE CONTROLS 248

13.1 Non immune controls for ant-Vinculin and anti-Integrin β5 248
13.2 Non-immune controls for anti-Paxillin and anti-FAK 249

14 APPENDIX I: ETHICS CLEARANCE CERTIFICATE 250

LIST OF FIGURES

Figure **Page**

CHAPTER 1: INTRODUCTION

Figure 1.1 The general reaction of the conversion of cholesterol to pregnenolone catalyzed by P450scc. 7

Figure 1.2 The general reaction for the conversion of testosterone to estradiol catalyzed by aromatase. 9

Figure 1.3 The general hydroxylation reaction in which testosterone is converted to 19-Hydroxytestosterone. 10

Figure 1.4 The general hydroxylation reaction in which 19-Hydroxytestosterone is converted to 19-Oxotestosterone. 11

Figure 1.5 Aromatase is catalyzing the reduction of an aliphatic A-ring of the androgen. 12

Figure 1.6 A summary of the ovarian steroidogenesis and aromatization of androgens. 13

Figure 1.7 CYP19A1 structure. 14

Figure 1.8 Hormonal interaction of the hypothalamus, anterior lobe of the pituitary gland, and ovary. 17

Figure 1.9 The structure of cartoon aromatase. 20

Figure 1.10 Views of the active site of aromatase. 21

Figure 1.11 A putative active-site access channel from within the lipid bilayer. 22

Figure 1.12 The general interactions between the androgen androstenedione with the aromatase inhibitor exemestane. 25

Figure 1.13 Chemical structure of anastrozole. 30

Figure 1.14 Rat uterus layers histology image. 34

Figure 1.15 The rat estrous cycle. 36

Figure 1.16 Signaling pathways involved in the regulation of focal adhesions in the rat. 41

Figure 1.17 Cell adhesion and motility regulators: focal adhesion proteins. 43

CHAPTER 3: RESULTS

Figure 3.1: Graphical representation of the means of implantation sites of treatment regimes of day 6 of pregnancy in rats. 68

Figure 3.2: Uterine horns of day 6 pregnant Wistar rat treated with a single dose of 15mg/kg body weight of anastrozole which has superovulated and achieved pregnancy. 69

Figure 3.3: Graphical representation of the uterine epithelial cell microvilli density (MD) and microvilli surface beads (MSB) in pregnant rats. 71

Figure 3.4: Graphical representation of the uterine large surface protrusions (LSP) and membrane pores (MP) in pregnant rats. 72

Figure 3.5: SEM of the uterine epithelial cells from day 1 and implantation sites of day 6 pregnant rats. 73

Figure 3.6: SEM of the uterine epithelial cells from non implantation sites (NP) of day 6 pregnant rats. 74

Figure 3.7: Graphical representation of the surface uterine epithelial cell microvilli in pregnant rats. 76

Figure 3.8: Graphical representation of the uterine surface folding in pregnant rats. 77

Figure 3.9: SEM of the uterine surface folding from day 1 and day 6 implantation sites of pregnant rats. 78

Figure 3.10: SEM of the uterine surface folding from day 6 non implantation sites of pregnant rats. 80

Figure 3.11: Graphical representation of uterine epithelial cell apices in pregnant rats. 81

Figure 3.12: SEM of the uterine epithelial cells from day 1 and implantation sites of day 6 of pregnant rats. 82

Figure 3.13: SEM of the uterine epithelial cells from non implantation sites of day 6 of pregnancy in rats. 83

Figure 3.14: Graphical representation of cell borders of uterine epithelial cells in pregnant rats. 84

Figure 3.15: Graphical representation of the uterine surface glycocalyx in pregnant rats. 85

Figure 3.16: SEM of the uterine epithelial cells from day 1 and implantation site day 6 pregnant rats. 86

Figure 3.17: Graphical representation of uterine epithelial gland openings. 88

Figure 3.18: Graphical representation of surface uterine small secretions in pregnant rats. 89

Figure 3.19A: Graphical representation of microvilli density (MD), microvilli surface beads (MSB), large surface protrusions (LSP), and membrane pores (MP) as shown in Table 2.2 at day 1 and day 6 of pregnancy in rats. 91

Figure 3.19B: Graphical representation of microvilli length (ML), uterine surface folding (SF), and surface glycocalyx (SG) as shown in Table 2.2 at day 1 and day 6 of pregnancy in rats. 92

Figure 3.19C: Graphical representation of small secretions (SS), epithelial gland openings (EGO), and cell apices (CA) as shown in Table 2.2 at day 1 and day 6 of pregnancy in rats. 93

Figure 3.20: Vinculin and intergrin β5 expression in the surface luminal uterine epithelial cells of day 1 and day 6 pregnant rats. 96

Figure 3.21: Vinculin and intergrin β5 uterine epithelial localization. 97

Figure 3.22: Micrograph showing vinculin and integrin β5 expression and co-localization in luminal uterine epithelial cells from day 1 of pregnancy in rats. 99

Figure 3.23: Micrograph showing vinculin and integrin β5 expression and co-localization in luminal uterine epithelial cells from implantation sites of day 6 pregnant rats. 101

Figure 3.24: Graphical representation of paxillin and focal adhesion kinase (FAK) expression in luminal uterine epithelial cells in pregnant rats. 106

Figure 3.25: Graphical representation of paxillin and focal adhesion kinase (FAK) localization in the uterine epithelial cells in pregnant rats. 107

Figure 3.26: Micrograph showing paxillin and focal adhesion kinase (FAK) expression and localization in luminal uterine epithelial cells from day 1 of pregnancy in rats. 108

Figure 3.27: Micrograph showing paxillin and focal adhesion kinase (FAK) expression and co-localization in luminal uterine epithelial cells from implantation sites of day 6 pregnant rats. 110

Figure 3.28: Micrograph (H & E) of endometrium of day 1 and day 6 pregnant rats. 114

Figure 3.29: Graphical representation of vinculin and intergrin β5 gene expression in the surface luminal uterine epithelial cells of day 1 and day 6 pregnant rats. 119

Figure 3.30: Graphical representation of paxillin and focal adhesion kinase (FAK) gene expression in luminal uterine epithelial cells in pregnant rats. 123

APPENDIX D

Figure 9.1 Vinculin and integrin β5 melt curves. 189

Figure 9.2 FAK and paxillin melt curves. 190

Figure 9.3 Melt curves of reference genes. 191

Figure 9.4 Gel electrophoresis of genes of interest and reference genes. 192

APPENDIX H

Figure 13.1 Non-immune control micrograph for vinculin and integrin β5. 248

Figure 13.2 Non-immune control micrograph for paxillin and FAK. 249

LIST OF TABLES

Table **Page**

CHAPTER 2: MATERIALS AND METHODS

Table 2.1 Aanastrozole and CC dose regimes. 51

Table 2.2 The scoring system used to analyze the morphology of the surface uterine epithelial features from the SEM micrographs. 54

Table 2.3 A description of the scoring system for the focal adhesion protein expression and localization in the confocal images. 57

Table 2.4 Description of the requirements used to analyze primer sequences. 61

Table 2.5 Description of the real time PCR primer sequence characteristics. 62

Table 2.6 The composition of the 2x QuantiFast SYBR Green PCR master mix. 64

CHAPTER 3: RESULTS

Table 3.1 A summary of the scanning electron microscopy analysis of the eleven luminal uterine epithelial characteristics. 90

Table 3.2 A summary of vinculin and integrin β5 expression and localization. 103

Table 3.3 Summary table for paxillin and FAK expression and localization. 112

Table 3.4 Relative quantification (RQ) analysis of vinculin gene expression in the luminal surface uterine epithelial cells of day 1 and day 6 of pregnant rats. 117

Table 3.5 RQ analysis of integrin β5 gene expression in the luminal surface uterine epithelial cells of day 1 and day 6 of pregnant rats. 118

Table 3.6 RQ analysis of paxillin gene expression in the luminal surface uterine epithelial cells of day 1 and day 6 of pregnant rats. 121

Table 3.7 RQ analysis of FAK gene expression in the luminal surface uterine epithelial cells of day 1 and day 6 of pregnant rats. 122

APPENDIX D

Table 9.1 Components of master mix for cDNA synthesis. 188

Table 9.2 cDNA synthesis thermocycling conditions. 189

APPENDIX E

Table 10.1 Chemicals used in the study and their suppliers. 195

APPENDIX F

Table 11.1 Equipment and manufacturers. 197

APPENDIX G

Table 12.1 A summary of the analysis of variance using a one way ANOVA test to determine changes in the implantation means between various treatment regimes. 198

Table 12.2 A summary of comparisons of means of implantation sites using the Tukey-Kramer Absolute (Difference) HSD tests for treatment regimes at the 5 % level of significance. 198

Table 12.3 Means and standard deviations of implantation sites. 199

Table 12.4 The analysis of means using a Tukey-Kramer post hoc test in order to compare the number of implantation sites between treatment groups. 199

Table 12.5 A one way ANOVA summary of fit of microvilli density. 200

Table 12.6 Analysis of variance of microvilli density. 200

Table 12.7 Microvilli density means and standard deviations. 201

Table 12.8 The analysis of means using a Tukey-Kramer post hoc test in order to assess the changes in microvilli density between treatment groups. 201

Table 12.9 A one way ANOVA summary of fit of microvilli length. 202

Table 12.10 Analysis of variance of microvilli length. 202

Table 12.11 Means and standard deviations of microvilli length. 203

Table 12.12 The analysis of means using a Tukey-Kramer post hoc test in order to assess the changes in microvilli length between treatment groups. 203

Table 12.13 A one way ANOVA summary of fit of microvilli surface beads. 204

Table 12.14 Analysis of variance of microvilli surface beads. 204

Table 12. 15 Means and standard deviations of microvilli surface beads. 205

Table 12.16 The analysis of means using a Tukey-Kramer post hoc test in order to assess the changes in microvilli surface beads between treatment groups. 205

Table 12.17 A one way ANOVA summary of fit of large surface protrusions. 206

Table 12.18 Analysis of variance of large surface protrusions. 206

Table 12.19 Means and standard deviations of large surface protrusions. 207

Table 12.20 The analysis of means using a Tukey-Kramer post hoc test in order to assess the changes in large surface protrusions between treatment groups. 207

Table 12.21 A one way ANOVA summary of fit of uterine surface folding. 208

Table 12.22 Analysis of variance of uterine surface folding. 208

Table 12.23 Means and standard deviations of uterine surface folding. 209

Table 12.24 The analysis of means using a Tukey-Kramer post hoc test in order to assess the changes in uterine surface folding between treatment groups. 209

Table 12.25 A one way ANOVA summary of fit of surface glycocalyx. 210

Table 12.26 Analysis of variance of surface glycocalyx. 210

Table 12.27 Means and standard deviations of surface glycocalyx. 211

Table 12.28 The analysis of means using a Tukey-Kramer post hoc test in order to assess the changes in surface glycocalyx between treatment groups. 211

Table 12.29 A one way ANOVA summary of fit of membrane pores. 212

Table 12.30 Analysis of variance of membrane pores. 212

Table 12.31 Means and standard deviations of membrane pores. 213

Table 12.32 The analysis of means using a Tukey-Kramer post hoc test in order to assess the changes in membrane pores between treatment groups. 213

Table 12.33 A one way ANOVA summary of fit of small secretions. 214

Table 12.34 Analysis of variance of small secretions. 214

Table 12.35 Means and standard deviations of small secretions. 215

Table 12.36 The analysis of means using a Tukey-Kramer post hoc test in order to assess the changes in small secretions between treatment groups. 215

Table 12.37 A one way ANOVA summary of fit of epithelial gland openings. 216

Table 12.38 Analysis of variance of epithelial gland openings. 216

Table 12.39 Means and standard deviations of epithelial gland openings. 217

Table 12.40 The analysis of means using a Tukey-Kramer post hoc test in order to assess the changes in epithelial gland openings between treatment groups. 217

Table 12.41 A one way ANOVA summary of fit of cell apices. 218

Table 12.42 Analysis of variance of cell apices. 218

Table 12.43 Means and standard deviations of cell apices. 219

Table 12.44 The analysis of means using a Tukey-Kramer post hoc test in order to assess the changes in cell apices between treatment groups. 219

Table 12.45 A one way ANOVA summary of fit of cell borders. 220

Table 12.46 Analysis of variance of cell borders. 220

Table 12.47 Means and standard deviations of cell borders. 221

Table 12.48 The analysis of means using a Tukey-Kramer post hoc test in order to assess the changes in cell borders between treatment groups. 221

Table 12.49 A one way ANOVA summary of fit of vinculin protein expression. 222

Table 12.50 A summary of the analysis of variance using a one way ANOVA test to determine the expression of vinculin in the luminal uterine epithelial cells at day and day 6 of pregnancy in rats. 222

Table 12.51 Means and standard deviations of vinculin protein expression. 223

Table 12.52 The analysis of means using a Tukey-Kramer post hoc test in order to compare the expression levels of vinculin between treatment groups. 223

Table 12.53 A one way ANOVA summary of fit of integrin β5 protein expression. 224

Table 12.54 A summary of the analysis of variance using a one way ANOVA test to determine the expression of integrin β5 in the luminal uterine epithelial cells at day and day 6 of pregnancy in rats. 224

Table 12.55 Means and standard deviations of integrin β5 protein expression 225

Table 12.56 The analysis of means using a Tukey-Kramer post hoc test in order to compare the expression levels of integrin β5 between treatment groups. 225

Table 12.57 A one way ANOVA summary of fit of paxillin protein expression. 226

Table 12.58 A summary of the analysis of variance using a one way ANOVA test to determine the expression of paxillin in the luminal uterine epithelial cells at day and day 6 of pregnancy in rats. 226

Table 12.59 Means and standard deviations of paxillin protein expression. 227

Table 12.60 The analysis of means using a Tukey-Kramer post hoc test in order to compare the expression levels of paxillin between treatment groups. 227

Table 12.61 A one way ANOVA summary of fit of FAK protein expression. 228

Table 12.62 A summary of the analysis of variance using a one way ANOVA test to determine the expression of FAK in the luminal uterine epithelial cells at day and day 6 of pregnancy in rats. 228

Table 12.63 Means and standard deviations of FAK protein expression. 229

Table 12.64 The analysis of means using a Tukey-Kramer post hoc test in order to compare the expression levels of FAK between treatment groups. 229

Table 12.65 A one way ANOVA summary of fit of vinculin epithelial localization. 230

Table 12.66 Analysis of variance of vinculin epithelial localization. 230

Table 12.67 Means and standard deviations of vinculin epithelial localization. 231

Table 12.68 The analysis of means using a Tukey-Kramer post hoc test in order to compare the epithelial localization of vinculin between treatment groups. 231

Table 12.69 A one way ANOVA summary of fit of integrin β5 epithelial domain localization 232

Table 12.70 Analysis of variance of integrin β5 epithelial domain localization. 232

Table 12.71 Means and standard deviations of integrin β5 epithelial domain localization. 233

Table 12.72 The analysis of means using a Tukey-Kramer post hoc test in order to compare the epithelial localization of integrin β5 between treatment groups. 233

Table 12.73 A one way ANOVA summary of fit of paxillin epithelial localization. 234

Table 12.74 Analysis of variance of paxillin epithelial localization. 234

Table 12.75 Means and standard deviations of paxillin epithelial localization. 235

Table 12.76 The analysis of means using a Tukey-Kramer post hoc test in order to compare the epithelial localization of paxillin between treatment groups. 235

Table 12.77 A one way ANOVA summary of fit of FAK epithelial localization. 236

Table 12.78 Analysis of variance of FAK epithelial localization. 236

Table 12.79 Means and standard deviations of FAK epithelial localization. 237

Table 12.80 The analysis of means using a Tukey-Kramer post hoc test in order to compare the epithelial localization of FAK between treatment groups. 237

Table 12.81 A one way ANOVA summary of fit of vinculin normalised relative quantities (NRQ) 238

Table 12.82 Analysis of variance of vinculin normalised relative quantities (NRQ). 238

Table 12.83 Means and standard deviations of vinculin normalised relative quantities (NRQ) 239

Table 12.84 The analysis of NRQ means using a Tukey-Kramer post hoc test in order to compare vinculin gene expression between treatment groups. 240

Table 12.85 A one way ANOVA summary of fit of integrin β5 normalised relative quantities (NRQ) 241

Table 12.86 Analysis of variance of integrin β5 normalised relative quantities (NRQ). 241

Table 12.87 Means and standard deviations of integrin β5 normalised relative quantities (NRQ) 242

Table 12.88 The analysis of NRQ means using a Tukey-Kramer post hoc test in order to compare integrin β5 gene expression between treatment groups. 243

Table 12.89 A one way ANOVA summary of fit of paxillin normalised relative quantities (NRQ). 243

Table 12.90 Analysis of variance of paxillin normalised relative quantities (NRQ). 244

Table 12.91 Means and standard deviations of paxillin normalised relative quantities (NRQ) 244

Table 12.92 The analysis of NRQ means using a Tukey-Kramer post hoc test in order to compare paxillin gene expression between treatment groups. 245

Table 12.93 A one way ANOVA summary of fit of FAK normalised relative quantities (NRQ). 245

Table 12.94 Analysis of variance of FAK normalised relative quantities (NRQ). 246

Table 12.95 Means and standard deviations of FAK normalised relative quantities (NRQ). 246

Table 12.96 The analysis of NRQ means using a Tukey-Kramer post hoc test in order to compare FAK gene expression between treatment groups. 247

ABBREVIATIONS

ADS Aromatase deficiency syndrome

AEXS Aromatase excess syndrome

AI Aromatase inhibitor

ART Assisted reproductive technology

BLAST Basic local alignment search tool

CA Cell apices

CB Cell borders

CC Clomiphene citrate

C_T Threshold cycle

DAPI 4',6-diamidino-2-phenylindole

DEPC Diethy pyrocarbonate

ECM Extracellular matrix

EDTA Tris-ethylenediamine tetraacetic acid

EGO Epithelial gland openings

FA Focal adhesion

FAK Focal adhesion kinase

FITC Fluorescein isothiocyanate

HMDS Hexamethyldisilazane

IVF In vitro fertilization

ICSI Intra cytoplasmic sperm injection

IP Implantation sites

LSP Large surface protrusions

MD Microvilli density

ML Microvilli length

MM Membrane pores

MSB Microvilli surface beads

NCBI National center for biotechnology information

NP Non-implantation sites

NRQ Normalized relative quantities

OCP Oral contraceptive pill

PBS Phosphate buffered saline

PCOS Polycystic ovary syndrome

PCR Polymerase chain reaction

qPCR Quantitative real time polymerase chain reaction

RQ Relative quantification

SEM Scanning electron microscopy

SERM Synthetic estrogen receptor modulator

SF Uterine surface folding

SG Surface glycocalyx

SS Small secretions

TRITC Tetramethyl rhodamine isothiocyanat

CHAPTER ONE: INTRODUCTION

1.1 Background

1.1.1 Assisted reproductive technologies (ART) and their importance

Subfertility affects one in seven couples trying to conceive (Smulders *et al.*, 2010). Two common causes of infertility include anovulatory dysfunction and polycystic ovarian syndrome (PCOS); these are responsible for about 80-90% of female infertility (Kousta *et al.*, 1997; Homburg, 2005; March *et al.*, 2010; Misso *et al.*, 2012). About 22.6% of the ART treatment cycles done in Australia and New Zealand in 2009 resulted in a clinical pregnancy, and 17.2% resulted in a live delivery (Wang *et al.*, 2009). ART is the technology used primarily for infertility treatments to achieve pregnancy (Wang *et al.*, 2009). ART treatments have advanced considerably since the first *in vitro* fertilization (IVF) birth in 1978 (Nygren and Andersen, 2001). IVF is a process by which oocytes are fertilized by a sperm outside the body in a laboratory simulating similar conditions in the body and then the fertilized eggs are implanted back in the uterus for full-term completion of pregnancy (Kuang *et al.*, 2014). For many subfertile couples, ART is the last hope of having a child. For this reason, many different ART protocols have been developed and include combined oral contraceptive pill (OCP) given prior to hormone therapy in an IVF cycle (Smulders *et al.*, 2010); IVF and intra cytoplasmic sperm injection (ICSI) (Pandian, 2005); administration of super-ovulatory drugs and a combination of these (Wang *et al.*, 2009; Mattos *et al.*, 2011; Pasco *et al.*, 2012; Kuang *et al.*, 2014; Shalom-Paz *et al.,* 2014). Thus many ART procedures require superovulation.

Superovulation is a process of retrieving multiple eggs using drug-induced stimulation, which helps a woman to release more than one egg in a month (Kuang *et al.*, 2014).

1.1.2 Superovulation

1.1.2.1 Gonadotropins

One way to achieve superovulation is to stimulate ovaries with large doses of gonadotropins (Shalom-Paz *et al.*, 2014). This was once the method of choice in the 1990s (Belaisch-Allart *et al.*, 1998), but gonadotropins are now used as second-line therapy for women with PCOS who have failed to respond to clomiphene citrate (CC) (Thessaloniki *et al.*, 2008). However, gonadotropins can be dangerous with serious life threatening side effects such as haemoconcentration, hypovolaemia and thromboembolism, which may result in death (Bergh and Navot, 1992) and thus their relegation to a second-line treatment (Thessaloniki *et al.*, 2008). Gonadotropin treatments are associated with a high risk of ovarian hyperstimulation (DiMarzo *et al.*, 1992), in which ovaries get large and are filled with fluid in response to the gonadotropin treatments (Abbas and Rouzi, 2013). Hyperstimulated ovaries release factors that cause a woman's blood vessels to leak fluid into the pelvis (DiMarzo *et al.*, 1992; Abbas and Rouzi, 2013). In addition, gonadotropins require invasive daily injections with constant monitoring of the ovarian response (Gibreel *et al.*, 2012). This is costly, time-consuming, invasive and additionally compliance is uncomfortable, unpleasant and difficult (Farquhar *et al.*, 2004). These side effects coupled with the relatively high risk of multi-follicular development and multiple pregnancies (Bruna-Catalan *et al.*, 2011), mean that this approach is usually reserved as the last resort (Lee and Ledger, 2011).

1.1.2.2 Clomiphene citrate

Chlomiphene citrate (CC) was first synthesized in 1956 (nearly sixty years ago) by Dr Palopoli as a prospective post coital contraceptive. Clomiphene citrate (CC) went to clinical trials in 1960 as a superovulatory drug and has been widely used since 1967 as such (Clark and Markaverich, 1982; Dickey and Holtcamp, 1996). Clomiphene citrate (CC) is a non steroidal compound, which is made up of enclomiphene and zuclomiphene isomers (Rostami-Hodjegan *et al.*, 2004). Clomiphene citrate (CC) is structurally similar to estrogen; and thus also classified as a synthetic estrogen receptor modulator (SERM). CC, therefore, blocks estrogenic hypothalamic receptors, resulting in blocking the hypothalamus-pituitary axis to endogenous circulating estrogens (Kurl and Morris, 1978). This in turn, triggers the release of follicle stimulating hormone (FSH) from the anterior pituitary due to modifications in GnRH pulsatility (Kerin *et al.*, 1985). In summary, the competitive inhibition of estrogen binding to its receptors results in a quantifiable drop of circulating estrogen to the hypothalamus, thus leading to increased gonadotropin secretion and the subsequent induction of ovulation.

Clomiphene citrate (CC) is the first-line and most commonly used oral agent for the induction of ovulation (Casper and Mitwally, 2011) because it is safe, inexpensive, available and easy to administer orally and additionally its side effects are fairly minor (Brown *et al.*, 2009). Side effects may include hot flushes, breast discomfort, abdominal distension, nausea and vomiting, sleeplessness, headache, mood swings, dizziness, hair loss and bilateral visual disturbances (Racette *et al.*, 2010).

Earlier studies have noted that successful ovulation occurs in 60-90% of women who are treated with clomiphene citrate (CC) (Homburg, 2005; Neveu *et al.*, 2007; Nutu *et al.*, 2010) while pregnancy rates are only 10-20% (Neveu *et al.*, 2007). The total CC-treated pregnancy rates are approximately 10 times lower than "natural" rates (Hosie *et al.*, 2008; Nutu *et al.*, 2010). These strikingly low pregnancy rates in women who are treated with CC are disappointing (Sharma *et al.*, 2014), possibly due to a wide variation among patients in the metabolism of the zuclomiphene (Rostami-Hodjegan *et al.*, 2004), and this may contribute to the variation in response to the drug (Rostami-Hodjegan *et al.*, 2004). Clearly an alternative and better substitute ovulatory drug, which is superior to clomiphene citrate (CC), is sought.

In addition, Dickey *et al.*, (1996) have noted an increased number of spontaneous abortions and miscarriages in CC treated women when compared to natural pregnancies. Furthermore, clomiphene citrate (CC) has been shown to have deleterious peripheral anti estrogenic actions at the level of the endometrium and cervical mucus, partly explaining the discrepancy in ovulation and pregnancy rates (Randall and Templeton, 1991; Benda, 1992; Dickey *et al.*, 1996; Healy *et al.*, 2003; Homburg, 2005; Hosie *et al.*, 2008; Brown *et al.*, 2009).

Clomiphene citrate (CC) also reduces endometrial thickness (Lacin *et al.*, 2001), blood flow (Hsu *et al.,* 1995), embryo development (Birkenfeld *et al.*, 1986), decidualization (Nutu *et al.*, 2010), quality of oocytes (London *et al.*, 2000) and thus affecting pregnancy rates (Brown *et al.*, 2009). Although it has been proposed that the antiestrogenic effects of CC may lead to early pregnancy failure (Healy *et al.*, 2003; Homburg, 2005; Hosie *et al.*, 2008; Brown *et al.*,

2009), the precise molecular events underlying CC-induced uterine anomalies remain incompletely understood (Nutu *et al.*, 2010). Earlier studies have suggested that the aberrant apoptotic activities of the uterine stromal cells after chronic CC treatment maybe a mechanism whereby the implantation process is disrupted (Nutu *et al.*, 2010). This is thought to be facilitated through the activation of the caspase-3-mediated apoptotic pathway in which CC regulates the uterine stroma cell function and hence the implantation process and pregnancy outcome (Nutu *et al.*, 2010). Other studies done on CC have reported several congenital malformations among newborns (Biljan *et al.*, 2005; Lima *et al.*, 2014), which include holoprosencephaly (Eleftheriou *et al.*, 2010), cardiac malformation (Reefhuis *et al.*, 2011), craniosynostosis (Ardalan *et al.*, 2012), ovary and fallopian tube dysplasia (Lima *et al.*, 2014), duplication of the urethra, cleft palate and lip, inguinal hernia and neural tube defects (Sharma *et al.*, 2014). These observations are also noted in another study that demonstrates increased risks for birth defects in babies born to mothers using CC (Davies *et al.*, 2012). Forman *et al.*, (2007) have observed a higher malformation rate in newborns born from mothers treated with CC (2.6%) when compared to the newborns from mothers treated with letrozole (0%), which is an aromatase inhibitor usually used in breast cancer treatment (Forman *et al.*, 2007). Other studies have made similar observations (Badawy *et al.*, 2009; Davies *et al.*, 2012). The use of CC in ovulation induction is also associated with hypospadias (Sharma *et al.*, 2014). To the contrary, Sorensen *et al.*, (2005) have not found any increased risk of hypospadias with CC usage to induce ovulation (Sorensen *et al.*, 2005).

Furthermore, CC appears to significantly reduce the mean birth weight of newborns when compared to naturally conceived babies (Sharma *et al.*, 2014). Similarly, another study has

reported lower mean birth weight in babies born to mothers who received clomiphene citrate (CC) treatment when compared to letrozole treated women (Forman *et al.*, 2007). However, other investigators have not reported any difference in the birth weight among clomiphene citrate (CC), letrozole and spontaneous pregnancies (Badawy *et al.*, 2009).

Additionally, CC disrupts some of the well documented normal uterine surface ultrastructure seen at the time of implantation (Parr and Parr, 1989; Murphy and Shaw 1994; Hosie *et al.*, 2003; Scholtz *et al.*, 2008). For example, typical surface morphological features associated with implantation include the change from long thin fairly dense microvilli at day 1 of pregnancy to a flattened uterine surface with few and short microvilli, at the time of implantation in rats and humans. With CC treatment, the uterine epithelial cells retain the long microvilli reminiscent of day 1 of pregnancy in rats (Hosie *et al.*, 2003). Similarly, recessed uterine epithelial cell borders are seen at day 6 of pregnancy, with CC treatment the cell borders are raised (Hosie *et al.*, 2003). Other ultrastructural uterine surface features associated with implantation include a decrease in the thickness of the glycocalyx, the presence of pinopods (uterodomes) and small secretions (Murphy & Shaw, 1994; Hosie *et al.*, 2003; Scholtz *et al.*, 2008).

These observations of the abnormalities that are seen in the female reproductive tract (including the uterus), embryos and newborns after CC treatment in both rodents and humans combined with the significant low pregnancy rates associated with CC treatments demand investigative studies for a potential substitute ovulatory drug, which is better than CC as the current first line drug for ovulation induction and probably long overdue. Moreover, some

women with PCOS are resistant to CC (Thessaloniki *et al.*, 2008; Casper and Mitwally, 2011), hence the need for an alternative better oral ovulation induction agent, which has proven superiority to CC that could be used without the risk of hyperstimulation and with minimal monitoring and thus emerging as the new first-line treatment for anovulatory or ovulatory infertility for more than half a century (Dickey and Holtcamp, 1996).

1.1.2.3 Aromatase inhibitors and their mechanism of action

1.1.2.3.1 Biosynthesis of steroid hormones

Steroid hormones are derived from cholesterol; they belong to a class of biologically active compounds in vertebrates (Kraemer *et al.*, 2013). The cholesterol side-chain cleavage enzyme (P450scc) catalyzes the conversion of cholesterol, a C27 compound, to pregnenolone, a C21 sreroid as shown in Figure 1.1 (Davydov *et al.*, 2012).

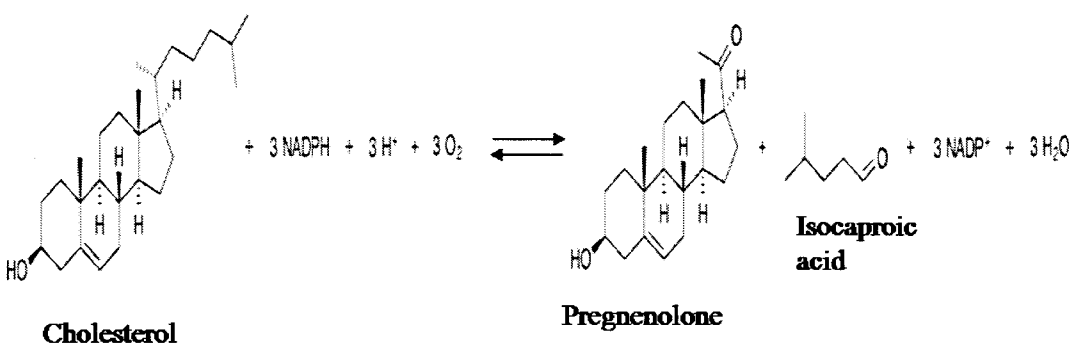


Figure 1.1: The general reaction of the conversion of cholesterol to pregnenolone catalyzed by P450scc. This involves two hydroxylation steps of the cholesterol side-chain which generate, first, the 22R-hydroxycholesterol and then the 20alpha, 22R-

dihydroxycholesterol. The bond between carbons 20 and 22 is then cleaved, and thus forming pregnenolone and isocaproic acid (Davydov *et al.*, 2012).

In other words, this process proceeds via three sequential monooxygenation reactions: two stereospecific hydroxylations with formation first of 22R-hydroxycholesterol (22-HC) and then 20α,22R-dihydroxycholesterol (20,22-DHC), followed by C20-C22 bond cleavage (Davydov *et al.*, 2012). Pregnenolone is then converted to progesterone by a bifunctional enzyme complex (Chapman *et al.*, 2005).

Pregnenolone and progesterone are the starting substrates for the three groups of steroids: the C21 steroids of glucocorticoids and minerocorticoids, the C19 steroids of androgens, and the C18 steroids of estrogens (Petrunak *et al.*, 2014). Progesterone is converted by hydroxylation to corticosterone, which is further modified into a mineralcorticoid called aldosterone, which helps in controlling electrolyte homeostasis, which influences blood pressure (Petrunak *et al.*, 2014). Cortisol, the main glucocorticoid that promotes carbohydrate metabolism and is involved in immune and stress responses, is formed from 17alpha-hydroxyprogesterone (Petrunak *et al.*, 2014). Testosterone is formed from pregnenolone by two pathways, delta5 pathway via dehydroepiandrosterone and delta4 pathway via androstenedione (Ghosh *et al.*, 2009). Estrogens, estradiol and estrone, are formed from testosterone and androstenedione respectively by oxidative elimination of the angular C19 methyl group and subsequent aromatization of the A-ring (Ghosh *et al.*, 2009). The three sequential hydroxylation and aromatization reactions of the androgens testosterone and androstenedione are catalyzed by an

aromatase resulting in the formation of estrogens. In summary, these steps involve two successive hydroxylation of the 19-methy group of the androgens, followed by simultaneous elimination of the angular methyl group as formate and aromatization of the A-ring as shown in Figure 1.2 (Ghosh *et al.*, 2010).

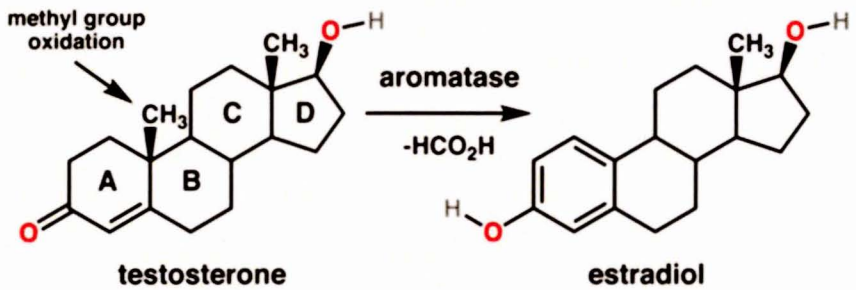


Figure 1.2: The general reaction for the conversion of testosterone to estradiol catalyzed by aromatase. Steroids are composed of four fused rings labeled A-D. Aromatase converts the ring labeled "A" into an aromatic state. Aromatase catalyzes the oxidative removal of the C19-methyl group to form an A-ring which is in its aromatic state (Ghosh *et al.*, 2010).

The three sequential hydroxylation and aromatization reactions of converting androgens into estrogens are as shown and described in Figures 1.3, 1.4 and 1.5.

First hydroxylation step:

Testosterone + reduced flavoprotein + oxygen <=> 19-Hydroxytestosterone + oxidized flavoprotein + H_2O.

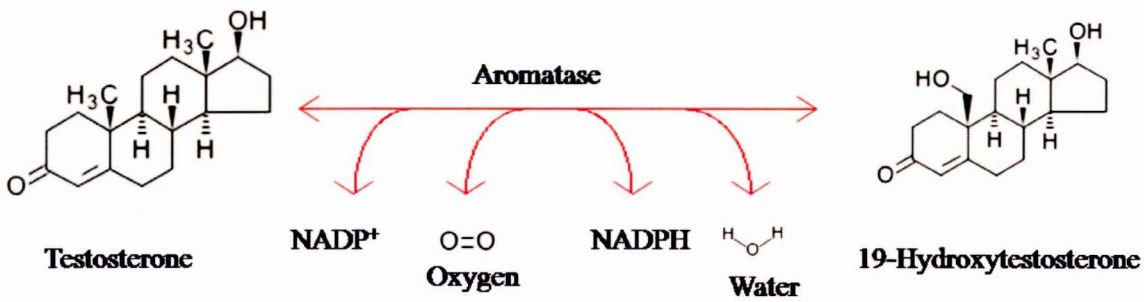


Figure 1.3: The general hydroxylation reaction in which testosterone is converted to 19-Hydroxytestosterone. The reaction is catalyzed by aromatase and proceeds in collaboration with nicotinamide adenine dinucleotide phosphate-cytochrome P450 reductase, which is conjugated with aromatase and supplies nicotinamide adenine dinucleotide phosphate, an essential co- enzyme for hydroxylation to aromatase (Mouriec *et al.*, 2009).

Second hydroxylation step:

19-Hydroxytestosterone + Reduced flavoprotein + Oxygen <=> 19-Oxotestosterone + Oxidized flavoprotein + $2H_2O$.

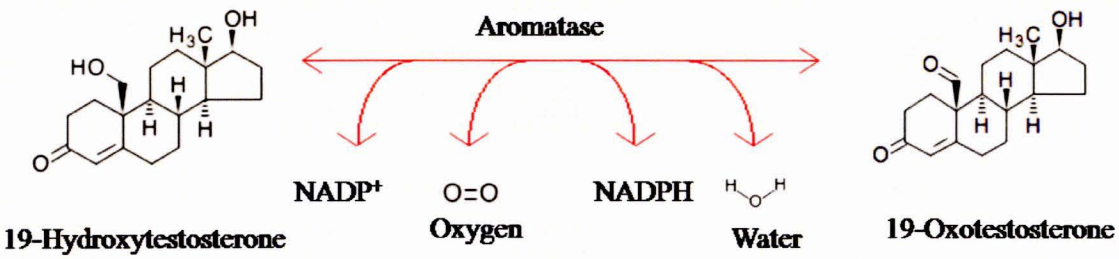


Figure 1.4: The general hydroxylation reaction in which 19-Hydroxytestosterone is converted to 19-Oxotestosterone. The reaction is catalyzed by aromatase and proceeds in collaboration with nicotinamide adenine dinucleotide phosphate-cytochrome P450 reductase, which supplies nicotinamide adenine dinucleotide phosphate to aromatase for the hydroxylation process (Mouriec *et al.*, 2009).

Third aromatization step

19-Oxotestosterone + Reduced flavoprotein + Oxygen <=> Estradiol + Formate + Oxidized flavoprotein + H_2O

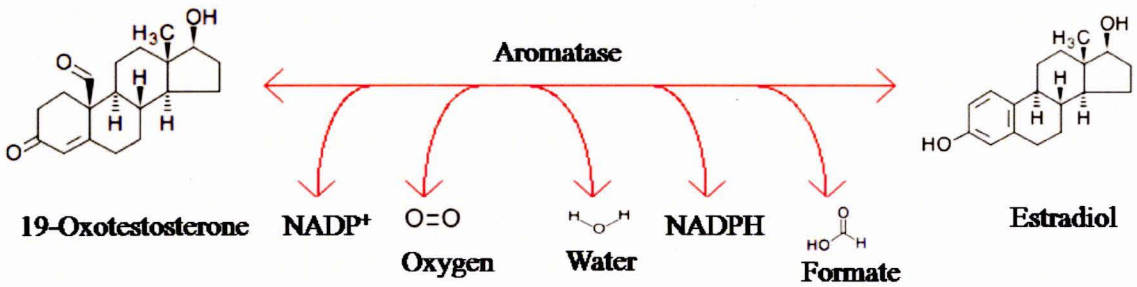


Figure 1.5: Aromatase is catalyzing the reduction of an aliphatic A-ring of the androgen to yield an aromatic A-ring of the estradiol while hydrogen or electrons are transferred from the reduced flavoprotein and one other donor, and one atom of oxygen is incorporated into one donor (Mouriec *et al.*, 2009).

In summary, during steroidogenesis, cholesterol enters the mitochondrion for prognenolone and progesterone production, which are then converted to androstenedione. This is followed by the conversion of androstenedione and testosterone to estrogens, estrone and estradiol respectively, catalyzed by aromatase as presented in Figure 1.6 (Attar and Bulun, 2006).

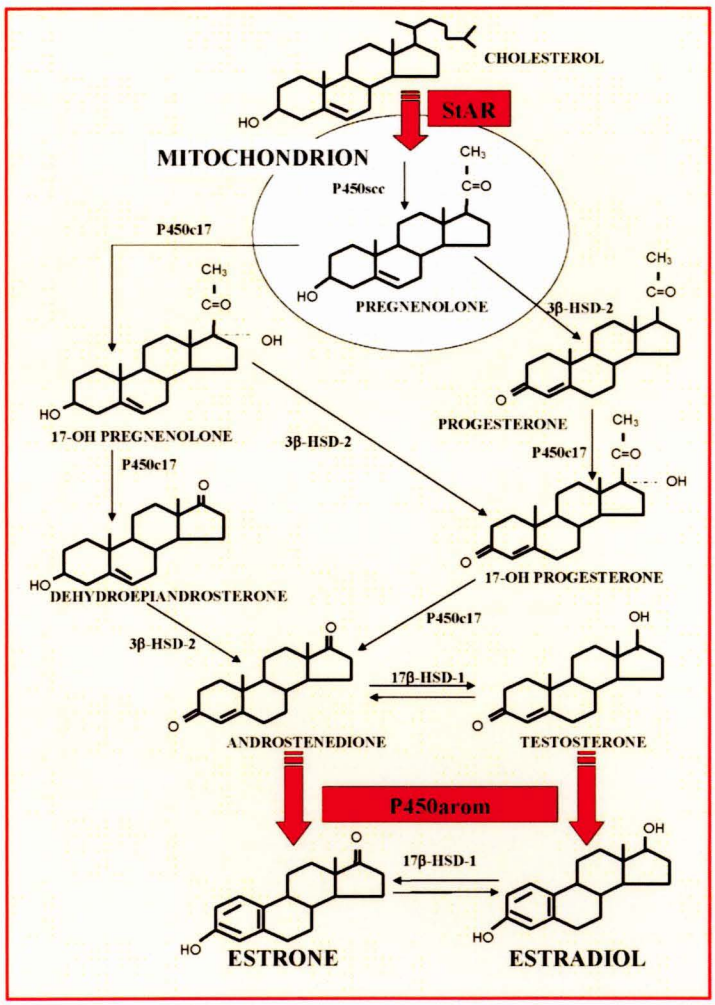


Figure 1.6: A summary of the ovarian steroidogenesis and aromatization of androgens: cholesterol enters the mitochondrion, facilitated by StAR for prognenolone and progesterone production, which are then converted to androstenedione (Attar and Bulun, 2006). This is followed by the conversion of androstenedione to estrone, catalyzed by aromatase (P450arom), for estrogen production. P450scc = side-chain cleavage enzyme cytochrome P450; P450c17 = 17-hydroxylase (17/20-lyase) cytochrome P450; 3β-HSD-2 = 3β-hydroxysteroid dehydrogenase type 2; 17β-HSD-1 = 17β-hydroxysteroid dehydrogenase type 1 (Attar and Bulun, 2006).

1.1.2.3.2 Aromatase

Human aromatase is an enzyme and a product of the CYP19 gene on chromosome 15q21.1 (Figure 1.7) (Shozu *et al.*, 2014), and it is monomeric, comprised of an iron-containing haem group and a polypeptide chain of 503 amino-acid residues. Aromatase is a member of the cytochrome P450 superfamily (EC 1.14.14.1), which are monooxygenases that catalyze many reactions involved in steroidogenesis (Shozu *et al.*, 2014).

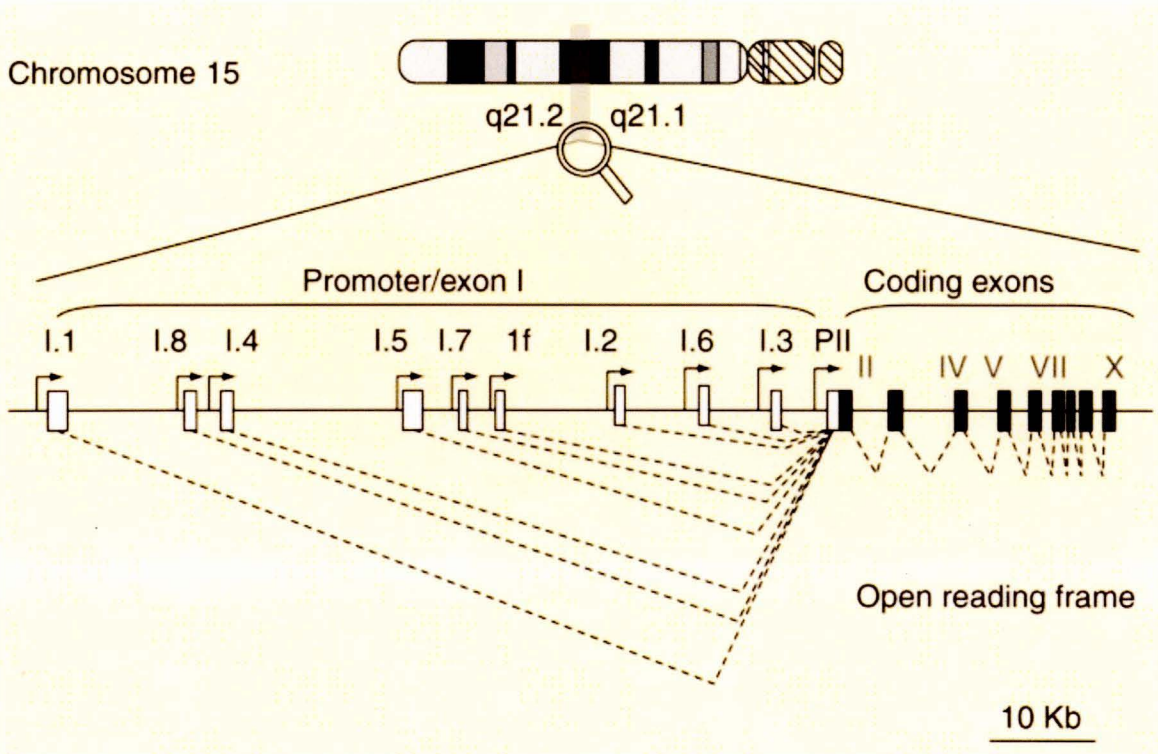


Figure 1.7: CYP19A1 structure (Shozu *et al.*, 2014). Open boxes represent aromatase exon, Is and L-shaped arrows in front of the boxes represent corresponding promoters. Closed boxes represent aromatase exons II–X encoding the open reading frame. Broken lines represent the splicing patterns (Shozu *et al.*, 2014). The entire gene spans 123 kb and is composed of at least 10 coding exons and upstream 5′ non-coding exons (exon Is). Each exon I possesses a unique

upstream promoter sequence that allows tissue-specific alternative use, and therefore, tissue-specific regulation (Shozu *et al.*, 2014). For example, the most proximal promoter (PII) is almost exclusively expressed in the gonadal tissues, whereas exons 1f and I.4, which are located upstream of PII, are almost exclusively expressed in the brain and adipose tissues, respectively. The most upstream promoter (I.1) is exclusively expressed in the placenta (Shozu *et al.*, 2014).The primary transcripts from exon Is are spliced to a common splicing acceptor site located in exon II so that the secondary mRNAs share exons II–X, which encode the full-length aromatase enzyme. Thus, all *CYP19A1* mRNAs encode the same protein, irrespective of exon I, which contains the transcriptional start site (Shozu *et al.*, 2014).

Aromatase is also called estrogen synthetase or estrogen synthase. It is an integral membrane protein of the endoplasmic reticulum, anchored to the membrane by the amino terminal transmembrane domain with the glycosylated N-terminal residue inside the lumen of the endoplasmic reticulum (Shozu *et al.*, 2014), in addition to other membrane-associating regions. What is remarkable is that aromatase is the only known enzyme in vertebrates capable of catalyzing the aromatization of androgens to estrogens (Simpson *et al.*, 1994, Ghosh *et al.*, 2009). Aromatase inhibitors, therefore, constitute a frontline therapy for estrogen-dependent breast cancer (Eisen *et al.*, 2008). In a three step process, each step requiring 1 mol of O_2, 1 mol of NADPH, and coupling with its redox partner cytochrome P450 reductase, aromatase converts androstenedione, testosterone and 16α-hydroxytestosterone to estrone, 17β-estradiol and 17β,16α-estriol, respectively (Ghosh *et al.*, 2010; Shozu *et al.*, 2014). As noted earlier, the first two steps are C19-methyl hydroxylation steps, and the third involves the aromatization of the steroid A-ring, unique to aromatase (Ghosh *et al.*, 2010).

Aromatase activity has been demonstrated in both reproductive (ovaries, placenta and breasts) and non-reproductive (adipose tissue, brain, muscle, fibroblasts, liver and osteoblasts) tissues (Nelson & Bulun, 2001; Gennari *et al.*, 2011; Stocco, 2012; Rettberg *et al.*, 2014). While aromatase is predominantly expressed in the ovaries of premenopausal women (Bartsch *et al.*, 2012), it is also highly expressed in the placenta of pregnant women (Wang *et al.*, 2014).

In the ovary, the precursors to the estrogens are produced by the highly vascularized layer of cuboidal cells of the theca interna (Qiu *et al.*, 2014). The fully differentiated cells of the theca interna possess ultrastructural features characteristic of steroid-secreting cells and thus they respond to the luteinizing hormone (LH) stimulation to synthesize and secrete androgens which are modified into estrogens by the ovarian granulosa cells (Qiu *et al.*, 2014) and exert a negative feedback effect on the FSH release from the pituitary gland (Campbell and Reece, 2005; Christensen *et al.*, 2012) as shown in Figure 1.8 (Campbell and Reece, 2005).

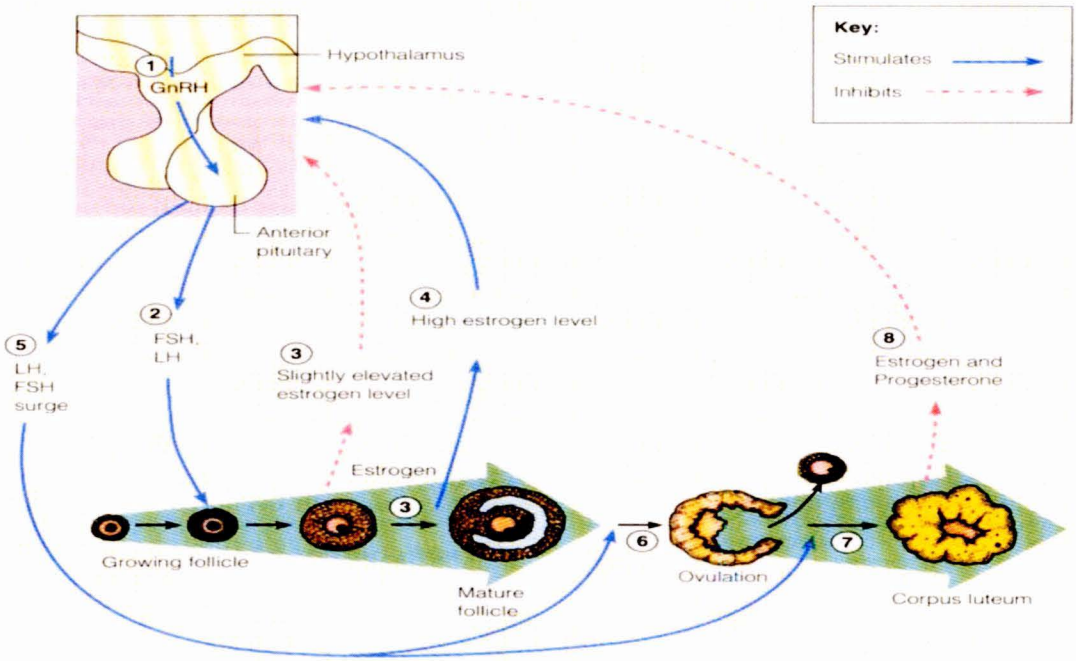


Figure 1.8: Hormonal interaction of the hypothalamus, anterior lobe of the pituitary gland, and ovary (Campbell and Reece, 2005). Production of estrogens is regulated through a negative feedback system. The estrogen can feedback on the system and inhibit further release of estrogens (Campbell and Reece, 2005). Such inhibition occurs at the level of the anterior lobe of the pituitary gland and the hypothalamus. The system is activated in response to low estrogen hormone levels (Campbell and Reece, 2005; Christensen *et al.*, 2012).

In other words, the hypothalamic-pituitary-gonadal axis coordinates the reproductive hormonal regulation that drives the ovary to ovulation. The primary signal from the central nervous system is the gonadotropin-releasing hormone (GnRH), which modulates the activity of the anterior pituitary small and medium-sized gonadotropes with round nuclei in the pars distalis (Childs *et al.*, 1992), and thus regulating the follicle stimulating hormone (FSH) and

luteinizing hormone (LH) release (Christensen *et al.*, 2012). As ovarian follicles develop, they release estrogen, which negatively regulates further release of GnRH and FSH. As estrogen levels peak, they trigger the surge release of GnRH, which leads to LH release inducing ovulation (Christensen *et al.*, 2012).

As noted in Figure 1.8, when the aromatization of androgens to estrogens is inhibited, a reduction of the circulating estrogens as described earlier for CC causes similar modifications in the hypothalamic–pituitary–ovary axis, including: the release of the hypothalamic –pituitary axis from estrogenic negative feedback and causing the increase of FSH secretion, resulting in the growth of ovarian follicles (Tiboni *et al.*, 2008).

1.1.2.3.3 Aromatase involvement in disease

Over expression and/or dysregulated expression of aromatase plays a role in the pathogenesis of various diseases, such as breast cancer, endometrial cancer, endometriosis and uterine fibroid development (Ishikawa *et al.*, 2009). In addition, placental aromatase protects the fetus from virilization through the clearance of potentially hazardous adrenal androgens (Shozu *et al.*, 2014).

Moreover, aromatase excess syndrome (AEXS), which was formerly known as familial gynecomastia, is a genetic autosomal dominant disease, which is characterized by increased extraglandular aromatization of steroids that presents with heterosexual precocity in males and isosexual precocity in females thus leading to pre- or peri-pubertal onset of gynecomastia (Fukami *et al.*, 2014). AEXS is caused by a mutational subchromosomal inversion of CYP19A

(Shozu *et al.*, 2014). The symptoms of AEXS are exclusively related to estrogen excess and are not life-threatening unlike those of common gynecomastia, which have a variety of well-established etiologies, especially secondary gynecomastia (Fukami *et al.*, 2014). Serum estrogen levels are elevated in 80% of AEXS patients, but are normal in 20%; therefore, a normal serum estrogen level does not exclude a diagnosis of aromatase excess syndrome (Shozu *et al.*, 2014). However, the use of aromatase inhibitors ameliorates gynecomastia (Fukami *et al.*, 2014).

Alternatively, aromatase deficiency syndrome (ADS) is a rare autosomal recessive disorder, which is the result of aromatase deficiency and thus leading to androgen excess and estrogen deficiency in the absence of normal aromatase activity (Ito *et al.*, 1993; Gagliardi *et al.*, 2014). This disorder is caused by the duplication in the aromatase gene, which occurs within the aromatase α-helix, and thus likely able to disrupt the substrate (androgen) and cofactor (protoporphyrin IX) binding, resulting in a lack of estrogen synthesis (Gagliardi *et al.*, 2014). In adult females, manifestations include delay of puberty, breast hypoplasia and primary amenorrhoea with polycystic ovaries (Ito *et al.*, 1993; Gagliardi *et al.*, 2014).

1.1.2.3.4 Structure of human aromatase

Aromatase enzyme has a unique active site specific for androgen binding thus making the enzyme highly substrate selective (Ghosh *et al.*, 2009). This androgenic specificity makes aromatase different from most P450s. Based on the crystallized structure of the human aromatase (Ghosh *et al.*, 2009), the enzyme has an androgen-specific cleft that binds its natural substrate androstenedione molecule snugly as shown in Figures 1.9 and 1.10 (Ghosh *et al.*, 2009). Hydrophobic and polar residues exquisitely complement the steroid backbone

(Ghosh *et al.*, 2009; 2010). The relative juxtaposition of the hydrophobic amino-terminal region and the opening to the catalytic cleft, as also demonstrated in Figure 1.11, shows why membrane anchoring is necessary for the lipophilic substrates to gain access to the active site (Ghosh *et al.*, 2009).

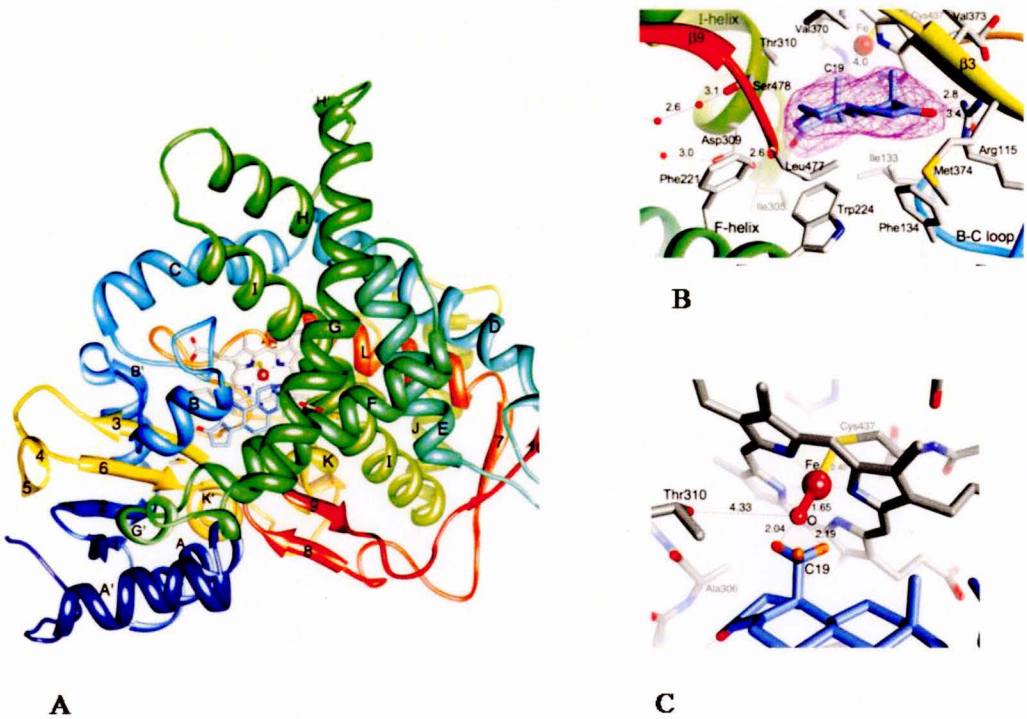


Figure 1.9: The structure of cartoon aromatase (Ghosh *et al.*, 2009). (A) This diagram shows the overall structure of aromatase. The N terminus, starting at residue 45, is coloured dark blue and the C terminus ending at residue 496 is coloured red. The α-helices are labelled from A to L and β-strands are numbered from 1 to 10. The haem group, the bound androstenedione molecule at the active site and its polar interactions are shown. (B) A close-up view of the active site showing the bound androstenedione molecule (Ghosh *et al.*, 2009). (C) Modelling of Fe(III) as an oxyferryl Fe(IV) = O moiety. The C19-methyl hydrogen atoms are shown at the calculated ideal positions. Important side chains, haem and water molecules

are depicted in element colours: grey, C; blue, N; red, O; yellow, S; firebrick, Fe; orange, H. The haem is a cofactor required for enzyme to be catalytically active. The C atoms of androstenedione are coloured cornflower blue. Distances are in angstroms. The directions of view into the active site are roughly similar in all panels. These illustrations were prepared with Chimera (Ghosh *et al.*, 2009).

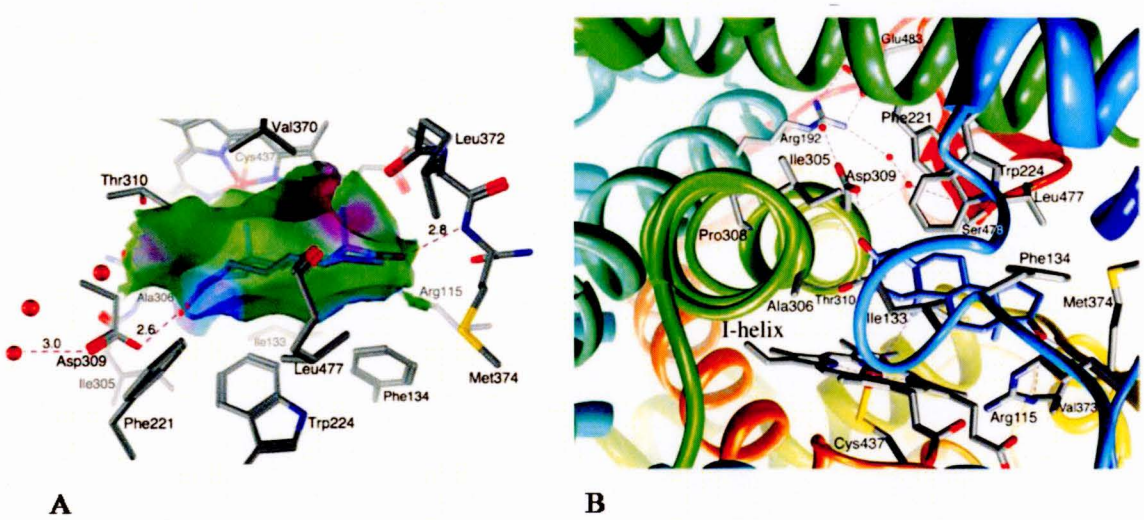


Figure 1.10: Views of the active site of aromatase (Ghosh *et al.*, 2009). (A) A van der Waals interaction surface cast by the protein and haem atoms at the active site. The semi-transparent surface, coloured green for hydrophobic interactions and magenta for polar interactions, closely resembles the shape, size and puckering of the steroid backbone (Ghosh *et al.*, 2009). (B) A view along the I-helix axis from its N-terminal end. The disruption to the helicity of the backbone at residues Pro 308-Asp 309-Thr 310 causes the helix axis to displace by about 3.5Å, allowing the side chain of Asp 309 to interact with the 3-keto oxygen of the steroid (Ghosh *et al.*, 2009).



Figure 1.11: A putative active-site access channel from within the lipid bilayer (Ghosh *et al.*, 2009). (A) The solvent-excluded surface of aromatase excludes the steroid binding pocket and haem from the protein interior by forming a 'pouch'-like cleft that has the only opening to the protein exterior through a channel, roughly at the arrowhead (Ghosh *et al.*, 2009). The course of the polypeptide chain is shown in rainbow colours. Residues Arg 192, Asp 309, Ser 478 and Glu 483 border this channel from the protein interior; three water molecules, part of the proton relay network, are within the channel. The inset is a view along this channel at the arrowhead, showing the locations of water molecules and opening to the active site (Ghosh *et al.*, 2009). (B) A proposed membrane integration model. The opening to the active-site access channel rests on the lipid bilayer surface, allowing the steroids to enter the aromatase active site directly from within the bilayer, roughly along the arrow shown (Ghosh *et al.*, 2009). The model suggests lipid integration/ association of the N terminus up to helix A, and other loops near the C terminus. The orientation of aromatase is roughly the same in both panels (Ghosh *et al.*, 2009).

Put together, the structure of aromatase as shown in Figures 1.9, 1.10 and 1.11 generally demonstrates the binding mode of androstenedione in the catalytically active oxidized high-spin ferric state of the enzyme (Pettersen *et al.*, 2004; Ghosh *et al*,. 2009). The hydrogen bond

forming interactions and tight packing hydrophobic side chains that complement the puckering of the steroid backbone provide the molecular basis for the exclusive androgenic specificity of the aromatase (Ghosh *et al.*, 2009; 2010). The location of the catalytic residues and water molecules clarifies the mechanism of the aromatization process. The structure also suggests a membrane integration model indicative of the passage of steroids through the lipid bilayer (Ghosh *et al.*, 2009; 2010). This molecular basis for the enzyme's androgenic specificity and unique catalytic mechanism can be used for developing the next-generation aromatase inhibitors (Ghosh *et al.*, 2010).

1.1.2.3.5 Aromatase inhibitors

Aromatase inhibitors (AIs) were originally developed for the treatment of advanced breast cancer in postmenopausal women (Dukes *et al.*, 1996). For example, aminoglutethimide and fadrozol were the first and second generation AIs respectively (Lee & Ledger, 2011). However, these caused a wide array of problems, which ranged from low potency, lack of specificity to adverse side effects (Holzer *et al.*, 2006). Therefore, a second and the third-generation AIs were engineered and these include non-steroidal anastrozole and letrozole, and steroidal exemestane. Unlike the first and second generation AIs, anastrozole and letrozole are highly potent, reversible and more specific in inhibiting aromatase activity (Dukes *et al.*, 1996; Mitwally & Casper, 2001; Lee & Ledger, 2011).

As described in Figures 1.9, 1.10 and 1.11, the structural and molecular basis of aromatase defines its unique specificity for the synthesis of estrogens from androgens, and this explains how aromatase inhibitors actually work (Ghosh *et al.*, 2009; 2010). Earlier studies done on the human aromatase have investigated the roles of the key amino acid residues in the active site,

at the intermolecular interface, inside the access channel, and at the lipid-protein boundary for their roles in enzyme function and higher-order organization (Ghosh *et al.*, 2013). Aromatase is inactivated when the active site residue D309 is replaced with an N, consistent with its proposed involvement in the aromatization process (Ghosh *et al.*, 2013). Additionally, a mutation of the R192 at the lipid interface is pivotal to the proton relay network in the access channel, resulting in the loss of aromatase activity (Ghosh *et al.*, 2012; 2013). Furthermore, mutation of K440 and Y361 of the haem-proximal region significantly interferes with the substrate binding, enzyme activity, and haem stability (Ghosh *et al.*, 2013). Moreover, the D-E loop deletion mutant Del7 that disrupts the intermolecular interaction drastically reduces the aromatase activity. Furthermore, it has been demonstrated that mutations in the intermolecular interface change the quaternary organization of the enzyme in solution (Ghosh *et al.*, 2013). Aromatase inhibitors (AIs), therefore, may act on these critical amino acid residues (Figure 1.12) in the active site and access channel to interfere with the enzyme activity and haem stability thus preventing the aromatization of androgens to estrogens (Ghosh *et al.*, 2013).

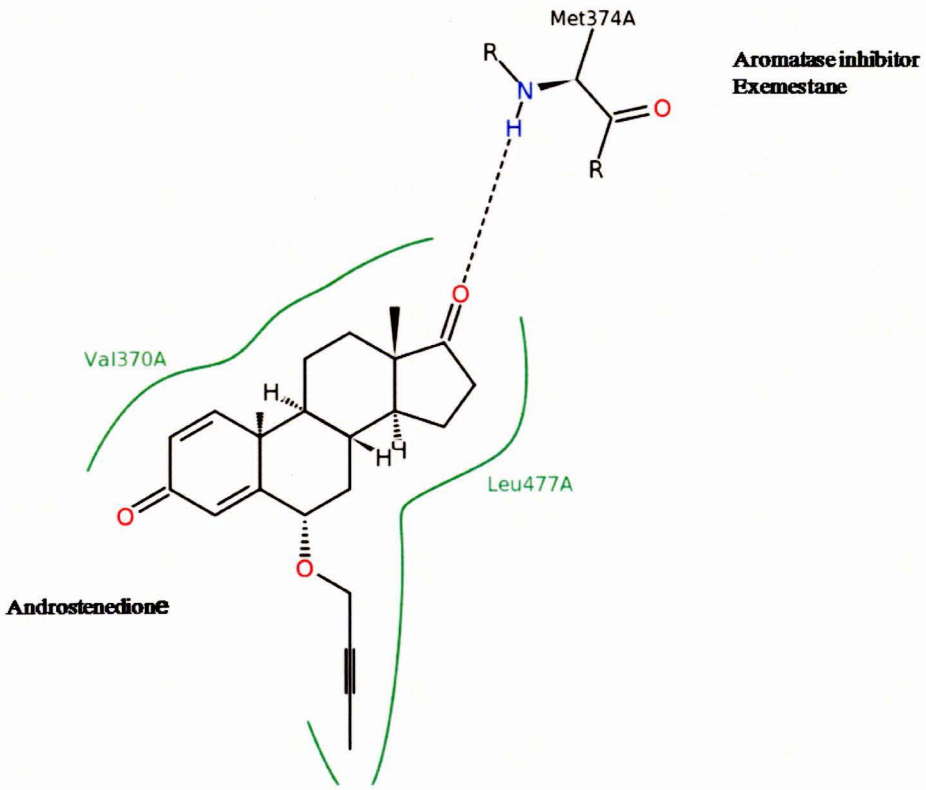


Figure 1.12: The general interactions between the androgen androstenedione with the aromatase inhibitor exemestane (Ghosh *et al.*, 2013). The black dashed lines are hydrogen bonds, salt bridges, metal interactions; the green solid lines are hydrophobic side chain residue interactions. Note: the covalent bonds to proteins are not displayed. Aromatase inhibitors (AIs) may interfere with the hydrogen bond forming interactions as shown in Figure 1.12, and also the hydrophobic side chain residues of the active site and access channel that complement the puckering of the steroid back bone (Figures 1.9-1.11), and thus affecting the aromatase-androgen specificity, and eventually inactivating the enzyme culminating into prevention of the aromatization process (Ghosh *et al.*, 2013).

Besides being highly specific, their easy compliance and oral administration make the third generation AIs an attractive alternative to other therapies. Letrozole, for example, apart from its role as a breast cancer treatment, has been used successfully to treat a variety of oestrogen-dependant conditions, including endometriosis and adenomyosis (Dietrich, 2010; Patwardhan *et al.*, 2008), uterine fibroids (Parsanezhad *et al.*, 2010) and endometrial stromal sarcoma (Sylvestre and Dunton, 2010).

Aromatase inhibitors were introduced for ovulation induction in 2001 (Franik *et al.*, 2014). Letrozole is at least as effective as CC in ovulation induction and probably more cost effective second-line option after CC failure in comparison to gonadotropins, especially in developing countries (Quintero *et al.*, 2007; Sharma *et al.*, 2014). Letrozole was being used in India for infertility treatment mainly as a second line drug after CC failure until October 2011 when the Ministry of Health and Family Welfare suspended its use in infertile women (Sharma *et al.*, 2014) because of its link with congenital malformations (Biljan *et al.*, 2005). The main concerns regarding the use of letrozole in ovulation induction are that letrozole might interrupt the normal aromatase function in tissues during fetal development and could be potentially teratogenic (Sharma *et al.*, 2014).

Ovulation induction studies have been conducted using letrozole (Casper and Mitwally, 2011; Lee & Ledger, 2011). Some investigators have reported an increase in congenital malformations following letrozole treatment. Letrozole treatment has been associated with a higher risk of congenital cardiac and bone malformations (Biljan *et al.*, 2005; Tiboni *et al.*, 2008). Other malformations associated with letrozole treatment include paraumbilical hernia,

congenital deafness, congenital talipus equino varus (CTEV) and albinism (Sharma *et al.*, 2014). On the contrary, Simerpal *et al.*, (2008) found no evidence of birth defects with letrozole use. Moreover, Sharma *et al.*, (2014) found that the overall rate of congenital malformations is not significantly higher in the natural conception group when compared to the letrozole group. In conclusion, it appears that the incidence of congenital malformations among children born following natural conception is comparable to that with the letrozole group according to some data (Tulandi *et al.*, 2006; Sharma *et al.*, 2014). In addition, other ovulation induction studies done with either letrozole or CC have shown that the congenital malformations and chromosomal abnormalities are comparable between the two groups (2.4% in the letrozole group; 4.8% in the CC group) but the rate of all congenital cardiac anomalies are significantly higher (P=0.02) in the CC group (1.8%) compared to the letrozole group (0.2%) (Tulandi *et al.*, 2006).

In another superovulation study done in mice, letrozole has been shown not to increase the risk to spindle assembly and blastocyst formation in oocytes as evidenced by the characteristics of the meiotic spindle and pre-implantational development of the embryos using Polscope imaging (Ganesh *et al.*, 2010). To put it in plain words, the risk of chromosomal anomalies appears to be low with letrozole use (Ganesh *et al.*, 2010). However, regarding its use during pregnancy, animal data has suggested that gestational exposure of letrozole is associated with embryo and fetal toxicity at a concentration much lower than 1% of the human dose (Gerardin and Pereira, 2002). Additionally, Tiboni *et al.*, (2008) have observed that exposing rats to letrozole at a dose lower than the recommended human therapeutic dose during pregnancy result in a marked increase in intrauterine lethality. The plasma half-lives of the standard doses of letrozole (2.5mg once a day) and anastrozole (1mg once a day) are 2-4 days and 41-48hrs

respectively (Buzdar, 2003). The time to steady-state plasma levels is 60 days for letrozole and 7 days for anastrozole (Buzdar, 2003). The long half-life and pharmacological profile of letrozole may contribute to the birth defects observed in developing embryos, and thus reducing its efficacy and tolerability benefits over other superovulatory drugs such as anastrozole (Buzdar, 2003). This means that letrozole should not necessarily be regarded as a safe ovulation induction agent although it may not adversely affect morphogenesis when administered before fertilization (Tiboni *et al.*, 2008).

Moreover, letrozole has some adverse effects, which include gastrointestinal disturbances, asthenia, hot flushes, headache and back pain (Holzer *et al.*, 2006). Letrozole, however, seems to be at least as effective as CC for induction of ovulation, live birth, and pregnancy rates in subfertile women with anovulatory PCOS with some potential advantages over CC (Casper & Mitwally, 2012; Franik *et al.*, 2014; Sharma *et al.*, 2014).

Earlier studies done with letrozole and anastrozole in women with PCOS, have reported comparable ovulation rate (62-63.4%) and pregnancy rate (12-15%), with significantly lower number of mature follicles and thinner endometrium in the letrozole group (Badawy *et al.*, 2008). Consequently, the use of letrozole as a first line therapy for women with anovulation is not fully conclusive and still remains debatable (Kamath and George, 2011; Misso *et al.*, 2012).

Anastrozole has a slightly better preclinical profile than letrozole with regard to teratology (Buzdar, 2003; Goss, 2003). Previous ovulation induction studies have been done on

anastrozole in women with CC- resistant PCOS (Wu *et al.*, 2007). Anastrozole appears to increase the endometrial thickness, pregnancy rates and reduce the number of ovulatory follicles when compared to CC (Wu *et al.*, 2007). Similarly, Griesinger *et al.*, 2009 have noted that the mean number of follicles greater than 15mm in size is higher in the CC group than in the anastrozole group on the day of the luteinizing hormone (LH) surge, thus more follicular growth in the CC group is noted. These observations are in agreement with other studies which have seen that anastrozole is associated with thicker endometrium, slightly higher pregnancy rates and fewer mature growing follicles when compared with CC (Badway *et al.*, 2009). However, when anastrozole and letrozole are compared in inducing ovulation in women with PCOS, the pregnancy rate is insignificantly higher in the anastrozole than letrozole patients (Badway *et al.*, 2008), and the endometrium is thicker in the anastrozole than in the letrozole patients, as mentioned earlier (Badway *et al.*, 2008). These studies have also noted more follicles in the patients treated with anastrozole than in those who are treated with letrozole. Additionally, the time taken to reach a dominant follicle is longer in the letrozole patients than in the anastrozole patients (Badway *et al.*, 2008). Put together, these observations seem to indicate that anastrozole is clinically effective in ovulation induction (Tredway & Schertz, 2011), but it has not been widely studied in reproductive medicine (Tredway & Schertz, 2011). Understanding the effects of anastrozole on implantation *in vivo* enables manipulation of uterine receptivity to control fertility and to improve the outcome of assisted reproductive procedures (Hosie *et al.*, 2003; Karaer *et al.*, 2005). Anastrozole could be a potential alternative drug used for hyperovulation or just to promote fertility in patients, particularly those suffering from polycystic ovary syndrome or are unresponsive to CC.

1.1.2.3.6 Chemistry of anastrozole

Anastrozole is a compound with a chemical formula of $C_{17}H_{19}N_5$. The chemical structure of anastrozole is shown in Figure 1.13. Anastrozole has a molecular weight of 293.3663. The brand names for anastrozole are anastrole and arimidex while the chemical IUPAC name is 2-[3-(2-cyanopropan-2-yl)-5-(1,2,4-triazol-1-ylmethyl)-2-methylpropanenitrile. Anastrozole belongs to the benzyl cyanides, which are compounds containing an acetonitrile with one hydrogen atom replaced by a phenyl group as shown in Figure 1.13 (Khile *et al.*, 2006).

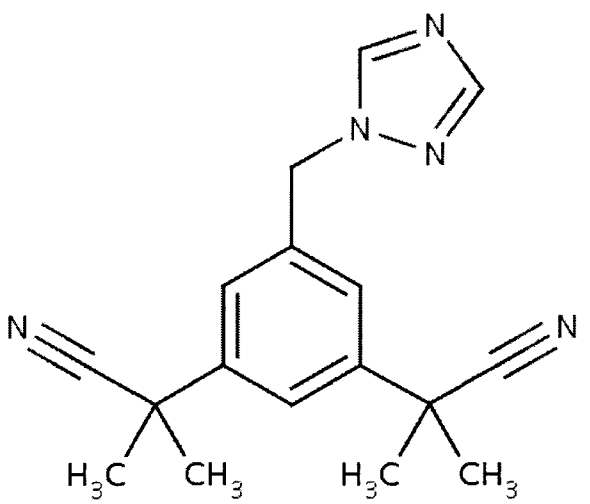


Figure 1.13: Chemical structure of anastrozole adapted from Khile *et al.*, (2006).

The half-life for anastrozole in humans is reported as being 41-48 hours (Plourde *et al.*, 1995; Buzdar, 2003; Franik *et al.*, 2014). Anastrozole is a white powder with a melting point of 130.14^{0}C. Anastrozole has moderate aqueous solubility (0.5 mg/mL at 25°C); its solubility is

independent of pH in the physiological range. Anastrozole is freely soluble in methanol, acetone, ethanol, and tetrahydrofuran, and very soluble in acetonitrile. For clinical use, anastrozole contains lactose, magnesium stearate, hydroxypropylmethylcellulose, polyethylene glycol, povidone, sodium starch glycolate, and titanium dioxide as inactive ingredients (Khile *et al.*, 2006; Mauras *et al.*, 2009).

Anastrozole is rapidly absorbed into the systemic circulation following oral administration. Anastrozole is metabolized mainly by N-dealkylation, hydroxylation, and glucuronidation to inactive metabolites. The primary metabolite is an inactive triazole (Khile *et al.*, 2006; Mauras *et al.*, 2009). The hepatic metabolism accounts for approximately 85% of anastrozole elimination while renal elimination accounts for approximately 10% of the total clearance (Khile *et al.*, 2006). In rats, the lethality is greater than 100 mg/kg. It is a non-carcinogen, but not readily biodegradable (Khile *et al.*, 2006; Mauras *et al.*, 2009).

1.1.2.3.7 Aromatase inhibitor mechanism of action

Multiple mechanisms of action for aromatase inhibitors as superovulatory agents have been suggested in earlier studies (Mitwally and Casper, 2002; Chen, 2011). Aromatase inhibitors (AIs) appear to be reversible competitive inhibitors as they block the active site and therefore their action would be dose dependent. The AI competes with the aromatase itself. The more AIs present the less aromatase would bind to the active site (Berg *et al.*, 2012).

As indicated earlier, AIs may interfere with the hydrogen bond forming interactions as shown in Figure 12, and also the hydrophobic side chain residues of the active site and access channel

that complement the puckering of the steroid back bone, and thus affecting the aromatase-androgen specificity, and preventing the enzyme from binding and in that way blocking the enzyme activity, culminating into prevention of the aromatization process (Ghosh *et al.*, 2009; 2010; 2013). For example, AIs may inactivate aromatase by replacing the active site residue D309 with an N, consistent with its proposed involvement in the aromatization process (Ghosh *et al.*, 2013). Additionally, AIs may change some of the crucial side chain residues at the active site and access channel responsible for its specificity. As noted earlier, a mutation of the R192 at the lipid interface, pivotal to the proton relay network in the access channel, results in the loss of aromatase activity (Ghosh *et al.*, 2013). Furthermore, mutation of K440 and Y361significantly interferes with the substrate binding, enzyme activity, and haem stability (Ghosh *et al.*, 2013). These mechanisms interfere with the aromatization of androgens to estrogens and thus preventing the feedback by estrogen on the gonadotropin releasing hormone and gonadotropin secretion.

Aromatase inhibitors may also act locally in the ovary by increasing expression of FSH receptors, which increases follicular sensitivity to FSH. This may result from the accumulation of intraovarian androgens, since conversion of androgen substrate to estrogen is blocked (Mitwally and Casper, 2002). In addition, Weil *et al.*, (1999) have reported the stimulatory role of androgens in follicular growth in primates. Furthermore, follicular androgen accumulation may stimulate insulin-like growth factor 1, which promotes folliculogenesis (Adashi, 1993).

1.1.3 Reproduction and early pregnancy

1.1.3.1 Anatomy of the rat uterus

The uterus is the muscular organ that accommodates the developing embryo. In a female rat, the vagina is a short tube lying dorsal to the urinary bladder. The vagina divides into two uterine horns that extend toward the kidneys. Superior to uterine horns are ovaries and are connected to the uterine horns by thin, short oviducts. Inferiorly, the two uterine horns join and open into the vagina via two separate cervices. The wall of the uterine horns is organized into three layers: endometrium, myometrium and perimetrium (Dykes and Watson, 2007) as shown in Figure 1.14.

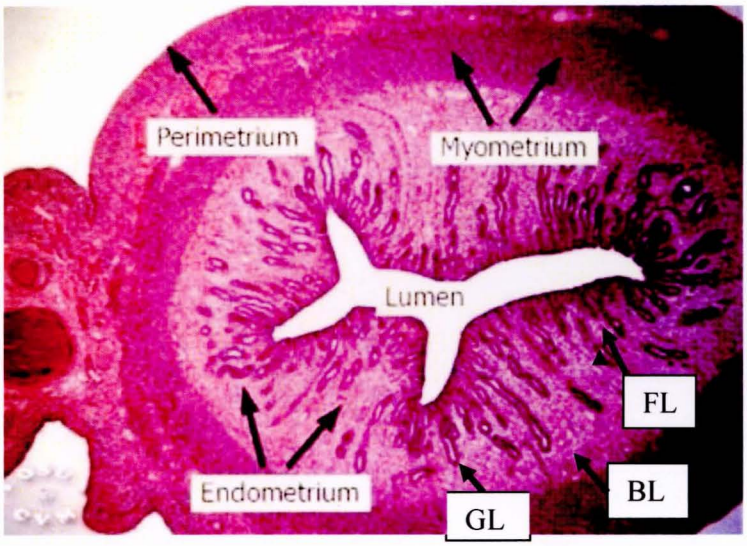


Figure 1.14: Histology of rat uterus showing layers courtesy of OSU College of Veterinary Medicine. Copyright © Charlotte L. Ownby. Reprinted with permission. This section shows the three main layers of the uterus in proestrus stage of the estrous cycle: endometrium, myometrium and perimetrium. The myometrium consists of smooth muscle and connective tissue and contains large blood vessels that give rise to the vessels that supply the endometrium. The endometrium has a simple columnar epithelium and has many simple tubular glands (GL) which secret glycogen for the embryo; it has a basal layer (BL) and functional layer (FL).

The endometrium is multilayered and dynamic. It overlies the myometrium and comprises a functional layer and a basal layer. The luminal surface of the endometrium consists of a simple columnar epithelium overlying a thick lamina propria, which contains numerous blood vessels and simple tubular glands (Diedrich *et al.*, 2007). The basal layer is attached to the myometrium and serves as a base for endometrial regeneration (Gargett *et al.*, 2012). The endometrium has several different cell types, which include luminal and glandular epithelial

cells, stromal cells, lymphocytes and other leucocytes. The numbers, activity, structure and function of these cells not only change throughout the reproductive cycle, but also during pregnancy (Diedrich *et al.*, 2007).

The myometrium is the middle and largest layer; it is composed of an inner circular and outer longitudinal smooth muscle layer. The myometrium plays a role in embryo spacing and spreading along the length of the uterine horn during implantation in the female rat (Pusey *et al.*, 1980). The myometrium is covered by the perimetrium, which is a thin outer connective tissue layer.

1.1.3.2 Estrous cycle of female rats and vaginal cytology

In most mammals the female undergoes a spontaneous cycle of reproductive preparedness at least during some times of the year. This cycle is referred to as the estrous cycle in non-primates and the menstrual cycle in primates where it is associated with a more extensive buildup and breakdown of the uterine mucosal lining (Rudolph *et al.*, 2012).

The estrous cycle of female rats is much shorter than the human reproductive cycle, consisting of 4 days and characterized as proestrus, estrus, metestrus and diestrus as shown in Figure 1.15 (Long and Evans, 1922). The cytological changes of the vagina reflect the level of estrogens during the estrous cycle (Marcondes *et al.*, 2002). A vaginal smear taken during diestrus, when the level of estrogens is low, the vaginal epithelium is thin and the cells of the basal layer of the vaginal epithelium appear. Leukocytes are abundant in the stroma and the vaginal smear should consist of stringy mucus in which are entangled a large number of leukocytes and a few

small, round or oval shaped nucleated epithelial cells (Marcondes *et al.*, 2002). As the cycle changes to proestrus, to estrous and with the concomitant increase in estrogen, the vaginal epithelium undergoes an increased mitotic activity resulting in many rows of epithelial cells, the outer layer consisting of squamous and cornified epithelial cells. The proestrus stage smear contains round and nucleated medium sized epithelial cells whereas the estrus stage smear predominantly has cornified epithelial cells (Marcondes *et al.*, 2002).

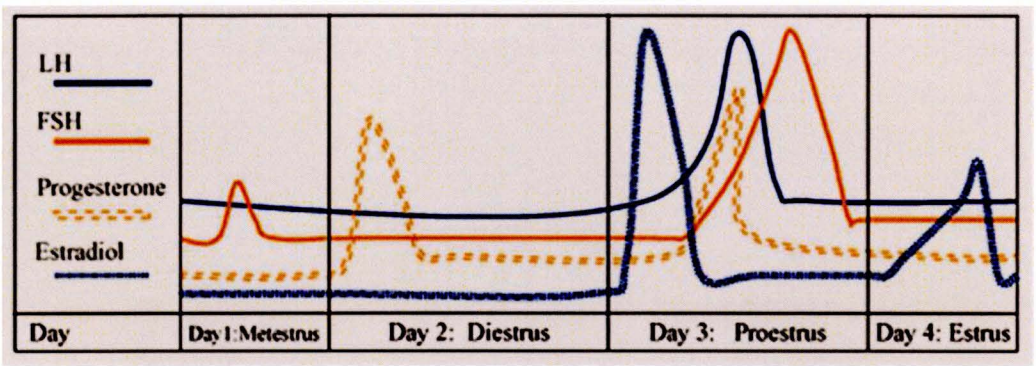


Figure 1.15: The rat estrous cycle. The rat estrous cycle consists of about 4 days and is controlled by hormones (Long and Evans, 1922). Progesterone increases sharply, beginning early in the postovulation phase (diestrus) on day 2 and drops sharply in late diestrus on day 2. At approximately noon of the start of the follicular phase (proestrus), estrogen levels markedly surge, causing a rapid peaking of LH and FSH between about 4 p.m. to 6 p.m. of proestrus and an increased progesterone secretion. The gonadotropin surge triggers ovulation. All these hormones return to the baseline levels when ovulation occurs (estrus) on day 4. Finally there is a brief temporary peak of estradiol on the evening of estrus. Diestrus is the luteal phase. Proestrus is the beginning of the follicular phase (Emanuele *et al.*, 2002).

During the estrous cycle, the luteinizing hormone (LH), follicle stimulating hormone (FSH) and prolactin remain low and increase in the afternoon of proestrus phase. Estrogen levels begin to increase and reach peak levels during proestrus and return to baseline at estrus (Sportnitz *et al.*, 1999). Progesterone secretion also increases during diestrus due to the corpus luteum activity with a decrease afterwards. Then progesterone rises to reach its second peak towards the end of proestrus (Sportnitz *et al.*, 1999). Ovulation occurs from the beginning of proestrus to the end of estrus (Marcondes *et al.*, 2002).

1.1.3.3 Fertilization and pre-implantation embryo development

Fertilization is the process by which male and female gametes fuse to form a zygote. The sperm penetrates the corona radiate and zona pellucida to reach the oocyte. Fertilization usually occurs in the fallopian tube (Gilbert, 2010). Soon after fertilization, the egg responds by altering the structure of the zona pellucida to prevent binding of other sperms, which inturn prevents polyspermy (Gilbert, 2010). The fertilized egg metabolism is acitivated for proper embryo development. For example, phospholipase C (PLC) cleaves a membrane lipid into two parts: Di-acetyl-glycerol (DAG) and Inositol triphosphate (IP_3), which stimulates increased oxygen consumption, DNA synthesis, protein synthesis, rearrangement of the cytoplasm of the zygote to create new molecular interactions (Gilbert, 2010). This is followed by cleavage in which the zygote undergoes a series of rapid mitotic divisions that give rise to many smaller cells called blastomeres forming a blastula (Gilbert, 2010). A blastula differentiates into a morula, which later develops a cavity or blastocele and therefore, the embryo at this stage is

called a blastocyst. The blastocyst is the one that implants onto a receptive uterus (Gilbert, 2010).

1.1.3.4 Uterine receptivity and blastocyst implantation

Implantation is a process by which the blastocyst makes the first physical and physiological contact with the maternal uterine luminal epithelium (Enders and Schlafke, 1969; Paria *et al.*, 2001; Reese *et al.*, 2001). The blood vessels of the embryo are later brought into functional communication with the maternal circulation leading to the establishment of a functional placenta and pregnancy (Dey *et al.*, 2004). Under the influence of ovarian steroid hormones, an optimal "window" for implantation is created when the activated developing blastocyst overlaps with a brief period of uterine receptivity (Psychoyos, 1986; Paria *et al.*, 2001; Reese *et al.*, 2001; Dey *et al.*, 2004) during which the uterine environment is favorable to blastocyst acceptance and implantation. One of the earliest significant events of the implantation process in most species including humans and rodents is the adhesion of the blastocyst to a receptive uterine luminal epithelium (Enders and Schlafke, 1969; Wynn and Jollie, 1989; Murphy and Shaw, 1994; Paria *et al.*, 2001). A non-receptive uterine luminal epithelium forms an epithelial barrier that is refractory to invasive elements, including blastocycts (Murphy and Shaw, 1994; Poon, *et al.*, 2014). In preparation for implantation, the plasma membrane of uterine epithelial cells undergoes a reversible plasma membrane transformation for the uterus to be receptive and adhesive (Png and Murphy, 1997; Murphy, 2004). Earlier studies have observed common basolateral and apical morphological and molecular alterations, which are termed 'plasma membrane transformation' occurring across species during early pregnancy (Murphy, 1995; 2004). These alterations are important in uterine receptivity (Murphy, 2004). During this

period, the luminal uterine epithelium loses long regular microvilli, which become short irregular and flat (Murphy and Shaw, 1994; Png and Murphy, 2002); large, rounded, smooth-surfaced protrusions (uterodomes) also appear in a receptive uterus (Novotny *et al.*, 1999; Nikas and Psychoyos, 1997; Murphy, 2000). In addition, cholesterols increase in the apical plasma membrane (Dey *et al.*, 2004) while the luminal epithelial surface glycocalyx is significantly reduced as pregnancy progresses (Murphy, 2000). The basolateral plasma membrane also undergoes considerable alterations during early pregnancy (Murphy, 2004).

After successful fertilization and prior to implantation, the blastocyst assumes a particular orientation as it approaches the endometrium, a process called apposition (Diedrich *et al.*, 2007). The blastocyst then adheres onto the uterine epithelial layer before it penetrates it and invades the stroma (Enders *et al.*, 1986; Diedrich *et al.*, 2007). Uterine epithelial cells, therefore, are the first site of interaction between the maternal and foetal cells during early pregnancy, and they allow the blastocyst to penetrate them from the apical surface (Murphy, 2004). Blastocyst implantation is a complex process that requires interaction between a developed competent blastocyst and receptive uterus (Emiliani *et al.*, 2005; Urman *et al.*, 2005; Wang and Dey, 2006; Diedrich *et al.*, 2007). In other words, the activation of the blastocyst, a process by which it gains competency to attach onto the receptive uterus, is a prerequisite for successful implantation. Highly coordinated expression, activation and reorganization of adhesion molecules play an important role during implantation (Aplin and Kimber, 2004; Kaneko *et al.*, 2011). Implantation failure is thought to occur as a consequence of impairment of embryo developmental potential or impairment of uterine receptivity and the embryo-uterine dialogue (Diedrich *et al.*, 2007).

1.1.4 The cytoskeleton and focal adhesion dynamics

The cytoskeleton is an internal framework of a cell, which is largely composed of actin filaments, intermediate filaments and microtubules. In addition to participating in cellular shape maintenance, cytokinesis, phagocytosis and intracellular transport processes, the actin cytoskeleton essentially creates cell motility in animals (Lele *et al.*, 2008). Cytoskeletal reorganization is an ongoing process when cells adhere, move or invade extracellular substrates. In order for cells to adhere, they employ focal adhesions (Fabry *et al.*, 2011).

The focal adhesion (FA) is a specialized structure formed where bundles of actin filaments are anchored to transmembrane receptors of the integrin family through a complex of adaptor and signaling proteins enabling cells to adhere, spread and migrate (Gilmore and Burridge, 1996). FAs provide sites of mechanical attachment to the extracellular matrix (ECM) and are sites where adhesion-associated signal transductions are initiated (Fabry *et al.*, 2011). FA formation is triggered by the binding of transmembrane integrin receptors to the ECM molecules, such as fibronectin, vitronectin, collagen (Hirata *et al.*, 2014). The binding of ligands to integrins on the extracellular side promotes recruitment of various intracellular proteins to the cytoplasmic tails of integrins that mechanically link them to the actin cytoskeleton (Hirata *et al.*, 2014). Integrin signaling requires the non-receptor tyrosine kinase activities of the focal adhesion kinase (FAK) and src proteins as well as the adaptor protein functions of FAK, src and Shc to initiate downstream signaling events (Lu and Rounds, 2012) as illustrated in Figure 1.16.

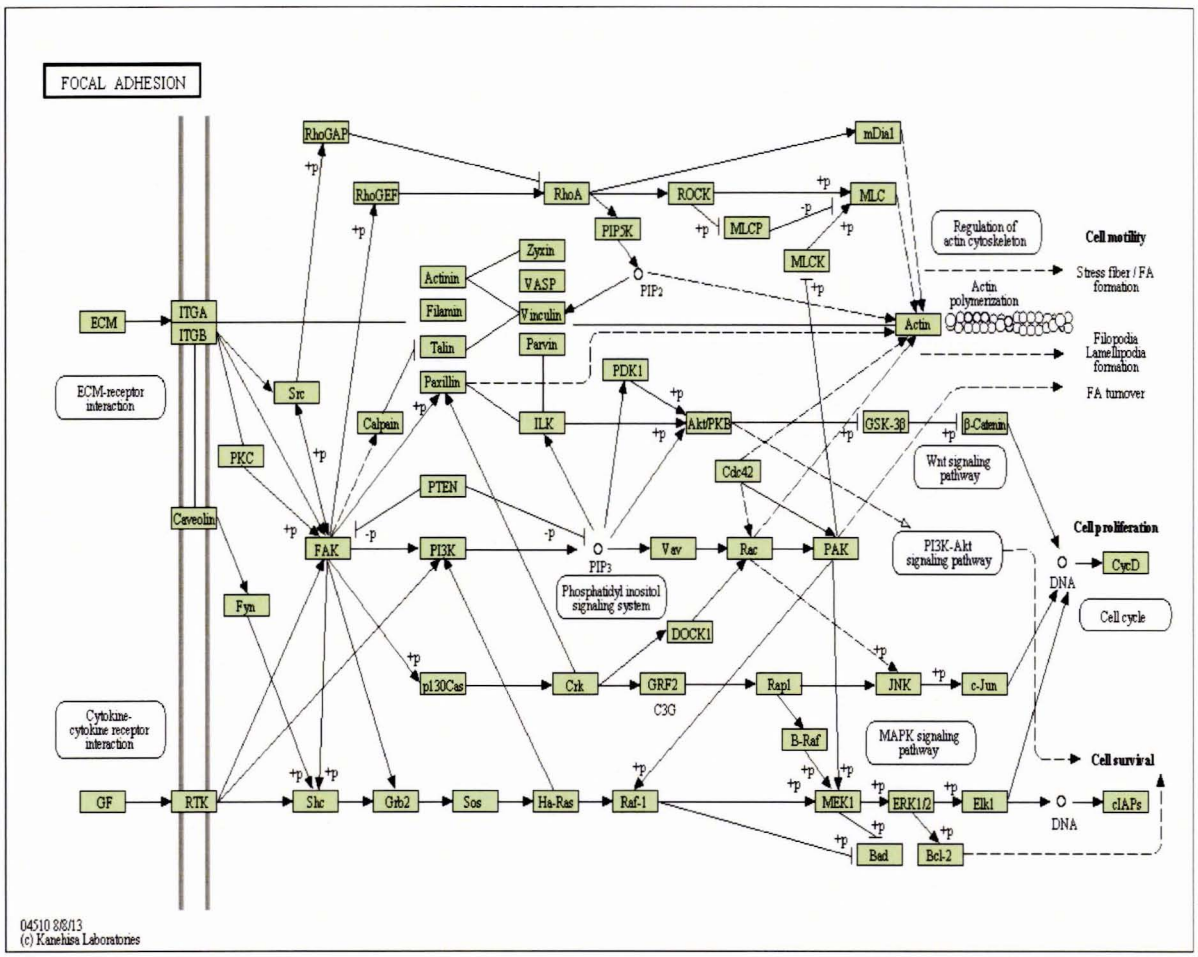


Figure 1.16: Signaling pathways involved in the regulation of focal adhesions in the rat (adapted from (Petit & Thiery, 2000; Berman *et al.*, 2003; Mitra *et al.*, 2005). Some of the constituents of focal adhesions participate in the structural link between membrane receptors and the actin cytoskeleton, while others are signalling molecules, including different protein kinases and phosphatases, their substrates, and various adapter proteins. Integrin signaling is dependent upon the non-receptor tyrosine kinase activities of the FAK and src proteins as well as the adaptor protein functions of FAK, src and Shc to initiate downstream signaling events (Lu and Rounds, 2012). These signalling events culminate in reorganization of the actin cytoskeleton; a prerequisite for changes in cell shape and motility, gene expression and

pregnancy (Lele *et al.*, 2008; Salgia, 2009; Fabry *et al.*, 2011; Kaneko *et al.*, 2011). Moreover, the implantation of blastocysts into the endometrial stroma cells is regulated by the Rho GTPases RhoA, Rac 1 and Cdc42, which is a FAK dependent remodeling process (Grewal *et al.*, 2010).

In addition, the focal adhesion proteins talin and α-actinin must also link the cytoplasmic domain of β-integrins with actin filaments in order to have a direct mechanical coupling between integrins and the actin cytoskeleton (Critchley *et al.,* 2004). Vinculin, acting as another linker protein, also binds actin filaments, talin and α-actinin as noted in Figure 1.17 (Critchley *et al.,* 2004; Salgia, 2009). Vinculin strengthens the connections between integrins and actin filaments in order to support force transfer from the cytoskeleton to the extracellular matrix (Choquet *et al.*, 1997).

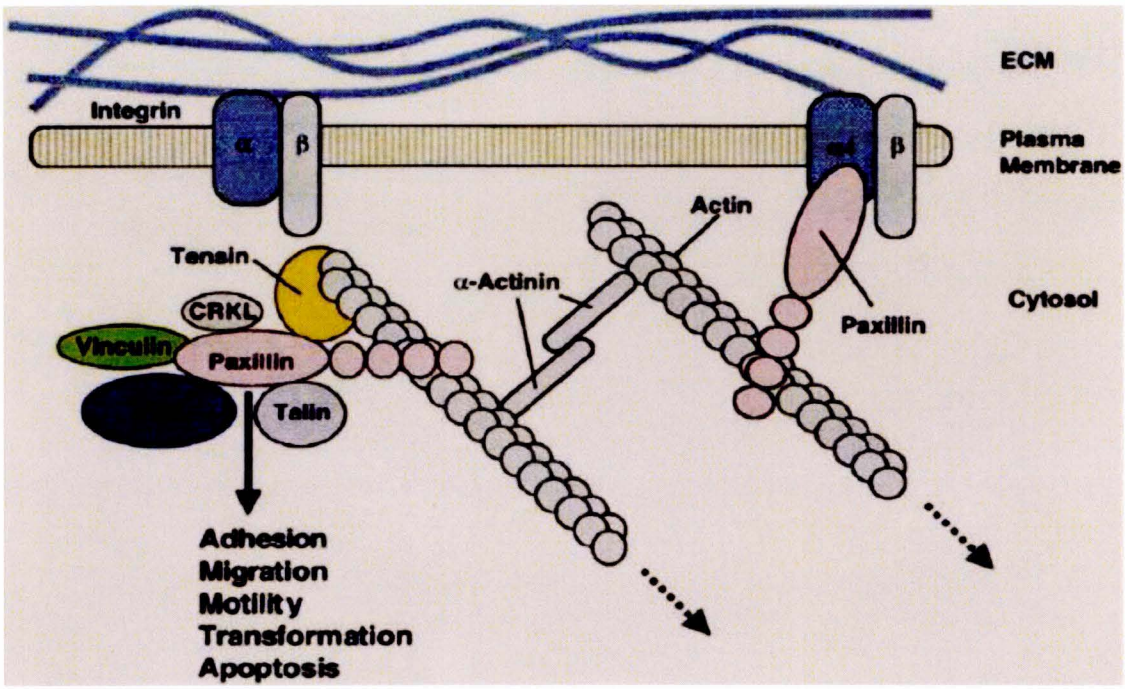


Figure 1.17: Cell adhesion and motility regulators: focal adhesion proteins (Salgia, 2009). Paxillin interacts with the integrin $\alpha_4\beta_1$ and is a key mediator in cytoskeletal interactions. A complex formed by paxillin and other cytoskeletal members talin, vinculin, FAK, and CRKL can lead to membrane reorganization and separation of focal adhesions leading to migration and motility. Constitutively, active paxillin can mediate these functions more aggressively. Many functions of the cytoskeletal protein complex are also shown, which include adhesion, migration, transformation and apoptosis (Salgia, 2009).

Other studies have provided evidence to suggest that the binding of vinculin to actin and talin can be regulated by phosphatidyl-inositol-4-5-bisphosphate (Gilmore and Burridge, 1996) and inhibited by acidic phospholipids (Weekes *et al.,* 1996). Clearly, the structural links between actin filaments and integrins are regulated in at least some cell types, and it would not be

unreasonable to hypothesize that agents known to alter cell behavior may do so by affecting the expression or function of actin binding proteins such as vinculin, talin, α-actinin, paxillin, and signaling molecules such as FAK which are recruited to focal adhesions (Mwakikunga *et al.*, 2011). Focal adhesions are dynamically assembled and disassembled by cells including uterine luminal epithelial cells (Kaneko *et al.*, 2008; Hosie *et al.*, 2008; Kaneko *et al.*, 2011) and these mechanisms are likely governed by the modulation of cross-talk between their constituent proteins, which influence their gene expression and morphology.

1.2 Problem statement

As noted earlier, gonadotropin injections are medically dangerous, invasive and their compliance is not easy. They are also associated with multiple pregnancies (Bruna-Catalan *et al.*, 2011). Similarly, PCOS patients are resistant to CC (Casper & Mitwally, 2011). Therefore, an alternative to gonadotropins and CC as ovulation induction agents is sought. AIs such as letrozole and anastrozole, which are used to treat breast cancer, have been suggested as alternatives to gonadotropins and CC due to their easy compliance and oral administration (Lee & Ledger, 2011). The use of letrozole as a first line therapy for women with anovulation is not fully conclusive and still remains debatable (Kamath *et al.*, 2011). Additionally, its association with low pregnancy rates and more importantly its suggestion of possible birth defects raises an investigative quest to conduct research on other potential superovulatory drugs (Tiboni *et al.*, 2008). Anastrozole is clinically effective in ovulation induction (Tredway & Schertz, 2011), but it has not been well researched in reproductive medicine (Tredway & Schertz, 2011). Investigating its effect on implantation and early pregnancy is a positive step towards its acceptance as a possible long overdue better and safe alternative to CC. Further

research should focus on its effects on embryo development. Understanding the effects of anastrozole on the endometrium at the time of implantation *in vivo* enables manipulation of uterine receptivity to control fertility and to improve the outcome of assisted reproductive procedures (Paria, *et al.*, 2001; Hosie *et al.*, 2003; Karaer *et al.*, 2005).

As mentioned, despite many advances in recent years in assisted reproductive technologies (ART), the rates of implantation are still low (Andersen *et al.,* 2005); therefore, the search for predictors of implantation is ongoing. It is, therefore, important to identify potential molecular candidates that are used in implantation and determine their expression levels in the presence of an alternative ART superovulator such as anastrozole. Since blastocyst adhesion onto the endometrium is at the center of the implantation process (Enders *et al.*, 1986), this means that focal adhesion proteins are employed. The expression and distribution of focal adhesion proteins paxillin and talin in the rat uterine epithelial cells are associated with uterine receptivity (Kaneko *et al.*, 2008). In other words, the dynamics of focal adhesions are crucial at the time of implantation. Disassembly of the basal focal adhesions along the uterine epithelial cells makes cells less adherent to the underlying basement membrane, and this facilitates their removal, hence, enabling embryonic trophoblast cells to invade the endometrial decidual cells beneath. Since previous studies have demonstrated that focal adhesion proteins are more likely regulated in uterine epithelia to change cell behavior (Kaneko *et al.,* 2009), and that super-ovulatory drugs can alter expression of key molecules in the uterine epithelial cells during implantation (Hosie *et al.,* 2003), anastrozole may act on the focal adhesion proteins during implantation. To date, anastrozole regulation of focal adhesion proteins in the uterine epithelial cells during implantation has not been established.

In addition, previous studies have demonstrated that the plasma membrane of the uterine epithelial cells undergoes a remarkable change in structure, known as 'the plasma membrane transformation' of early pregnancy (Murphy, 2004), which is observed during the window of receptivity (Murphy, 2004). In view of this, a sequential change in the morphology of the plasma membrane transformation is postulated.

1.3 Aim and specific objectives

The overall aim of the study is to investigate the effects of anastrozole on the expression of focal adhesion proteins on the endometrium *in vivo* during implantation, which will enable manipulation of uterine receptivity to control fertility and improve the outcome of assisted reproductive procedures. The specific objectives are to:

1. Determine the optimal dose for anastrozole as a superovulator in the Wistar rats.

2. Determine the effects of anastrozole on the uterine morphology (surface uterine folding, microvilli density, microvilli length, microvilli surface beads, surface glycocalyx, large surface protrusions, cell borders and cell apices) during early pregnancy using scanning electron microscopy (SEM), and to compare it as a superovulator to CC in similar situations.

3. Investigate the effectiveness of anastrozole and clomiphene citrate as superovulators whose evidence will be found in the number of blastocysts implanted in the rats upon administration.

4. Determine the gene and protein expression levels and localization of focal adhesion proteins vinculin, integrin β5, paxillin, and FAK in the rat uterine epithelial cells during implantation *in vivo*.

2 CHAPTER TWO: MATERIALS AND METHODS

This study was approved by the University of the Witwatersrand Animal Ethics Committee with a clearance certificate number: 2012/11/03 as shown in Appendix I. The project was divided into two parts. Part one was a preliminary dose response study of anastrozole, where the aim was to determine the optimal dose of anastrozole that could give the highest number of implantation sites upon administration in the Wistar rats. Therefore, only day 6 pregnant rats were used in the preliminary study because the investigators were only interested in the number of blastocysts implanted with different anastrozole dose regimes. The optimal dose of anastrozole (15mg/kg) determined from this study was used in the second part of the project, and this part included both day 1 and day 6 pregnant rats. The second part of the project (main study) employed scanning electron microscopy (SEM), immunofluorescence and confocal microscopy and quantitative real time polymerase chain reaction (qPCR) techniques to determine the ultrastructure of the surface uterine epithelium during early pregnancy; and to determine the expression levels and localization of focal adhesion proteins vinculin, integrin β5, paxillin, and focal adhesion kinase (FAK) in the rat uterine luminal epithelial cells during implantation in vivo.

2.1 Animals

Thirty five female virgin in bred Wistar rats were used in the preliminary dose response study to determine the optimal dose of anastrozole required to superovulate rats in the main study. Only day 6 pregnant rats were used in the preliminary study. A chlomiphene citrate (CC) treatment group was also used as a control to compare with the anastrozole treatment groups. Rats were housed in plastic cages at 21^0C under a controlled 12 hour light-dark cycle. They

were provided with water and food *ad libitum* (Dukes *et al.,* 1996). Vaginal smears were obtained from all female rats to confirm that they had regular cycles for two cycles before drug administration (Jaramillo *et al.*, 2012; Singletary *et al.*, 2005). Thirty five mature female rats, 12 to 14 weeks old and weighing 200-250g, were randomly divided into 7 groups of 5 rats each. Vaginal smear was done in the late afternoon (Kaneko *et al.*, 2008) and rats in pro-oestrus were treated with the drugs or placebo then caged overnight with males of proven fertility. The morning of finding the vaginal plug or presence of spermatozoa in the smear was designated as day 1 of pregnancy (Kaneko *et al.*, 2008).

2.2 Rationale for the doses

A daily dose of 1mg/kg anastrozole (Sigma-Aldrich Co., St. Louis, MO, USA) for 5 days is the standard recommended dose to achieve ovulation in humans (Franik *et al.*, 2014). A 12-14 week mature female Wistar rat weighs between 200-250g with a 4-day estrous cycle, so a single dose of anastrozole administered at pro-estrus was deemed appropriate. Kilic-Okman *et al.*, (2003) employed a similar regime using letrozole. Earlier studies have suggested that the standard 1mg/kg anastrozole of body weight dose is too low for optimal follicle recruitment and ovulation, so higher doses are recommended (Al-Omari *et al.*, 2004; Casper and Mitwally, 2009). A single 25 mg/kg anastrozole dose has been successful in inducing ovulation in mice and is associated with favorable embryo development (Karaer *et al.*, 2005). However, in this preliminary work, a drug concentration study with anastrozole was carried out to determine the optimal dose to be used to superovulate and achieve pregnancy in the Wistar rats. Dose rates were therefore chosen starting at 1mg/kg. The chlomiphene citrate dose of 1.25mg/kg

(Sigma-Aldrich Co., St. Louis, MO, USA) was adopted from earlier studies (Hosie *et al.*, 2003) and used as a comparison.

2.3 Drug preparation and administration

Anastrozole has moderate aqueous solubility and previous studies have used normal saline as a vehicle for anastrozole (Karaer *et al.*, 2005; Fatum *et al.*, 2006). In this study, the vehicle for all of the drugs was normal saline and each injection consisted of 0.2ml normal saline (Fatum *et al.*, 2006) including the drug per injection per rat. All injections were intraperitoneal. The four anastrozole dose regimes for the preliminary dose response study were: 25mg, 15mg, 10mg, and 1mg/kg body weight which were made as shown in Appendix A.

2.4 Treatment regimes for the dose response study

Treatment regimes: Group 1 was left untreated (negative control). Group 2 (carrier control group) received the vehicle sterile saline. Groups 3, 4, 5 and 6 received a single dose of 1mg/kg, 10mg/kg, 15mg/kg and 25mg/kg of body weight anastrozole, respectively in the proestrous phase intraperitoneally. Group 7 received 1.25mg/kg of body weight CC; n=5 in each group, all 0.2ml intraperitoneal injections (Table 2.1).

Table 2.1 shows anastrozole and CC dose regimes made up to 0.2ml normal saline for the 7 groups of mature female Wistar rats undergoing ovulation stimulation.

Groups	Treatments	Number of rats
1	Untreated*	5
2	Saline (vehicle)*	5
3	1 mg/kg anastrozole	5
4	10 mg/kg anastrozole	5
5	15 mg/kg anastrozole*	5
6	25 mg/kg anastrozole	5
7	1.25mg/kg chlomiphene citrate*	5

* Rats also used in the main study.

2.5 Tissue preparation

Pregnant rats were sacrificed on day 6 at the time of implantation using a lethal dose (0.35 ml) of Euthanase, intraperitoneally (1 ml/kg is recommended; Kyron Labs, South Africa). Once deeply unconscious, the abdominal cavity was opened and the rats to be sacrificed on day 6 of pregnancy were injected intravenously using the inferior vena cava with 0.1ml of 1% high molecular weight vital dye Pontamine sky blue (Sigma, St. Louis, MO, USA) in normal saline (0.9% NaCl) (Pakrasi *et al.*, 2007), in order to distinguish implantation sites from non-implantation sites. This dye quickly localizes in the implantation sites due to increased vascularization and vascular permeability during early pregnancy (Psychoyos, 1986). After removal of the uterine horns, implantation sites were counted and recorded. The uterus was cut into1cm pieces separating implantation and non-implantation sites and prepared for scanning electron microscopy (SEM), confocal microscopy and qPCR.

2.6 Animals for the main study (SEM, confocal microscopy and qPCR)

A further twenty similar female rats to be sacrificed on day 1 of pregnancy were used in the main study. Five rats were treated with 15mg/kg anastrozole, (as this was found to be the optimal dose), five were treated with 1.25mg/kg CC, five were treated with saline alone and five were untreated. These matched the groups in the earlier study where the animals were sacrificed on day 6 of pregnancy (see Table 2.1).

2.6.1 Scanning Electron Microscopy (SEM)

The method used was adopted from previous studies (Hosie and Murphy, 1995). The uterine pieces of implantation and non-implantation sites were split into 5mm pieces briefly fixed in 2.5% buffered gluteraldehyde, to harden, (SPI-Chem, West Chester, PA, USA) then cut into half-moons exposing the endometrial surface (Hosie and Murphy, 1995) and fixed again in 2.5% buffered gluteraldehyde for a total of 1 hr; washed 3 times in 0.1M Na_2PO_4 buffer over 24 hrs, then incubated in 1% buffered osmium (SPI-Chem, West Chester, PA, USA) for 1 hr followed by 5 washes of dH_2O for three min each. Tissues were then incubated in 1% aqueous thiosemicarbazide (SPI-Chem, West Chester, PA, USA) for 10 min, followed by 5 washes of dH_2O for three min each. The uterine pieces were again incubated in 1% buffered osmium for 30 min (Araujo *et al.*, 2003) followed by 5 washes of dH_2O for three min each; dehydrated through a graded series of alcohols, immersed twice in pure hexamethyldisilazane (HMDS) (SPI-Chem, West Chester, PA, USA) for 30 seconds and allowed to dry in a desiccator for 24 hours before being mounted on aluminum stubs and sputter coated with carbon using an Emitech K950X coater. The tissue was examined in a SEM FEI NOVA 600 Nanolab (EDS) or the Gemini Zeiss Ultra Plus with a working distance of 2.5mm running at 1kV. After viewing

each specimen, micrographs were taken at magnifications of 5,000x, 10,000x, 20,000x, 50,000x, 100,000x and 120,000x in at least 3 areas per specimen chosen randomly. At least 100 specimens per treatment group were viewed.

2.6.1.1 Data analysis for the dose response study and SEM study

JMP10 (SAS Institute, Cary, NC, USA) was used for statistical comparisons of means of implantation sites between treatment groups using a one way ANOVA followed by a Tukey-Kramer HSD. Differences were considered statistically significant when $p<0.05$. For the high resolution SEM micrographs, assessment of the epithelial surface morphology was made using a scoring system summarised in Table 2.2. The assessment criteria were similar to those used in previous studies (Scholtz *et al.*, 2008) as shown in Table 2.2. A total of 15 images per criteria were assessed to generate the results. The parameters were scored by two researchers using a random blinded method and then analyzed using a one way ANOVA followed by a Tukey-Kramer HSD. Differences were considered statistically significant when $p<0.05$.

Table 2.2: The scoring system used to analyze the morphology of the surface uterine epithelial features from the SEM micrographs of day 1 and 6 of pregnancy of control, 15mg/kg anastrozole treated and 1.25mg/kg CC treated rats (Hosie *et al.*, 2003; Scholtz *et al.*, 2008).

Surface epithelial characteristics	Scoring system
Microvilli density	Relative number of microvilli per cell (1, sparse; 2, medium density; 3, dense)
Microvilli length	Whether they are short or long (1, short; 2, medium; 3, long)
Microvilli surface "beads"	Number of beads seen on microvilli (0, none; 1, some; 2, many)
Surface glycocalyx	Surface glycocalyx seen (0, none; 1, little; 2 much)
Cell borders	Whether recessed or obvious between cells (1,sunken; 2, flat; 3, raised)
Cell apices	Whether they were flat or bulge into the lumen (1, flat; 2, slightly raised; 3, raised)
Surface folding	Extent to which endometrium had folded (1, smooth; 2, folded; 3, very folded)
Large surface protrusions (pinopods)	Number of large surface protrusions seen on the cell surface (0, none; 1, some; 2, many)
Secretions	Number of small secretion vesicles seen of the cell surface (0, none; 1, some; 2, many)
Epithelial gland openings	Number of epithelial gland openings seen on the epithelial surface (0, none; 1, some; 2, many)
Membrane pores	Number of membrane pores seen on the cell surface (0, none; 1, some; 2, many)

2.6.2 Immunofluorescence and confocal microscopy

2.6.2.1 Tissue processing and sectioning

All histological glass slides that were used in this study were gelatin-coated (Rajamohamedsait and Sigurdsson, 2012) in order to stick the tissue sections to the glass slides during the staining and washing process. Using standard procedures, samples for immunofluorescence and confocal microscopy, and hematoxylin and eosin (H&E) staining were fixed in 10% buffered formalin for 48 hours (Karaer *et al.*, 2005), then placed in an automatic tissue processor (Shandon Citadel 1000, Labotek, South Africa) in which samples were incubated in a series of 70%, 95%, 95%, 95%, 100%, 100%, 100% ethanol, then in chloroform and finally in paraffin wax. Samples were then embedded in paraffin wax. Histological sections (5μm) were cut using a Leica 2035 Biocut microtome (Leica, Nussloch, Germany) fitted with a disposable blade and then dewaxed overnight by placing them in an oven at 60^0C, then immersed in histoclear for 5 minutes and then repeated in fresh histoclear for 5 minutes, rehydrated through a graded series of ethanol (100%, 100%, 95%, 80%, 70% and 60%) for 30 seconds each, then washed in running water for 5 minutes (Faolain *et al.*, 2005; Karaer *et al.*, 2005).

2.6.2.2 Immunofluorescence

The immunolocalization and double labeling protocol was adopted and modified from previous studies (Mohan *et al.*, 2008; Kaneko *et al.*, 2011; Mwakikunga *et al.*, 2011). De-waxed sections of uterus from each group were washed 3 times, 2 min each with PBS. This was followed by a 10 min incubation in 30% H_2O_2 (Sigma-Aldrich Co., St. Louis, MO, USA)

in methanol to block endogenous peroxidase activity (Mwakikunga *et al.*, 2011), and then washed 3 times, 2 min each with PBS. Sections were then permeabilized for 30 minutes in 0.1% Triton-X 100 (Sigma-Aldrich Co., St. Louis, MO, USA) in PBS, and incubated for 30 minutes in blocking solution (5% (v/v) normal goat serum (Sigma-Aldrich Co., St. Louis, MO, USA) in PBS. All primary and secondary antibodies were diluted in blocking solution (1:100) (Mwakikunga *et al.*, 2011). Sections were incubated with primary antibodies mouse monoclonal anti-Vinculin, rabbit polyclonal anti-Integrin β5, rabbit monoclonal anti-FAK, and mouse monoclonal anti-Paxillin (Abcam, Cambridge, MA, USA) for 24 hours at 4°C (double staining: vinculin with integrin β5; paxillin with FAK) (Mohan *et al.*, 2008; Kaneko *et al.*, 2011). After washing with PBS 3 times 5 min each, sections were incubated with fluorescein isothiocyanate (FITC) conjugated to AffiniPure Goat anti-mouse IgG secondary antibody (Abcam) and rodamine conjugated Goat anti-rabbit IgG secondary (Abcam) at a dilution of 1:100 (Mwakikunga *et al.*, 2011) for 30 min in the dark followed by 3 PBS washes of 5 min each. Sections were also counterstained with DAPI to label nuclei. Expression and localization of vinculin, integrin β5, FAK and paxillin were examined under the Zeiss LSM 780 confocal microscope (Carl Zeiss, Jena, Germany) and images were acquired using the Zeiss LSM software (Carl Zeiss, Jena, Germany). The focal adhesion protein expression levels and localization in the confocal images were scored using a scoring method modified from previous studies (Englund *et al.,* 2001) as shown in Table 2.3. A JMP10 software (SAS Institute, Cary, NC, USA) was used for the statistical comparisons of means of focal adhesion protein expression of vinculin, integrin-β5, paxillin and focal adhesion kinase (FAK) among treatment groups using a one way ANOVA followed by a Tukey-Kramer *post hoc* analysis. Differences were considered statistically significant when $p < 0.05$.

Table 2.3: A description of the scoring system for the focal adhesion protein expression and localization in the confocal images among treatment groups adopted from previous studies (Englund *et al.*, 2001; Mwakikunga *et al.*, 2011).

Epithelial immunohistochemical characteristics	Scoring system
Protein expression	Whether the epithelia and blastocysts are positively stained or not: (0, negative staining, intensity absent) (1, positive staining and 1 to 10% positively stained epithelium, low intensity) (2, positive staining and 11 to 50% positively stained epithelium, medium intensity) (3, positive staining and 51 to 100% positively stained epithelium, high intensity)
Main epithelial domain protein localization	Protein localization in the epithelium (1, basal; 2, apical; 3,lateral; 4, basolateral; 5, basal and apical)
Additional protein localization	Additional protein localization (1, cytoplasmic; 2, perinuclear; 3, evenly distributed in epithelial cell; 4, stroma)

2.6.3 Hematoxylin and Eosin (H&E) staining

The hematoxylin and eosin protocol was adopted from previous studies (Mohan *et al.*, 2008). De-waxed and hydrated sections of uterus from each group were incubated in Mayer's hematoxylin for 5 min, and then washed for 2min in tap water. In order to differentiate, this was followed by dipping the sections 3 times in 1% acid alcohol (Sigma-Aldrich Co., St. Louis, MO, USA). Sections were then washed in running water for 5 min until the nuclei were

bright blue and then counter-stained with eosin for 1 min and washed briefly in running water. Sections were passed up through a graded series of alcohols, and then into histoclear for 5 minutes, mounted with Entellan (Sigma-Aldrich Co., St. Louis, MO, USA) and cover-slipped and then viewed under the Axioskop 2 Plus system (Carl Zeiss, Jena, Germany). Images were captured with an Axio HRc digital camera (Carl Zeiss, Jena, Germany). The micrographs were examined and the tissues described to give an overall and comparative view of the uterine tissues between treatment groups.

2.6.4 Real time quantitative polymerase chain reaction (qPCR)

Polymerase chain reaction (PCR) is a technique that allows exponential amplification and detection of short sequences of DNA within a longer double stranded DNA template (Wilhelm and Pingoud, 2003; Ding and Cantor, 2004; Wang and Kaltenboeck, 2005). The technique uses a pair of primers that are complementary to a defined sequence on each of the two strands of the DNA. These primers are extended by DNA polymerases so that copies are made of designated sequences leading to exponential amplification (Arya *et al.*, 2005; Wang and Kaltenboeck, 2005). The real time quantitative polymerase chain reaction (qPCR) technique collects data throughout the PCR process as it occurs, thus amplifying and detecting DNA sequences using fluorescent dyes that correlate PCR product concentration to fluorescence intensity (Wong and Medrano, 2005). Therefore, the qPCR technique enables sensitive and specific quantification of the initial target sequence amounts and PCR products accumulated during the amplification cycle (Ding and Cantor, 2004; Wang and Kaltenboeck, 2005).

In this study, the qPCR was performed for the quantitation of gene expression of the focal adhesion proteins vinculin, integrin β5, paxillin and FAK in the uterine epithelial cells from

day 1 and day 6 pregnant rats of all treatment regimes. The uterine horns for each day 6 pregnant rat were further divided into implantation and non-implantation sites. The house keeping genes, *β-actin*, 18Sr RNA and Lactate dehydrogenase A (Ldha) were used as reference genes (Al-Bader and Al-Sarraf, 2005; Hong *et al.*, 2006; Li *et al.*, 2013).

2.6.4.1 RNA extraction

The RNA extraction protocol is standard and is similar to that described by the GeneJET RNA purification kit supplier (Thermo Scientific Inc., 2011). Please refer to Appendix D for details of the procedure. The purified RNA for downstream applications was stored at -80°C.

2.6.4.2 RNA assessment: Nanodrop method

The RNA concentration (ng/µl), the level of protein contamination in the sample (260/280 ratio) and the level of contaminants from the preparations such as guanidine salts (260/230 ratio) were measured using the Nanodrop method. The ideal 260/280 ratio is between 1.8 and 2.1 while the 260/230 ratio should be above 1.5 ideally 2.

The nanodrop spectrophotometer was wiped with RNase-free water with a clean laboratory paper before initiating it with 1.5µl of RNase-free water. The nucleic acid and RNA (constant=40) were then selected. The machine was further blanked with 1.5µl of RNase-free water before running each of the 1.5µl RNA samples. The RNA to be considered for downstream experiments had the only peak in the curve at 260 and no peaks at 220-230 or 280. The high peak at 230 and false high at 280 usually indicates salt contamination.

2.6.4.3 Genomic DNA removal from RNA preparations

As recommended by the supplier, (Thermo Scientific Inc., 2011), 1µg of RNA was mixed with 1 µl of 10X reaction buffer (100 mM Tris-HCl (ph 7.5 at 25°C), 25 mM $MgCl_2$, 1mM $CaCl_2$) and 1µl DNase 1, RNase-free. To the mixture, DEPC treated water was added to make a 10µl total volume. The mixture was then incubated at 37°C for 30 minutes. DNase 1, which is an endonuclease, was added to digest single- and double-stranded DNA by hydrolyzing phosphodiester bonds producing mono- and oligodeoxyribonucleotides with 5'-phosphates and 3'–OH groups. DNase 1 was then inactivated by heating the mixture at 65°C for 10 minutes. In order to prevent hydrolyzing RNA during heating with divalent cations, 1µl 50mM EDTA was added prior to heating.

2.6.4.4 Designing Primers

The National Center for Biotechnology Information (NCBI) website (http://www.ncbi.nlm.nih.gov) was accessed to get into the primer-BLAST (Basic Local Alignment Search Tool) page from where primers were taken. The NM number (RefSeq GenBank Accession Number) for the primer sequence from Abcam (http://www.abcam.com) was used to identify primers.

The PCR product size was set between 70 and 150. After getting the forward (F) and reverse (R) sequences, they were copied and exported into a primer designing tool to get primers with a maximum PCR product size set at 1000. The Eurofins mwg/operon website (http://www.econ.mwgdna.com) was used to analyze the primer sequences. Primers were either accepted or rejected based on whether they satisfied the following primer sequence requirements or not as indicated in Table 2.4.

Table 2.4: Description of the requirements used to analyze primer sequences for them to be accepted or rejected for the study (http://www.econ.mwgdna.com).

Primer characteristics	Primer requirements
Primer length	The optimal primer length was set at 20 base pairs
Melting temperatures	The minimum and maximum melting temperatures were 57°C and 62°C respectively
Primer melting temperature difference	Maximum difference between forward and reverse primer be 2°C
GC content	GC content was between 50% and 80%; 5 nucleotides at the 3' end should have no more than 2 Gs or Cs
Amplicon (product) length	Amplicon length to be between 70 and 150 (the smaller the product the more efficient the primer is)
Runs	Runs such as AAAA be avoided and should not be more than 4 identical in a row

A description summary of the requirements used to accept or reject primers to be used in the study (http://www.econ.mwgdna.com).

The oligoanalyzer website (http://www.idtdna.com) was also used to check primer specificity, splice variants and secondary structures (hairpins and dimers) and single nucleotide polymorphisms (SNPs) of nucleotide sequence variations. The last 5 base pairs on the 3' end should not have SNPs because variations that occur in functional regions of genes might cause significant changes in the transcribed sequences, which can lead to changes in protein expression (Hemani *et al.*, 2014) thus affecting phenotypic behavior such as metabolism or cell signaling. Table 2.5 shows the real time PCR primer sequences which met these requirements and were finally purchased (Whitehead Scientific, Cape Town, South Africa).

Table 2.5: Description of the real time PCR primer sequence characteristics for the genes of interest and reference genes used in the study.

Gene symbol	Gene name	RefSeq GenBank Accession Number	5'-3' primer sequence	Position of primer on template	GC content	Amplicon length (bp)
Vcl	Vinculin	NM 001107248.1	F: 5'- GTT CCC GGT TTT CTG TTG CC -3' (20 bases)	40—59	55%	139
			R: 5'- GCC CTC GTG CAT AAT CA -3' (20 bases)	178--159	55%	
Itgb5	Integrin, beta 5	NM 147139.2	F: 5'- GTG CGA CAG CTT TTC CTG TG -3' (20 bases)	1694--1713	55%	97
			R: 5'- AAT GTA ACC GAC GTG GCA CT -3' (20bases)	1790--1771	50%	
Pxn	Paxillin	NM 001012147	F: 5'- AGT GTT CTT GTC AGA GGA GCC -3' (21 bases)	171--190	52.3%	112
			R: 5'- GCT GCC ATT GGT CTA AGG GG -3' (20 bases)	282--263	60%	
Ptk2	Protein tyrosine kinase 2 (focal adhesion kinase)	NM 013081.2	F: 5'- ATC AAG GCG TGT ACC TGA GC -3' (20 bases)	2360--2379	55%	86
			R: 5'- GGT CAA ACT GGC GCA TTG TT -3' (20 bases)	2445--2426	50%	
Actb	Actin, beta	NM 031144.3	F: 5' - GCA GGA GTA CGA TGA GTC CG -3' (20 bases)	1155--1174	60%	74
			R: 5' – ACG CAG CTC AGT AAC AGT CC -3' (20 bases)	1228--1209	55%	
Ldha	Lactate dehydrogenase A	NM 017025.1	F: 5' – CCG TTA CCT GAT GGG AGA AA -3' (20 bases)	613--632	50%	108
			R: 5' – ACG TTC ACA CCA CTC CAC AC -3' (20 bases)	720--701	55%	
18s	18Sr RNA	X01117.1	F: 5' – GTT GGT TTT CGG AAC TGA GGC -3' (21 bases)	895--915	52.4%	204
			R: 5' – GTC GGC ATC GTT TAT GGT CG -3' (20 bases)	1098--1079	55%	

2.6.4.5 Complimentary DNA (cDNA) synthesis

Standard cDNA synthesis protocol was used similar to the one used by the supplier of the high capacity cDNA reverse transcription kit (Thermo Fisher Scientific Inc., 2011). (Please see Appendix D for details of the protocol).

2.6.4.6 Real-time quantitative polymerase chain reaction (qPCR)

Real-time quantitative polymerase chain reaction (qPCR) allows the copying of a DNA molecule exponentially by using a DNA polymerase enzyme that tolerates elevated temperatures as described in Appendix D. Following the reverse transcription, a QuantiFast SYBR Green PCR kit was used to provide rapid real-time quantification of cDNA targets. The kit was already optimized by the manufacturer (Thermo Fisher Scientific Inc., 2011) for use with a 7500 real-time PCR cycler (Applied Biosystems). The 2x QuantiFast SYBR Green PCR master mix included HotStarTaq *Plus* DNA polymerase, QuantiFast SYBR Green PCR buffer, SYBR Green, and ROX passive reference dye (Thermo Fisher Scientific Inc., 2011). The HotStarTaq *Plus* DNA polymerase was a modified form of QIAGEN *Taq* DNA polymerase that was supplied in an inactive state to prevent the formation of misprimed products and primer dimers during the reaction setup. The enzyme was activated at the start of the reaction by a 5-minute, 95°C incubation step. The concentration of the polymerase in the master mix was optimized to allow short extension times in the combined annealing/extension step of each PCR cycle as in Appendix D.

QuantiFast SYBR Green PCR buffer contained a balanced combination of KCl and (NH4)2SO4, which promoted a high ratio of specific to nonspecific primer binding during the annealing step of each PCR cycle (QuantiFast SYBR Green PCR Handbook, 2011). This created better primer annealing conditions, leading to increased PCR specificity. The 2x QuantiFast SYBR Green PCR master mix from the supplier (Thermo Fisher Scientific Inc., 2011) contained the following as shown in the Table 2.6:

Table 2.6: The composition of the 2x QuantiFast SYBR Green PCR master mix

Component	Description
HotStarTaq *Plus* DNA Polymerase	HotStarTaq *Plus* DNA Polymerase was a modified form of a recombinant 94 kDa DNA polymerase, originally isolated from *Thermus aquaticus*.
QuantiFast SYBR Green PCR buffer	Tris·Cl, KCl, (NH4)2SO4, MgCl2, and additives enabling fast cycling, including Q-Bond®
dNTP mix	Contained dATP, dCTP, dGTP, and Dttp
Fluorescent dyes	SYBR Green and ROX SYBR Green binds all double-stranded DNA molecules, emitting a fluorescent signal upon binding. The excitation and emission maxima of SYBR Green are at 494 nm and 521 nm respectively. ROX is a passive reference dye that compensated for differences in fluorescence detection between wells due to slight variations in reaction volume or to differences in well position.
RNase-free water	Ultrapure quality

Boxes of microAmp 8-tube strips and 8-cap strips, filtered tips, autoclaved eppendorfs and rack holders were sterilized in the UV hoods for 30 minutes. The master mix and DNA samples were allowed to thaw on ice in separate boxes. The reaction layout was set up on the PCR computer. The forward and reverse primers were allowed to thaw on ice. The master mix, primers and nuclease free water were brought into the master mix UV hood. The master mix, forward and reverse primers and nuclease free water were aliquoted into one 1.5ml eppendorf according to the volume required for the total number of reactions. Then, 16µl of master mix was aliquoted into each reaction tube to which 4µl of cDNA (10ng) was added to make a total of 20µl. The amplification cycling conditions were as follows: 95^0C for 10min, (95^0C for 15sec, 60^0C for 1min in 40 cycles), 95^0C for 15sec, 60^0C for 1min, 95^0C for 30sec, 60^0C for 15sec.

2.6.4.7 PCR product gel electrophoresis

Agarose gel electrophoresis is a method used to separate DNA fragments by size. The addition of ethidium brodium to the gel allows visualization of these fragments thus enabling one to estimate the size of the separated bands by comparing them to known fragment of the molecular weight marker. The standard 1% gel electrophoresis was performed to confirm single correct product as shown in Appendix D.

2.6.4.8 SYBR green qPCR data analysis

The $2^{-\Delta\Delta CT}$ method, as in Appendix D, was used to determine the gene expression fold change relative to the control following drug treatment regimes (Schmittgen and Livak, 2008). The data were first normalized using the three reference genes β-actin, 18S rRNA and Lactate

dehydrogenase A; then the fold change was calculated (Schmittgen and Livak, 2008). The JMP10 software was used to conduct statistical analyses on the data. A one way ANOVA followed by a Tukey-Kramer *post hoc* analysis was performed to compare the means of normalized relative quantities (NRQ) between treatment groups. Differences were considered statistically significant when $p < 0.05$.

3 CHAPTER THREE: RESULTS

The project was divided into two parts. Part one was a preliminary dose response study of anastrozole, where the aim was to determine the optimal dose of anastrozole that could give the highest number of implantation sites upon administration in the Wistar rats. The second part of the project (main study) employed hematoxylin and eosin (H&E) staining, scanning electron microscopy (SEM), immunofluorescence and confocal microscopy, and quantitative real time polymerase chain reaction (qPCR) techniques to determine the ultrastructure of the surface uterine epithelium during early pregnancy; and to determine the expression levels (fluorescence intensities reflecting protein quantities) and localization of focal adhesion proteins vinculin, integrin β5, paxillin, and focal adhesion kinase (FAK) in the rat uterine epithelial cells and blastocysts during implantation in vivo. The hematoxylin and eosin (H&E) staining technique was employed to have a general overview of the histological changes of the uterine endometria between treatment groups with regard to the uterine surface luminal epithelia, stroma cells, intercellular ground substance, epithelial glands and blood vessels.

3.1 Preliminary dose response study of anastrozole

A comparison of means of implantation sites between treatment groups was done using a one way ANOVA followed by a Tukey-Kramer HSD in order to determine the optimal dose and effectiveness of anastrozole as a superovulator. The most effective dose was the one that had the greatest number of implantation sites at day 6 of pregnancy and to an extent compare it with the CC treated and control animals. Differences were considered statistically significant when $p<0.05$. The rationale for this was that CC is generally associated with low implantation rates and therefore increased implantation sites are seen as an advantage.

3.1.1 Optimal anastrozole dose

As demonstrated in Figures 3.1, 3.2 and Appendix G, the results for the one way ANOVA and Tukey-Kramer HSD show that a significant increase of implantation sites is achieved in the 15mg/kg anastrozole treated rats, 16.6 ± 0.8 (mean ± SE) in comparison to control group, 7.8 ± 0.8 ($p<0.0001$). There is also a significant statistical difference in the number of implantation sites between CC treated group, 11.6 ± 0.8 and control group (untreated), 7.8 ± 0.8 ($p<0.0315$); CC treated group, 11.6 ± 0.8 and the 15mg/kg anastrozole treated rats, 16.6 ± 0.8 ($p<0.0022$). No significant difference is observed between the 25mg/kg anastrozole group, 10.6 ± 0.8 and control, 7.8 ± 0.8 ($p<0.2026$); 25mg/kg anastrozole and CC group ($p<0.9715$). The CC treated group and the 25mg/kg anastrozole group seem to have a similar response in this regard.

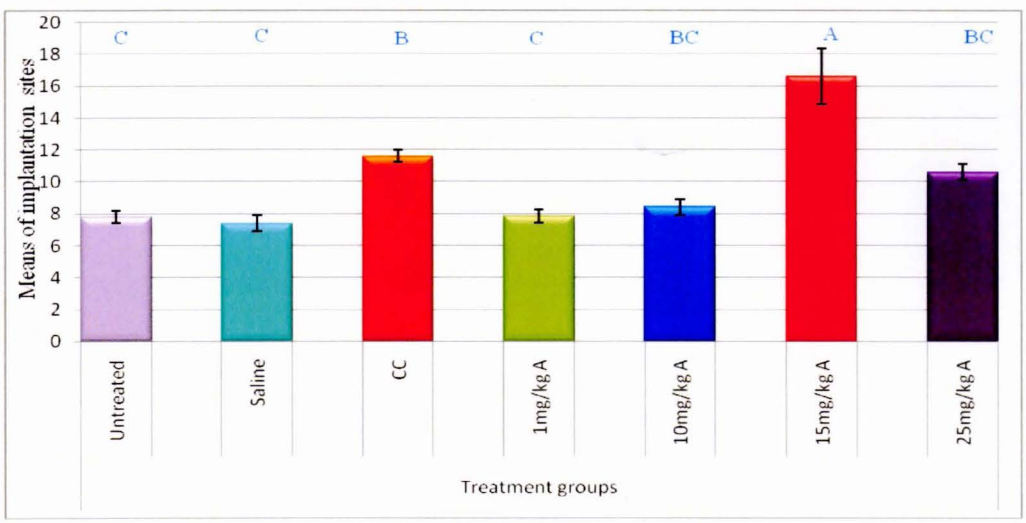


Figure 3.1: Graphical representation of the means of implantation sites of treatment regimes of day 6 of pregnancy in rats. Groups that are not connected by the same letter are significantly different as shown on top of each bar in the graph. A significant increase of implantation sites is achieved in the 15mg/kg anastrozole treated rats, 16.6 ± 0.8 (mean ± SE)

in comparison to control group, 7.8 ± 0.8 ($p<0.0001$). There is also a significant difference in the number of implantation sites between chlomiphene citrate (CC) treated group, 11.6 ± 0.8 and control group (untreated), 7.8 ± 0.8 ($p<0.0315$).

Implantation sites

The high molecular weight vital dye Pontamine sky blue was used to distinguish implantation sites from non-implantation sites because the dye quickly localizes in the implantation sites due to increased vascularization and vascular permeability during early pregnancy. Figure 3.2 shows the localization of Pontamine sky blue in implantation sites of a day 6 (15mg/kg) anastrozole treated pregnant rat which has undergone superovulation and achieved pregnancy.

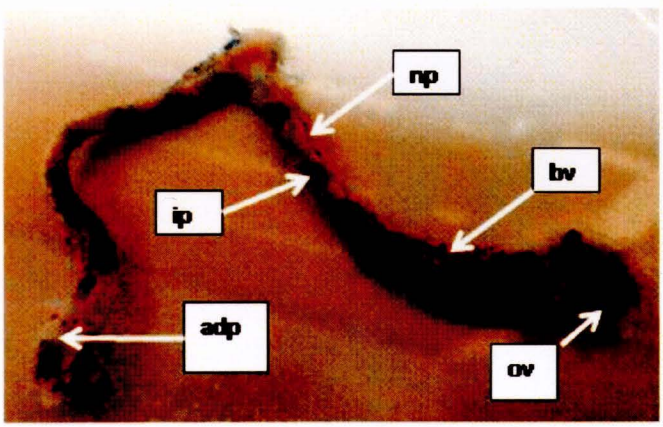


Figure 3.2: Uterine horns of day 6 pregnant Wistar rat treated with a single dose of 15mg/kg body weight of anastrozole which has superovulated and achieved pregnancy showing implantation sites (ip), non-implantation sites (np), ovaries (ov) blood vessels (bv) and adipose tissue (adp).

The mean number of implantation sites from day 6 pregnant rats treated with different anastrozole doses and chlomiphene citrate in this study show that the 15mg/kg anastrozole is the optimum dose that is able to give the highest number of implantation sites upon administration in the Wistar rats as shown in Figures 3.1 and 3.2 suggesting that anastrozole may allow just enough of the intermediates and E_2 to be present with regard to the hormone profiles for ovulation and successful implantation of the embryo because anastrozole is a competitive inhibitor of aromatase in the conversion of androgens to estrogens. Essentially, it may appear that there is blocking of E_2 and increasing of androgens in anastrozole treated rats compared to controls. Progesterone (P) is probably also high as E_2 is low. In CC treated rats, estrogen receptors are blocked and thus increased E_2, but androgens are presumably low. The effect of anastrozole in the level of E_2 and P may change the E_2/P ratio at day 6 of pregnancy, suggesting its effect on endometrial maturation and therefore improving receptivity.

3.2 Scanning Electron Microscopy (SEM)

The following parameters were tested as shown in Table 2.2. These were microvilli density (MD), microvilli length (ML), microvilli surface "beads" (MSB), surface glycocalyx (SG), cell borders (CB), cell apices (CA), uterine surface fording (SF), large surface protrusions (pinopods) (LSP), small secretions (SS), epithelial gland openings (EGO) and membrane pores (MP). The results of the one way ANOVA in each case demonstrate a significant difference at $p<0.0001$. The results of the *post hoc* analysis, the Tukey-Kramer HSD tests in each case clearly separate the day 1 and day 6 groups. In some cases there are overlaps. With regard to the Tukey-Kramer connecting letters report analysis, levels not connected by the same letter are considered significantly different.

3.2.1 Microvilli density (MD), microvilli surface beads (MSB), large surface protrusions (LSP) and membrane pores (MP)

In the MD, MSB, LSP, and MP all of the day 1 group together and all of the day 6 all group together, there are no other significant differences or overlaps as shown in Figures 3.3, 3.4, 3.5, 3.6 and Appendix G. However, microvilli generally change from long thin microvilli of medium density at day 1 of pregnancy, in terms of distribution as shown in Figures 3.4, 3.5 and 3.6 to short irregular sparse microvilli at day 6 in implantation sites (IP), as the non-implantation sites (NP) retain relatively denser and longer microvilli. In all groups, more membrane pores are visible at day 6 than at day 1 of pregnancy as seen in Figures 3.4, 3.5 and 3.6. Large surface protrusions are mostly noted but not limited to anastrozole treated rats at day 6 (Figures 3.4 and 3.5 and Appendix G).

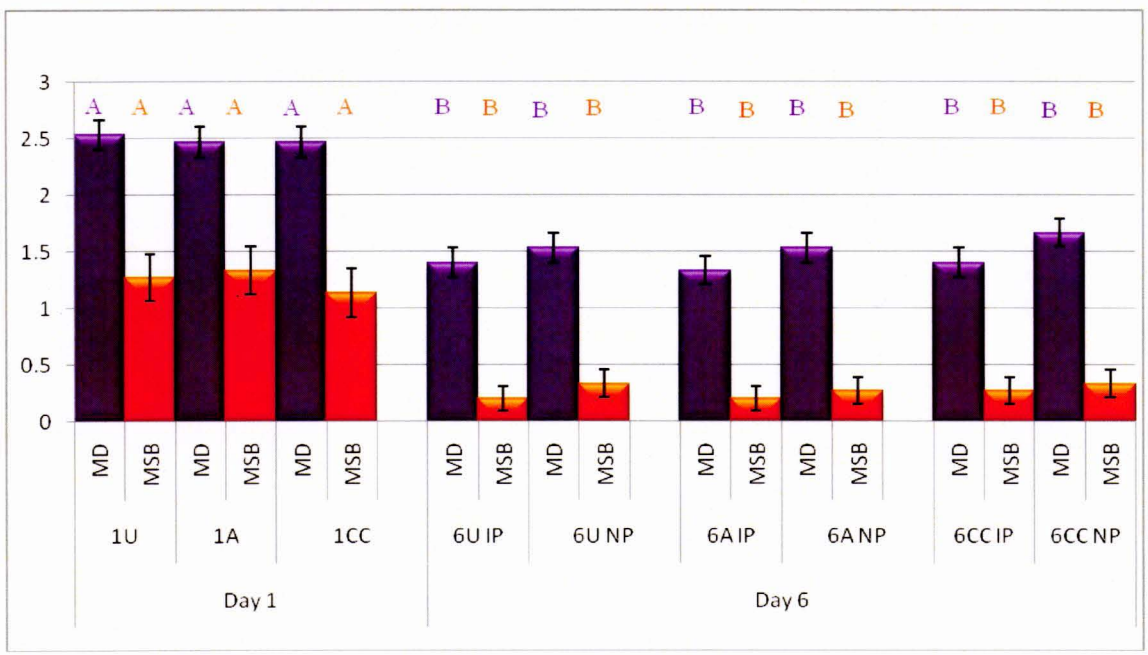


Figure 3.3: Graphical representation of the uterine epithelial cell microvilli density (MD) and microvilli surface beads (MSB) in pregnant rats. Groups that are not connected by the

same letter are significantly different as shown on top of each bar in the graph. In the MD and MSB all of the day 1 group together and all of the day 6 all group together, there are no overlaps and are clearly separated. In summary, there is a significant difference in microvilli density between day 1 groups and day 6 groups ($p<0.0001$). A significant difference is also observed in microvilli surface beads between day 1 groups and day 6 groups ($p<0.0001$). Long thin microvilli of medium to dense in terms of distribution at day 1 in all groups are replaced by short irregular sparse microvilli at day 6 in all groups. Microvilli surface beads also get reduced as pregnancy progresses from day 1 to day 6.

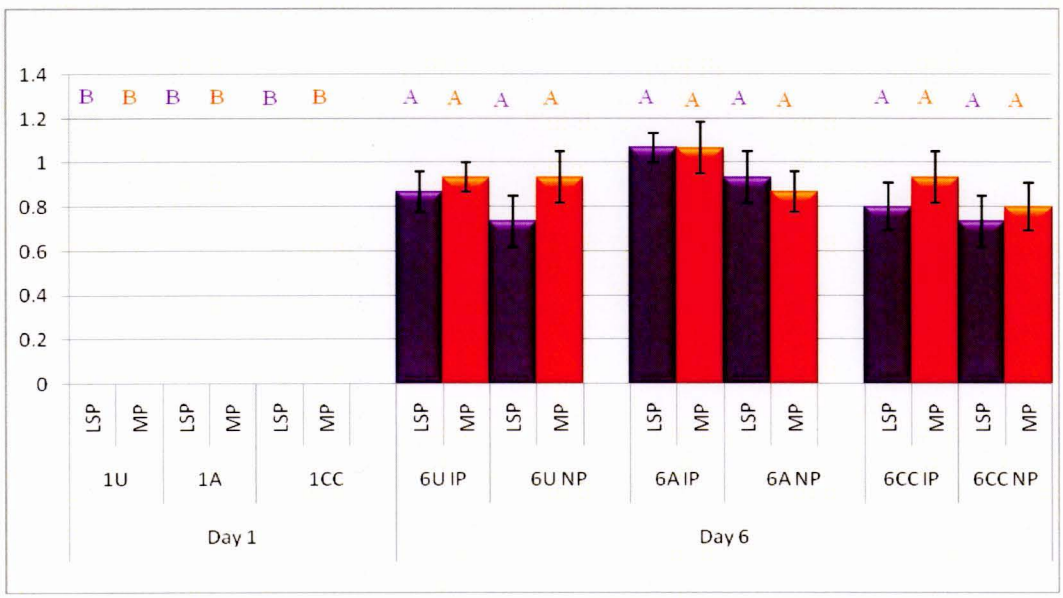


Figure 3.4: Graphical representation of the uterine large surface protrusions (LSP) and membrane pores (MP) in pregnant rats. Groups that are not connected by the same letter are significantly different as shown on top of each bar in the graph. In the LSP and MP all of the day 1 group together and all of the day 6 all group together, there are no overlaps and are clearly separated. There is a significant difference in large surface protrusions between day 1

groups and day 6 groups ($p<0.0001$). A significant difference is also observed in membrane pores between day 1 groups and day 6 groups ($p<0.0001$) (Appendix G). In all groups, more membrane pores are visible at day 6 than at day 1 of pregnancy as also seen in Figures 3.5 and 3.6 due to membrane flattening at day 6. Large surface protrusions are mostly noted but not limited to anastrozole treated rats at day 6.

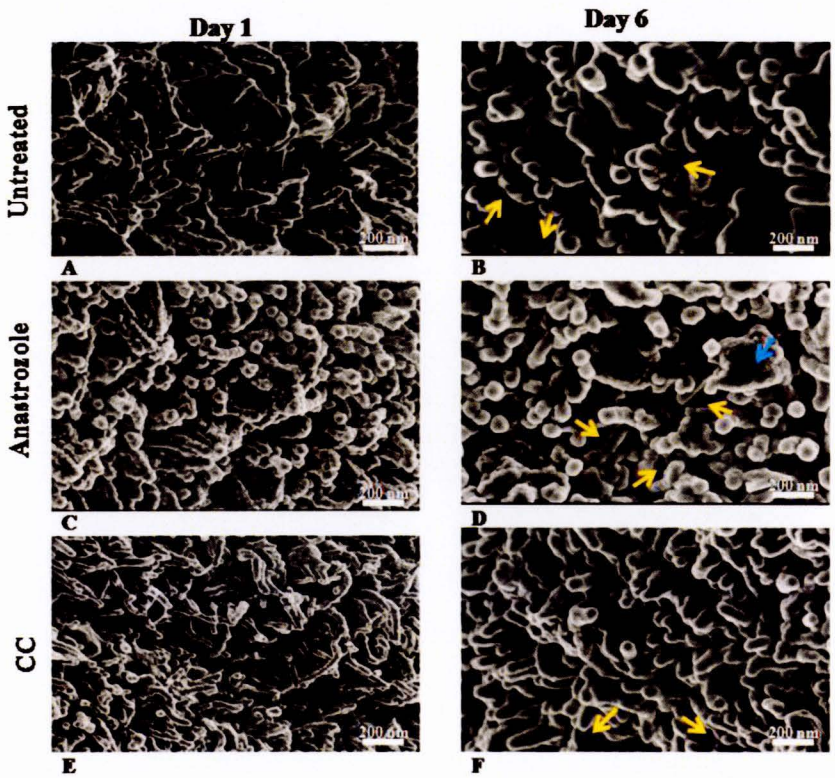


Figure 3.5: SEM of the uterine epithelial cells from day 1 and implantation sites of day 6 pregnant rats. (A) Untreated rat (control) showing long thin microvilli of medium to dense covering; note that the cell membrane cannot be seen between the microvilli. (B) Control rat showing short irregular microvilli and membrane pores (yellow arrow). (C) 15mg/kg anastrozole treated rat showing long thin surface-beaded microvilli of medium to dense in

terms of distribution. (D) Anastrozole treated rat showing short irregular microvilli, which generally look smaller than in control rat, but with numerous pinopods (blue arrow) in the process of membrane flattening; note also the numerous membrane pores. (E) Chlomiphene citrate (CC) treated rats showing long thin microvilli of medium to dense. (F) Day 6 CC treated rat showing short irregular sparse microvilli.

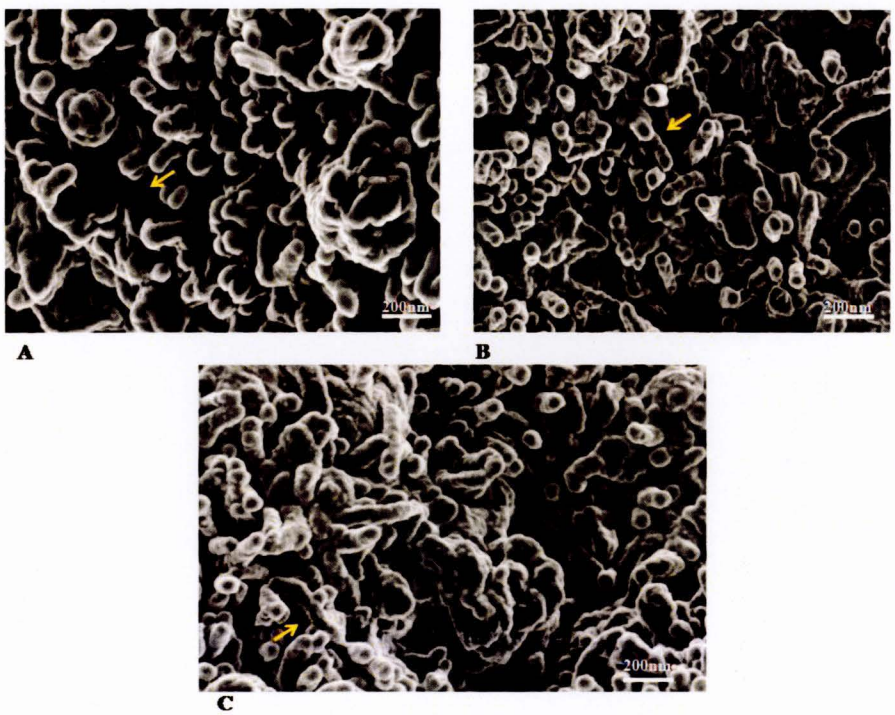


Figure 3.6: SEM of the uterine epithelial cells from non implantation sites (NP) of day 6 pregnant rats. (A) Untreated (control) rat showing a mixture of short irregular microvilli and relatively long microvilli of sparse to medium density. (B) 15mg/kg anastrozole treated rat showing short irregular microvilli and some returning long thin microvilli of sparse to medium density. (C) Chlomiphene citrate (CC) treated rat showing relatively longer microvilli of sparse to medium density. Note that some membrane pores (yellow arrows) are still evident in all the treatment groups.

3.2.2 Microvilli length (ML)

According to the Tukey-Kramer connecting letters report analysis, groups not connected by the same letter are considered significantly different. Day1 are all on level A and day 6 on level B, clearly separating the groups. Generally, microvilli change from the regular long thin microvilli at day 1 to short irregular microvilli at day 6 of pregnancy. However, day 1 anastrozole, day 1 untreated (U), day 6 chlomiphene citrate non implantation (CC NP) and day 6 untreated non implantation (U NP) also group together linking the day 1U and all day 6 NP groups (excluding the anastrozole NP group) suggesting a general retention of relatively longer microvilli in non implantation sites at day 6. What is also notable is that the microvilli in the anastrozole implantation sites (IP) and NP groups are the shortest as shown in Figures 3.5, 3.6 and 3.7 and Appendix G).

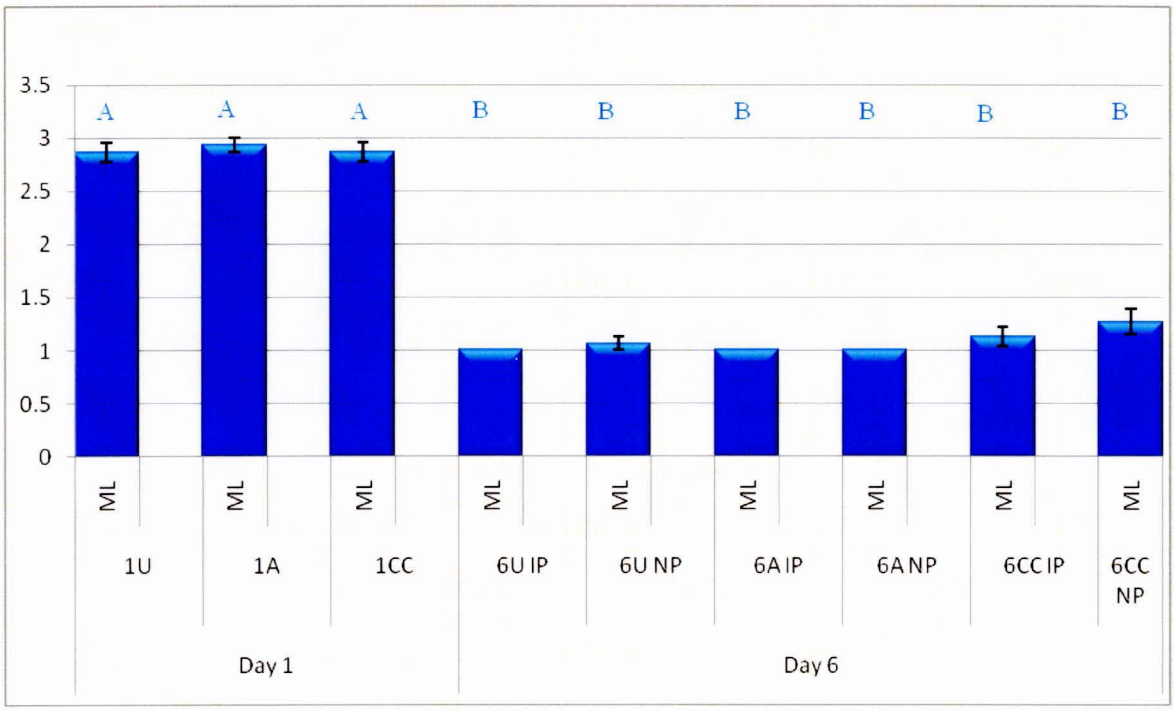


Figure 3.7: Graphical representation of the surface uterine epithelial cell microvilli in pregnant rats. Microvilli change from the regular long thin microvilli at day 1 to short irregular microvilli at day 6 of pregnancy in all treatment groups. Groups that are not connected by the same letter are significantly different as shown on top of each bar in the graph. In summary, there is a significant difference in microvilli length between day 1 groups and day 6 groups ($p<0.0001$) (Appendix G). Relatively longer microvilli in non implantation sites at day 6 are generally retained. Note: the microvilli in the anastrozole implantation sites (IP) and NP sites at day 6 are the shortest.

3.2.3 Uterine surface folding (SF)

Similarly, day 1 are all on level A and day 6 on level C, clearly separating the groups as seen above. However, in this instance the 'B' connecting group consists of day 1U, day 6CC NP, day 6U NP and day 6 anastrozole NP. The result suggests that in all treatments the NP sites remain folded as represented in Figures 3.8, 3.9 and 3.10 and Appendix G.

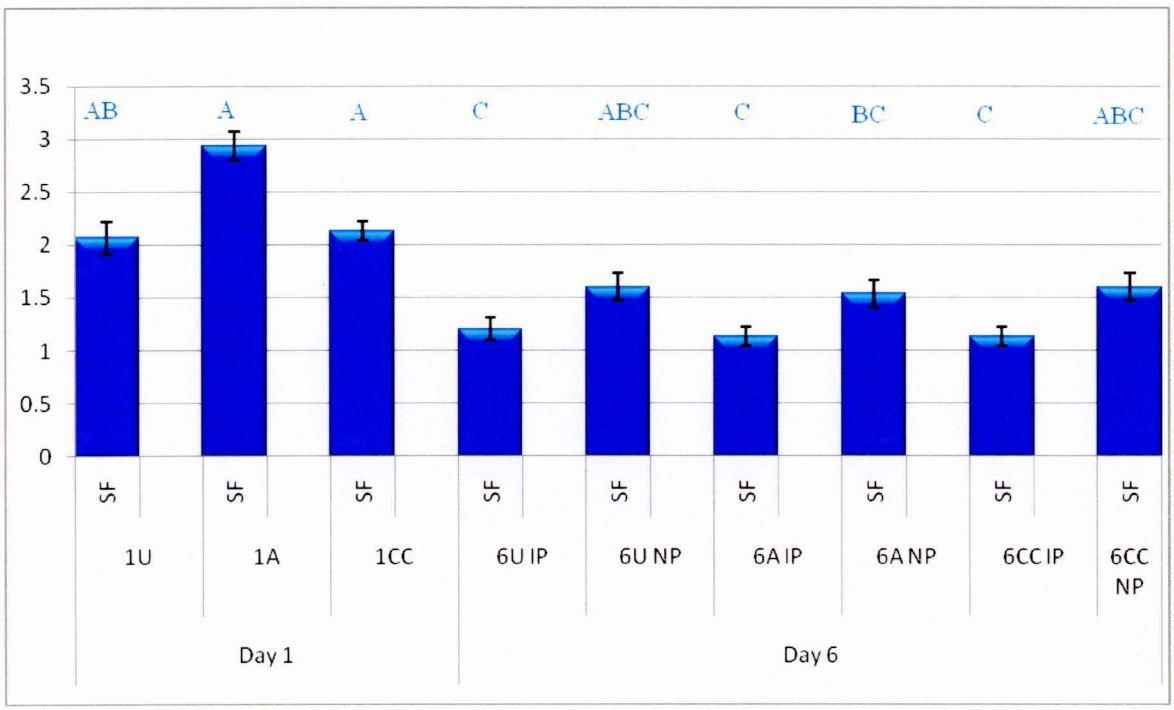


Figure 3.8: Graphical representation of the uterine surface folding in pregnant rats. Groups that are not connected by the same letter are significantly different as shown on top of each bar in the graph. There is a significant difference in the uterine folding between day 1 groups and day 6 groups ($p<0.0001$) (Appendix G). The deep surface folds of the uterine epithelium at day 1 of pregnancy in a rat change to smooth uterine surface with few folds at day 6 of pregnancy. The NP sites in all treatment groups remain slightly folded.

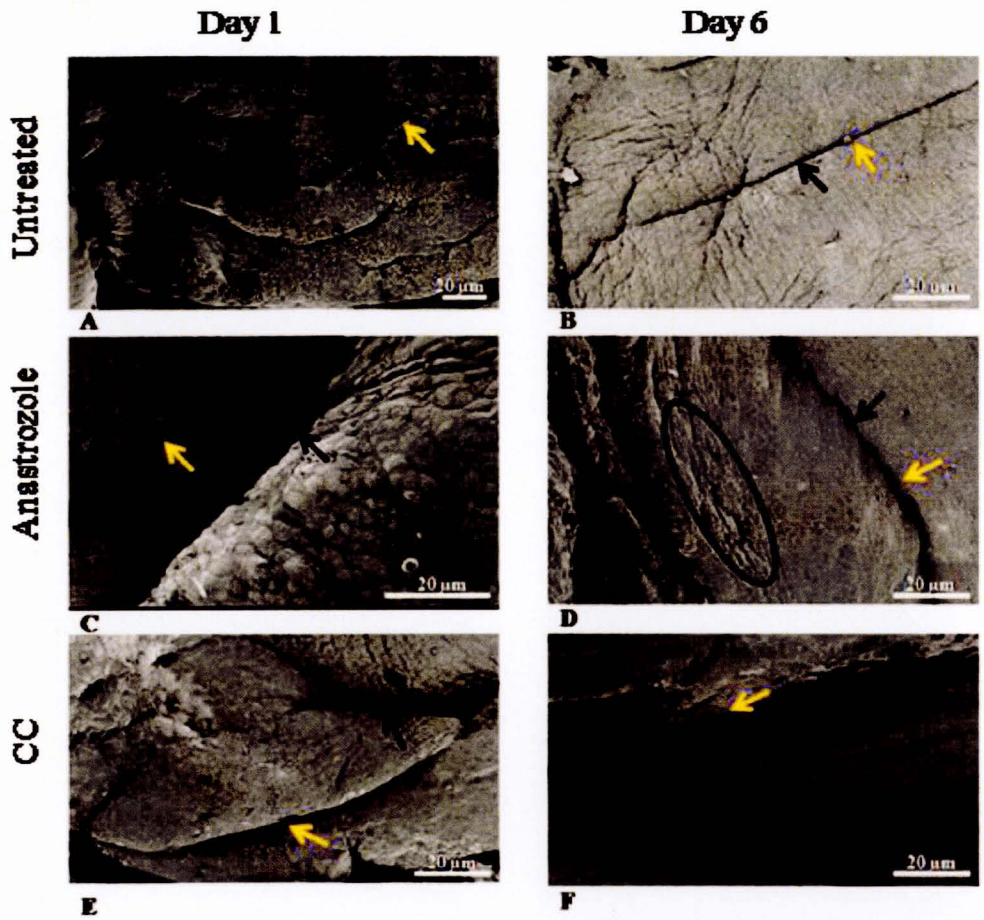


Figure 3.9: SEM of the uterine surface folding from day 1 and day 6 implantation sites of pregnant rats. (A) The surface uterine epithelium from day 1 of pregnancy of the untreated rat (control) showing deep surface folding (black arrow) and uterine gland openings (yellow arrow). (B) Day 6 untreated rat showing smooth uterine surface and few folds (black arrows) and some gland openings (yellow arrows). (C) The surface uterine epithelium from day 1 anastrozole treated rat showing deep surface folding (black arrows) and some gland openings (yellow arrows). (D) Day 6 of anastrozole treated rat showing smooth uterine surface and few folds (black arrows) and some gland openings (yellow arrows); note numerous pinopods,

black oval encircled in (D). (E) The surface uterine epithelium from day 1 chlomiphene citrate (CC) treated rat showing deep surface folding (black arrows) and some gland openings (yellow arrows). (F) Day 6 CC treated rat showing smooth uterine surface with few folds and some gland openings.

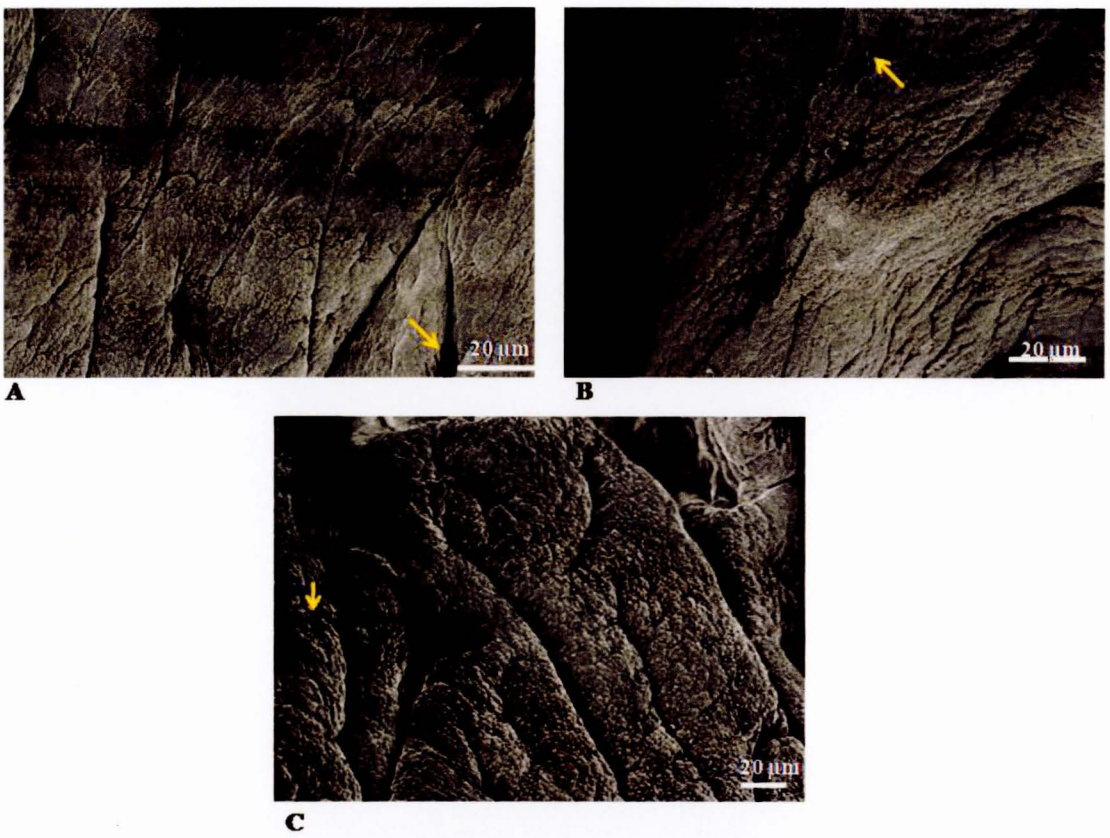


Figure 3.10: SEM of the uterine surface folding from day 6 non implantation sites of pregnant rats. (A) Day 6 untreated (control) rat showing smooth to slightly folded uterine surface (black arrow) and some gland openings (yellow arrow). (B) Day 6 of anastrozole treated rat showing smooth uterine surface and few folds (black arrow) and some gland openings (yellow arrow). (C) Day 6 chlomiphene citrate (CC) treated rat showing uterine surface with some folds and gland openings.

3.2.4 Cell apices (CA)

In the CA groups, the results are clustered into 4 levels. Level A includes day 6 anastrozole IP, day 6U IP, day 6 anastrozole NP and day 6U NP. The second level includes the above groups except for day 6 anastrozole IP and includes day 6CC IP. Thus grouping all the day 6 tissue except for day 6CC NP. The third level includes all of the day 6 NP as well as day 6CC IP and day 1U. The last group includes all of the day 1 groups as well as day 6CC NP and 6CC IP. Generally, anastrozole seems to maintain slight doming of the cell apices while chlomiphene citrate (CC) appears to flatten cell apices at day 6 as shown in Figures 3.11, 3.12 and 3.13 and Appendix G.

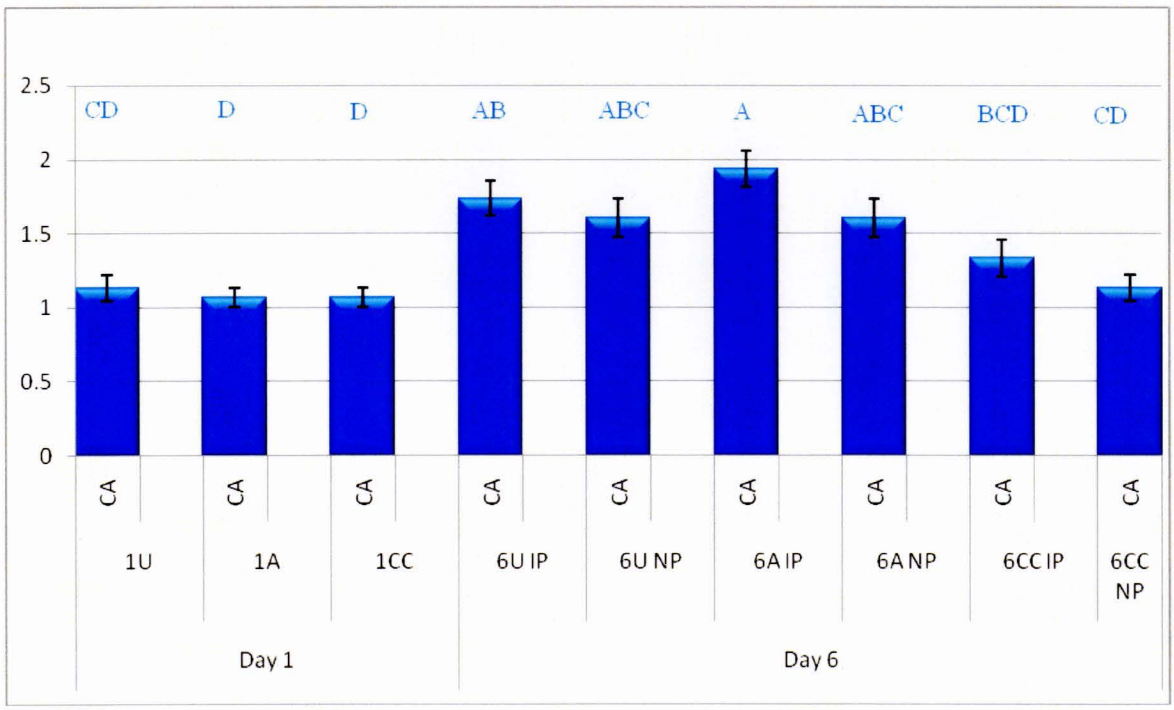
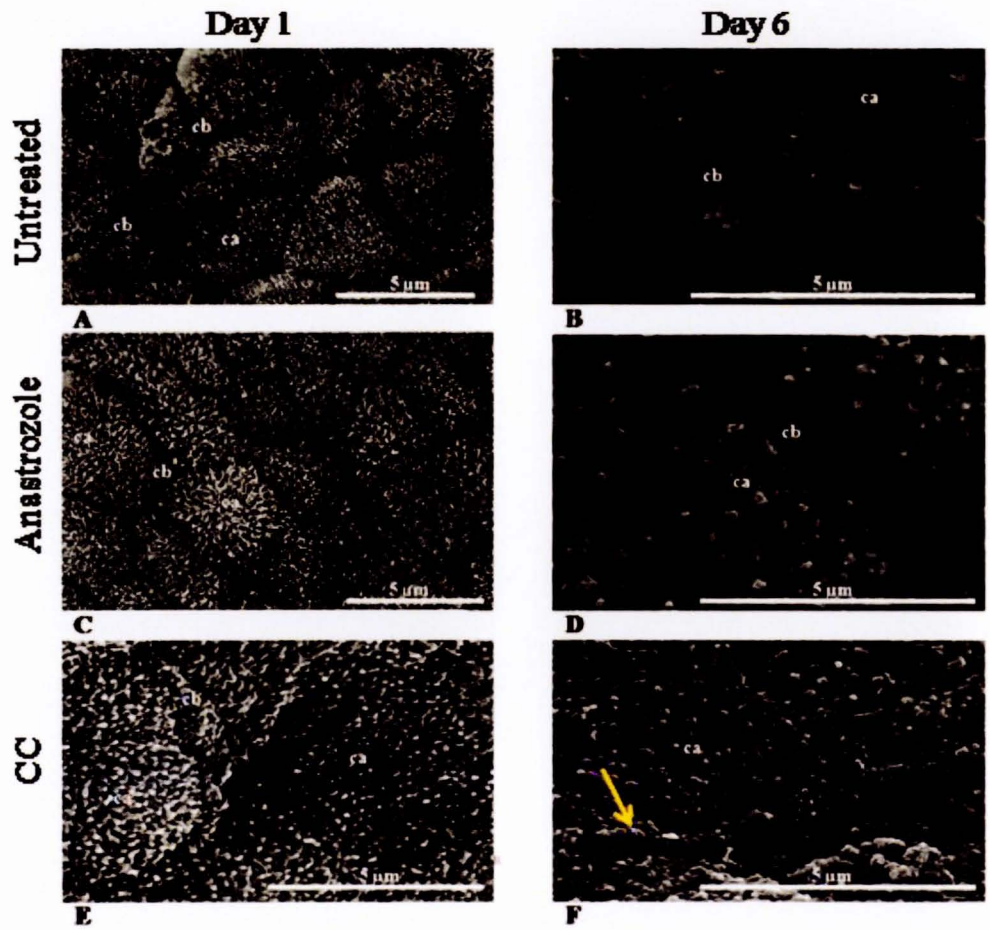


Figure 3.11: Graphical representation of uterine epithelial cell apices in pregnant rats. Groups that are not connected by the same letter are significantly different as shown on top of each bar in the graph. There is a significant difference in the cell apices between day 1 groups

and day 6 groups ($p<0.0001$) (Appendix G). Generally, anastrozole seems to maintain slight doming of the cell apices while chlomiphene citrate (CC) appears to flatten cell apices at day 6 of pregnancy in Wistar rats.



Figure

Figure 3.12: SEM of the uterine epithelial cells from day 1 and implantation sites of day 6 of pregnant rats. (A) The uterine epithelial cells from day 1 untreated rat (control) showing flat cell borders (cb) and slightly bulged cell apices (ca). (B) The uterine epithelial cells from the implantation site of day 6 untreated rat (control) showing flat cb and slightly bulged ca. (C) Day 1 anastrozole treated rat showing flat cb and slightly bulged ca. (D) Day 6

implantation site of the anastrozole treated rat showing flat cb and slightly bulged ca. (E) Day 1 chlomiphene citrate (CC) treated rat showing slightly raised cb and flat ca. (F) Day 6 chlomiphene citrate (CC) treated rat showing raised cb (arrow) and flat ca.

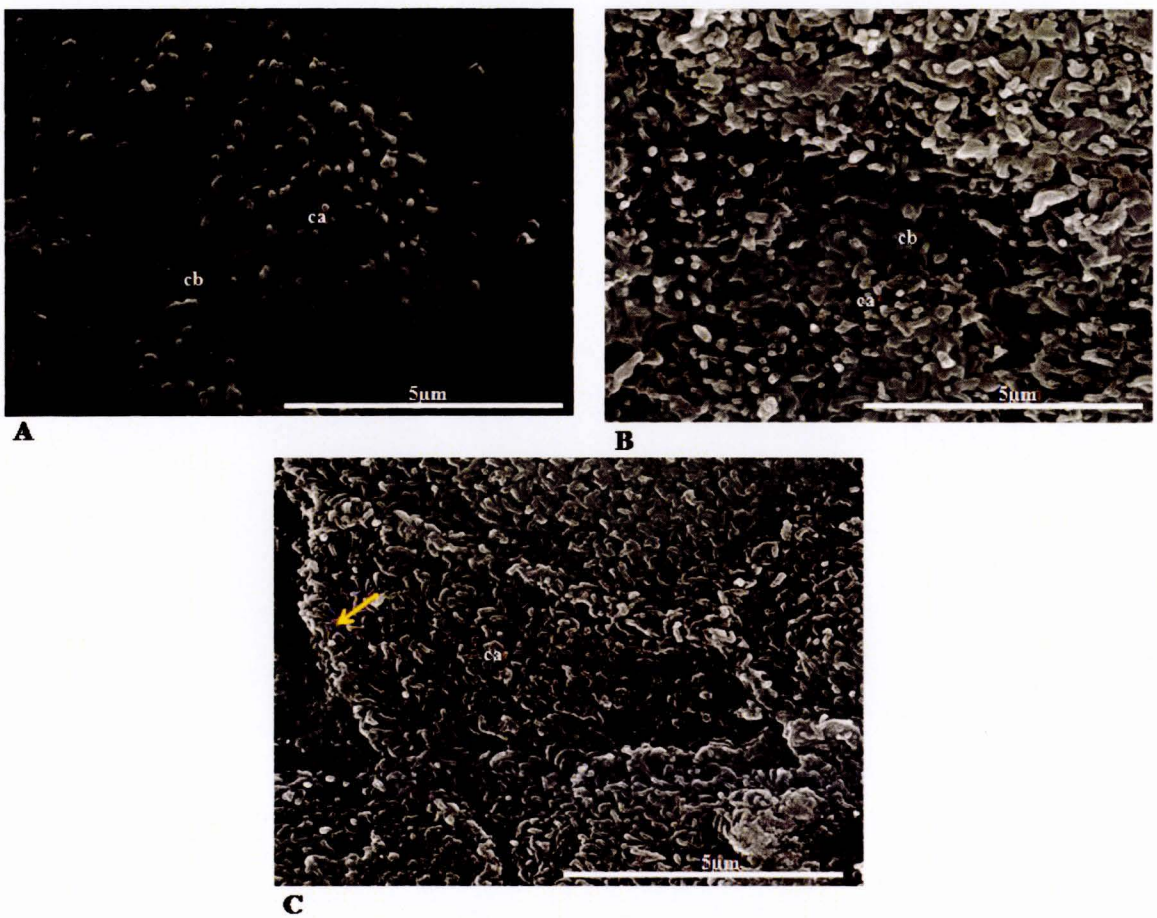


Figure 3.13: SEM of the uterine epithelial cells from non implantation sites of day 6 of pregnancy in rats. (A) The uterine epithelial cells from the non implantation site of day 6 untreated rat (control) showing flat cell borders (cb) and slightly bulged cell apices (ca). (B) Day 6 anastrozole treated rat showing flat cb and slightly bulged ca. (C) Day 6 chlomiphene citrate (CC) treated rat showing raised cb (arrow) and flat ca.

3.2.5 Cell borders (CB)

In the CB group, there are 2 levels of results (Appendix G). Levels that are not connected by the same letter are significantly different as shown on top of each bar in Figure 3.15. Specifically only day 6CC NP is different from day 1 anastrozole, day 6 anastrozole IP and day 6U IP suggesting that anastrozole appears to maintain flat cell borders in uterine epithelial cells during implantation compared to chlomiphene citrate (CC) treated animals which show raised cell borders as represented in Figures 3.12, 3.13, 3.14 and Appendix G.

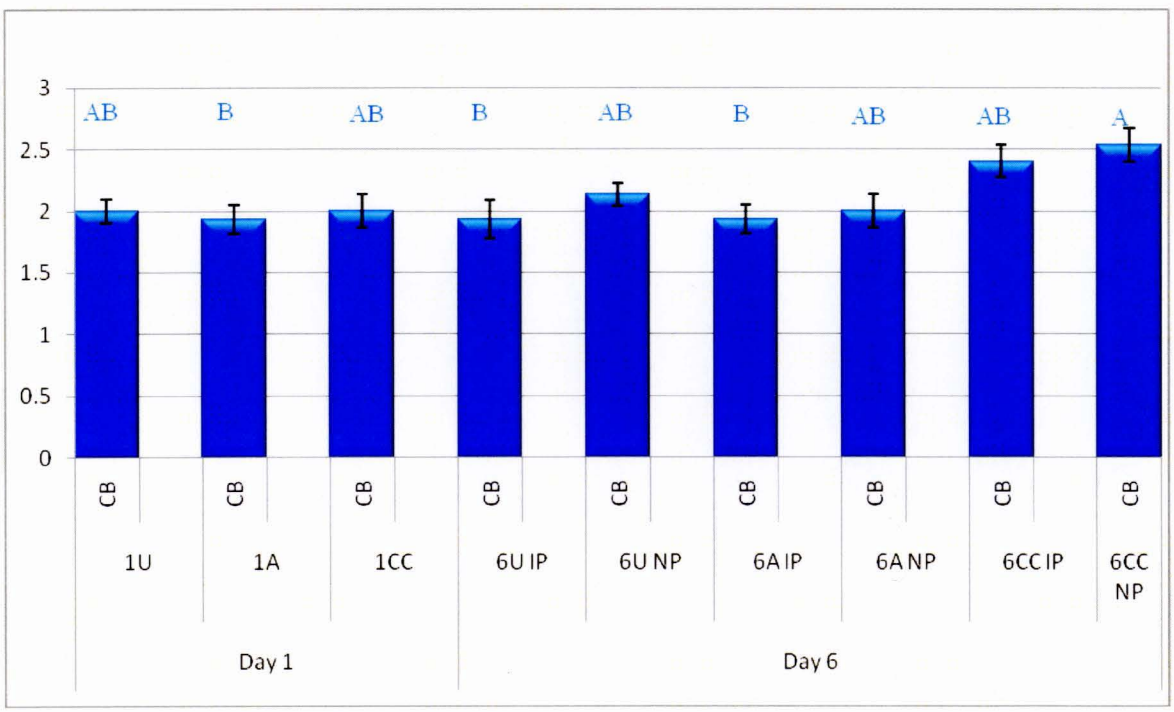


Figure 3.14: Graphical representation of cell borders of uterine epithelial cells in pregnant rats. There is a significant difference in cell borders between day 6 non-implantation sites of chlomiphene citrate treated and day 6 implantation sites of anastrozole treated ($p<0.0265$) (Appendix G). There is also a significant difference in cell borders between day 6 non-implantation sites of chlomiphene citrate treated and day 6 implantation sites of

untreated rats ($p<0.0265$) (Appendix G). Anastrozole appears to maintain flat cell borders in uterine epithelial cells during implantation compared to chlomiphene citrate (CC) treated animals which show raised cell borders at day 6 of pregnancy.

3.2.6 Surface glycocalyx (SG)

Day 1 are all on level A and day 6 on level C, clearly separating the groups as seen in the ML and SF groups. However this time the connecting group consists of day 1 anastrozole, day 6 anastrozole IP and day 6 anastrozole NP (Appendix G). This result shows that the three anastrozole groups are similar in this regard, and appear to retain the glycocalyx to some extent as shown in Figures 3.15 and 3.16.

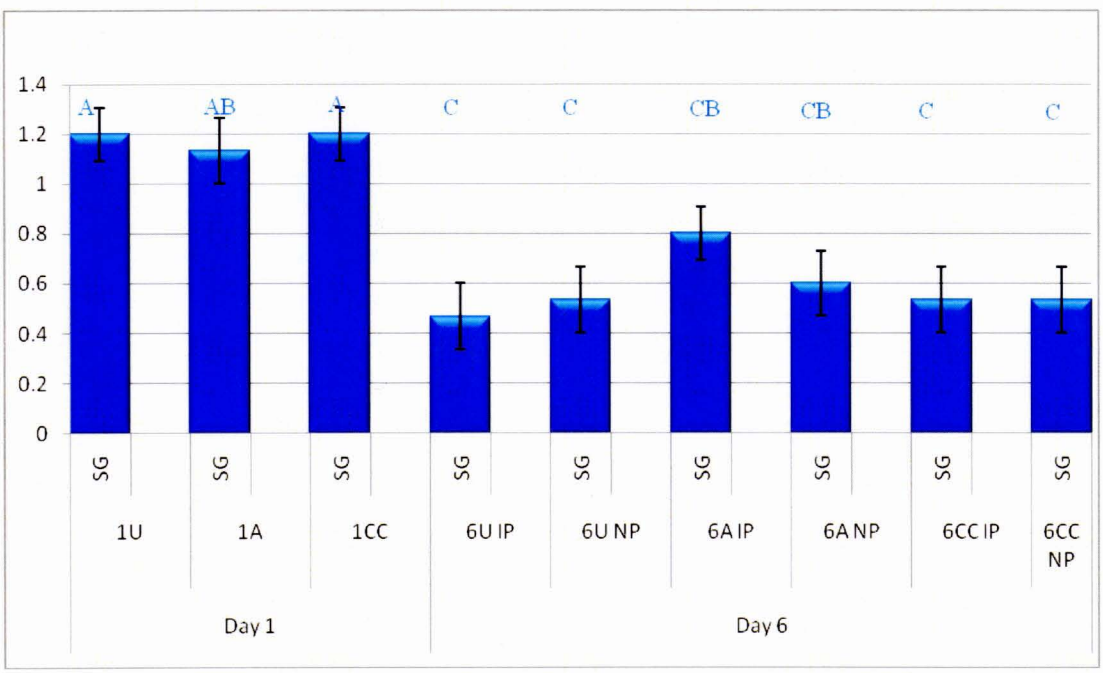


Figure 3.15: Graphical representation of the uterine surface glycocalyx in pregnant rats. Groups that are not connected by the same letter are significantly different as shown on top of each bar in the graph. There is a significant difference in the uterine surface glycocalyx

between day 1 groups and day 6 groups ($p<0.0001$) (Appendix G). The surface glycocalyx decreases as pregnancy progresses; note: anastrozole appears to retain the glycocalyx to some extent in implantation sites at day 6 of pregnancy.

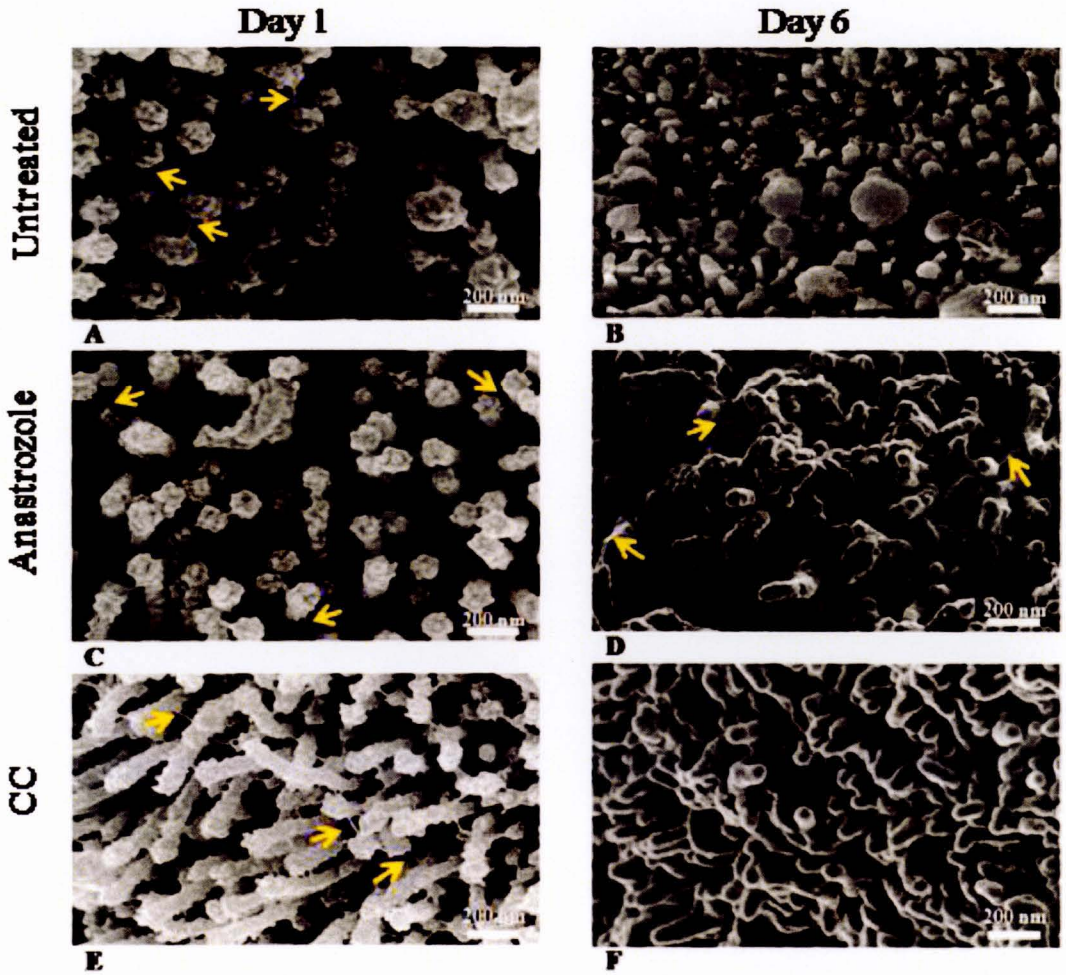


Figure 3.16: SEM of the uterine epithelial cells from day 1 and implantation site day 6 pregnant rats. (A) Day 1 untreated rat showing numerous glycocalyx molecules (yellow arrows). (B) Day 6 implantation site from untreated rat showing short irregular microvilli with no glycocalyx seen (C) Day 1 anastrozole treated rat showing numerous glycocalyx molecules

(D) Day 6 implantation site from untreated rat showing short irregular microvilli with some glycocalyx (E) Day 1 chlomiphene citrate (CC) treated rat showing numerous glycocalyx molecules. (F) Day 6 implantation site from CC treated rat showing short irregular microvilli without glycocalyx observed.

3.2.7 Epithelial gland opening (EGO)

In the EGO group, there are 4 separate levels identified (Appendix G). Groups that are not connected by the same letter are significantly different as shown on top of each bar in Figure 3.17. The day 1 group is isolated except that day 6 anastrozole NP is also included in this level. The day 6 group is also isolated except that it shares the day 6 anastrozole NP with the day 1 level. There are no day 6s or day 1s that are significantly different from each other. In the connecting groups, the first includes day 1 chlomiphene citrate (CC) and 1U as well as day 6 anastrozole NP and 6CC IP, possibly suggesting that the chlomiphene citrate implantation sites at day 6 are still not fully developed. The second connecting group includes day 1U and all of the day 6s except 6U NP, suggesting that the glands remain the same in untreated rats, in the non-implantation sites. Generally, there are more gland openings observed in day 1 groups than in day 6 groups as shown in Figure 3.17 and Appendix G.

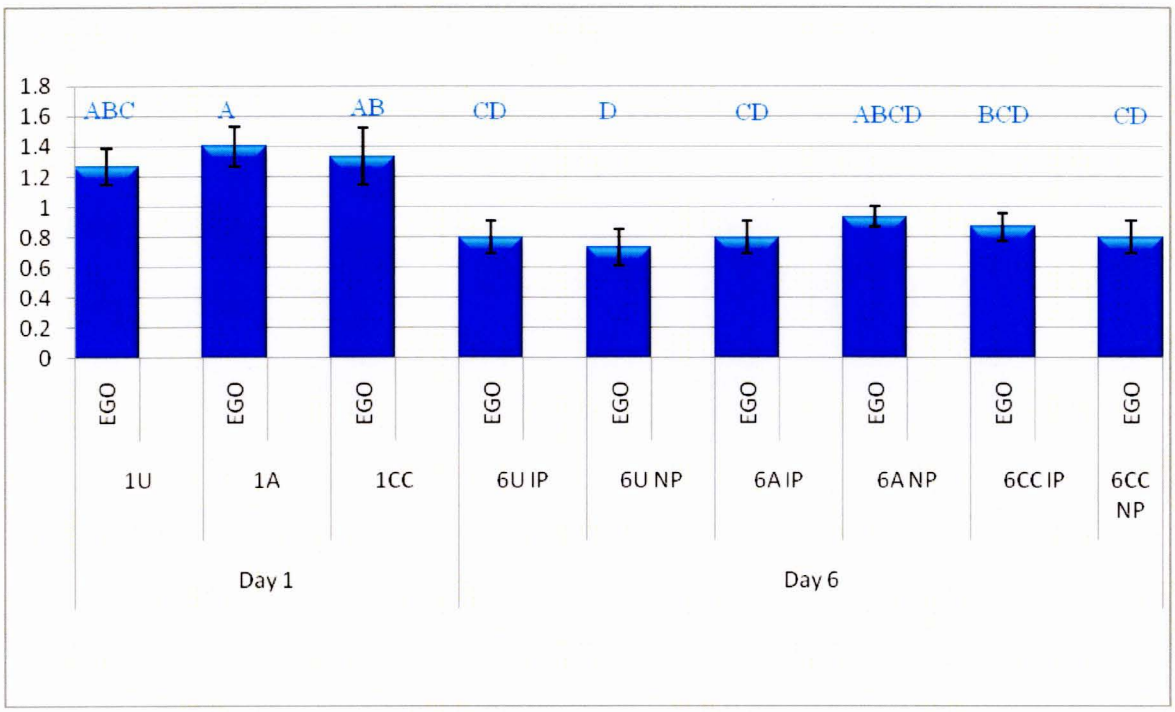


Figure 3.17: Graphical representation of the uterine epithelial gland openings in pregnant rats. Groups that are not connected by the same letter are significantly different as shown on top of each bar in the graph. There is a significant difference in the uterine epithelial gland openings between day 1 groups and day 6 groups ($p<0.0001$) (Appendix G). Generally, there are more gland openings observed in day 1 groups than in day 6 groups.

3.2.8 Small secretions (SS)

In the SS group again 4 levels are seen (Appendix G). First the day 1 and day 6 groups are separated (level A and D) respectively. However, there is an over-lap where day 1U, 1CC and day 6 anastrozole NP are grouped as are day 1CC, day 6 anastrozole NP, 6 anastrozole IP and 6CC IP. Generally day1 groups have the most abundant small secretions followed by day 6

implantation sites (except for day 6 anastrozole NP, which clusters with the day 1 groups) as shown in Figure 3.18, Table 3.1, Figures 3.19A - 3.19C and Appendix G.

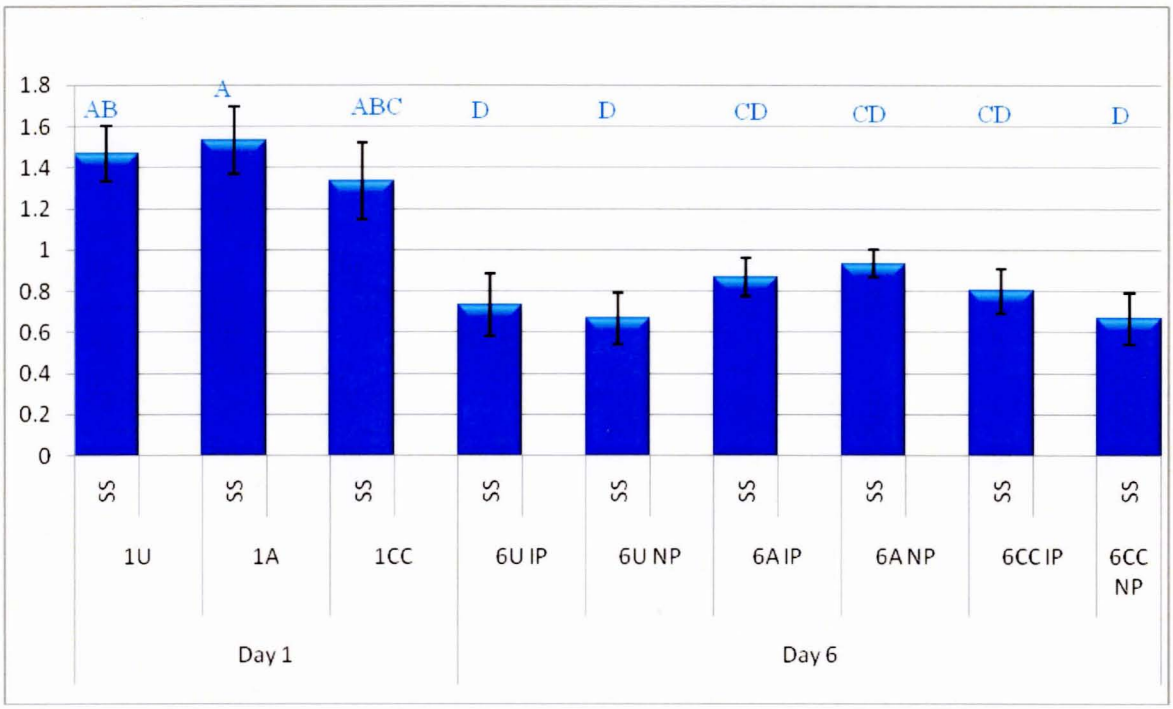


Figure 3.18: Graphical representation of the surface uterine small secretions in pregnant rats. There is a significant difference in the surface uterine small secretions between day 1 groups and day 6 groups ($p<0.0001$) (Appendix G). Generally day 1 groups have the most abundant small secretions followed by day 6 implantation sites.

Table 3.1: A summary of the scanning electron microscopy analysis of the eleven luminal uterine epithelial characteristics are as described in Table 2.2.

	Day 1			Day 6					
TR	U	A	CC	U IP	U NP	A IP	A NP	CC IP	CC NP
SF	Folded	Folded	Folded	Smooth	Smooth to slightly folded	Smooth	Smooth with few folds	Smooth with few folds	Folded
CA	Slightly bulged	Slightly bulged	Flat	Slightly bulged	Slightly bulged	Slightly bulged	Slightly bulged	Flat	Flat
CB	Flat	Flat	Slightly raised	Flat	Flat	Flat	Flat	Raised	Raised
MD	Medium to dense	Medium to dense	Medium to dense	Medium/s parse	Medium/ sparse	Medium/s parse	Medium/s parse	Medium/ Sparse	Medium/ Sparse
ML	Long thin	Long thin	Long thin	Very short irregular	Mixture of short and long	Very short irregular	Very short irregular	Short irregular	Relatively long
MSB	Many	Many	Many	Some	Some	Some	Some	Some	Some
LSP	None	None	None	Many	Some	Many	Many	Some	Some
SG	Numerous	Numerous	Numerous	None	None	Some	None	None	None
MP	Not seen	Not seen	Not seen	Some	Some	Some	Some	Some	Some
SS	Many	Many	Many	Some	Some	Some	Some	Some	Some
EGO	Many	Many	Many	Some	Some	Some	Some	Some	Some

Note: TR = Treatment groups

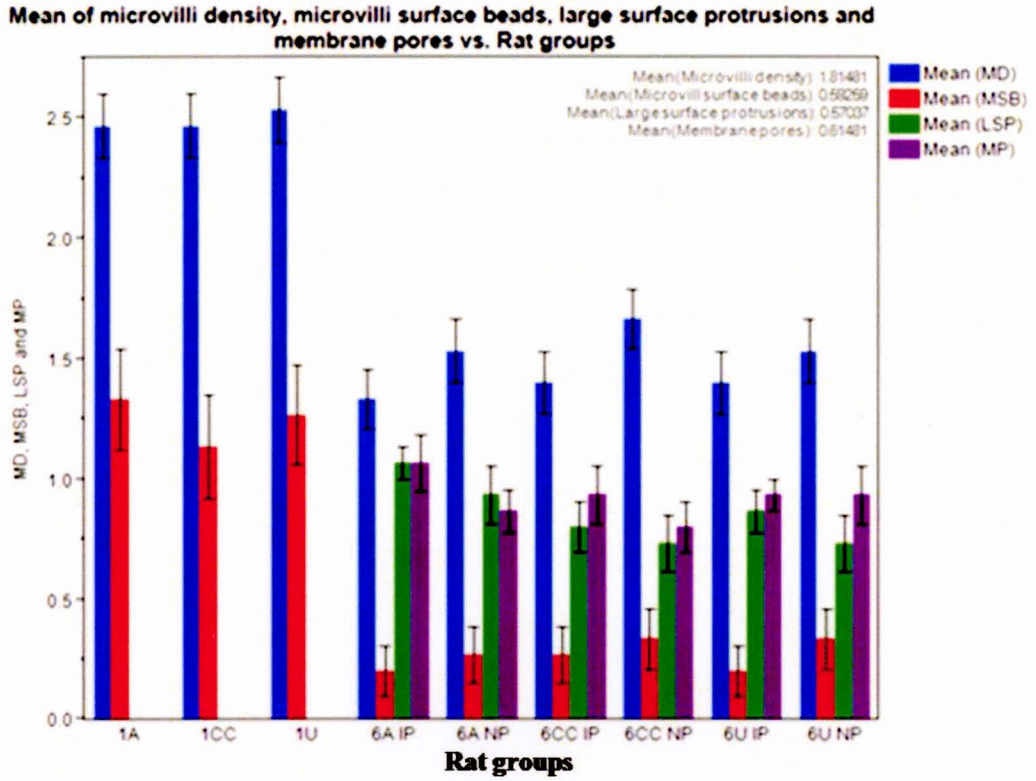


Figure 3.19A: Graphical representation of microvilli density (MD), microvilli surface beads (MSB), large surface protrusions (LSP), and membrane pores (MP) as shown in Table 2.2 at day 1 and day 6 of pregnancy in rats. In the MD, MSB, LSP, and MP all of the day 1 group together and all of the Day 6 all group together, there are no overlaps and are clearly separated. Long thin microvilli of medium to dense in terms of distribution at day 1 in all groups are replaced by short irregular sparse microvilli at day 6 in all groups. Surface glycocaly generally decreases as pregnancy progresses in all groups. However, anastrozole appears to retain some specific glycocalyx at day 6 possibly to be used in implantation. Large cell surface protrusions are mostly seen but not limited to anastrozole treated rats at day 6.

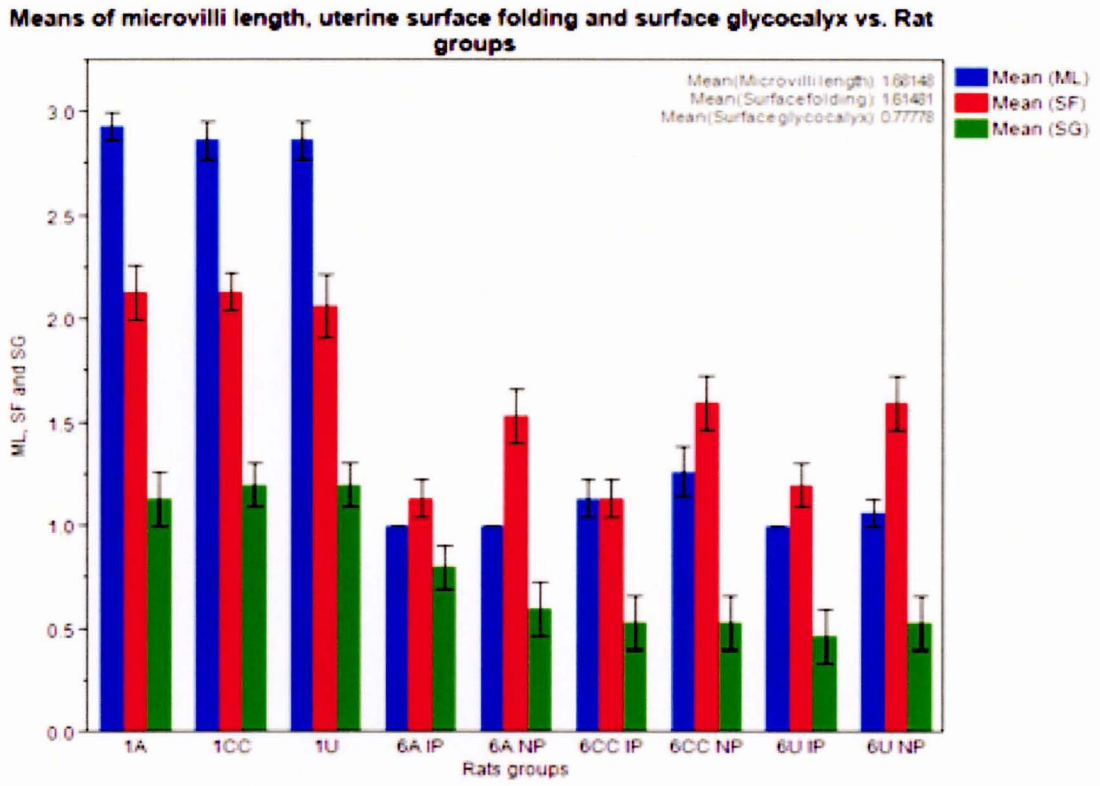


Figure 3.20B: Graphical representation of microvilli length (ML), uterine surface folding (SF), and surface glycocalyx (SG) as shown in Table 2.2 at day 1 and day 6 of pregnancy in rats. Long thin microvilli at day 1 are replaced by short irregular sparce microvilli at day 6 in all groups; note that the microvilli in the anastrozole NP and IP groups are the shortest. The deep surface uterine folds at day 1 become smoothened at day 6 in implantation sites while non-implantation sites remain folded in all groups. The surface glycocalyx decreases as pregnancy progresses; note: anastrozole appears to retain the glycocalyx to some extent.

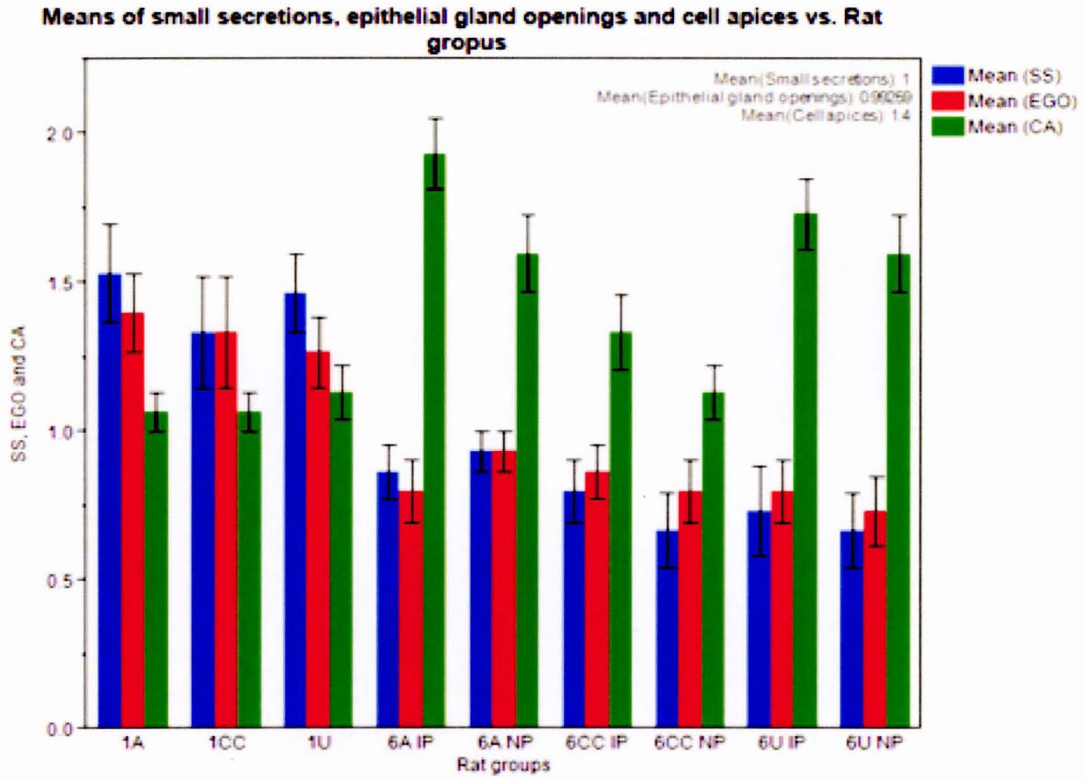


Figure 3.21C: Graphical representation of small secretions (SS), epithelial gland openings (EGO), and cell apices (CA) as shown in Table 2.2 at day 1 and day 6 of pregnancy in rats. Generally day 1 groups have the most secretions followed by day 6 implantation sites. Anastrozole seems to enhance slight doming of the cell apices while chlomiphene citrate (CC) appears to flatten cell apices. Generally more gland openings and secretions are seen in day 1 groups compared to day 6 groups.

3.3 Immunofluorescence for the focal adhesion protein vinculin, integrin β5, paxillin and focal adhesion kinase (FAK) in luminal surface uterine epithelial cells of day 1 and day 6 of pregnancy in rats

The assembly, disassembly and reorganization of focal adhesion proteins during early pregnancy are part of the process of plasma membrane transformation (Kaneko *et al.*, 2011). During implantation, focal adhesion proteins disassemble from the base of the epithelium to facilitate the detachment of the uterine luminal epithelium to allow the embryo to invade the endometrium (Kaneko *et al.* 2011). At the same time, they assemble and become localized apically to assist in the adhesion of the blastocyst onto the endometrium (Kaneko *et al.*, 2011; 2012).

The following parameters were tested as shown in Table 2.3. These were focal adhesion protein expression levels, that is, the fluorescence intensities reflecting protein quantities and the main epithelial domain protein localization. A total of 15 images per animal were assessed to generate the results. The parameters were scored by two researchers using a random blinded method and then analyzed using a one way ANOVA followed by a Tukey-Kramer HSD. The results of the one way ANOVA in each case demonstrate a significant difference at $p<0.0001$. The results of the *post hoc* analysis, the Tukey-Kramer HSD tests in each case clearly separate day 1 and day 6 groups. In some cases there are overlaps.

3.3.1 Vinculin and integrin β5

Vinculin and integrin β5 are co-localized at the base of the uterine epithelium at day 1 of pregnancy whereas at day 6 they disassemble from the basal focal adhesions and co-localize and increase their expression apically as noted in Figures 3.20, 3.21, 3.22, 3.23 and Appendix G. Additionally, vinculin is also expressed in the perinuclear region at day 1 and relocates apically at day 6 of pregnancy as seen in Figures 3.20, 3.21, 3.22, 3.23 and Appendix G. Moreover, there is a significant difference in the expression levels of both vinculin and integrin β5 between untreated (control) and chlomiphene citrate (CC) treated rats, anastrozole and CC treated rats at both day 1 and day 6 as seen in Figures 3.20, 3.21, 3.22, 3.23 and Appendix G suggesting that CC seems to decrease their expression. Although there is no significant difference in the expression levels between untreated and anastrozole treated rats at day 1 and day 6, the means for vinculin and integrin β5 expression are higher in the anastrozole treated groups suggesting that anastrozole seems to enhance their expression in order to assist in the implantation process of the embryo. The non-immune controls were used to validate and determine non-specific binding of the secondary antibody on other targets within the epithelium; there is lack of non-specific staining as seen in Appendix I.

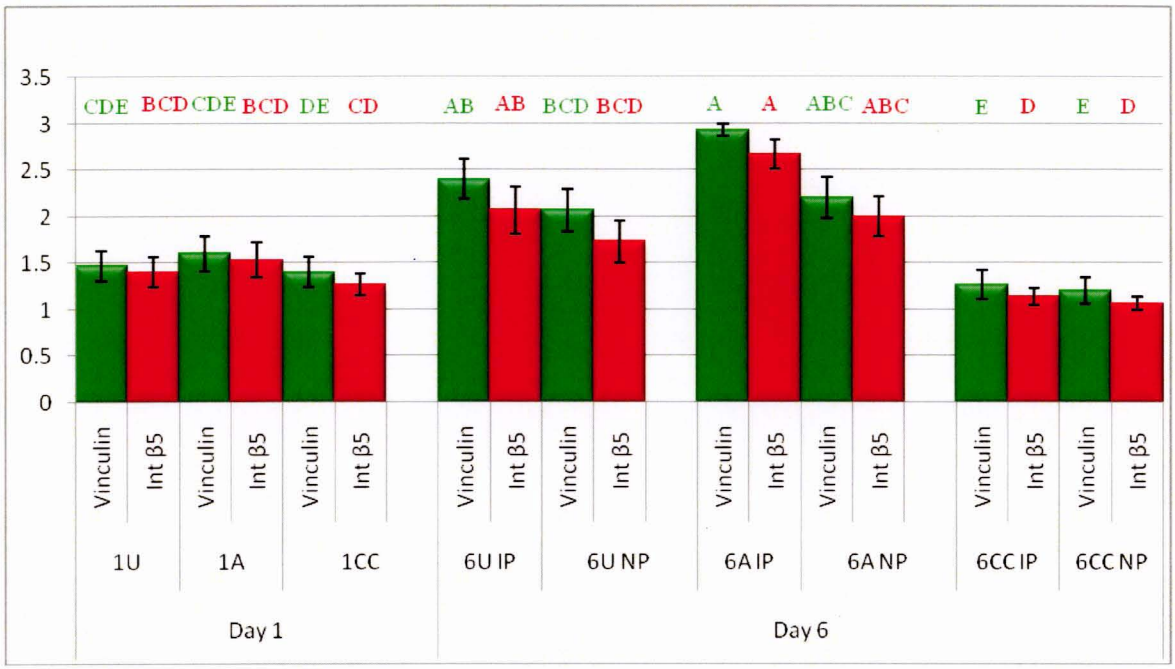


Figure 3.22: Vinculin and intergrin β5 expression in the surface luminal uterine epithelial cells of day 1 and day 6 pregnant rats. There is a significant difference in the expression of vinculin and integrin β5 between anastrozole day 1 and day 6 ($p<0.0001$) (Appendix G), untreated (control) day 1 and day 6 ($p<0.0001$) (Appendix G), untreated day 6 and CC day 6 ($p<0.0001$) (Appendix G). No significant difference in vinculin and integrin β5 expression is noted between chlomiphene citrate day 1 and chlomiphene citrate day 6 ($p>0.05$) (Appendix G), untreated day 6 and anastrozole day 6 ($p>0.05$) (Appendix G). Note: chlomiphene citrate (CC) seems to decrease their expression while anastrozole seems to enhance their expression as pregnancy progresses.

In addition, based on the scoring system for the main epithelial domain protein localization as described in Table 2.3, (1, basal; 2, apical; 3, lateral; 4, basolateral; 5, basal and apical) (Englund *et al.,* 2001; Mwakikunga *et al.*, 2011), vinculin and integrin β5 are co-localized at

the base of the uterine epithelium at day 1 of pregnancy whereas at day 6 they disassemble from the basal focal adhesions and co-localize and increase their expression apically as noted in Figures 3.20, 3.21, 3.22, 3.23 and Appendix G.

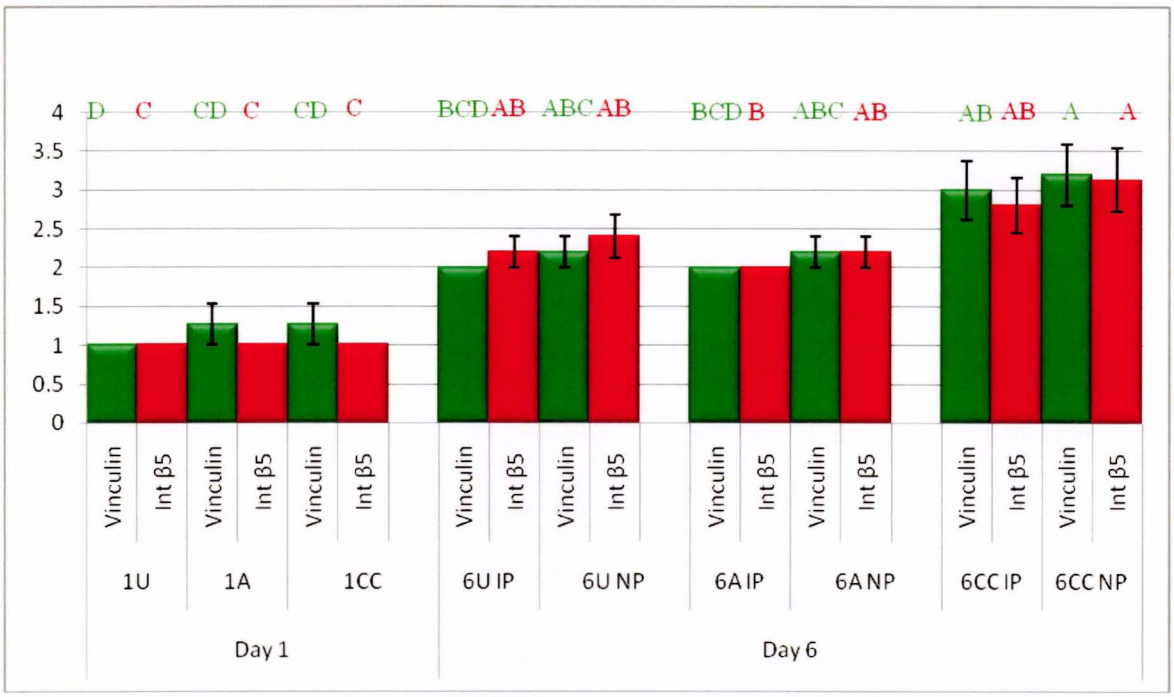


Figure 3.23: Vinculin and intergrin β5 uterine epithelial localization. Vinculin and integrin β5 are co-localized at the base of the uterine epithelium at day 1 of pregnancy whereas at day 6 they disassemble from the basal focal adhesions and co-localize and significantly increase their expression apically ($p<0.0001$) as also noted in Figures 3.22, 3.23 and Appendix G. Note: vinculin is also expressed in the perinuclear region at day 1 and relocates apically at day 6 of pregnancy in the untreated and anastrozole treated rats as seen in Figures 3.22 and 3.23. Vinculin and integrin β5 also colocalize and significantly increase their expression on the basolateral membrane of the uterine epithelial cells in the chlomiphene citrate (CC) day 6 rats

compared to day 1 groups ($p<0.05$), which may impede blastocyst invasion during implantation. Note: numerical scale on the left represents the scoring system average scores.

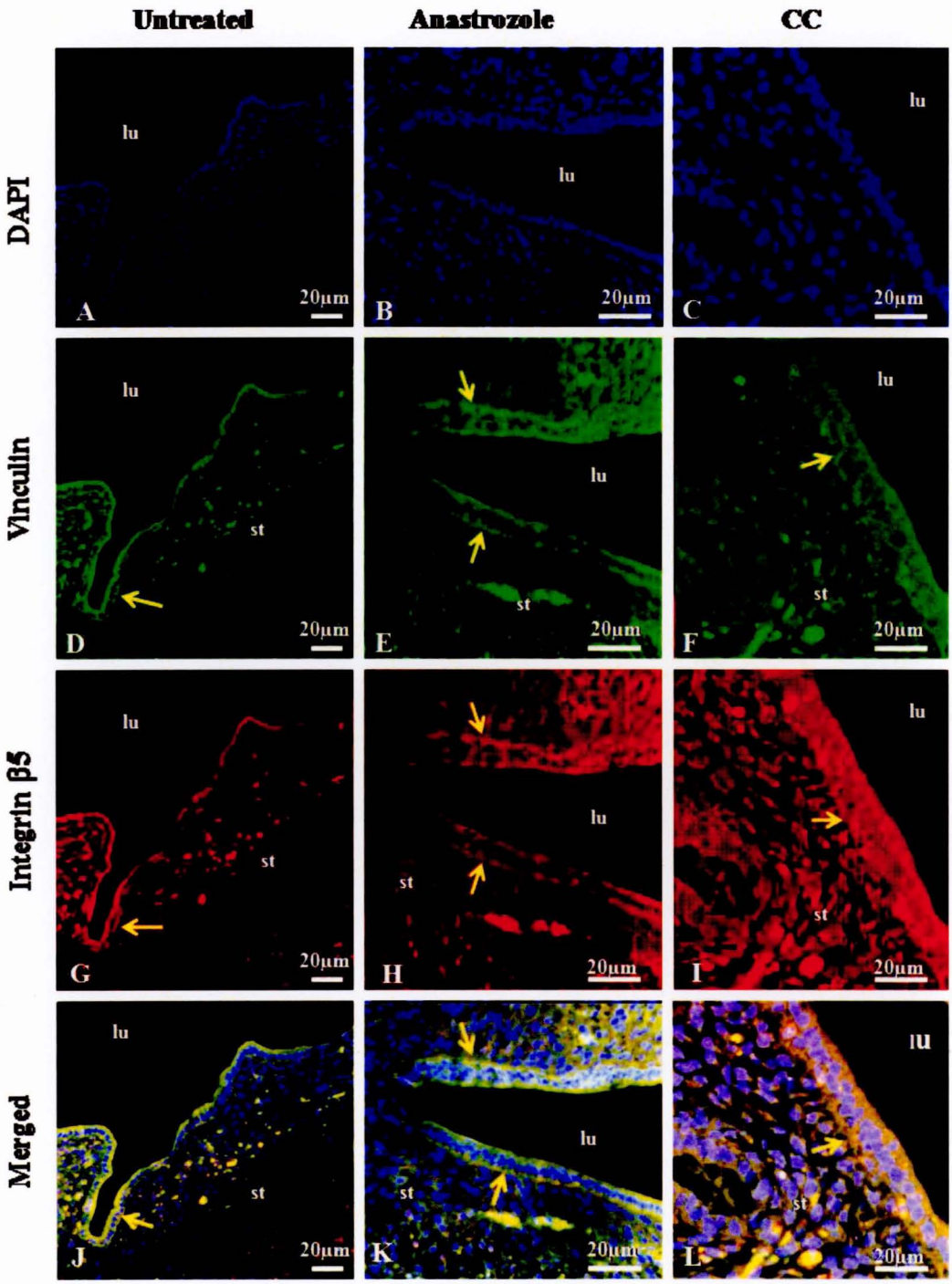


Figure 3.24: Micrograph showing vinculin and integrin β5 expression and co-localization in luminal uterine epithelial cells from day 1 of pregnancy in rats. (A), (B) and (C) show

nuclei stained with DAPI (blue). (D) and (E) A distinct band of vinculin (green, FITC) expression at the base of the uterine epithelium (yellow arrow) is noted in both untreated and anastrozole treated rats. (F) The basal expression of vinculin in chlomiphene citrate (CC) treated rat is not as high as in (D) and (E). (G) and (H) A distinct band of integrin β5 (red, rodamine) expression at the base of the uterine epithelium (yellow arrow) is noted in both untreated and anastrozole treated rats. (I) The basal expression of integrin β5 in CC treated rat is not as high as in (G) and (H). (J), (K) and (L) Vinculin and integrin β5 co-localize basally on day 1 of pregnancy. All images are representative of staining from the 5 rats in each of the treatment regimes.

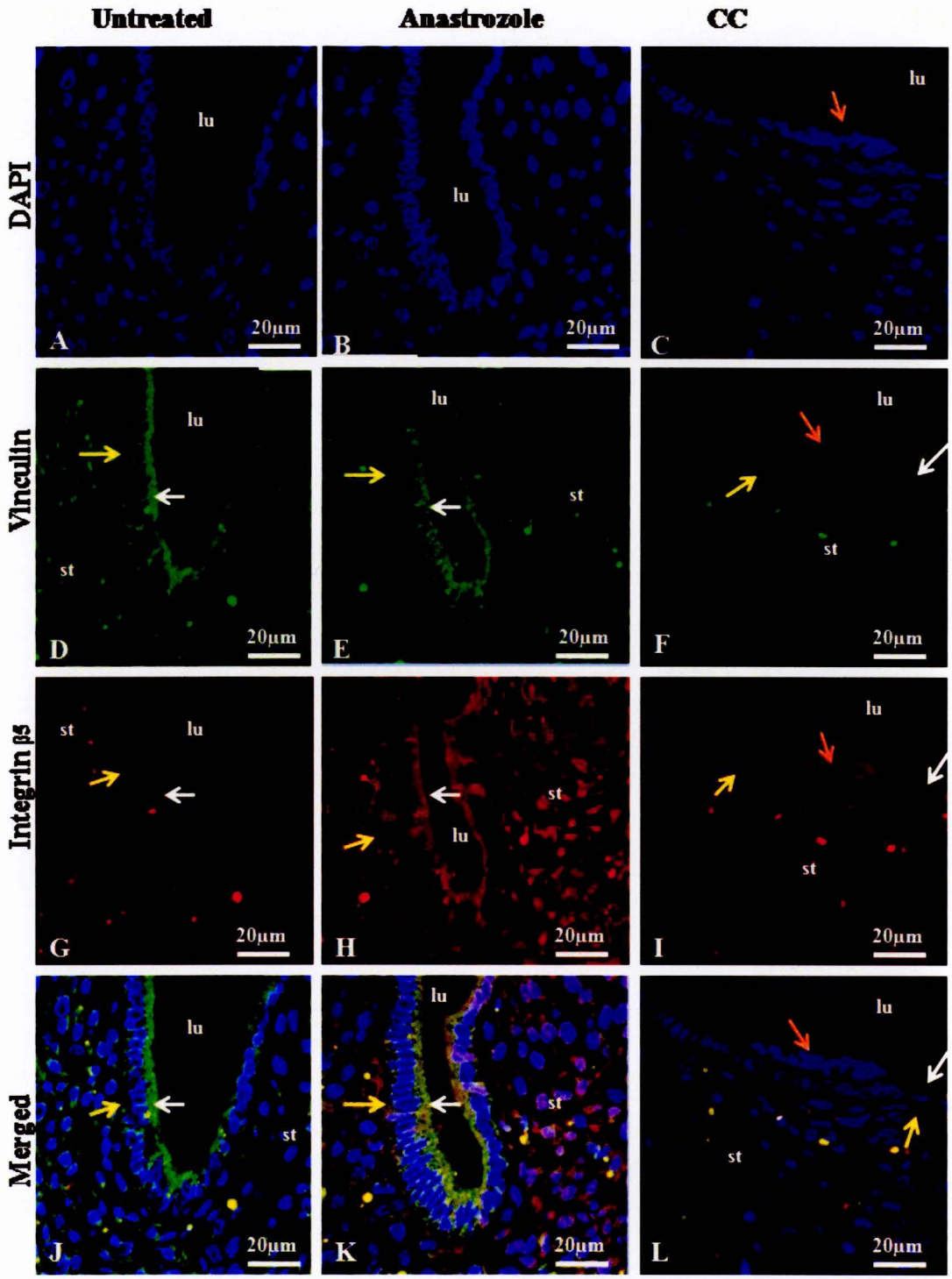


Figure 3.25: Micrograph showing vinculin and integrin β5 expression and co-localization in luminal uterine epithelial cells from implantation sites of day 6 pregnant rats. (A), (B)

and (C) show nuclei stained with DAPI (blue); orange arrow shows the embryo. (D) and (E) Vinculin (green, fluorescein isothiocyanate (FITC) disassemble from the base of the epithelium (yellow arrows) and become highly expressed apically (white arrows) in both untreated and anastrozole treated rats. (F) The apical expression of vinculin in chlomiphene citrate (CC) treated rat is down-regulated. (G) and (H) Integrin β5 (red, rodamine) disassemble from the base of the epithelium (yellow arrows) and become highly expressed apically (white arrows) in both untreated and anastrozole treated rats. (I) The apical expression of integrin β5 in CC treated rat is down-regulated. (J), (K) and (L) Vinculin and integrin β5 co-localize apically on day 6 of pregnancy. All images are representative of staining from the 5 rats in each of the treatment regimes.

Table 3.2: A summary of vinculin and integrin β5 expression and localization

		Vinculin	Integrin β5
Day 1	Untreated	Medium intensity expression in focal adhesions at the base of the epithelium with some sparse perinuclear region expression	Medium intensity expression in focal adhesions at the base of the epithelium
	Anastrozole	Medium to high intensity expression in the basal region of the epithelium with some sparse perinuclear region expression	Medium to high intensity expression in the basal region of the epithelium
	CC	Medium intensity expression in focal adhesions at the base of the epithelium	Medium intensity expression in focal adhesions at the base of the epithelium
Day 6 IP	Untreated	High intensity apical cytoplasmic expression	High intensity apical cytoplasmic expression
	Anastrozole	High intensity apical cytoplasmic expression	High intensity apical cytoplasmic expression
	CC	Low intensity apical cytoplasmic expression	Low intensity apical cytoplasmic expression
Day 6 NP	Untreated	High intensity apical cytoplasmic expression	High intensity apical cytoplasmic expression
	Anastrozole	High intensity apical cytoplasmic expression	High intensity apical cytoplasmic expression
	CC	Low intensity apical cytoplasmic expression	Low intensity apical cytoplasmic expression

3.3.2 Paxillin and focal adhesion kinase (FAK)

Like vinculin and integrin β5, paxillin is localized in focal adhesions at the base of the uterine epithelial cells at day 1 of pregnancy whereas at day 6, paxillin disassembles from the basal focal adhesions and localizes and significantly increases its expression apically ($p<0.0001$) as noted in Figures 3.24, 3.25, 3.26, 3.27, Table 3.3 and Appendix G. Additionally, FAK is faintly expressed at the basal aspect of the uterine epithelial cells while moderately expressed at the cell-to-cell contact at day 1 in all groups from where it disassembles and relocates apically and becomes more intensely expressed at day 6 of pregnancy in untreated and anastrozole treated rats ($p<0.05$) (Appendix G). Although paxillin is localized apically at day 6, its expression is significantly down-regulated with chlomiphene citrate (CC) treatment ($p<0.05$) (Appendix G) suggesting its interference with the implantation process. However, there is a significant difference in the expression levels of paxillin and FAK between untreated (control) and chlomiphene citrate (CC) treated rats ($p<0.0001$), anastrozole and CC treated rats at day 6 ($p<0.0001$) as seen in Figures 3.24, 3.25, 3.26, 3.27, Table 3.3 and Appendix G suggesting that chlomiphene citrate appears to decrease their expression. Although there is no significant difference between untreated and anastrozole treated rats at day 6 ($p>0.05$) (Appendix G), the means for paxillin and FAK expression are higher in the anastrozole treated than in the untreated groups suggesting that anastrozole seems to enhance their expression probably to take part in the implantation process of the embryo. As seen in Figure 3.25, paxillin and FAK do not co-localize in focal adhesions at the base of the epithelium at day 1, but they co-localize and significantly increase their expression apically at day 6 ($p<0.0001$) (Appendix G) suggesting their role in the implantation process. In general, with regard to the ovarian hormones, the expression of paxillin and FAK in the anastrozole treated

group appears to be due to the blocking of estrogens and increasing of androgens compared to controls during implantation. Progesterone is probably also high as estrogen is low. In the chlomiphene citrate (CC) group, estrogen receptors are blocked, but androgens are presumably low during implantation. The non-immune controls were used to validate and determine non-specific binding of the secondary antibody on other targets within the epithelium; there is no non-specific binding as seen in Appendix G.

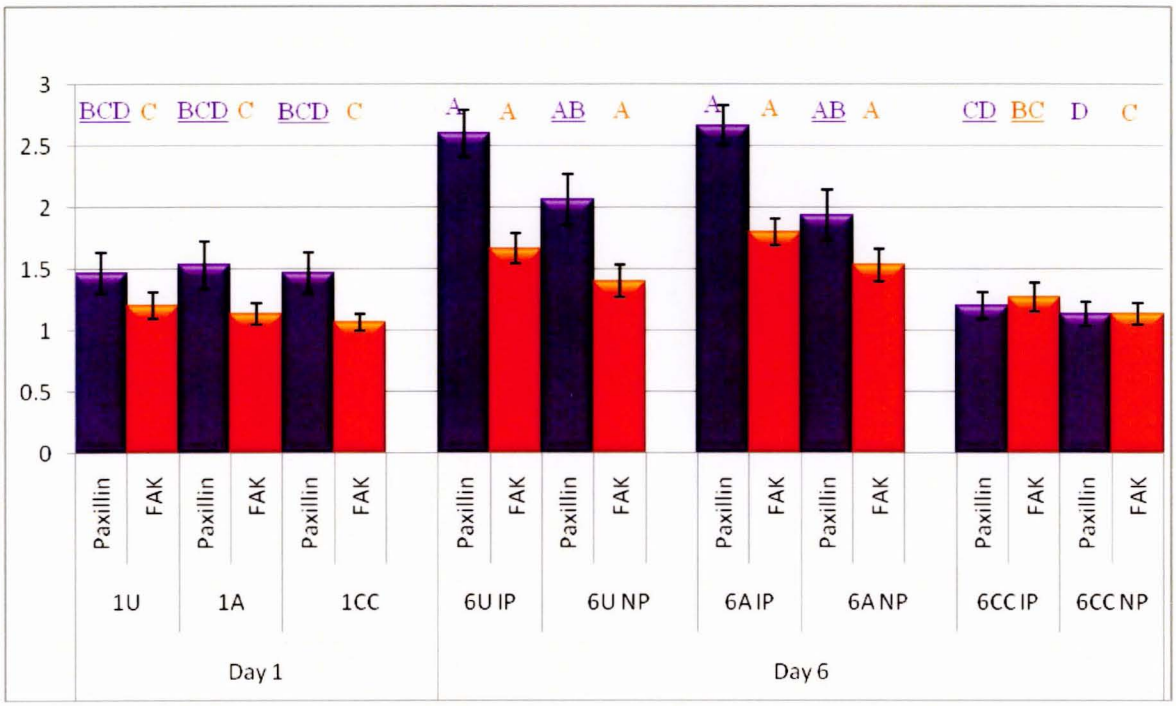


Figure 3.26: Graphical representation of paxillin and focal adhesion kinase (FAK) expression in luminal uterine epithelial cells in pregnant rats. There is a significant difference in the expression levels of paxillin and FAK between untreated (control) and chlomiphene citrate (CC) treated rats ($p<0.0001$) (Appendix G), anastrozole and CC treated rats at day 6 ($p<0.0001$) suggesting that CC appears to decrease their expression. No significant difference is noted between untreated and anastrozole treated rats at day 6 ($p>0.05$) (Appendix G), although the means for paxillin and FAK expression are higher in the anastrozole treated than in the untreated groups.

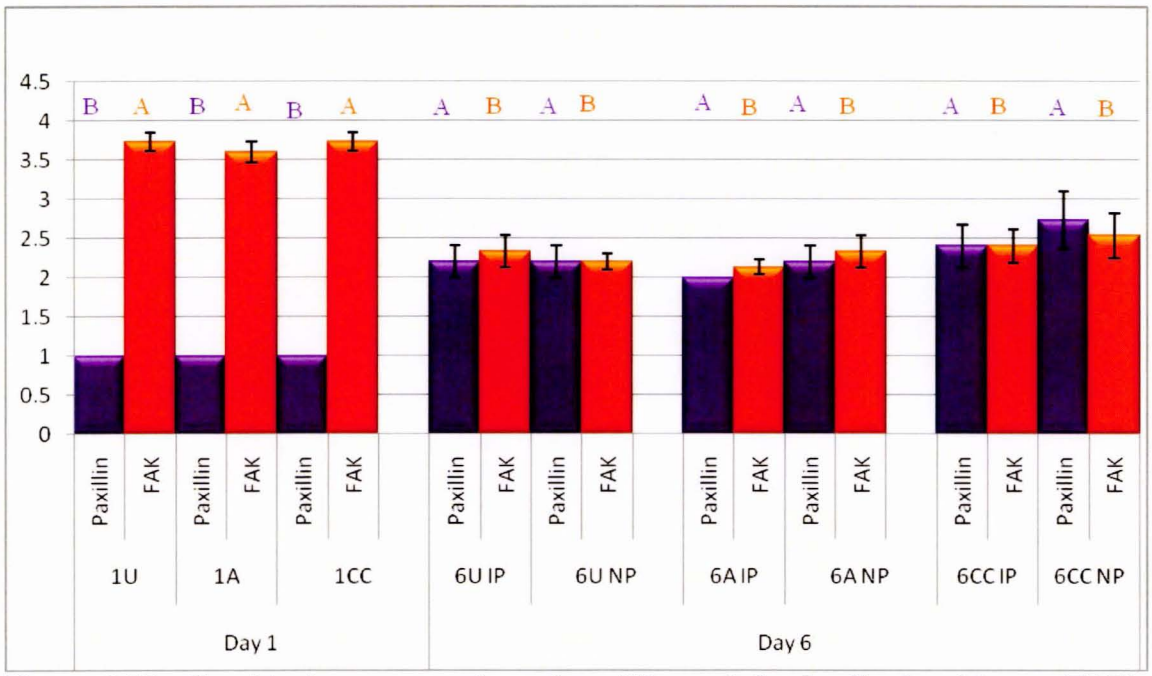


Figure 3.27: Graphical representation of paxillin and focal adhesion kinase (FAK) localization in the uterine epithelial cells in pregnant rats. Paxillin is localized in focal adhesions at the base of the uterine epithelial cells at day 1 of pregnancy whereas at day 6, paxillin disassembles from the basal focal adhesions and localizes apically. FAK is faintly expressed at the base of the uterine epithelial cells while moderately expressed at the cell-to-cell contact (lateral aspect) of the uterine epithelial cells at day 1 in all groups from where it disassembles and relocates apically and becomes more intensely expressed ($p<0.05$) (Appendix G) at day 6 of pregnancy in untreated and anastrozole treated rats. Note: numerical scale on the left represents the scoring system average scores as described previously.

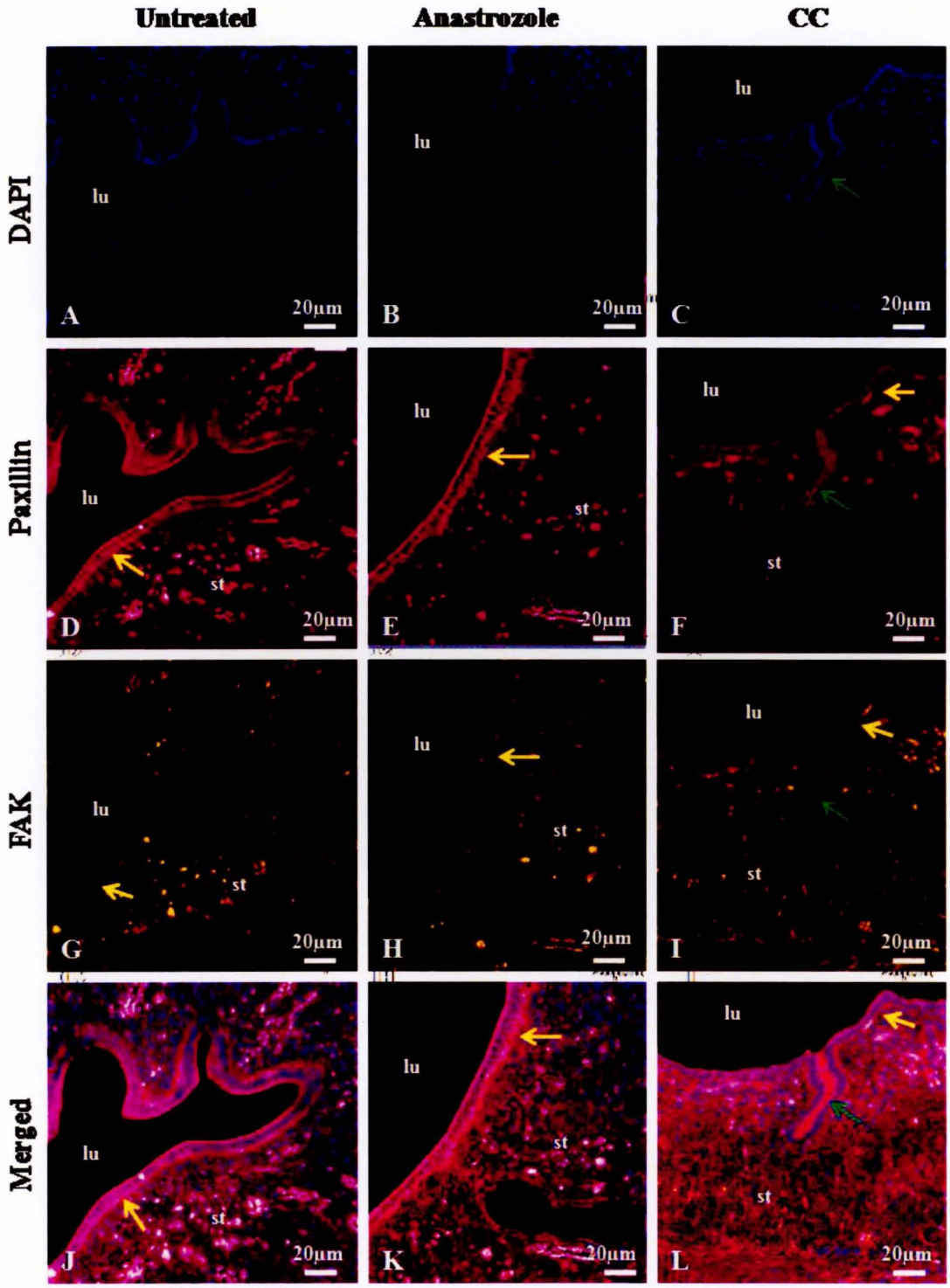


Figure 3.28: Micrograph showing paxillin and focal adhesion kinase (FAK) expression and localization in luminal uterine epithelial cells from day 1 of pregnancy in rats. (A),

(B) and (C) show nuclei stained with DAPI (blue). (D) and (E) A distinct band of paxillin (magenta, FITC) expression at the base of the uterine epithelium (yellow arrow) is noted in both untreated and anastrozole treated rats. (F) The basal expression of paxillin in chlomiphene citrate (CC) treated rat is not as high as in (D) and (E). (G), (H) and (I) Very faint band of focal adhesion kinase (FAK) (orange, rodamine) expression is noted at the base of the uterine epithelium (yellow arrow) in untreated, anastrozole treated and chlomiphene citrate (CC) treated rats. FAK expression of medium intensity is also noted on the lateral domain of the epithelium. (K) and (L) Paxillin and FAK do not co-localize basally on day 1 of pregnancy. All images are representative of staining from the 5 rats in each of the treatment regimes.

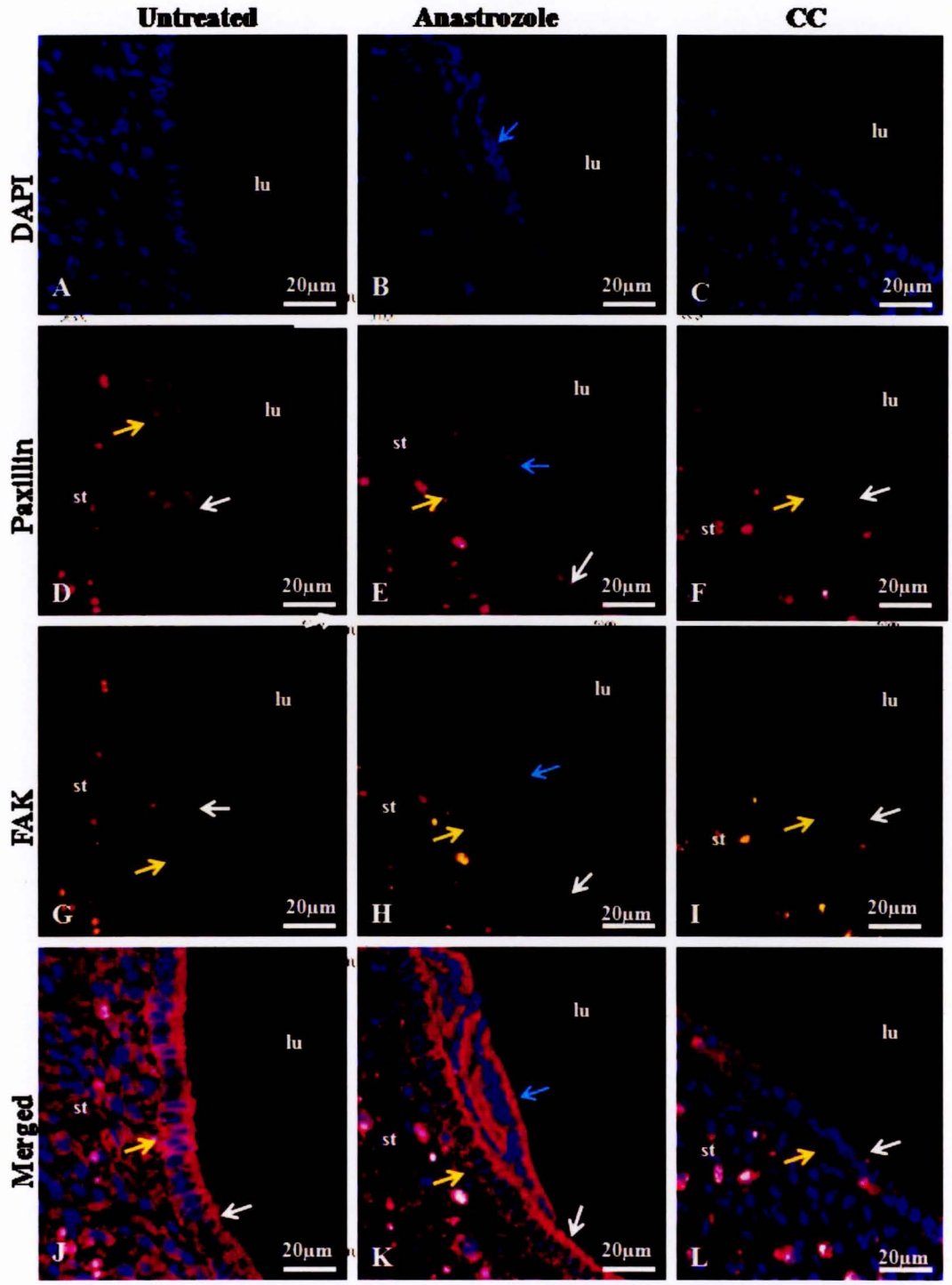


Figure 3.29: Micrograph showing paxillin and focal adhesion kinase (FAK) expression and co-localization in luminal uterine epithelial cells from implantation sites of day 6

pregnant rats. (A), (B) and (C) show nuclei stained with DAPI (blue); blue arrow shows the embryo. (D) and (E) paxillin (Magenta, fluorescein isothiocyanate (FITC) disassemble from the base of the epithelium (yellow arrows) and increases apically (white arrows) in both untreated and anastrozole treated rats. (F) The apical expression of paxillin in chlomiphene citrate (CC) treated rat is reduced. (G) and (H) Focal adhesion kinase (FAK) (orange, rodamine) become increased apically (white arrows) in both untreated and anastrozole treated rats. (I) The apical expression of FAK in chlomiphene citrate (CC) treated rats is significantly unchanged. (J), (K) and (L) Paxillin and FAK co-localize apically on day 6 of pregnancy. All images are representative of staining from the 5 rats in each of the treatment regimes.

Table 3.3: Summary table for paxillin and FAK expression and localization

		Paxillin	FAK
Day 1	Untreated	Medium intensity expression in focal adhesions at the base of the epithelium	Medium intensity expression on the lateral aspect of the epithelial cells
	Anastrozole	Medium intensity expression in focal adhesions at the base of the epithelium	Medium intensity expression on the lateral aspect of the epithelial cells
	CC	Medium intensity expression in focal adhesions at the base of the epithelium	Medium intensity expression on the lateral aspect of the epithelial cells
Day 6 IP	Untreated	High intensity apical cytoplasmic expression	High intensity apical cytoplasmic expression
	Anastrozole	High intensity apical cytoplasmic expression	High intensity apical cytoplasmic expression
	CC	Low intensity apical cytoplasmic expression	Medium to low intensity apical cytoplasmic expression
Day 6 NP	Untreated	High intensity apical cytoplasmic expression	High intensity apical cytoplasmic expression
	Anastrozole	High intensity apical cytoplasmic expression	High intensity apical cytoplasmic expression
	CC	Low intensity apical cytoplasmic expression	Medium to low intensity apical cytoplasmic expression

3.4 Hematoxylin and eosin (H&E) staining

The standard hematoxylin and eosin protocol (Mohan *et al.*, 2008) was performed in order to have a general overview of the uterine endometrial histological changes, if any, between treatment groups. The changes in the uterine surface luminal epithelium, stroma cells, epithelial glands, blood vessels were considered. All images were captured with an Axio HRc digital camera (Carl Zeiss, Jena, Germany). All the images in Figure 3.29 are representative of staining from the 5 rats in each of the treatment regimes).

Generally, the untreated, anastrozole and CC treated day 1 rats respectively show a simple cuboidal to low columnar surface luminal uterine epithelium with simple tubular glands. The spiral arteries extend from stratum basale to just below the epithelium as noted in Figure 3.28. The stroma cells (fibroblasts) are relatively small in size.

The day 6 untreated and anastrozole treated rats show a simple columnar surface luminal epithelium with a mixture of secretory and non-secretory cells. Some of the epithelial cells have accumulation of glycogen in the basal portions (Figure 3.28). The stroma is edematous and the stroma cells have decidualised (are larger and pale) with abundant intercellular ground substance. The glands have lengthened, coiled and have become saw toothed with secretions (nutrients such as glycogen) in their lumen.

However, day 6 CC treated rats show a reduced or delayed decidualization of the stroma. Interestingly, the base of the uterine luminal epithelium where focal adhesions are located appears to be intact as well as cell-to-cell contact, which might be interfering with blastocyst invasion during implantation. (All images are representative of staining from the 5 rats in each of the treatment regimes).

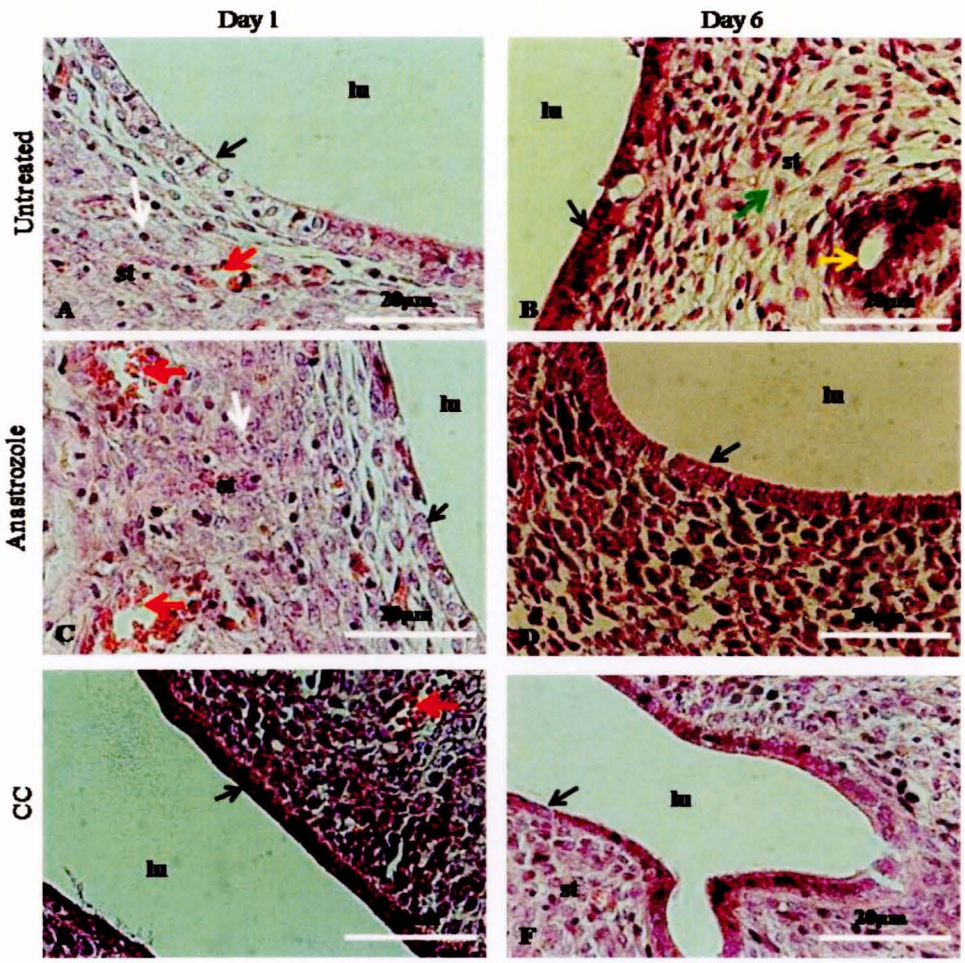


Figure 3.30: Micrograph (H & E) showing the endometrium of day 1 and day 6 pregnant rats. (A), (C) and (E) are day 1 untreated, anastrozole and CC treated rats respectively all showing the simple cuboidal to low columnar surface luminal epithelia (black arrows). Note: spiral arteries (red arrow) extend from stratum basale to just below the epithelium. The stroma cells (fibroblasts) are relatively small in size (white arrow). (B) and (D) are day 6 untreated and anastrozole treated rats respectively. The surface luminal epithelium is simple columnar. Note: the centrally located oval to round nuclei due to the accumulation of glycogen in the basal portions of some epithelial cells. The stroma is edematous and the stroma cells (green arrow) have decidualised (are larger and pale) with abundant intercellular ground substance.

The glands (yellow arrow) have lengthened, coiled and have become saw toothed with secretions (nutrients such as glycogen) in their lumen. (F) Day 6 CC treated rat showing a reduced or delayed decidualization of the stroma. Note: the base of the uterine luminal epithelium where focal adhesions are located appears to be intact as well as cell-to-cell contact interfering with blastocyst invasion during implantation. (All images are representative of staining from the 5 rats in each of the treatment regimes).

3.5 Real-time quantitative polymerase chain reaction (qPCR) of gene expression of vinculin, integrin β5, paxillin and FAK in the uterine epithelial cells from day 1 and day 6 pregnant rats

The comparative C_T method ($2^{-\Delta\Delta CT}$ method), as shown in Appendix D, was used to determine the gene expression fold change relative to the control following drug treatment regimes (Schmittgen and Livak, 2008). The data were first normalized using the three reference genes β-actin, 18S rRNA and Lactate dehydrogenase A; then the fold change was calculated (Schmittgen and Livak, 2008). The JMP10 software was used to conduct statistical analyses on the data. A one way ANOVA followed by a Tukey-Kramer *post hoc* analysis was performed to compare the means of normalized relative quantities (NRQ) between treatment groups. Differences were considered statistically significant when $p < 0.05$.

3.5.1 Relative quantification (RQ) analysis of vinculin and integrin β5 gene expression in the uterine epithelial cells from day 1 and day 6 pregnant rats

At day 1 of pregnancy, vinculin gene expression in uterine luminal epithelial cells is fairly similar (1.2-fold increase) in the anastrozole treated rats relative to the calibrator sample (day 1 untreated rats). This is also true for integrin β5 gene expression (1.01-fold increase) suggesting that anastrozole does not retard vinculin and integrin β5 gene expression in the process of endometrial readiness for implantation. Vinculin and integrin β5 gene expression in uterine luminal epithelial cells, however, is down-regulated (0.77-fold decrease) and (0.79-fold decrease) respectively with chlomiphene citrate (CC) treatment at day 1 of pregnancy relative to the calibrator sample as shown in Tables 3.4, 3.5 and Figure 3.29 suggesting that CC seems to decrease their expression. Interestingly, like the immunofluorescence experiments, at day 6 of pregnancy vinculin and integrin β5 gene expression are significantly up-regulated (more than 1.5-fold increase) ($p<0.0001$) (Appendix G) in uterine luminal epithelial cells in the implantation and non-implantation sites in the anastrozole treated group relative to the calibrator sample (Tables 3.4, 3.5, Figure 3.29 and Appendix G). A significant increase in the integrin β5 gene expression is also noted in uterine luminal epithelial cells of day 6 implantation sites in the untreated group (more than 1.5-fold increase) ($p<0.0001$) (Appendix G) while it has remained similar (1.04-fold increase) ($p>0.05$) (Appendix G) in the non-implantation sites relative to the calibrator sample (Tables 3.4, 3.5 and Figure 3.29) suggesting that anastrozole appears to enhance their expression to probably assist in the implantation process of the embryo. However, vinculin gene expression in uterine luminal epithelial cells is down-regulated with CC treatment at day 6 in implantation sites (0.96-fold decrease) and non-implantation sites (0.93-fold decrease) relative to the calibrator sample.

This is also true for integrin β5 gene expression (0.86-fold decrease and 0.42-fold decrease) respectively suggesting that chlomiphene citrate (CC) seems to decrease their expression, which may lag endometrial receptivity. In general, there is an increase in vinculin and integrin β5 gene expression at day 6 of pregnancy in uterine luminal epithelial cells in untreated and anastrozole treated groups, as reflected in the immunofluorescence experiments suggesting that anastrozole favours implantation.

Table 3.4: Relative quantification (RQ) analysis of vinculin gene expression in the luminal surface uterine epithelial cells of day 1 and day 6 of pregnant rats. A fold change of 1.5 or more represents a significant difference in gene expression ($p<0.05$).

Sample	Vin Ave C_T	*RFG Ave C_T	ΔC_T	$\Delta\Delta C_T$	Log_{10} ($2^{-\Delta\Delta CT}$)	Fold change $2^{-\Delta\Delta CT}$
**1U	24.40 ± 0.01	22.81 ± 0.03	1.59 ± 0.03	0 ± 0.03	0	**1** (0.97 to 1.02)
1A	24.14 ± 0.06	22.75 ± 0.04	1.39 ± 0.07	-0.2 ± 0.07	0.08	**1.2** (1.09 to 1.21)
1CC	24.81 ± 0.13	22.82 ± 0.06	1.99 ± 0.14	0.4 ± 0.14	-0.11	**0.77** (0.69 to 0.84)
6U IP	23.96 ± 0.03	22.59 ± 0.09	1.37 ± 0.09	-0.22 ± 0.09	0.08	**1.2** (1.09 to 1.24)
6U NP	23.91 ± 0.07	22.37 ± 0.04	1.54 ± 0.08	-0.05 ± 0.08	0.02	**1.04** (0.98 to 1.09)
6A IP	23.17 ± 0.03	22.19 ± 0.02	0.98 ± 0.04	-0.61 ± 0.04	0.20	**1.6** (1.5 to 1.6)
6A NP	24.19 ± 0.07	23.17 ± 0.03	1.02 ± 0.08	-0.57 ± 0.08	0.18	**1.5** (1.4 to 1.5)
6CC IP	25.18 ± 0.28	23.52 ± 0.05	1.66 ± 0.08	0.07 ± 0.08	-0.02	**0.96** (0.90 to 1.01)
6CC NP	25.26 ± 0.11	23.56 ± 0.05	1.7 ± 0.12	0.11 ± 0.12	-0.03	**0.93** (0.85 to 1.01)

C_T - threshold cycle, SEM - standard error of the mean, * - endogenous control, ** - calibrator sample. ΔC_T = C_T (Target) – C_T (Endogenous control). $\Delta\Delta C_T$ = ΔC_T (Target - ΔC_T (Calibrator).

Table 3.5: RQ analysis of integrin β5 gene expression in the luminal surface uterine epithelial cells of day 1 and day 6 of pregnant rats. A fold change of 1.5 or more represents a significant difference in gene expression ($p<0.05$).

Sample	Int β5 Ave C_T	*RFG Ave C_T	ΔC_T	$\Delta\Delta C_T$	Log_{10} ($2^{-\Delta\Delta CT}$)	Fold change $2^{-\Delta\Delta CT}$
**1U	27.8 ± 0.02	22.81 ± 0.03	4.99 ± 0.04	0 ± 0.04	0	**1** (0.97 to 1.03)
1A	27.64 ± 0.07	22.75 ± 0.04	4.89 ± 0.08	-0.1 ± 0.08	0.03	**1.07** (1.01 to 1.13)
1CC	27.39 ± 0.05	22.05 ± 0.06	5.34 ± 0.08	0.35 ± 0.08	-0.10	**0.79** (0.74 to 0.83)
6U IP	26.88 ± 0.06	22.59 ± 0.09	4.29 ± 0.11	-0.7 ± 0.11	0.21	**1.63** (1.51 to 1.75)
6U NP	26.96 ± 0.02	22.37 ± 0.04	4.59 ± 0.04	-0.4 ± 0.04	0.12	**1.32** (1.29 to 1.35)
6A IP	26.30 ± 0.06	22.19 ± 0.02	4.11 ± 0.06	-0.88 ± 0.06	0.27	**1.85** (1.77 to 1.92)
6A NP	27.41 ± 0.02	23.17 ± 0.03	4.24 ± 0.04	-0.75 ± 0.04	0.23	**1.68** (1.64 to 1.73)
6CC IP	28.74 ± 0.08	23.52 ± 0.05	5.22 ± 0.09	0.23 ± 0.09	-0.07	**0.86** (0.8 to 0.91)
6CC NP	29.83 ± 0.01	23.56 ± 0.05	6.27 ± 0.05	1.28 ± 0.05	-0.38	**0.42** (0.4 to 0.43)

C_T - threshold cycle, SEM - standard error of the mean, * - endogenous control, ** - calibrator sample. ΔC_T = C_T (Target) – C_T (Endogenous control). $\Delta\Delta C_T$ = ΔC_T (Target - ΔC_T (Calibrator).

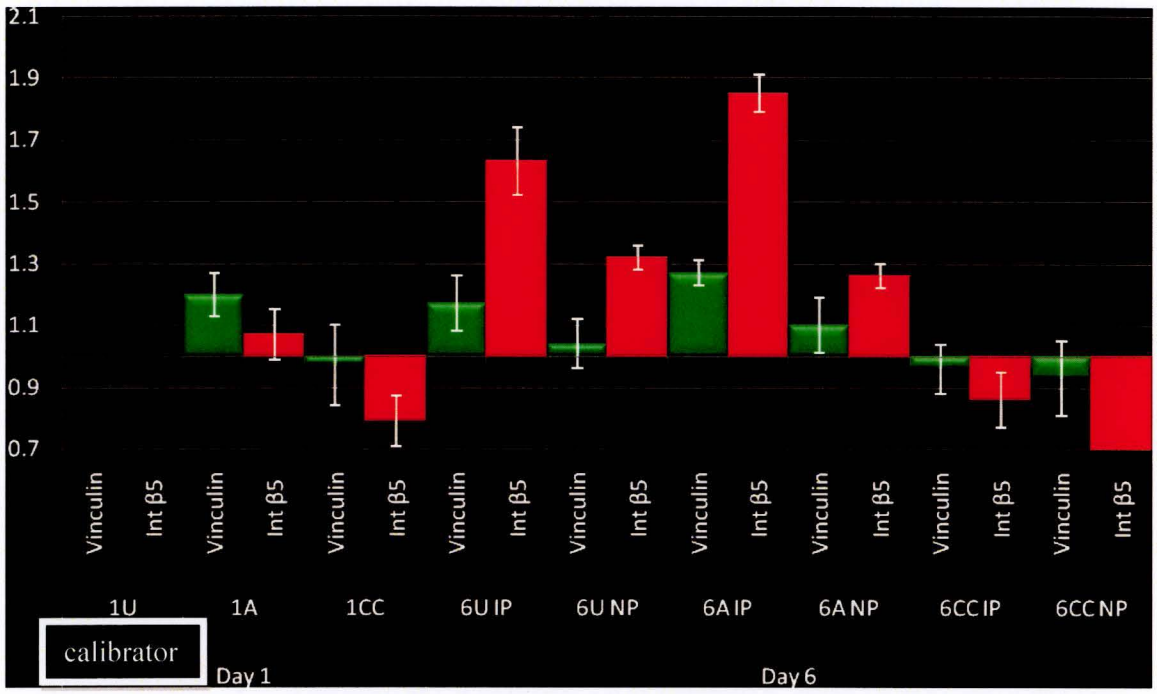


Figure 3.31: Graphical representation of vinculin and intergrin β5 gene expression in the surface luminal uterine epithelial cells of day 1 and day 6 pregnant rats. There is a significant difference in the gene expression of vinculin and integrin β5 between anastrozole day 1 and day 6 ($p<0.0001$) (Appendix G), untreated (control) day 1 and day 6 ($p<0.0001$) (Appendix G), untreated day 6 and CC day 6 ($p<0.0001$) (Appendix G). No significant difference is noted between CC day 1 and CC day 6 ($p>0.05$) (Appendix G), untreated day 6 and anastrozole day 6 ($p>0.05$) (Appendix G). Note: Generally, chlomiphene citrate (CC) seems to decrease their expression while anastrozole seems to enhance their expression as pregnancy progresses.

3.5.2 Relative quantification (RQ) analysis of paxillin and focal adhesion kinase (FAK) gene expression in the uterine epithelial cells from day 1 and day 6 pregnant rats

At day 1 of pregnancy, paxillin gene expression is fairly similar (1.02-fold increase) ($p>0.05$) (Appendix G) in uterine luminal epithelial cells in the anastrozole treated rats relative to the calibrator sample (day 1 untreated rats). This is also true for FAK gene expression (1.02-fold increase) ($p>0.05$) (Appendix G) suggesting that anastrozole favors their expression in readiness for implantation. Paxillin gene expression is slightly down-regulated (0.59-fold decrease) in uterine luminal epithelial cells in the chlomiphene citrate (CC) treated group when compared to the calibrator sample suggesting that CC seems to decrease its expression. This is also true for FAK gene expression (0.64-fold decrease) as shown in Tables 3.6, 3.7, Figure 3.30 and Appendix G. Notably, at day 6 of pregnancy, paxillin and FAK gene expression are significantly up-regulated (more than 1.5-fold increase) ($p<0.0001$) (Appendix G) in uterine luminal epithelial cells in the implantation and non-implantation sites in the anastrozole treated group relative to the calibrator sample (Tables 3.4, 3.5, Figure 3.29 and Appendix G) suggesting that anastrozole increases their expression in order perhaps to take a role in the implantation process. A significant increase in the paxillin gene expression is also noted in the day 6 implantation sites in the untreated group (more than 1.5-fold increase) ($p<0.05$) (Appendix G) while it has remained similar (1.32-fold increase) ($p>0.05$) (Appendix G) in the non-implantation sites relative to the calibrator sample (Tables 3.6, 3.7 and Figure 3.30). On the other hand, paxillin is down-regulated with chlomiphene citrate (CC) treatment in uterine luminal epithelial cells at day 6 in implantation sites (0.92-fold decrease) and non-implantation sites (0.89-fold decrease) relative to the calibrator sample suggesting that CC decreases its expression, and this may interfere with the implantation process of the embryo.

Interestingly, chlomiphane citrate (CC) seems not to down-regulate FAK gene expression in uterine luminal epithelial cells in implantation and non-implantation sites at day 6 (1.57-fold increase ($p<0.05$) (Appendix G) and 1.25-fold increase ($p>0.05$) (Appendix G) respectively, when compared to the calibrator sample (Table 3.7 and Figure 3.30) suggesting that FAK could disrupt cell signaling with chlomiphene citrate (CC) treatment.

In general, there is an increase in paxillin and FAK gene expression in uterine luminal epithelial cells in untreated and anastrozole treated rats, as pregnancy progresses, as reflected in the immunofluorescence experiments in order to perhaps assist in implantation.

Table 3.6: RQ analysis of paxillin gene expression in the luminal surface uterine epithelial cells of day 1 and day 6 of pregnant rats. A fold change of 1.5 or more represents a significant difference in gene expression ($p<0.05$) (Appendix G).

Sample	Pax Ave C_T	*RFG Ave C_T	ΔC_T	$\Delta\Delta C_T$	Log_{10} ($2^{-\Delta\Delta CT}$)	Fold change $2^{-\Delta\Delta CT}$
**1U	22.82 ± 0.03	22.81 ± 0.03	0.01 ± 0.04	0 ± 0.04	0	**1** (0.97 to 1.03)
1A	22.74 ± 0.03	22.75 ± 0.04	-0.01 ± 0.05	-0.02 ± 0.05	0.09	**1.02** (0.98 to 1.05)
1CC	22.83 ± 0.03	22.05 ± 0.06	0.78 ± 0.07	0.77 ± 0.07	-0.23	**0.59** (0.56 to 0.62)
6U IP	21.25 ± 0.02	22.59 ± 0.09	-1.34 ± 0.09	-0.58 ± 0.09	0.18	**1.5** (1.4 to 1.59)
6U NP	21.96 ± 0.03	22.37 ± 0.04	-0.41 ± 0.05	-0.42 ± 0.05	0.12	**1.32** (1.29 to 1.35)
6A IP	21.21 ± 0.04	22.19 ± 0.02	-0.98 ± 0.04	-0.99 ± 0.04	0.3	**2** (1.93 to 1.92)
6A NP	22.45 ± 0.06	23.17 ± 0.03	-0.72 ± 0.07	-0.73 ± 0.07	0.22	**1.66** (1.58 to 1.74)
6CC IP	23.66 ± 0.03	23.52 ± 0.05	0.14 ± 0.06	0.13 ± 0.06	-0.04	**0.92** (0.88 to 0.95)
6CC NP	23.75 ± 0.05	23.56 ± 0.05	0.19 ± 0.07	0.18 ± 0.07	-0.05	**0.89** (0.84 to 0.93)

C_T - threshold cycle, SEM - standard error of the mean, * - endogenous control, ** - calibrator sample. ΔC_T = C_T (Target) – C_T (Endogenous control). $\Delta\Delta C_T$ = ΔC_T (Target - ΔC_T (Calibrator).

Table 3.7: RQ analysis of FAK gene expression in the luminal surface uterine epithelial cells of day 1 and day 6 of pregnant rats. A fold change of 1.5 or more represents a significant difference in gene expression ($p<0.05$) (Appendix G).

Sample	FAK Ave C_T	*RFG Ave C_T	ΔC_T	$\Delta\Delta C_T$	Log_{10} ($2^{-\Delta\Delta CT}$)	Fold change $2^{-\Delta\Delta CT}$
**1U	25.64 ± 0.02	22.81 ± 0.03	2.83 ± 0.04	0 ± 0.04	0	**1** (0.97 to 1.03)
1A	25.55 ± 0.06	22.75 ± 0.04	2.8 ± 0.07	-0.03 ± 0.07	0.09	**1.02** (0.97 to 1.07)
1CC	25.54 ± 0.02	22.05 ± 0.06	3.49 ± 0.06	0.66 ± 0.06	-0.19	**0.64** (0.61 to 0.66)
6U IP	24.11 ± 0.07	22.59 ± 0.09	1.52 ± 0.11	-1.31 ± 0.11	0.40	**2.5** (2.3 to 2.68)
6U NP	25.19 ± 0.02	22.37 ± 0.04	2.82 ± 0.04	-0.01 ± 0.04	0.04	**1.01** (0.98 to 1.04)
6A IP	23.50 ± 0.17	22.19 ± 0.02	1.31 ± 0.17	-1.52 ± 0.17	0.46	**2.89** (2.55 to 3.23)
6A NP	24.84 ± 0.02	23.17 ± 0.03	1.67 ± 0.08	-1.16 ± 0.08	0.35	**2.24** (2.11 to 2.36)
6CC IP	25.7 ± 0.02	23.52 ± 0.05	2.18 ± 0.05	-0.65 ± 0.05	0.20	**1.57** (1.52 to 1.62)
6CC NP	26.07 ± 0.06	23.56 ± 0.05	2.51 ± 0.08	-0.32 ± 0.08	0.10	**1.25** (1.18 to 1.32)

C_T - threshold cycle, SEM - standard error of the mean, * - endogenous control, ** - calibrator sample. ΔC_T = C_T (Target) – C_T (Endogenous control). $\Delta\Delta C_T$ = ΔC_T (Target - ΔC_T (Calibrator).

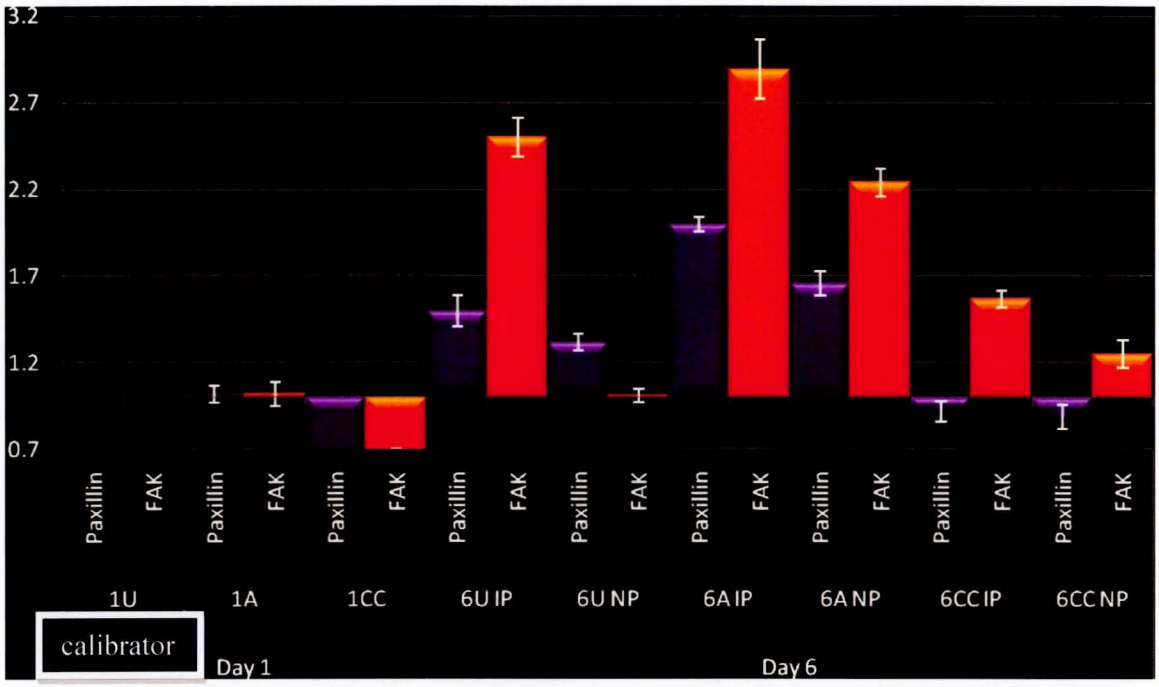


Figure 3.32: Graphical representation of paxillin and focal adhesion kinase (FAK) gene expression in luminal uterine epithelial cells in pregnant rats. There is a significant difference in the gene expression levels of paxillin and FAK between untreated (control) and chlomiphene citrate (CC) treated rats ($p<0.0001$) (Appendix G), anastrozole and CC treated rats at day 6 ($p<0.0001$) (Appendix G) suggesting that CC appears to decrease their expression. No significant difference is noted between untreated and anastrozole treated rats at day 6 ($p>0.05$) (Appendix G) although the means for paxillin and FAK expression are higher in the anastrozole treated than in the untreated groups. Compared to the calibrator sample, chlomiphane citrate (CC) seems not to down-regulate FAK gene expression in uterine luminal epithelial cells in implantation and non-implantation sites at day 6 (1.57-fold increase ($p<0.05$) (Appendix G).

4 CHAPTER FOUR: DISCUSSION AND CONCLUSIONS

4.1 Introduction and general structure

The overall aim of the study was to investigate the effects of anastrozole on the expression of focal adhesion proteins on the endometrium *in vivo* during implantation, which would enable manipulation of uterine receptivity to control fertility and improve the outcome of assisted reproductive procedures. The structure of this chapter follows the structure of the project design. The project was divided into two parts. Part one was a preliminary dose response study of anastrozole, where the aim was to determine the optimal dose of anastrozole that could give the highest number of implantation sites upon administration in the Wistar rats. The second part of the project (main study) employed scanning electron microscopy (SEM), immunofluorescence and confocal microscopy, hematoxylin and eosin (H&E) staining, and quantitative real time polymerase chain reaction (qPCR) techniques to determine the effects of anastrozole on the ultrastructure of the surface uterine epithelium during early pregnancy and to compare it as a superovulator to chlomiphene (CC) in similar situations; and to determine the expression levels (fluorescence intensities reflecting protein quantities) and localization of focal adhesion proteins vinculin, integrin β5, paxillin, and focal adhesion kinase (FAK) in the rat uterine epithelial cells during implantation in vivo. The hematoxylin and eosin (H&E) staining technique was employed to have a general overview of the histological changes of the uterine endometria between treatment groups with regard to the uterine surface luminal epithelia, stroma cells, intercellular ground substance, epithelial glands and blood vessels.

4.2 Anastrozole dose response study

A comparison of means of implantation sites between treatment groups was done using a one way ANOVA followed by a Tukey-Kramer HSD in order to determine the optimal dose and effectiveness of anastrozole as a superovulator. The most effective dose was the one that had the greatest number of implantation sites at day 6 of pregnancy and to compare it with the chlomiphene citrate (CC) treated and control animals. Differences were considered statistically significant when $p<0.05$. The rationale for this was that CC is generally associated with low implantation rates and therefore increased implantation sites are seen as an advantage.

The high molecular weight vital dye Pontamine sky blue was used to distinguish implantation sites from non-implantation sites because the dye quickly localizes in the implantation sites due to increased vascularization and vascular permeability during early pregnancy.

In this study, a significant increase in the number of implantation sites was found in the 15mg/kg of body weight anastrozole treated rats, 16.6 ± 0.8 (mean $\pm$ SE) (Appendix G) in comparison to control group (untreated), 7.8 ± 0.8 ($p<0.0001$) (Appendix G). There is also a significant difference in the number of implantation sites between chlomiphene citrate treated group, 11.6 ± 0.8 and control group, 7.8 ± 0.8 ($p<0.0315$) (Appendix G); chlomiphene citrate treated group, 11.6 ± 0.8 (Appendix G) and the 15mg/kg anastrozole treated rats, 16.6 ± 0.8 ($p<0.0022$) (Appendix G). Earlier investigators also have noted an average of 7.2 embryos produced per pregnancy in normal untreated rats (Jaramillo *et al.,* 2012). This seems to indicate that the 15mg/kg anastrozole superovulates and achieves pregnancy in the Wistar rats. This evidence also confirms earlier hypotheses and findings that suggest that the standard

1mg/kg anastrozole of body weight dose is too low for optimal follicle recruitment and ovulation in rats, so they have recommended higher doses (Badawy *et al.*, 2008; Tredway and Schertz, 2011).

The 15mg/kg anastrozole appears to be so effective in causing ovulation and achieving pregnancy suggesting that anastrozole may allow just enough of the intermediates and E_2 to be present with regard to the hormone profiles for ovulation and successful implantation of the embryo because anastrozole is a competitive inhibitor of aromatase in the conversion of androgens to estrogens (Buzdar, 2011). Essentially, it may appear that there is blocking of E_2 and increasing of androgens in anastrozole treated rats compared to controls. Progesterone (P) is probably also high as E_2 is low (Cortinez *et al.*, 2005). In CC treated rats, estrogen receptors are blocked and thus increased E_2 (Cortinez *et al.*, 2005), but androgens are presumably low. The effect of anastrozole in the level of E_2 and P may change the E_2/P ratio at day 6 of pregnancy, suggesting its effect on endometrial maturation and therefore improving receptivity.

The current study also found no significant difference in the mean number of implantation sites between the 25mg/kg anastrozole group, 10.6 ± 1.1 and control, 7.8 ± 0.8 ($p<0.2026$) (Appendix G); 25mg/kg anastrozole and chlomiphene citrate group ($p<0.9715$) (Appendix G). This suggests that the effectiveness of higher anastrozole doses in ovulation stimulation and achieving pregnancy has a threshold as indicated by decreased implantation sites observed in the 25mg/kg anastrozole treated rats in the present study. In contrast, previous studies done in mice have noted that the 25 mg/kg anastrozole dose has been successful in inducing ovulation in mice and is associated with favorable embryo development (Karaer *et al.*, 2005). It could be speculated, therefore, that the anastrozole optimal dose could be species specific.

Notably, the present study has provided strong evidence that the 15mg/kg anastrozole dose superovulates and favours implantation in the Wistar rats and additionally appears to be dose specific. Together with the observed varying optimal doses among different species suggest that they could be species specific and therefore should be (and probably is worth) investigated in humans (Badawy *et al.*, 2008; Mitwally and Casper 2002).

4.3 Uterine surface ultrastructure

A high resolution SEM was also performed in this study to determine the effects of anastrozole on the surface uterine morphology during early pregnancy and to compare it as a superovulator to chlomiphene citrate (CC) in similar situations. The uterine morphological characteristics which were studied in day 1 and 6 pregnant rats include microvilli density, microvilli length, microvilli surface "beads", large surface protrusions (pinopods), membrane pores, uterine surface fording, surface glycocalyx, epithelial gland openings, small secretions, cell apices and cell borders. Day 6 of pregnancy is when attachment of the blastocyst has begun (Murphy 2004).

The results of the present study show that day 1 and 6 anastrozole groups have similar morphology to the control ($p>0.05$) (Appendix G) and significantly different to chlomiphene citrate (CC) group ($p<0.0001$) (Appendix G). This study observes a change from long thin microvilli of medium density at day 1 of pregnancy, in terms of distribution, to short irregular sparse microvilli at day 6 in implantation sites, as the non-implantation sites retain relatively denser and longer microvilli in all groups. Moreover, microvilli in implantation sites of day 6 anastrozole group are the shortest. As expected, more membrane pores are also visible at day 6

than at day 1 of pregnancy in all groups suggesting that the uterine epithelium apical membrane surface flattens as it approaches the day of implantation to facilitate blastocyst-uterus apposition and adhesion. Similarly, previous studies have reported that in a receptive uterus, long, thin, regular microvilli at day 1,which are under the control of estrogen hormones, are replaced by flattened irregular projections that promote apical membrane flattening at day 6 of pregnancy, which are modulated by progesterone (Murphy, 2004) in implantation sites, as the non-implantation sites retain relatively longer and more dense microvilli as also reported by Scholtz *et al.*, (2008), except in the anastrozole group where the microvilli are the shortest. It could be postulated that the decrease in microvilli density and length also possibly allow the membrane pores to be more visible in a receptive uterus at day 6 of pregnancy in this study. Apical membrane flattening is part of the 'plasma membrane transformation' in which the uterine surface epithelium undergoes apical and basal alterations to become receptive to the blastocyst (Murphy, 2004). Therefore, anastrozole would appear to promote the apical membrane flattening of the uterine surface epithelium and thus its significance in enhancing the uterine receptivity to the blastocyst implantation.

The current study has also observed a significant change from the deep uterine surface folding at day 1, believed to be estrogen controlled, to smooth uterine surface at day 6 in implantation sites ($p<0.0001$) (Appendix) as non-implantation sites remain folded in all groups ($p>0.05$) (Appendix). Earlier studies have reported similar observations in which implantation sites have smooth uterine surface while the non-implantation sites seem to retain deep transverse uterine folds during early pregnancy in rats (Hosie *et al.*, 2003; Scholtz *et al.*, 2008). The implication of this uterine morphological change is to promote the flattening of uterine surface

in order to facilitate the blastocyst apposition and implantation at day 6 of pregnancy. With respect to hormonal signaling, it would appear that anastrozole enhances the co-relationship of progesterone and estrogen hormones during early pregnancy in order to establish a receptive uterus as suggested by other studies (Hewitt and Korach, 2000).

Intriguingly, anastrozole also appears to retain surface uterine glycocalyx to some extent during implantation in the current study. Glycocalyx molecules generally are reduced as pregnancy progresses (Hosie *et al.*, 2003) as this might facilitate the apposition of the blastocyst and uterine cellular surfaces in the implantation process. However, specific glycocalyx molecules used in implantation are retained during implantation (Murphy, 2004). Moreover, glucosamine trisaccharides and mucin 13 are some of the glycocalyx molecules that are believed to be retained during early pregnancy to contribute to the success of blastocyst implantation (Murphy and Turner, 1991; Poon *et al.*, 2014). On the contrary, CC decreases the expression of glucosamine trisaccharides on the rat uterine surface (Hosie *et al.*, 2003). Because of the limitations with the use of SEM to study the molecular glycocalyx composition in this study, it would seem that further molecular and immunofluorescence studies on the glycocalyx of the luminal surface uterine epithelial cells are necessary to better elucidate the types of glycocalyx molecules that are retained during implantation with anastrozole treatment. It is not surprising, however, to observe some glycocalyx in the anastrozole treated rats at day 6 of pregnancy, which could be used in implantation. These results taken together, indicate that the surface uterine epithelial characteristics observed in anastrozole treated rats enhance uterine receptivity, suggesting that anastrozole achieves a better uterine environment for pregnancy when compared to chlomiphene citrate (CC).

Furthermore, the uterine epithelial cells from day 1 of all groups show flat cell borders and slightly bulged cell apices while those from the implantation sites of day 6 untreated and anastrozole treated rats show flat cell borders and slightly bulged cell apices. It is interesting to note that day 6 chlomiphene citrate treated rats have raised cell borders and flat cell apices in the present study. If the current study had treated the rats with an anti-progesterone drug such as RU486 or Mifepristone, raised cell borders would likely be observed in day 6 implantation and non-implantation sites as noted earlier in some studies done in rats (Scholtz *et al.*, 2008). These findings from the present study strongly confirm earlier observations in which chlomiphene citrate (CC) seems to disrupt some of the well documented normal uterine surface ultrastructure seen at the time of implantation (Murphy and Shaw 1994; Hosie *et al.*, 2003; Scholtz *et al.*, 2008) among which the recessed uterine epithelial cell borders seen at day 6 of pregnancy, with CC treatment these cell borders are raised (Hosie *et al.*, 2003). Additionally, CC appears to cause similar uterine cell border morphology to RU486 suggesting that CC might interfere with progesterone activity during early pregnancy. Moreover, Bonhoff *et al.*, (1996) have speculated that such an impaired endometrial morphological development during early pregnancy with CC treatment, which is a sensitive interval in preparation for implantation, might lead to an effective asynchrony between embryonic and uterine development and unfavourably influence the outcome of implantation. Other researchers have also suggested that the aberrant apoptotic activities of the uterine stromal cells after chronic CC treatment maybe a mechanism whereby the implantation process is disrupted (Nutu *et al.*, 2010). This means that CC can cause apoptosis in some cell types. In this regard, it is also tempting to speculate that the raised borders of uterine epithelial cells in the CC treated rats could be an apoptotic characteristic activity due to CC treatment in the present study although previous studies seem to contradict with this hypothesis because

these studies have suggested that CC does not disrupt the normal apoptotic activity seen at implantation, but does change the morphology of the luminal epithelium, which could influence successful implantation (Hosie and Stewart, 2006). While ovarian hormones regulate the morphology of the luminal epithelium, the complex apoptotic pathways in the uterus are not specifically regulated by ovarian hormones alone (Hosie and Stewart, 2006). However, in the current study, anastrozole appears to effectively cause ovulation and to promote implantation in the Wistar rats suggesting that there is blocking of E_2 and increasing of androgens in anastrozole treated rats compared to controls because anastrozole is a competitive inhibitor of aromatase in the conversion to androgens to estrogens (Buzdar, 2011). Progesterone (P) is probably also high as E_2 is low (Cortinez *et al.*, 2005). In CC treated rats, estrogen receptors are blocked and thus increased E_2, but androgens are presumably low. The effect of anastrozole in the level of E_2 and P may change the E_2/P ratio at day 6 of pregnancy, suggesting its effect on endometrial maturation including surface uterine epithelial morphological changes such as cell borders, and therefore improving receptivity. All in all, if the hypothesis regarding the raised cell borders in CC treated rats in the present study is true, anastrozole continues to achieve a better uterine environment for pregnancy when compared to CC. In summary, these observations of the abnormalities that are seen in the uterus after CC treatment in this study combined with the significant low pregnancy rates associated with CC treatments (Casper and Mitwally, 2011), make anastrozole a potential substitute oral ovulatory drug, which has proven superiority to CC that could be used without the risk of hyperstimulation and with minimal monitoring and thus emerging as the new first-line treatment for anovulatory or ovulatory infertility.

It is also of interest to note that large surface protrusions (pinopods) are mostly noted but not limited to anastrozole treated rats at day 6 of pregnancy in this study. These observations further demonstrate an improved uterine surface morphology in anastrozole treated rats in which anastrozole seems to promote short irregular sparse microvilli, flat cell borders, slightly doming cell apices and most importantly large cell surface protrusions (pinopods) believed to be associated with successful implantation (Nikas, 1997; Creus *et al.*, 2003; Hosie *et al.*, 2003; Murphy, 2004; Scholtz *et al.*, 2008). Pinopods, which mediate endocytosis, appear in a receptive uterus (Nikas, 1997; Murphy, 2004) and seem to be among the important markers of the window of implantation and thus used in clinical fertility programs (Adams *et al.*, 2001; Creus *et al.*, 2003). These pinopods are believed to promote apical uterine surface membrane flattening (Nikas, 1997). Earlier studies have reported a potential deleterious effect of CC on endometrial pinopod formation (Creus *et al.*, 2003). On the contrary, Cortinez *et al.*, (2005) have observed normal morphology of the endometrium and full formation of pinopods during the implantation window when aromatase inhibitors such as letrozole are used (Cortinez *et al.*, (2005). It will be important to consider the implications of the increase in the number of pinopods observed in anastrozole treated rats at day 6 and what this observation suggests about the possible additional functions for pinopods. It could be speculated that these pinopods might also contain adhesion molecules which are believed to be crucial in the process of embryo implantation (Kaneko *et al.*, 2008). If this is true, indeed anastrozole promotes a better uterine environment for embryo implantation and thus a particularly interesting finding of this study. However, transmission electron microscopy (TEM) and molecular studies would be recommended to ascertain whether anastrozole affects the composition of pinopods in order to clarify their additional significance in implantation and their involvement in fertility-promoting strategy.

Earlier studies have shown that aromatase inhibitors (AIs) may act on critical amino acid residues in the active site and access channel to interfere with the aromatase enzyme activity and haem stability and thus preventing the aromatization of androgens to estrogens (Ghosh *et al.*, 2010; Ghosh *et al.*, 2013). Anastrozole, therefore, inhibits aromatase enzyme, which in turn reduces estradiol levels (Ghosh *et al.*, 2010). An earlier study has demonstrated that administration of aromatase inhibitors results in increased follicle stimulating hormone and luteinizing hormone (Sinha *et al.*, 1998). Fatum *et al.* (2006) have observed that anastrozole treatment during follicular phase does not hamper follicular development, oocyte fertilization *in vivo* or embryo development in mice. Other studies have shown that aromatase inhibitors achieve a better uterine environment including increased blood flow and endometrial thickness; these parameters are both associated with higher pregnancy rates (Adams *et al.*, 2001; Murphy, 2004; Karaer *et al.*, 2005). These studies support the findings of the current work in which anastrozole seems to promote blastocyst implantation in the Wistar rats.

Put together, our evidence for increased implantation sites in the Wistar rats treated with the 15mg/kg anastrozole suggests that this particular dose superovulates and favors implantation in this species. It also confirms earlier studies that suggest higher anastrozole doses for ovulation induction, but to a limit as observed in the 25mg/kg of body weight anastrozole treated rats. The surface uterine epithelial morphology further demonstrates that anastrozole is implantation friendly. The observed success of anastrozole in inducing ovulation and achieving pregnancy in the Wistar rats is provocative and warrants further research. Most importantly, anastrozole may indeed be a suitable replacement or alternative drug used for

hyperovulation or just to promote fertility in patients, particularly those suffering from polycystic ovary syndrome or are unresponsive to chlomiphene citrate (CC).

4.4 Focal adhesion protein dynamics in rat uterus

During implantation, focal adhesion proteins disassemble from the base of the epithelium to facilitate the detachment of the uterine luminal epithelium to allow the embryo to invade the endometrium (Kaneko *et al.* 2011). At the same time, they assemble and become localized apically to assist in the adhesion of the blastocyst onto the endometrium (Kaneko *et al.*, 2011; 2012). In order to further ascertain the effectiveness of anastrozole as a superovulator, one of the objectives of this study was to determine the effects of anastrozole on the expression levels (fluorescence intensities reflecting protein quantities) and the main epithelial domain localization of focal adhesion proteins vinculin, integrin β5, paxillin, and focal adhesion kinase (FAK) in the rat uterine epithelial cells during implantation *in vivo* and to compare it to chlomiphene citrate (CC) in similar situations.

4.4.1 Gene and protein expression of vinculin and integrin β5

In the current study, the focal adhesion proteins vinculin and integrin β5 are co-localized at the base of the uterine epithelium at day 1 of pregnancy whereas at day 6, they disassemble from the basal focal adhesions and co-localize and significantly increase their expression apically ($p<0.0001$) (Appendix G). Additionally, vinculin is also expressed in the perinuclear region at day 1 and relocates apically at day 6 of pregnancy. Moreover, there is a significant difference in the protein expression levels of both vinculin and integrin β5 between untreated (control) and chlomiphene citrate (CC) treated rats ($p<0.0001$) (Appendix G), anastrozole and chlomiphene citrate (CC) treated rats at both day 1 and day 6 ($p<0.0001$) (Appendix G) suggesting that CC seems to decrease their expression. Although there is no significant difference in the expression levels between untreated and anastrozole treated rats at day 1 and day 6 ($p>0.05$) (Appendix G), the means for vinculin and integrin β5 protein expression are higher in the anastrozole treated groups (Appendix G) suggesting that anastrozole seems to enhance their expression in order to assist in the implantation process of the embryo.

In the present study, the vinculin and integrin β5 gene expression in uterine luminal epithelial cells at day 1 of pregnancy agrees with the protein expression. Vinculin gene expression is fairly similar (1.2-fold increase) ($p>0.05$) (Appendix G) in the anastrozole treated rats relative to the calibrator sample (day 1 untreated rats). This is also true for integrin β5 gene expression (1.01-fold increase) ($p>0.05$) (Appendix G) suggesting that anastrozole does not retard vinculin and integrin β5 gene expression in the process of endometrial readiness for implantation. Vinculin and integrin β5 gene expression in uterine luminal epithelial cells,

however, is down-regulated (0.77-fold decrease) and (0.79-fold decrease) respectively with chlomiphene citrate (CC) treatment at day 1 of pregnancy relative to the calibrator sample suggesting that CC seems to decrease their expression. Interestingly, like the immunofluorescence experiments, at day 6 of pregnancy vinculin and integrin β5 gene expression are significantly up-regulated (more than 1.5-fold increase) ($p<0.0001$) (Appendix G) in uterine luminal epithelial cells in the implantation and non-implantation sites in the anastrozole treated group relative to the calibrator sample. A significant increase in the integrin β5 gene expression is also noted in uterine luminal epithelial cells of day 6 implantation sites in the untreated group (more than 1.5-fold increase) ($p<0.0001$) (Appendix) while it has remained similar (1.04-fold increase) ($p>0.05$) (Appendix G) in the non-implantation sites relative to the calibrator sample suggesting that anastrozole appears to enhance their expression to probably assist in the implantation process of the embryo. However, vinculin gene expression in uterine luminal epithelial cells is down-regulated with chlomiphene citrate (CC) treatment at day 6 in implantation sites (0.96-fold decrease) and non-implantation sites (0.93-fold decrease) relative to the calibrator sample. This is also true for integrin β5 gene expression (0.86-fold decrease and 0.42-fold decrease) respectively suggesting that chlomiphene citrate (CC) seems to decrease their expression, which may lag endometrial receptivity. In general, there is an increase in vinculin and integrin β5 gene expression at day 6 of pregnancy in uterine luminal epithelial cells in untreated and anastrozole treated groups, as reflected in the immunofluorescence experiments suggesting that anastrozole favours implantation.

Vinculin is one of the core and best characterized focal adhesion (FA) proteins (Humphries *et al.*, 2007; Carisey *et al.*, 2013). Tyrosine phosphorylation of vinculin modifies focal adhesion dynamics and cell tractions (Kupper *et al.*, 2010). Vinculin regulates the recruitment and release of other core focal adhesion proteins in a force dependent manner and interacts with the talin-integrin complex and thus drives the recruitment and release of core FA components (Humphries *et al.*, 2007; Carisey *et al.*, 2013). Earlier studies have shown that lack of cytoskeletal connecting proteins like vinculin, talin and focal adhesion kinase (FAK) reduces the overall cellular binding strength (Carisey *et al.*, 2013). Moreover, the structural links between actin filaments and integrins are regulated in at least some cell types and it would not be unreasonable to hypothesize that agents known to alter cell behavior may do so by affecting the expression or function of actin binding proteins such as vinculin, talin, α-actinin, paxillin, and signaling molecules such as focal adhesion kinase (FAK) which are recruited to focal adhesions (Mwakikunga *et al.*, 2011). As mentioned earlier, focal adhesions disassemble from the base of uterine luminal epithelial cells at the time of implantation to facilitate their removal so that the implanting blastocyst can invade into the underlying endometrial decidual cells during early pregnancy in the rat (Kaneko *et al.*, 2009). In their study, another core FA protein talin shows a major distributional change between different hormone regimes. Talin is highly concentrated along the basal cell surface of uterine luminal epithelial cells in response to estrogen treatment which is observed at day 1 of pregnancy. However, this prominent staining of talin is absent in response to progesterone alone or progesterone in combination with estrogen, which is also observed at the time of implantation (Kaneko *et al.*, 2009). This supports one of the important findings of the present study as noted in the immunofluorescence experiments in which vinculin and integrin β5 disassemble from the base

of the uterine epithelium at day 1 of pregnancy and co-localize and increase their expression apically at day 6 of pregnancy to facilitate the implantation process.

Of particular significance, the disassembly of vinculin and integrin β5 from the basal focal adhesions and their apical expression increase at day 6 of pregnancy in the anastrozole treated rats means that anastrozole favours implantation. Moreover, integrin $\alpha_V\beta_3$ is required for endometrial receptivity (Zhang *et al.*, 2011). Other studies have demonstrated that human preimplantation embryos constitutively express integrin β3 and integrin β5 subunit proteins (Bloor *et al.*, 2002). Put together, this means that integrins play a role in the implantation process and could be regulated by agents that are known to alter cell behavior such as anastrozole and chlomiphene citrate (CC).

On the other hand, the decrease in the apical vinculin and integrin β5 expression with chlomiphene citrate (CC) treatment at day 6 in the current study suggests that CC might negatively affect the implantation process in this regard. This agrees with earlier studies that have also observed a decrease in uterine integrin β_3 expression in chlomiphene citrate (CC) treated patients during the window of implantation suggesting that chlomiphene citrate (CC) might affect the expression of uterine receptivity markers (Palomino *et al.*, 2005). On the contrary, other studies have noted that chlomiphene citrate (CC) does not affect the secretion of integrin α3, integrin αV and integrin β1 during the implantation window in patients with unexplained infertility (Lacin *et al.*, 2001). All in all, chlomiphene citrate (CC) appears to negatively affect the implantation process by down-regulating the expression of key

implantation markers such as vinculin and integrin β5 and thus being associated with low pregnancy rates.

Additionally, other studies done on the effects of letrozole and chlomiphene citrate (CC) on the expression of integrin $\alpha_V\beta_3$ during implantation in rats show that the expression of integrin $\alpha_V\beta_3$ in the CC group is significantly lower than in the letrozole and saline groups (Bao *et al.*, 2009). This study further shows that letrozole affects the HOXA 10 in uterine epithelium, but has no effect on the expression of integrin $\alpha_V\beta_3$ suggesting that CC suppresses uterine receptivity more than letrozole (Bao *et al.*, 2009). Similar observations are made by previous studies in which the expression of the molecular markers of endometrial receptivity, integrin $\alpha_V\beta_3$ and glycodelin, are decreased in endometrial biopsy specimens from women with PCOS when ovulation is induced with clomiphene citrate (Gonzalez *et al.*, 2001; Jakubowicz *et al.*, 2001). Interestingly, these observations agree with the results of the current study in which integrin β_5 expression in the uterine luminal epithelial cells of CC treated rats is significantly lower than anastrozole and untreated groups during implantation ($p<0.0001$) (Appendix G). However, in the present study, integrin β_5 disassembles from the basal focal adhesions and later get localized at the apical plasma membrane of the rat uterine luminal epithelial cells at the time of implantation as also noted by Kaneko *et al.*, (2011) in their studies with integrin β_3. As stated earlier, the implication of this disassembly of focal adhesions is to facilitate the removal of the uterine luminal epithelial cells for blastocyst invasion. The focal adhesion proteins are then localized apically to promote adhesion of the blastocyst during implantation.

Integrin β_5 associates with α_V to form an RGD dependent receptor for fibronectin, vitronectin or osteopontin (Felding-Habermann and Cheresh, 1993; Liaw *et al.*, 1995). Therefore, integrin β_5 is a component of focal adhesions. Moreover, integrin β_5, β_3 and α_V are apically distributed in uterine epithelial cells during implantation (Aplin *et al.*, 1996) suggesting their crucial role in the implantation process. Similarly, Creus *et al.*, (2003) have shown that the human endometrial maturity is characterized by integrin $\alpha_V\beta_3$ expression and pinopod formation. Therefore, this clearly shows that integrins (including integrins β5) are pivotal with regard to blastocyst-uterus interaction during early pregnancy.

Viewed in its totality, anastrozole seems to enhance the focal adhesion protein vinculin and integrin β5 expression at day 6 suggesting that anastrozole is implantation friendly as also evidenced by its high implantation rates in this study. In order to justify the vinculin and integrin β5 protein expression at day 6 of pregnancy in the anastrozole group, the results from the gene expression experiments are consistent with the immunofluorescence results.

4.4.2 Gene and protein expression paxillin and focal adhesion kinase (FAK)

In this study, paxillin is localized in focal adhesions at the base of the uterine epithelial cells at day 1 of pregnancy; at day 6 paxillin disassembles from the basal focal adhesions and localizes and significantly increases its expression apically ($p<0.0001$) (Appendix G). Additionally, FAK is faintly expressed at the basal aspect of the uterine epithelial cells while moderately expressed at the cell-to-cell contact at day 1 in all groups from where it disassembles and relocates apically and becomes significantly more intensely expressed ($p<0.05$) (Appendix G) at day 6 of pregnancy in untreated and anastrozole treated rats.

Although paxillin is localized apically at day 6, its expression is significantly down-regulated with chlomiphene citrate (CC) treatment ($p<0.05$) (Appendix G) suggesting its interference with the implantation process. However, there is a significant difference in the expression levels of paxillin and FAK between untreated (control) and chlomiphene citrate (CC) treated rats ($p<0.0001$) (Appendix G), anastrozole and chlomiphene citrate (CC) treated rats at day 6 ($p<0.0001$) (Appendix G) suggesting that CC appears to decrease their expression. Although there is no significant difference between untreated and anastrozole treated rats at day 6 ($p>0.05$) (Appendix G) in uterine luminal epithelial cells, the means for paxillin and FAK expression are higher in the anastrozole treated than in the untreated groups suggesting that anastrozole seems to enhance their expression probably to help in the implantation process of the embryo. Paxillin and FAK do not co-localize in focal adhesions at the base of the epithelium at day 1, but they co-localize and significantly increase their expression apically at day 6 ($p<0.0001$) (Appendix G) suggesting their role in the implantation process.

With regard to the paxillin and FAK gene expression experiments in this study, at day 1 of pregnancy, paxillin gene expression is fairly similar (1.02-fold increase) ($p>0.05$) (Appendix G) in uterine luminal epithelial cells in the anastrozole treated rats relative to the calibrator sample (day 1 untreated rats). This is also true for FAK gene expression (1.02-fold increase) ($p>0.05$) (Appendix G) suggesting that anastrozole favors their expression in readiness for implantation. Paxillin gene expression is slightly down-regulated (0.59-fold decrease) in uterine luminal epithelial cells in the chlomiphene citrate (CC) treated group when compared to the calibrator sample suggesting that CC seems to decrease its expression. This is also true for FAK gene expression (0.64-fold decrease). Notably, at day 6 of pregnancy, paxillin and

FAK gene expression are significantly up-regulated (more than 1.5-fold increase) ($p<0.0001$) (Appendix G) in uterine luminal epithelial cells in the implantation and non-implantation sites in the anastrozole treated group relative to the calibrator sample suggesting that anastrozole increases their expression in order perhaps to take a role in the implantation process. A significant increase in the paxillin gene expression is also noted in the day 6 implantation sites in the untreated group (more than 1.5-fold increase) ($p<0.0001$) (Appendix G) while it has remained similar (1.32-fold increase) ($p>0.05$) (Appendix G) in the non-implantation sites relative to the calibrator sample. On the other hand, paxillin is significantly down-regulated with chlomiphene citrate (CC) treatment in uterine luminal epithelial cells at day 6 in implantation sites (0.92-fold decrease) ($p<0.05$) and non-implantation sites (0.89-fold decrease) ($p<0.05$) relative to the calibrator sample suggesting that chlomiphene citrate (CC) decreases its expression, and this may interfere with the implantation process of the embryo. Interestingly, chlomiphene citrate (CC) seems not to down-regulate FAK gene expression in uterine luminal epithelial cells in implantation and non-implantation sites at day 6 (1.57-fold increase ($p<0.05$) (Appendix G) and 1.25-fold increase ($p>0.05$) respectively) when compared to the calibrator sample suggesting that FAK could disrupt cell signaling with chlomiphene citrate (CC) treatment.

In general, there is an increase in paxillin and FAK gene expression in uterine luminal epithelial cells in the untreated and anastrozole treated rats, as pregnancy progresses, as reflected in the immunofluorescence experiments in order to perhaps assist in implantation.

Focal adhesion kinase (FAK) is phosphorylated on tyrosine residues upon integrin-mediated adhesion to a substratum (Zhao and Guan, 2009). FAK exhibits a high degree of evolutionary conservation between species at the amino acid level (>94%) suggesting that it might play a crucial function in the cell (Corsi *et al.*, 2006). FAK is important in maintenance of normal cell survival, and disruption of FAK signaling results in loss of substrate adhesion and apoptosis of anchorage-dependent cells such as endothelial cells (Lu and Rounds, 2011). FAK is a key component of cell-substratum adhesions, known as focal adhesion complexes, and it maintains cell adhesion to integrins via PI3 kinase/AKt signaling (Lu and Rounds, 2011). FAK activity is dependent upon small GTPase signaling.

Maturity of focal adhesions enhances FAK's catalytic activity and increases FAK tyrosine phosphorylation (Mitra et al., 2005). FAK autophosphorylation at tyrosine 397(Y3a7) leads to recruitment of Src and Src-family kinases as well as to an increased phosphorylation of other focal adhesion proteins such as paxillin (Mitra *et al.*, 2005). It is not surprising, therefore, that anastrozole appears to enhance the gene and protein expression of FAK and paxillin during implantation in the present study.

Other studies have demonstrated that site-specific FAK phosphorylation is also triggered by mechanical forces and determines physiological cellular responses to shear stress and cyclic stretch. In these studies, FAK has been noted to have multitude of phosphorylation sites, making it an ideal anchor for participating in mechanotransduction (Cabodi *et al.*, 2010). Similarly, some investigators have found that FAK associates with multiple cell surface receptors and is at a point of convergence of integrin and growth factor mechanical signaling pathway (Long *et al.*, 2010).

FAK stabilizes the cytoskeleton by promoting focal adhesion turn-over through a rho-kinase (ROCK)-dependent pathway (Nehru *et al.*, 2013). FAK inhibition disrupts integrin β5 signaling anchorage mechanism (Tancioni *et al.*, 2014).

Of special note, progesterone enhances vascular endothelial cell migration via activation of FAK (Zheng *et al.*, 2012). Additionally, progesterone has been seen to enhance breast cancer cell motility and invasion via extranuclear activation of FAK (Fu *et al.*, 2010). This means that progesterone can regulate FAK activities. This is clearly consistent with the findings of the present study in which the high FAK expression on the apical uterine epithelium together with paxillin, vinculin and integrin β5 in the anastrozole and control groups coincides with the implantation period, which is also progesterone controlled (Diao *et al.*, 2011). Moreover, progesterone is known to highly up-regulate junctional adhesion molecule 2 (Jam 2) in the luminal epithelium of receptive rat uterus via tyrosine phosphorylation of Stat 3 suggesting that Jam 2 may play a role in the interaction between blastocyst and receptive uterus (Su *et al.*, 2012). Other studies have suggested that the up-regulation of the adhesion molecule ICAM 1 in the uterine epithelium in rats is under the control of progesterone at the time of implantation (Lecce *et al.*, 2011). As in the current study, the focal adhesion proteins, which are receptivity markers, appear to be up-regulated during the progesterone controlled, implantation period, in both day 6 anastrozole and control groups. Taken together, anastrozole continues to demonstrate that it enhances the uterine receptivity during implantation.

While it is also interesting and understandable to note from the results of the present study that chlomiphene citrate (CC) seems not to down-regulate FAK gene expression in implantation and non-implantation sites at day 6 (1.57-fold increase and 1.25-fold increase respectively) when compared to the calibrator sample, CC appears to down regulate FAK protein expression in uterine luminal epithelial cells at day 6 of pregnancy. This discrepancy in the results of this study raises the question of the normal molecular dogma of DNA-mRNA-protein. However, it could be argued that this is one of the limitations of real-time qPCR in that detection of the presence of an mRNA provides no information on whether that mRNA will be translated into a protein or indeed whether a functional protein is translated at all (Derveaux *et al.*, 2010). In summary, this means that some of the FAK mRNAs might have not been translated into functional proteins in uterine luminal epithelial cells at day 6 of pregnancy in the chlomiphene citrate (CC) treated animals, and thus their increased gene and decreased protein expression as suggested by Derveaux *et al.*, 2010. It follows, therefore, that not all mRNAs are translated into proteins, and thus the decreased FAK protein expression in uterine luminal epithelial cells in the chlomiphene citrate (CC) treated rats at day 6 of pregnancy in the immunofluorescence experiments in this study suggesting that FAK down regulation might affect the attachment of the blastocyst onto the uterus during implantation. If this study had found that chlomiphene citrate (CC) significantly increased FAK protein expression, the question of whether this specific biological change interferes with implantation and pregnancy rates would still be a matter of debate.

Moreover, FAK and vinculin have been shown to strengthen cellular stiffness in mouse embryonic fibroblasts (Klemm *et al.*, 2009). FAK is also known to be crucial in the

coordination of the appropriate mechanical properties to cell-cell contacts through cadherin-catenin-actin interactions in which focal adhesions sense the physical properties of the extracellular matrix (ECM) and organize the cytoskeleton accordingly (Quadri, 2011). Other studies have suggested that FAK is a mediator of crosstalk between integrin-mediated FAs and intercellular adherens junctions (Zachary, 2003). This clearly shows that FAK is at the centre of focal adhesion assembly, and therefore, anastrozole might positively affect its expression during implantation (Kaneko *et al.*, 2012).

Immunofluorescence and focal adhesion localization studies done in rats during early pregnancy have revealed that FAK does not localize at the site of focal adhesions, instead it is localized to the site of cell-to-cell contact and colocalise with ZO-1 at day 1 of pregnancy (Kaneko *et al.*, 2012), and this is also observed in other cell types (Quadri and Bhattacharya, 2007). At day 6 of pregnancy, FAK expression increases at the apical region of the rat uterine luminal epithelial cells, regulated by progesterone (Kaneko *et al.*, 2012). It is not surprising, therefore, to see in the current study that FAK re-locates and significantly increases its expression apically ($p<0.05$) (Appendix G) in the rat uterine epithelial cells at day 6 in both untreated and anastrozole treated rats. Moreover, junctional barrier complexes undergo major alterations during the plasma membrane transformation of uterine epithelial cells in early pregnancy (Murphy, 2000). These morphological and molecular alterations allow the conclusion that while paracellular permeability is reduced by the time of blastocyst attachment, the epithelial cells are paradoxically less firmly attached to each other, and to their extracellular environment (Murphy, 2000). Taken together, anastrozole still continues to demonstrate that it promotes the uterine environment for implantation.

Actin filaments play a role in the dynamics of paxillin assembly and disassembly (Hu *et al.*, 2006) and tyrosine phosphorylation is an important element in paxillin dynamics at focal adhesions (Hu *et al.*, 2006). In addition, FAK is targeted to the focal adhesion (FA) complexes via direct binding to paxillin (Liu *et al.*, 2002) and p130Cas (Polte and Hanks, 1997). Activated Src also binds to the Src-binding domain (SBD) of p130Cas. Multiple interactions between FAK, Src, p130Cas, and paxillin regulate the dynamic FA assembly and disassembly, as reviewed by Playford and Schaller (2004). Disruption of these interactions causes cell detachment (Playford and Schaller, 2004; Zouq *et al.*, 2009).

Furthermore, earlier hormonal studies done on rats have demonstrated that paxillin expression is along the basal cell surface of the uterine epithelial cells with estrogen treatment (Kaneko *et al.*, 2009). On the other hand, there is a reduction or no staining of paxillin at the basal surface of uterine epithelial cells with progesterone treatment, which is also observed at the time of implantation (Kaneko *et al.*, 2009). This is in agreement with the observation in this study in which paxillin is seen to disassemble from the basal surface of the uterine epithelial cells then relocates and increases its expression apically in uterine luminal epithelial cells at day 6 of pregnancy in untreated and anastrozole treated rats. The implication of this is for the blastocyst to easily invade the endometrium. The increase in the paxillin protein expression in uterine luminal epithelial cells of the untreated and anastrozole treated groups and the decrease in the chlomiphene citrate (CC) treated group at day 6 of pregnancy are consistent with the paxillin gene expression experiments in this regard. Earlier studies have further shown that neonatal exposure to Bisphenol A alters rat uterine implantation-associated gene expression and reduces the number of implantation sites (Varayoud *et al.*, 2011). This means that gene

expression of receptivity markers in the rat uterine epithelial cells during implantation could be regulated by chemicals. It is not surprising, therefore, to observe in the present study that chlomiphene citrate (CC) generally down-regulates gene expression of the focal adhesion proteins in uterine luminal epithelial cells during implantation. All in all, this seems to suggest that anastrozole supports the implantation process.

4.5 Hematoxylin and eosin (H&E) staining

The standard hematoxylin and eosin protocol (Mohan *et al.*, 2008) was performed in order to have a general overview of the uterine endometrial histological changes, if any, between treatment groups. The changes in the uterine surface luminal epithelium, stroma cells, epithelial glands and blood vessels were considered.

Generally, the untreated, anastrozole and chlomiphene citrate (CC) treated day 1 rats respectively show a simple cuboidal to low columnar surface luminal epithelium with simple tubular glands. The spiral arteries extend from stratum basale to just below the epithelium. The stroma cells (fibroblasts) are relatively small in size.

The day 6 untreated and anastrozole treated rats show a simple columnar surface luminal epithelium with a mixture of secretory and non-secretory cells. Some of the epithelial cells have accumulation of glycogen in the basal portions. The stroma is edematous and the stroma cells have decidualised (are larger and pale) with abundant intercellular ground substance. The glands have lengthened, coiled and have become saw toothed with secretions (nutrients such as glycogen) in their lumen. This is a typical normal endometrial morphology observed during

early pregnancy as reported by other studies (Creus *et al.*, 2003) suggesting that anastrozole is implantation friendly.

However, day 6 chlomiphene citrate (CC) treated rats show a reduced or delayed decidualization of the stroma. This agrees with earlier studies that have shown that chlomiphene citrate (CC) inhibits decidualization of the endometrium in pregnant women (Nutu *et al.*, 2010). Interestingly, the base of the uterine luminal epithelium where focal adhesions are located appears to be intact and has cell-to-cell contact, which might be interfering with blastocyst invasion during implantation. Moreover, earlier studies have demonstrated that chlomiphene citrate (CC) reduces endometrial thickness (Lacin *et al.*, 2001), blood flow, embryo development and pregnancy rates (Bao *et al.*, 2009). This agrees with what other researchers have observed in which chlomiphene citrate (CC) seems to induce morphological abnormalities in the rat uteri (Randall and Templeton, 1991; Reefhuis *et al.*, 2011) suggesting that chlomiphene citrate (CC) may disrupt blastocyst implantation, and is thus associated with low pregnancy rates.

4.6 Conclusions and recommendations

In conclusion, the evidence for increased implantation sites in the Wistar rats treated with the 15mg/kg anastrozole in this study suggests that this particular dose superovulates and favors implantation in this species. It also confirms earlier studies that suggest higher anastrozole doses for ovulation induction. It is also important to note that anastrozole is a competitive inhibitor of aromatase in the conversion of androgens to estrogens (E_2); therefore, the 15mg/kg anastrozole dose, which is so effective in causing ovulation, may allow just enough of the intermediates and E_2 to be present with regard to the hormone profiles for ovulation and successful implantation of the embryo. Essentially, it may appear that there is blocking of E_2 and increasing of androgens in anastrozole treated rats compared to controls. Progesterone (P) is probably also high as E_2 is low. In chlomiphene citrate (CC) treated rats, estrogen receptors are blocked and thus increased E_2, but androgens are presumably low. The effect of anastrozole in the level of E_2 and P may change the E_2/P ratio at day 6 of pregnancy, suggesting its effect on endometrial maturation and therefore improving receptivity. The advantage of anastrozole therapy over chlomiphene citrate (CC) may be the lower E_2/P ratio and increased levels of FSH and LH. Therefore, measuring parameters such as the intermediates, estrogens and androgens in future studies may be of use in determining hormonal profiles for implantation.

The surface uterine epithelial morphology further demonstrates that anastrozole is implantation friendly. This study observes a change from long thin microvilli of medium density at day 1 of pregnancy, in terms of distribution, to short irregular sparse microvilli at

day 6 in implantation sites, as the non-implantation sites retain relatively denser and longer microvilli in all groups. Moreover, microvilli in implantation sites of day 6 anastrozole group are the shortest. The main implication of this morphological change is to flatten the apical membrane as part of the 'plasma membrane transformation' in which the uterine surface epithelium undergoes apical and basal alterations to become receptive to the blastocyst (Murphy, 2004). Therefore, anastrozole appears to promote the apical membrane flattening of the uterine surface epithelium and thus its significance in enhancing the uterine receptivity to the blastocyst implantation.

This study has further revealed an interesting finding in which anastrozole appears to retain surface uterine glycocalyx to some extent during implantation. Glycocalyx molecules generally are reduced as pregnancy progresses (Hosie *et al.*, 2003) as this might facilitate the apposition of the blastocyst and uterine cellular surfaces in the implantation process. However, specific glycocalyx molecules used in implantation are retained during implantation (Murphy, 2004). Therefore, the observed glycocalyx in the anastrozole treated rats at day 6 of pregnancy could be used in implantation suggesting that anastrozole achieves a better uterine environment for pregnancy when compared to chlomiphene citrate (CC). Further molecular studies could be employed to determine the types of glycocalyx molecules that are retained in the anastrozole treated rats during implantation.

Furthermore, the surface uterine ultrastructure findings from the present study strongly confirm earlier observations in which chlomiphene citrate (CC) seems to disrupt some of the well documented normal uterine surface ultrastructure seen at the time of implantation (Murphy and Shaw 1994; Hosie *et al.*, 2003; Scholtz *et al.*, 2008) among which the recessed

uterine epithelial cell borders seen at day 6 of pregnancy, with chlomiphene citrate (CC) treatment these cell borders are raised (Hosie *et al.*, 2003).

Another important finding of the present study is that large surface protrusions (pinopods) are mostly noted but not limited to anastrozole treated rats at day 6 of pregnancy. These observations further demonstrate an improved uterine surface morphology in anastrozole treated rats. Other than promoting the apical uterine surface membrane flattening (Nikas, 1997), the current study seems to speculate that the additional significance of these pinopods is that they could also contain adhesion molecules which are believed to be crucial in the process of embryo implantation (Kaneko *et al.*, 2008). If this is true, indeed anastrozole promotes a better uterine environment for embryo implantation and thus a particularly interesting finding of this study. However, transmission electron microscopy (TEM) and molecular studies would be recommended to ascertain whether anastrozole affects the composition of pinopods in order to clarify their additional significance in implantation and their involvement in fertility-promoting strategy.

The immunofluorescence and gene expression findings of the focal adhesions proteins vinculin, integrin β5, paxillin and FAK, which are uterine receptivity markers have also strongly demonstrate that anastrozole is implantation friendly. It will be interesting to see in future studies why FAK is not down-regulated with chlomiphene citrate (CC) treatment in uterine luminal epithelial cells during implantation in rats and if this could disrupt cell signaling. Most importantly, anastrozole may indeed be a suitable replacement or alternative drug used for hyperovulation or just to promote fertility in patients, particularly those suffering from polycystic ovary syndrome or are unresponsive to chlomiphene citrate (CC). In summary, these findings make anastrozole a potential substitute oral ovulatory drug, which

has proven superiority to chlomiphene citrate (CC) that could be used without the risk of hyperstimulation and with minimal monitoring and thus emerging as the new first-line treatment for anovulatory or ovulatory infertility.

5 REFERENCES

Abbas, S.M. & Rouzi, A.A. (2013) Pregnancy with 15 live fetuses and severe ovarian hyperstimulation syndrome after ovulation induction and intrauterine insemination. *Clin Exp Obstet Gynecol* 40(2): 297-299.

Adams, S.M., Gayer, N., Terry, V. & Murphy, C.R. (2001) Manipulation of the folicular phase: Uterodomes and pregnancy – is there a correlation? *BMC Pregnancy and Childbirth* 1: 2.

Adashi, E. (1993) Intraovarian regulation: the proposed role of insulin-like growth factors. *Ann N Y Acad Sci* 687: 10-12.

Al-Bader, M.D. & Al-Sarraf, H.A. (2005) Housekeeping gene expression during fetal brain development in the rat-validation by semi-quantitative RT-PCR. *Brain Res Dev Brain Res* 156(1): 38-45.

Al-Omari, W.R., Sulaiman, W. & Al-Hadithi, N. (2004) Comparison of two aromatase inhibitors in women with clomiphene resistant polycystic ovary syndrome. *Int J Gynecol Obstet* 85: 289-291.

Amos, W.B. & White, J.G. (2003) How the confocal laser scanning microscope entered biological research. *Biol Cell* 95(6): 335-342.

Andersen, A.N., Gianaroli, L., Felberbaum, R., de Mouzon, J. & Nygren, K.G. (2005) Assisted reproductive technology in Europe, 2001. Results generated from European registers by ESHRE. *Hum Reprod* 20: 1158-1176.

Aplin, J.D. & Kimber, S.J. (2004) Trophoblast-uterine interactions at implantation. *Reprod Biol Endocrinol* 2: 48.Doc: 10.1186/1477-7827-2-48.

Aplin, J.D., Spanswick, C., Behzad, F., Kimber, S.J. & Vicovac, C. (1996) Integrins β5, β3 and αv are apically distributed in endometrial epithelium. *Mol Hum Reprod* 2(7): 527-534.

Araujo, C.C., Teran, F.C., Oliveira, R.A., *et al.* (2003) Comparison of hexamethyldisilazane and critical point drying treatments for SEM analysis of anaerobic biofilms and granular sludge. *J Electron Microsc (Tokyo)* 52(4): 429-433.

Ardalan, M., Rafati, A., Nejat, F., Farazmand, B., Majed, M. & El Khashab, M. (2012) Risk factors associated with craniosynostosis: a case control study. *Pediatr Neurosurg* 48(3):152-156.

Arya, M., Shergill, I.S., Williamson, M., Gommersall, L., Arya, N. & Patel, H.R. (2005) Basic principles of real-time quantitative PCR. *Expert Rev Mol Diagn* 5(2): 209-219.

Attar, E. & Bulun, S.E. (2006) Aromatase inhibitors: the next generation of therapeutics for endometriosis? *Fertil Steril* 85(5): 1307-1318.

Badawy, A., Mosbah, A. & Shady, M. (2008) Anastrozole or letrozole for ovulation induction in clomiphene-resistant women with polycystic ovarian syndrome: a prospective randomized trial. *Fertil Steril* 89: 1209-1212.

Badawy, A., Aal, I.A. & Abulatta, M. (2009) Chlomiphene citrate or anastrozole for ovulation induction in women with polycystic ovarian syndrome? A prosepective controlled trial. *Fertil Steril* 92(3): 860-863.

Bao, S.H., Sheng, S.L., Peng, Y.F. & Lin, Q.D. (2009) Effects of letrozole and clomiphene citrate on the expression of HOXA10 and integrin avb3 in uterine epithelium of rats. *Fertil Steril* 91: 244-248.

Bartsch, R., Bago-Horvath, Z., Berghoff, A., *et al.* (2012) Ovarian function suppression and fulvestrant as endocrine therapy in premenopausal women with metastatic breast cancer. *Eur J Cancer* 48(13): 1932-1938.

Belaisch-Allart, J., Bachelot, A. & de Mouzon, J. (1998) Ovulation stimulation. *Contracept Fertil Sex* 26(7-8): 473-475.

Benda, J.A. (1992) Clomiphene's effect on endometrium in infertility. *Int J Gynecol Pathol* 11: 273-282.

Berg, J.M., Tymoczko, J.L., Stryer, L. & Gatto Jr, G.J. (2012) Biochemistry. 7th ed. Freeman and Company. New York. Pp. 725-945.

Bergh, P.A. & Navot, D. (1992) Ovarian hyperstimulation syndrome: a review of pathophysiology. *J Assist Reprod Genet* 9: 429-438.

Berman, A.E., Kozlova, N.I. & Morozevich, G.E. (2003) Integrins: structure and signaling. *Biochemistry (Mosc)* 68: 1284-1299.

Biljan, M.M., Hemming, R. & Brassard, N. (2005) The outcome of 150 babies following treatment with letrozole or letrozole with gonadotropins. *Fertil Steril* 84(Supp 1): 1-231.

Birkenfeld, A., Beier, H.M. & Schenker, J.G. (1986) The effects of chlomiphene citrate on early embryonic development, endometrium and implantation. *Hun Reprod* 1(6): 387-395.

Bloor, D.J., Metcalfe, A.D., Rutherford, A., Brison, D.R. & Kimber, S.J. (2002) Expression of cell adhesion molecules during human preimplantation embryo development. *Mol Hum Reprod* 8(3): 237-245.

Bogner, A., Jouneau, P.H., Thollet, G., Basset, D. & Gauthier, C. (2007) A history of scanning electron microscopy developments: towards wet-STEM imaging. *Micron* 38(4): 390-401.

Bonhoff, A.J., Naether, O.G.J. & Johannisson, E. (1996) Effects of chlomiphene citrate stimulation on endometrial structure in infertile women. *Hum Reprod* 11(4): 844-849.

Boruah, B.R. & Neil, M.A. (2009) Laser scanning confocal microscope with programmable amplitude, phase, and polarization of the illumination beam. *Rev Sci Instrum* 80(1): 013705.doi :10.1063/1.3072663.

Brown, J., Farquhar, C., Beck, J., Boothroyd, C. & Hughes, E. (2009) Clomiphene and anti-oestrogens for ovulation induction in PCOS. *Cochrane Database Syst Rev* Issue 4. Art No: CD002249.

Bruna-Catalan, I., Menabrito, M., *et al.* (2011) Ovulation induction with minimal dose of follitropin alfa: a case series study. *Reprod Biol Endocrinol* 9: 142.

Buzdar, A.U. (2003) Pharmacology and pharmacokinetics of the newer generation aromatase inhibitors. *Clin Cancer Res* 9: 468-472.

Cabodi, S., Di Stefano, P. & Leal Mdel, P., *et al.* (2010) Integrins and signal transduction. *Adv Exp Med Biol* 674: 43-54.

Caligioni, C. (2009) Assessing reproductive status/stages in mice. *Curr Protoc Neurosci* Appendix–4I. doi:10.1002/0471142301.nsa04is48.

Carisey, A., Tsang, R., Greiner A.M., *et al.* (2013) Vinculin regulates the recruitment and release of core focal adhesion proteins in a force-dependent manner. *Curr Bio* 23(4): 271-281.

Casper, R.F. & Mitwally, M.F. (2011) Use of the aromatase inhibitor letrozole for ovulation induction in women with polycystic ovarian syndrome. *Clin Obstet Gynecol* 54(4): 685-695.

Casper, R.F. & Mitwally, M.F. (2012) A historical perspective of aromatase inhibitors for ovulation induction. *Fertil Steril* 98: 1352-1355.

Chapman, J.C., Polanco, J.R., Min, S. & Michael, S.D. (2005) Mitochondrial 3 beta-hydroxysteroid dehydrogenase (HSD) is essential for the synthesis of progesterone by corpora lutea: an hypothesis. *Reprod Biol Endocrinol* 3: 11.

Chen, X. (2011) Five-day anastrozole group in infertility needs supplemental human chorionic gonadotropin. *Fertil Steril* 96(2): 135.

Childs, G.V., Unabia, G., Lee, B.L. & Rougeau, D. (1992) Heightened secretion by small and medium-sized luteinizing hormone (LH) gonadotropes late in the cycle suggests contributions to the LH surge or possible paracrine interactions. *Endocrinology* 130(1): 345-352.

Choi, S., Kim, P., Boutilier, R., Kim, M.Y., Lee, Y.J. & Lee, H. (2013). Development of a high speed laser scanning confocal microscope with an acquisition rate up to 200 frames per second. *Opt Express* 21(20): 23611-23618.

Choquet, D., Felsenfeld, D. P., & Sheetz, M. P. (1997) Extracellular matrix rigidity causes strengthening of integrin-cytoskeleton linkages. *Cell* 88: 39-48.

Christensen, A., Bentley, G.E., Cabrera, R., *et al.* (2012) Hormonal regulation of female reproduction. *Horm Metab Res* 44(8): 587-591.

Clark, J.H. & Markaverich, B.M. (1982) The agonistic-antagonistic properties of chlomiphene citrate: a review. *Pharmacol Ther* 15: 467-519.

Coons, A. H., Creech, H. J., Jones, R. N. & Berliner, E. (1942) The demonstration of pneumococcal antigens in tissues by the use of fluorescent antibody. *J Immunol* 45: 157-170.

Cortinez, A., De Carvalho, I., Vantman, D., Gabler, F., Iniquez, G. & Vega, M. (2005) Hormonal profile and endometrial morphology in letrozole-controlled ovarian hyperstimulation in ovulatory infertile patients. *Fertil Steril* 83(1): 110-115.

Corsi, J.M., Rouer, E., Girault, J.A. & Enslen, H. (2006) Organization and post-transcriptional processing of focal adhesion kinase. *BMC Genomics* 7: 198.

Costello, M.L., Mathieu-Costello, O. & West, J.B. (1992) Stress failure of alveolar epithelial cells studied by scanning electron microscopy. *Am Rev Respir Dis* 145: 1445-1455.

Creus, M., Ordi, J., Fabregues, F., *et al.* (2003) The effect of different hormone therapies on integrin expression and pinopode formation in the human endometrium: a controlled study. *Hum Reprod* 18(4): 683-693.

Critchley, D.R. (2004) Cytoskeletal proteins talin and vinculin in integrin-mediated adhesion. *Biochem Soc Trans* 32(5): 831-836.

Davies, M.J., Moore, V.M., Willson, K.J., *et al.* (2012) Reproductive technologies and the risk of birth defects. *N Engl J Med* 366: 1803-1813.

Davydov, R., Gilep, A.A., Strushkevich, N.V., Usanov, S.A. & Hoffman, B.M. (2012) Compound I is the reactive intermediate in the first monooxygenation step during conversion of cholesterol to pregnenolone by cytochrome P450scc EPR/ENDOR/cryoreduction/annealing studies. *J Am Chem Soc* 134(41): 17149-17156.

Derveaux, S., Vandesompele, J. & Hellemans, J. (2010) How to do successful gene expression analysis using real-time PCR. *Methods* 50(2010): 227-230.

Dey, S.K., Lim, H., Das, S.K., *et al.* (2004) Molecular cues to implantation. *Endocrine Reviews* 25(3): 341-373.

Diao, H., Paria, B.C., Xiao, S. & Ye, X. (2011) Temporal expression pattern of progesterone receptor in the uterine luminal epithelium. *Fertil Steril* 95(6): 2087-2093.

Dickey, R.P. & Holtkamp, D.E. (1996) Development, pharmacology and clinical experience with clomiphene citrate. *Hum Reprod Update* 2(6): 483-506.

Dickey, R.P., Taylor, S.N., Curole, D.N., Rye, P.H. & Pyrzak, R. (1996) Incidence of spontaneous abortion in clomiphene pregnancies. *Hum Reprod* 11: 2623-2628.

Diedrich, K., Fauser, B.C.J.M., Devroey, P. & Griesinger, G. (2007) The role of the endometrium and embryo in human implantation. *Hum Reprod Update* 13(4): 365-377.

Dietrich, J.E. (2010) An update on adenomyosis in the adolescent. *Curr Opin Obstet Gynecol* 22: 388-392.

DiMarzo, S.J., Kennedy, J.F., Young, P.E., Hebert, S.A., Rosenberg, D.C. & Villanueva, B. (1992) Effect of controlled ovarian hyperstimulation on pregnancy rates after intrauterine insemination. *Am Obstet Gynecol* 166: 1607-1612.

Ding, C. & Cantor, C.R. (2004) Quantitative analysis of nucleic acids - the last few years of progress. *J Biochem Mol Biol* 37(1): 1-10.

Dukes, M., Edwards, P.N., Large, M., Smith, I. & Boyle, T. (1996) The preclinical pharmacology of "arimidex" (anastrozole; ZD1033) - a potent, selective aromatase inhibitor. *J Steroid Biochem Molec Biol* 58(4): 439-445.

Dykes, M. & Watson, W. (2007) Anatomy crash course. 3rd ed. London. Pp.127-130.

Eisen, A., Trudeau, M., Shelley, W., Messersmith, H. & Pritchard, K. I. (2008) Aromatase inhibitors in adjuvant therapy for hormone receptor positive breast cancer: A systematic review. *Cancer Treat* 34:157-174.

Eleftheriou, G., Butera, R. & Manzo, L. (2012) Holoprosencephaly in clomiphene-induced pregnancy: a possible association? A case report and literature review. *Clin Exp Obstet Gynecol* 39(4):535-536.

Emanuele, M.A., Wezeman, F. & Emanuele, N.V. (2002) Alcohol's effects on female reproductive function. *Alcohol Res Health* 26(4): 274-281.

Emiliani, S., Delbaere, A., Devreker, F. & Englert, Y. (2005) Embryo-maternal interactive factors regulating the implantation process: implications in assisted reproductive. *Reprod Biomed Online* 10: 527-540.

Enders, A.C. & Schlafke, S. (1969) Cytological aspects of trophoblast-uterine interaction in early implantation. *Am J Anat* 125: 1-30.

Enders, A.C., Schlafke, S. & Hendrickx, A.G. (1986) Differentiation of the embryonic disc, amnion, and yolk sac in the rhesus monkey. *Am J Anat* 177: 161-185.

Englund, P., Lindroos, E., Nennesmo, I., Klareskog, L. & Lundberg, I.E. (2001) Skeletal muscle fibers express major histocompatibility complex class II antigens independently of inflammatory infiltrates in inflammatory myopathies. *Am J Pathol* 159(4): 1263-1273.

Fabry, B., Klemm, A.H., Kienle, S., Schaffer, T.E. & Goldmann, W.H. (2011) Focal adhesion kinase stabilizes the cytoskeleton. *Biophys J* 101(9): 2131- 2138.

Faolain, E.O., Hunter, M.B., Byrne, J.M., *et al.* (2005) Raman spectroscopic evaluation of efficacy of current paraffin wax section dewaxing agents. *J Histochem Cytochem* 53(1): 121-129.

Farquhar, C.M., Williamson, K., Brown, P.M., *et al.* (2004) An economic evaluation of laparoscopic ovarian diathermy versus gonadotropin therapy for women with clomiphene citrate resistant polycystic ovary syndrome. *Hum Reprod* 19: 1110-1115.

Fatum, M., Gyo, Y., Diana, P., Laufer, N. & Simon, A. (2006) Is estradiol mandatory for an adequate follicular and embryo development? A mouse model using aromatase inhibitor (anastrozole). *J Assist Reprod Genet* 23: 407-412.

Felding-Habermann, B. & Cheresh, D.A. (1993) Vintronectin and its receptors. *Curr Opin Cell Biol* 5(5):864-868.

Forman, R., Gil, S., Moretti, M., *et al.* (2007) Fetal safety of letrozole and clomiphene citrate for ovulation induction. *J Obstet Gynaecol Can* 29: 668-671.

Franik, S., Kremer, J.A.M., Nelen, W.L.D.M. & Farquhar, C. (2014) Aromatase inhibitors for subfertile women with polycystic ovary syndrome. *Cochrane Database Syst Rev*, Issue 2. Art. No.: CD010287. DOI: 10.1002/14651858.CD010287.pub2.

Fu, X.D., Goglia, L., Sanchez, A.M., *et al.* (2010) Progesterone enhances breast cancer cell motility and invasion via extranuclear activation of focal adhesion kinase. *Endocr Relat Cancer* 17(2): 431-443.

Fukami, M., Miyado., M., Nagasaki, K., Shozu, M. & Ogata, T. (2014) Aromatase excess syndrome: a rare autosomal dominant disorder leading to pre- or peri-pubertal onset of gynecomastia. *Pediatr Endocrinol Rev* 11(3): 298-305.

Gagliardi, L., Scott, H.S., Feng, J. & Torpy, D.J. (2014) A case of aromatase deficiency due to a novel CYP19A1 mutation. *BMC Endocr Disord* 14:16.doi:10.1186/1472-6823-14-16.

Ganesh, A., Chattopadhyay, R., Narendra Babu, K., Chakravarty, B.N. & Chaudhury, K. (2010) Analysis of spindle characteristics and embryo quality in mice stimulated with letrozole using Polscope imaging. *Fertil Steril* 93: 1477-1481.

Gargett, C.E., Nguyen, H.P. & Ye, L. (2012) Endometrial regeneration and endometrial stem/progenitor cells. *Rev Endocr Metab Disord* 13(4): 235-251.

Gennari, L., Merlotti, D. & Nuti, R. (2011) Aromatase activity and bone loss. *Adv Clin Chem* 54:129-164.

Gerardin, D.C.C. & Pereira, O.C.M. (2002) Reproductive changes in male rats treated perinatally with an aromatase inhibitor. *Pharmacol Biochem Behav* 71: 301-305.

Ghosh, D., Griswold, J., Erman, M. & Pangborn, W. (2009) Structural basis for androgen specificity and oestrogen synthesis in human aromatase. *Nature* 457:219-223.

Ghosh, D., Griswold, J., Erman, M. & Pangborn, W. (2010) X-ray structure of human aromatase reveals an androgen-specific active site. *J Steroid Biochem Mol Bio* 118(4-5):197-202.

Ghosh, D., Lo, J., Morton, D., Valette, D., *et al.* (2012) Novel aromatase inhibitors by structure-guided design. *J Med Chem* 55: 8464-8476.

Ghosh, D., Di Nardo, G. & Griswold, J. (2013) Structural basis for the functional roles of critical residues in human cytochrome P450 aromatase. *Biochemistry* 52: 5821-5829.

Gibreel, A., Maheshwari, A. & Bhattcharya, S. (2012) Clomiphene citrate in combination with gonadotropins for controlled ovarian stimulation in women undergoing in vitro fertilization. *Cochrane Database Syst Rev* 11: CD008528, doi: 10.100/14651858. CD008528.Pub2.

Goldstein, J., Newbury, D., Joy, D., *et al.* (2003) Scanning electron microscopy and X-ray microanalysis. 3rd ed. Kluwer Academic/Plenum New York. Pp 673-679.

Gonzalez, R.R., Palomino, A., Vantman, D., *et al.* (2001). Abnormal pattern of integrin expression at the implantation window in endometrium from fertile women treated with clomiphene citrate and users of intrauterine device. *Early Pregnancy* 5: 132-143.

Goss, P.E. (2003) Breast cancer prevention-clinical trials strategies involving aromatase inhibitors. *J Sterod Biochem and Mol Biol* 86: 487-493.

Grewal, S., Carver, J., Ridley, A.J. & Mardon, H.J. (2010) Human endometrial stromal cell Rho GTPases have opposing roles in regulatinf focal adhesion turnover and embryo invasion in vitro. *Biol Reprod* 83: 75-82.

Griesinger, G., von Otte, S., Schultze-Mosgau, A., Diedrich, K. & Schroer, A. (2009) Follicular and endocrine response to anastrozole versus clomiphene citrate administered in follicular phase to normoovulatory women: a randomized comparison. *Fertil Steril* 91:1831-1836.

Healy, S., Tan, S.L., Tulandi, T. & Biljan, M.M. (2003) Effects of letrozole on superovulation with gonadotropins in women undergoing intrauterine insemination. *Fertil Steril* 80: 1325-1329.

Hemani, G., Shakhbazov, K., Westra, H.J. *et al.*, (2014). Detection and replication of epistasis influencing transcription in humans. *Nature* 508: 249-253.

Hewitt, S.C. & Korach, K.S. (2000) Progesterone action and response in the alphaERKO mouse. *Steroids* 65: 551-557.

Hirata, H., Sokabe, M. & Lim, C.T. (2014) Molecular mechanisms underlying the force-dependent regulation of actin-to-ECM linkage at the focal adhesions. *Prog Mol Biol Transl Sci* 126: 135-154.

Hoebeeck, J., van der, L.R., Poppe, B., *et al.* (2005) Rapid detection of VHL exon deletions using real-time quantitative PCR. *Lab Invest* 85(1): 24-33.

Holzer, H., Casper, R. & Tulandi, T. (2006) A new era in ovulation induction. *Fertil Steril* 85(2): 277-284.

Homburg, R. (2005) Clomiphene citrate - end of an era? A mini review. *Hum Reprod* 20: 2043-2051.

Hong, E.J., Park, S.H., Choi, K.C., Leung, P.C. & Jeung, E.B. (2006) Identification of estrogen-regulated genes by microarray analysis of the uterus of immature rats exposed to endocrine disrupting chemicals. *Reprod Biol Endocrinol* 4

Hosie, M.T. & Murphy, C. (1995) A scanning and light microscope study comparing the effects of clomiphene citrate, estradiol 17-beta and progesterone on the structure of uterine luminal epithelial cells. *Eur J Morphol* 33(1): 39-50.

Hosie, M.J, Terry, V. & Murphy, C. (2003) Expression of glucosamine trisaccharides on the rat uterine surface is altered by clomiphene citrate. III. Relationship with implantation regimes and pregnancy. *Acta Histochem* 105(4): 329-338.

Hosie, M.J. & Stewart, C.M. (2006) Apoptosis is not altered by chlomiphene citrate in pseudopregnant rat uteri. *Acta Histochem* 108: 105-116.

Hosie M., Adamson, M. & Penny, C. (2008) Actin binding protein expression is altered in uterine luminal epithelium by clomiphene citrate, a synthetic estrogen receptor modulator. *Theriogenology* 69: 700-713.

Hsu, C.C., Kuo, H.C., Wang, S.T. & Huang, K.E. (1995) Interference with uterine blood flow by chlomiphene citrate in women with unexplained infertility. *Obstet Gynecol* 86(6): 917-921.

Hu, Y., Haga, J.H., Miao, H., Wang, Y., Li, Y. & Chien, S. (2006) Roles of microfilaments and microtubules in paxillin dynamics. *Biochem Biophys Res Commun* 348: 1463–1471.

Humphries, J.D., Wang, P., Streuli, C., Geiger, B., Humphries, M.J. & Ballestrem, C. (2007) Vinculin controls focal adhesion formation by direct interaction with talin and actin. *J Cell Biol* 179(5): 1043-1057.

Ishikawa, H., Reierstad, S., Demura, M., *et al.* (2009) High aromatase expression in uterine leiomyoma tissues of African-American women. *J Clin Endocrinol Metab* 94(5): 1752-1756.

Ito, Y., Fisher, C.R., Grumbach, M.M., Simpson, E.R. (1993) Molecular basis of aromatase deficiency in an adult female with sexual infantilism and polycystic ovaries. *Proc Natle Acad Sci USA.* 90(24): 11673-11677.

Jakubowicz, D.J., Seppala, M., Jakubowicz, S., *et al.* (2001) Insulin reduction with metformin increases luteal phase serum glycodelin and insulin-like growth factor-binding protein 1 concentrations and enhances uterine vascularity and blood flow in the polycystic ovary syndrome. *J Clin Endocrinol Metab* 86: 1126-1133.

Jaramillo, L.M., Balcazar, I.B. & Duran, C. (2012) Using vaginal wall impedance to determine estrous cycle phase in Lewis rats. *Lab Anim (NY)* 41(5):122-128.

Kamath, M.S. & George, K. (2011) Letrozole or clomiphene citrate as first line for anovulatory infertility: a debate. *Reprod Biol Endocrinol* 9(86): 1-4.

Kaneko, Y., Lindsay, L.A. & Murphy, C.R. (2008) Focal adhesions disassemble during early pregnancy in rat uterine epithelial cells. *Reprod Fertil Dev* 20(8): 892-899.

Kaneko, Y., Lecce, L. & Murphy, C.R. (2009) Ovarian hormones regulate expression of the focal adhesion proteins, talin and paxillin, in rat uterine luminal but not glandular epithelial cells. *Histochem Cell Biol* 132(6): 613-622.

Kaneko, Y., Lecce, L., Day, M.L. & Murphy, C.R. (2011) β_1 and β_3 integrins disassemble from basal focal adhesions and β_3 integrin is later localized to the apical plasma membrane of rat uterine luminal epithelial cells at the time of implantation. *Reprod Fertil Dev* 23: 481-495.

Kaneko, Y., Lecce, L., Day, M.L. & Murphy, C.R. (2012) Focal adhesion kinase localizes to sites of cell-to-cell contact in vivo and increases apically in rat uterine luminal epithelium and the blastocyst at the time of implantation. *J Morphol* 273(6): 639-650.

Karaer, O., Vatansever, H.S., Oruc, S., *et al.* (2005) The aromatase inhibitor anastrozole is associated with favourable embryo development and implantation markers in mice ovarian stimulation cycle. *Fertil Steril* 83(6): 1797-1806.

Kerin, J.F., Liu, J.H., Phillipou, G. & Yen, S.S. (1985) Evidence for a hypothalamic site of action of clomiphene citrate in women. *J Clin Endocrinol Metab* 61(2): 265-268.

Khile, A., Joshi, N. & Bhirud, S. (2006) Process for the preparation of anastrozole and intermediates thereof. *U.S. Patent* US20060189670.

Kilic-Okman, T., Kucuk, M. & Altaner, S. (2003) Comparison of the effects of letrozole and clomiphene citrate on ovarian follicles, endometrium, and hormone levels in the rat. *Fertil Steril* 80: 1330-1332.

Klemm, A.H., Diez, G., Alonso, J. & Goldman, W.H. (2008) Comparing the mechanical influences of vinculin, focal adhesion kinase and p53 in mouse embryonic fibroblasts. *Biochem Biophys Res Commun* 379: 799-801.

Kousta, E., White, D.M. & Franks, S. (1997) Modern use of clomiphene citrate in induction of ovulation. *Hum Reprod Update* 3: 359 - 365.

Kraemer, F.B., Khor, V.K., Shen, W.J. & Azhar, S. (2013) Cholesterol ester droplets and steroiddgenesis. *Mol Cell Endocrinol* 371(1-2): 15-19.

Kuang, Y., Hong, Q., Chen, Q., *et al.* (2014) Luteal-phase ovarian stimulation is feasible for producing competent oocytes in women undergoing in vitro fertilization/intracytoplasmic sperm injection treatment, with optimal pregnancy outcomes in frozen-thawed embryo transfer cycles. *Fertil Steril* 10(1): 105-111.

Kupper, K., Lang, N. Mohl, C., *et al.* (2010) Tyrosine phosphorylation of vinculin at position 1065 modifies focal adhesion dynamics and cell tractions. *Biochem Biophys Res Commun* 399(4): 560-564.

Kurl, R.N. & Morris, I.D. (1978) Differential depletion of cytoplasmic high affinity oestrogen receptors after the in vivo administration of the antioestrogens, clomiphene, MER-25 and tamoxifen. *Br J Pharmacol* 62: 487-493.

Lacin, S., Vatansever, S., Kuscu, N.K., *et al.* (2001) Clomiphene citrate does not affect the secretion of $\alpha 3$, α_v and β_1 integrin molecules during the implantation window in patients with unexplained infertility. *Hum Reprod* 16(11): 2305-2309.

Lecce, L., Kaneko, Y., Madawala, R. & Murphy, C.R. (2011) ICAM 1 and fibrinogen-γ are increased in uterine epithelial cells at the time of implantation in rats. *Mol Reprod Dev* 78: 318-327.

Lee, V.C. & Ledger, W. (2011) Aromatase inhibitors for ovulation induction and ovarian stimulation. *Clin Endocrinol* 74(5): 537-546.

Lele, T.P., Thodeti, C.K., Pendse, J. & Ingber, D.E. (2008) Investigating complexity of protein–protein interactions in focal adhesions. *Biochem Biophys Res* 369: 929-934.

Li, Y.Q., Bai, B., Zheng, Q.Q., Yan, H. & Zhuang, G.H. (2013) Quantitative study of metabolism-related genes expression in rat. *Biomed Environ Sci* 26(10): 808-819.

Liaw, L., Linder, V., Schwartz, S.M., *et al.* (1995) Osteopontin and beta 3 integrin are coordinately expressed in regenerating endothelium in vivo and stimulate Arg-Gly-Asp-dependent endothelial migration in vitro. *Circ Res* 77(4): 665-672.

Lima, S., Clemenson, A., Trombert, B., *et al.* (2014) Morphological and immunohistochemical analysis in ovaries and fallopian tubes of tamoxifen, letrozole and clomiphene-treated rats. *Arch Gynecol Obstet* 290: 553-559.

Liu, G., Guibao, C.D. & Zheng, J. (2002) Structural insight into the mechanisms of targeting and signaling of focal adhesion kinase. *Mol Cell Biol* 22: 2751-2760.

London, S.N., Young, D., Caldito, G. & Mailhes, J.B. (2000) Clomiphene citrate-induced perturbations during meiotic maturation and cytogenetic abnormalities in mouse oocytes *in vivo* and *in vitro*. *Fertil Steril* 73(3): 620-626.

Long, J.A. & Evans, H.M. (1922) The estrous cycle in the rat and its associated phenomena. *Memories of University of California* 6: 1–148.

Long, W., Yi, P., Amazit, L., *et al.* (2010) SRC-3Delta4 mediates the interactions of EGFR with FAK to promote cell migration. *Mol Cell* 37(3): 321-332.

Lu, Q. & Rounds, S. (2012) Focal adhesion kinase and endothelial cell apoptosis. *Microvasc Res* 83(1): 56-63.

March, W., Moore, V., Willson, K., Phillips, D., Norman, R. & Davies, M. (2010) The prevalence of polycystic ovary syndrome in a community sample assessed under contrasting diagnostic criteria. *Hum Reprod* 2: 544-551.

Marcondes, F.K., Bianchi, F.J. & Tanno, A.P. (2002) Determination of the estrous cycle phase of rats: some helpful considerations. *Braz J Biol* 62(4A): 609-614.

Mattos, M.C., Bastos, M.R., Guardieiro, M.M., *et al.* (2011) Improvement of embryo production by the replacement of the last two doses of porcine follicle-stimulating hormone with equine chorionic gonadotropin in Sindhi donors. *Anim Reprod Sci* 125(1-4): 119-123.

Mauras, N., Bishop, K., Merinbaum, D., Emeribe, U., Agbo, F. & Lowe, E. (2009) Pharmacokinetics and pharmacodynamics of anastrozole in pubertal boys with recent-onset gynecomastia. *J Clin Endocrinol Metab* 94(8):2975-2978.

Misso, M.L., Wong, J.L.A., Teede, H.J., *et al.* (2012) Aromatase inhibitors for PCOS: a systematic review and meta-analysis. *Hum Reprod update* 18(3): 301-312.

Mitra, S.K., Hanson, D.A. & Schlaepfer, D.D. (2005) Focal adhesion kinase: in command and control of cell motility. *Nat Rev Mol* Cell Biol 6: 55-68.

Mitwally, M.F.M. & Casper, R.F. (2001) Use of an aromatase inhibitor for induction of ovulation in patients with an inadequate response to clomiphene citrate. *Fertil Steril* 75:305-309.

Mitwally, M.F.M. & Casper, R.F. (2002) Aromatase inhibition for ovarian stimulation: future avenues for infertility management. *Curr Opin Obstet Gynecol* 14: 255-263.

Mohan, K.H., Sathish, P., Raghavendra, R., Sripathi, H. & Prabhu, S. (2008) Techniques of immunofluorescence and their significance. *Indian J Dermatol Venereol Leprol* 74(4): 415-419.

Mouriec, K., Lareyre, J.J., Tong, S.K., *et al.* (2009) Early regulation of brain aromatase (cyp19a1b) by estrogen receptors during zebrafish development. *Dev Dyn* 238: 2641-2651.

Murphy, C.R. & Turner, V.F. (1991) Glycocalyx carbohydrates of the uterine epithelial cells increase during pregnancy in the rat. *J Anat* 177: 109-115.

Murphy, C.R. & Shaw, T.J. (1994) Plasma membrane transformation: a common response of uterine epithelial cells during the peri-implantation period. *Cell Biol Int* 18: 1115-1128.

Murphy, C.R. (1995) The cytoskeleton of uterine epithelial cells: a new player in uterine receptivity and the plasma membrane transformation. *Hum Reprod Update* 1: 567-580.

Murphy, C.R. (2000) Understanding the apical surface markers of uterine receptivity: Pinopods or uterodomes? *Hum Reprod* 15: 2451-2454.

Murphy, C.R. (2004) Uterine receptivity and the plasma membrane transformation. *Cell Res* 14: 258-267.

Mwakikunga, A.R., Clubine, A.L. & Wiens, D.J. (2011) Homocysteine and cardiac neural crest cell cytoskeletal proteins in the chick embryo. *Int J Biol* 3(2): 43-56.

Nehru, V., Almeidal, F.N., Aspenstrom, P., *et al.* (2013) Interaction of RhoD and ZIP kinase modulates actin filament assembly and focal adhesion dynamics. *Biochem Biophys Res Commun* 433(2) : 163-169.

Nelson, L.R. & Bulun, S.E. (2001) Estrogen production and action. *J Am Acad Dermatol* 45(Suppl 3): S116-S124.

Neveu, N.G.L., St. Michel, P. & Lavoie, H.B. (2007) Comparison of clomiphene citrate, metformin, or the combination of both for first-line ovulation induction and achievement of pregnancy in 154 women with polycystic ovary syndrome. *Fertil Steril* 87: 113-120.

Nikas, G. (1997) Pinododes as markers of endometrial receptivity in clinical practice. *Hum Reprod* 14 (suppl 2): 99-106.

Nikas, G. & Psychoyos, A. (1997) Uterine pinopodes in peri-implantation human endometrium. Clinical relevance. *Ann N Y Acad Sci* 816: 129-142.

Novotny, R., Malinsky, J., Oborna, I. & Dostal, J. (1999) Ultrastructure of ometrial surface relief in normal menstrual cycle and after hormonal stimulation. *Acta Univ Palacki Olomuc Fac Med* 142: 47-55.

Nutu, M., Feng, Y., Egecioglu, E., *et al.* (2010) Stromal cell–specific apoptotic and antiestrogenic mechanisms may explain uterine defects in humans after clomiphene citrate therapy. *Am J Obstet Gynecol* 203: 65.e1-65.e10.

Nygren, K.G. & Andersen, A.N. (2001) Assisted reproductive technology in Europe, 1997 results generated from European registers by ESHRE. European IVF-monitoring program (EIM), for the European society of human reproduction and embryology (ESHRE). *Hum Reprod* 16: 384-391.

Odell, I.D. & Cook, D. (2013) Immunofluorescence techniques. *J Invest Dermatol* 133: 1-4.

Paddock, S.W. & Eliceiri, K.W. (2014) Laser scanning confocal microscopy: history, applications, and related optical sectioning techniques. *Methods Mol Biol* 1075: 9-47.

Pakrasi, P.L. & Tiwari, A. (2007) Evidence of increased endometrial vascular permeability at the time of implantation in the short-nosed fruit bat, Cyanopterus sphinx. *Anim Reprod Sci* 101(1-2): 179-185.

Palomino, W.A., Fuentes, A., Gonzalez, R.R., *et al.* (2005) Differential expression of endometrial integrins and progesterone receptor during the window of implantation in normo-ovulatory women treated with clomiphene citrate. *Fertil Steril* 83(3): 587-593.

Pandian, Z., Templeton, A., Serour, G. & Bhattacharya, S. (2005) Number of embryos for transfer after IVF and ICSI: a cochrane review. *Hum Reprod* 20(10): 2681-2687.

Paria, B.C., Song, H. & Dey, S.K. (2001) Implantation: molecular basis of embryo-uterine dialogue. *Int J Dev Biol* 45: 597-605.

Parr, M.B. & Parr, E.L. (1989) The implantation reaction (R.M. Wynn and W.P. Jollie, eds.) Plenum Medical Book Company, New York. pp 233-277.

Parsanezhad, M.E., Azmoon, M., Alborzi, S., *et al.* (2010) A randomized, controlled clinical trial comparing the effects of aromatase inhibitor (letrozole) and gonadotropin-releasing hormone agonist (triptorelin) on uterine leiomyoma volume and hormonal status. *Fertil Steril* 93: 192-198.

Pasco, R., Gardner, D.K., Walker, D.W. & Dickinson, H. (2012) A superovulation protocol for the spiny mouse (Acomys cahirinus). *Reprod Fertil Dev* 24(8): 1117-1122.

Patwardhan, S., Nawathe, A., Yates, D., *et al.* (2008) Systematic review of the effects of aromatase inhibitors on pain associated with endometriosis. *BJOG* 115: 818–822.

Petit, V. & Thiery, J.P. (2000) Focal adhesions: structure and dynamics. *Biol Cell* 92: 477-494.

Petrunak, E.M., DeVore, N.M., Porubsky, P.R. & Scott, E.E. (2014) Structure of human steroidogenic cytochrome P450 17A1 with substrates. *J Biol Chem* Pii:jbc.M114.610998.

Pettersen, E. F., Goddard, T.D., Huang, C.C., *et al.* (2004) UCSF Chimera- a visualization system for exploratory research and analysis. *J Comput Chem* 25:1605-1612.

Playford, M.P. & Schaller, M.D. (2004) The interplay between Src and integrins in normal and tumor biology. *Oncogene* 23: 7928-7946.

Plourde, P.V., Dyroff, M., Dowsett, M., Demers, L., Yates, R. & Webster, A. (1995) ARIMIDEX: a new oral, once a day aromatase inhibitor. *J Steroid Biochem Mol Biol* 53(1-6): 175-179.

Png, F.Y. & Murphy, C.R. (1997) The plasma membrane transformation does not last: Microvilli return to the apical plasma membrane of uterine epithelial cells after the period of uterine receptivity. *Eur J Morphol.* 35(1): 19-24.

Polte, T.R. & Hanks, S.K. (1997) Complexes of focal adhesion kinase (FAK) and Crk-associated substrate (p130(Cas)) are elevated in cytoskeleton-associated fractions following adhesion and Src transformation. Requirements for Src kinase activity and FAK proline rich motifs. *J Biol Chem* 272: 5501-5509.

Poon, C.E., Lecce, L., Day, M.L. & Murphy, C.R. (2014) Mucin 15 is lost but mucin 13 remains in the uterine luminal epithelial cells and the blastocyst at the time of implantation in the rat. *Reprod Fertil Dev* 26: 421-431

Pusey, J., Kelly, W.A., Bradshaw, J.M.C. & Porter, D.G. (1980) Myometrial activity and distribution of blastocysts in the uterus of the rat: interference by relaxin. *Biol Reprod* 23: 394-397.

Psychoyos, A. (1986) Uterine receptivity for implantation. *Ann N Y Acad Sci.* 476(1): 36-42.

Qiu, M., Liu, J., Han, C., *et al.* (2014) The influence of ovarian stromal/theca cells during in vitro culture on steroidogenesis, proliferation and apoptosis of granulosa cells derived from the goat ovary. *Reprod Dom Anim* 49: 170-176.

Quadri, S.K. (2011) Cross talk between focal adhesion kinase and cadherins: role in regulating endothelial barrier function. *Microvasc Res* 83: 3-11.

Quadri, S.K. & Bhattacharya, J. (2007) Resealing of endothelial junctions by focal adhesion kinase. *Am J Physiol Lung Cell Mol Physiol* 292: 334-342.

Quintero, R.B., Urban, R., Lathi, R.B., Westphal, L.M. & Dahan, M.H. (2007) A comparison of letrozole to gonadotropins for ovulation induction, in subjects who failed to conceive with clomiphene citrate. *Fertil Steril* 88: 879-885.

Racette, L., Casson, P., Claman, P., *et al.* (2010) Bilateral visual disturbances in patients on clomiphene citrate arise from the central nervous system. *Fertil Steril* 93: 1169-1172.

Rajamohamedsait, H.B. & Sigurdsson, E.M. (2012) Histological staining of amyloid and pre-amyloid peptides and proteins in mouse tissue. *Methods Mol Biol* 849: doi.10.1007/978-1-61779-551-0-28.

Randall, J.M. & Templeton, A. (1991) Transvaginal sonographic assessment of follicular and endometrial growth in spontaneous and clomiphene citrate cycles. *Fertil Steril* 56: 208-212.

Rao, R. & Shenoi, S.D. (2006) Indirect immunofluorescence to demonstrate lichen planus specific antigen (LPSA) in lichen planus. *Indian J Dermatol Venereol Leprol* 72: 350-352.

Reefhuis, J., Honein, M.A., Schieve, L.A. & Rasmussen, S.A. (2011) Use of clomiphene citrate and birth defects, National Birth Defects Prevention Study, 1997–2005. *Hum Reprod* 26(2): 451-7.

Reese, J., Das, S.K., Paria, B.C., *et al.* (2001) Global gene analysis to identify molecular markers of uterine receptivity and embryo implantation. *J Biol Chem* 276(47): 44137-44145.

Rettberg, J.R., Yao, J. & Brinton, R.D. (2014) Estrogen: a master regulator of bioenergetic systems in the brain and body. *Front Neuroendocrinol* 35(1): 8-30.

Rostami-Hodjegan, A., Lennard, M.S., Tucker, G.T. & Ledger, W.L. (2004) Minitoring plasma concentrations to individualize treatment with clomiphene citrate. *Fertil Steril* 81: 1187-1193.

Rudolph, M., Docke, W.D., Muller, A., *et al.* (2012) Induction of overt menstruation in intact mice. *PLos one* 7(3): e32922.doi:10.1371/journal.pone.0032922.

Salgia, R. (2009) Role of c-Met in cancer: Emphasis on lung cancer. *Semin Oncol* 36(2 Suppl 1): S52-S58.

Schmittgen, T.D. & Livak, K.J. (2008) Analyzing real-time PCR data by the comparative CT method. *Nat Protoc* 3(6): 1101-1108.

Scholtz, K.E., Penny, C.B. & Hosie, M.J. (2008) A high resolution SEM study of the effects of RU486, used as a postcoital contraceptive, on the rat uterus during early pregnancy. *Cell Biol Int* 32(4): 436-46.

Shalom-Paz, E., Marzal, A., Wiser, A., Hyman, J. & Tulandi, T. (2014) Does optimal follicular size in IUI cycles vary between clomiphene citrate and gonadotrophins treatments? *Gynecol Endocrinol* 30(2): 107-110.

Sharma, S., Ghosh, S., Singh, S., *et al.* (2014) Congenital malformations among babies born following letrozole or chlomiphene citrate for infertility treatment. *PLos One* 9(10): e108219 doi: 10.1371/Journal.pone.0108219.

Shozu, M., Fukami, M. & Ogata, T. (2014) Understanding the pathological manifestations of aromatase excess syndrome: lessons for clinical diagnosis. *Expert Rev Endocrinol Metab* 9(4): 397-409.

Simerpal, K.G., Moretti, M. & Koren, G. (2008) Is the use of letrozole to induce ovulation teratogenic? *Can Fam Physiacian* 54: 353-354.

Simpson, E. R., Mahendroo, M.S., Means, G.D., *et al.* (1994) Aromatase cytochrome P450, the enzyme responsible for estrogen biosynthesis. *Endocr* 15: 342-355.

Singletary, S.J., Kirsch, A.J., Watson, J., *et al.* (2005) Lack of correlation of vaginal impedance measurements with hormone levels in the rat. *Contemp Top Lab Anim Sci* 44(6): 37-42.

Sinha, S., Kaseta, J., Santner, L.M., *et al.* (1998) Effects of CGS20267 on ovarian aromatase and gonatropin levels in the rat. *Breast Cancer Res Treat* 48: 45-51.

Smulders, B., van Oirschot, S.M., Farquha, C., Rombauts, L. & Kremer, J.A. (2010) Oral contraceptive pill, progestogen or estrogen pretreatment for ovarian stimulation protocols for women undergoing assisted reproductive techniques. *Cochrane Database Syst Rev* 1: CD006109.

Sorensen, H.T., Pedersen, L., Skriver, M.V., *et al.* (2005) Use of clomifene during early pregnancy and risk of hypospadias: population based case–control study. *BMJ* 330: 126-7.

Spornitz, U.M., Socin, C.D. & David, A.A. (1999) Estrous stage determination in rats by means of scanning electron microscopic images of uterine surface epithelium. *The Anat Rec* 254: 116-126.

Stocco, C. (2012) Tissue physiology and pathology of aromatase. *Steroids* 77(1-2) : 27-35.

Su, R.W., Jia, B., Ni, H., *et al.* (2012) Junctional adhesion molecule 2 mediates the interaction between hatched blastocyst and luminal epithelium: induction by progesterone and LIF. *PLoS ONE* 7(4): e34325. doi:10.1371/journal.pone.0034325.

Sylvestre, V.T. & Dunton, C.J. (2010) Treatment of recurrent endometrial stromal sarcoma with letrozole: a case report and literature review. *Horm Cancer* 1(2): 112-115.

Takagi, S., Shimizu, T., Kuramoto, G., *et al.* (2014) Reconstruction of functional endometrium-like tissue in vitro and in vivo using cell sheet engineering. *Biochem Biophys Res Commun* 446(1): 335-340.

Tancioni, I., Uryu, S., Sulzmaier, F.J., *et al.* (2014) FAK inhibition disrupts a β5 integrin signaling axis controlling anchorage-independent ovarian carcinoma growth. *Mol Cancer Ther* 13(8): 2050-2061.

Thessaloniki ESHRE/ASRM-Sponsored PCOS Consensus Worksho Group. (2008) Consensus on infertility treatment related to polycystic ovary syndrome. *Fertil Steril* 89: 505-522.

Tiboni, G.M., Marotta, F., Rossi, C., *et al.* (2008) Effects of the aromatase inhibitor letrozole on in utero development in rats. *Hum Reprod* 23: 1719–1723.

Tredway, D.R. & Schertz, J.C. (2011) Anastrozole versus clomiphene citrate: which is better for ovulation induction? *Fertil Steril* 95: 1549-1551.

Tulandi, T., Martin, J., Al-Fadhli, R., *et al.* (2006) Congenital malformations among 911 newborns conceived after infertility treatment with letrozole or clomiphene citrate. *Fertil Steril* 85: 1761-1765.

Urman, B., Yakin, K. & Balaban, B. (2005) Recurrent implantation failure in assisted reproduction: how to counsel and manage. A. General considerations and treatment options that may benefit the couple. *Reprod Biomed Online* 11: 371-381.

Varayoud, J., Ramos, J.G., Bosquiazzo, V.L., *et al.* (2011) Neonatal exposure to Bisphenol A alters rat uterine implantation-associated gene expression and reduces the number of implantation sites. *Endocrinology* 152: 1101-1111.

Wang, H. & Dey, S.K. (2006) Roadmap to embryo implantation: Clues from mouse models. *Nat Rev Genet* 7: 185-199.

Wang, C. & Kaltenboeck, B. (2005) Advances in real-time PCR: application to clinical laboratory diagnostics. *Adv Clin Chem* 40: 219-259.

Wang, W.S., Liu, C., Li, W.J., Zhu, P., Li, J.N. & Sun, K. (2014) Involvement of CRH and hCG in the induction of aromatase by cortisol in human placental syncytiotrophoblasts. *Placenta* 35(1): 30-36.

Wang, Y.A., Chambers, G.M., Dieng, M. & Sullivan, E.A. (2009) Assisted reproductive technology in Australia and New Zealand. *Assisted reproduction technology series* no. 13. Cat. no. PER 47. Canberra: AIHW.

Weekes, J., Barry, S. T., & Critchley, D. R. (1996) Acidic phospholipids inhibit the intramolecular association between the n- and c-terminal regions of vinculin, exposing actin-binding and protein kinase c phosphorylation sites. *Biochem J* 314: 827-832.

Wehrend, A., Huchzermeyer, S. & Bostedt, H. (2005) Distribution of eosinophils and mast cells in the cervical tissue of non-gravid mares during diestrus. *Reprod Domest Anim* 40(6): 562-563.

Weil, S., Vendola, K., Zhou, J. & Bondy, C.A. (1999) Androgen and follicle-stimulating hormone interactions in primate ovarian follicle development. *J Clin Endocrinol Metab* 84: 2951-2956.

Wilhelm, J. & Pingoud, A. (2003) Real-time polymerase chain reaction. *Chebiochem* 4(11): 1120-1128.

Wong, M.L. & Medrano, J.F. (2005) Real-time PCR for mRNA quantitation. *Bio Techniques* 39: 75-85.

Wu, H.H., Wang, N.M., Cheng, M.L. & Hsieh, J.N. (2007) A randomized comparison of ovulation induction and hormone profile between the aromatase inhibitor anastrozole and clomiphene citrate in women with infertility. *Gynecol Endocrinol* 23: 76-81.

Wynn, R.M. & Jollie, W.P. (1989) Biology of the uterus. 2nd ed. New York. Pp. 233-277.

Zachary, I. (2003) VEGF signaling: integration and multi-tasking in endothelial cell biology. *Biochem Soc Trans* 31(6): 1171-1177.

Zhang, H.B., Feng, R.J & Ura, K. (2004) Utilizing the charging effect in scanning electron microscopy. *Sci Prog* 87(4): 249-268.

Zhang, D., Wei, J., Wang, J., Liu, S., Wang, X., Yan, Q. (2011) Difucosylated oligosaccharide Lewis Y is contained within integrin αVβ3 on RL95-2 cells and required for endometrial receptivity. *Fertil Steril* 95(4): 1446-1451.

Zhao, J. & Guan, J.L. (2009) Signal transduction by focal adhesion kinase in cancer. *Cancer Metastasis* 28(1-2): 35-49.

Zhao, M., Chang, C., Liu, Z., Chen, L.M. & Chen, Q. (2010) Treatment with low dose asprin increased the level of LIF and integrin β3 expression in mice during the implantation window. *Placenta* 31: 1101-1105.

Zheng, S., Huang, J., Zhou, K., *et al.* (2012) Progesterone enhances vascular endothelial cell migration via activation of focal adhesion kinase. *J Cell Mol Med* 16(2): 296-305.

Zhou, W., Apkarian, R.P., Wang, Z.L. & Joy, D. (2007) Scanning microscopy for nanotechnology. Springer New York. Pp 1-40.

Zimmermann, T., Rietdorf, J. & Pepperkok, R. (2003) Spectral imaging and its applications in lice cell microscopy. *FEBS Lett* 546(1): 87-95.

Zouq, N.K., Keeble, J.A., Lindsay, J., *et al.* (2009) FAK engages multiple pathways to maintain survival of fibroblasts and epithelia: differential roles for paxillin and p130Cas. *J Cell Sci* 122: 357-367.

6 APPENDIX A: SOLUTIONS AND RECIPES FOR VAGINAL SMEAR, DRUG PREPARATION AND SACRIFICE

6.1 Vaginal smear method of staining

Vaginal fluid was collected with a smoothened glass pipette filled with 10 µl of normal saline (NaCl 0.9%) by inserting the tip into the rat vagina, but not deeply and flushed gently three to five times with saline. The final flush was collected in the pipette tip for observation of the vaginal cytology (Caligioni, 2009). The vaginal fluid was placed on a glass slide and air dried (Singletary *et al.*, 2005). One drop of 1% toluidine blue was used to stain the specimen for 3-5 min at room temperature; then, gently washed under running tape water for ten seconds (Wehrend *et al.*, 2005). Slides were observed under a light microscope. A proestrus smear consisted of a predominance of round nucleated epithelial cells; an estrous smear primarily consisted of anucleated cornified cells; a metestrus smear consisted of the same proportion among leukocytes, cornified, and nucleated epithelial cells, and a diestrus smear consisted of a predominance of leukocytes (Marcondes *et al.*, 2002).

6.2 Normal saline (0.9%)

9g sodium chloride (NaCl) (ACE, Southdale, Gauteng, South Africa)

100ml distilled water (dH_2O)

6.3 Toluidine blue

1g Toluidine blue (ACE, Southdale, Gauteng, South Africa)

100ml 1% sodium borate in dH_2O (Saarchem Merck Chemicals, Gauteng, South Africa)

6.4 Vehicle for all drugs

0.9% NaCl

0.2ml NaCl per injection per rat

Anastrozole in 0.9% NaCl

A daily dose of 1mg/kg anastrozole for 5 days is the standard recommended dose in humans (Al-Omari *et al.*, 2004). A 12-14 week mature female Wistar rat weighs about 200-250g.

6.5 Four anastrozole dose regimes for the preliminary dose response study:

25mg/kg body weight (5mg anastrozole dissolved in 0.2ml of saline)

15mg/kg body weight (3mg anastrozole dissolved in 0.2ml of saline)

10mg/kg body weight (2mg anastrozole dissolved in 0.2ml of saline)

1mg/kg body weight (0.2mg anastrozole dissolved in 0.2ml of saline)

6.6 Chlomiphene citrate

1.25mg/kg of body weight chlomiphene citrate dose was adopted from previous studies (Hosie *et al.*, 2003).

(0.25mg chlomiphene citrate dissolved in 0.2ml of saline)

6.7 Anaesthesia: Anaket-Chanazine

0.1ml/100g body weight as recommended by the manufacturer (Centaur Labs, Bryanston, Gauteng, South Africa).

The Wistar rat weighs about 200g; 0.2ml was needed per animal.

0.16ml Anaket (Ketamine 100mg/ml) (Centaur Labs, Bryanston, Gauteng, South Africa)

0.04ml Chanazine (Xylazine 20mg/ml) (Centaur Labs, Bryanston, Gauteng, South Africa)

Mixture ratio of Anaket to Chanazine was 4:1

Route: intramuscular (IM)

6.8 Euthanasia: Euthapent solution

1ml Euthapent solution (200mg Pentobarbitone and 20ml Benzyl alcohol) per animal was injected intramuscular (IM) as recommended by the manufacturer (Kyron Labs (PTY) Ltd, Benrose, South Africa).

6.9 1% Pontamine sky blue

1g Pontamine sky blue (BDH Chemical Supplies, Poole, England, UK)

100ml distilled water (dH_2O)

Filtered before use

7 APPENDIX B: SOLUTIONS AND RECIPES FOR SCANNING ELECTRON MICROSCOPY (SEM)

7.1 The principle of the scanning electron microscopy and the rationale for using it in thecurrent study

The Scanning electron microscope (SEM) has enabled physical and life scientists to explore and study the surface morphology of cells, tissues and structures in more detail since 1935 when it was first built by the German scientist Max Knoll (Bogner *et al.*, 2007). The SEM uses an electron beam, which is produced by an electron gun, to trace over the specimen in order to create a high magnification and resolution 3-D image (Zhou *et al.*, 2007). As the electron beam traces over the object, it interacts with the surface of the object, dislodging secondary electrons from the surface of the specimen in unique patterns (Zhou *et al.*, 2007). A secondary electron detector attracts those scattered electrons and, depending on the number of electrons that reach the detector, registers different levels of brightness on a monitor (Goldstein *et al.*, 2003; Zhou *et al.*, 2007). Additional sensors detect backscattered electrons (electrons that reflect off the specimen's surface) and X-rays (emitted from beneath the specimen's surface) (Goldstein *et al.*, 2003). A high resolution image of the original specimen, with great surface ultrastractural detail, is then scanned onto a monitor for viewing. This makes the scanning electron microscope to be more superior to the conventional light microscope (Costello *et al.*, 1992; Zhang *et al.*, 2004; Zhou *et al.*, 2007).

SEM uses scanning coils, which create a magnetic field using fluctuating voltage, to manipulate the electron beam. The scanning coils are able to move the beam precisely back and forth over a defined section of the specimen. For example, one would increase the

magnification of an image by setting the electron beam to scan a smaller area of the sample (Goldstein *et al.*, 2003; Zhou *et al.*, 2007).

One of the objectives of this study was to determine the effects of anastrozole on the uterine surface ultrastructure during early pregnancy using scanning electron microscopy, and to an extent, to compare it as a superovulator to chlomiphene citrate in similar situations. The SEM was the most suitable tool to use in this regard. Additionally, its sample preparation is simple.

7.2 0.1M Phosphate buffer ($NaPO_4$), pH 7.4

Solution A: 0.1M of NaH_2PO_4 $2H_2O$ (ACE, Southdale, Gauteng, South Africa)

78g in 500ml distilled water

Solution B: 0.1M of Na_2HPO_4 $2H_2O$ (ACE, Southdale, Gauteng, South Africa)

8.9g in 500ml distilled water

140ml (solution A) + 360ml (solution B) = 500ml buffer

7.3 2.5% Gluteraldehyde

250ml gluteraldehyde (SPI-Chem, West Chester, PA, USA) + 1250ml buffer (0.1M $NaPO_4$) + 1000ml distilled water

7.4 1% Osmium tetroxide

Ampoule supplied contains 2ml of 4% osmium tetroxide (SPI-Chem, West Chester, PA, USA). Mix the 2ml of 4% osmium tetroxide with 6ml of phosphate buffer

7.5 1% Thiosemicarbizide

1g thiosemicarbizide (SPI-Chem, West Chester, PA, USA) in 100ml distilled water

7.6 Hexamethyldisilazane (HMDS)

Pure 100% hexamethyldisilazane (SPI-Chem, West Chester, PA, USA)

7.7 Graded alcohol solutions

100% ethanol (pure)

Distilled water (dH_2O)

50% ethanol (100ml): mix 50ml of pure ethanol with 50ml distilled water

70% ethanol (100ml): mix 70ml of pure ethanol with 30ml distilled water

80% ethanol (100ml): mix 80ml of pure ethanol with 20ml distilled water

95% ethanol (100ml): mix 95ml of pure ethanol with 5ml distilled water

8 APPENDIX C: SOLUTIONS AND RECIPES FOR IMMUNOFLUORESCENCE AND CONFOCAL MICROSCOPY

8.1 The principle of immunofluorescence and confocal microscopy and the rationale for using it in the study

The immunofluorescence technique was first developed by Coons and Kaplan in 1941 (Coons *et al.*, 1942). This technique involves antibodies that are conjugated to fluorescent dyes (fluorochromes) such as fluorescein isothiocyanate (FITC) or tetramethyl rhodamine isothiocyanate (TRITC), which bind directly or indirectly to the antigen of interest (Mohan *et al.*, 2008; Odell and Cook, 2013). Upon absorption of high energy light, the fluorochrome emits light at its own characteristic wavelength (fluorescence) and thus allows detection of antigen-antibody complexes and be able to visualize under a fluorescence or confocal microscope (Mohan *et al.*, 2008). In other words, it is a powerful technique that utilizes fluorescent-labeled antibodies to detect specific target antigens. This technique is widely used in both clinical laboratories and scientific research (Mohan *et al.*, 2008; Odell and Cook, 2013). The indirect immunofluorescence utilizes a two-step method, in which a primary, unlabeled antibody binds to the target, after which a fluorophore-labeled secondary antibody, directed against the primary antibody, is used to detect the first antibody (Mohan *et al.*, 2008; Odell and Cook, 2013). This technique is more complicated and time consuming than the direct immunofluorescence because it requires a second incubation period (Rao and Shenoi, 2006); however, it is more sensitive because more than one secondary antibody can bind to each primary antibody, which amplifies the fluorescence signal (Odell and Cook, 2013). Like the direct labeling, the indirect labeling can utilize double labeling in which the FITC is used

in conjunction with the TRITC to demonstrate co-localization of two proteins of interest in tissues (Mohan *et al.*, 2008; Kaneko *et al.*, 2011). Generally, fluorescence signals depend on the concentration and quality of the antibodies, proper handling of the specimen, and detection with the appropriate secondary antibodies (Odell and Cook, 2013).

Confocal microscopy became available for use in 1987 (Paddock and Eliceiri, 2014). The current laser scanning confocal microscope is designed from the conventional light microscope. The laser scanning confocal microscope generates high-resolution images and 3-D reconstructions of specimens (Boruah and Neil, 2009). The principle of confocal microscopy involves a laser light beam that is focused onto a fluorescent specimen through the objective lens (Boruah and Neil, 2009). The mixture of reflected and emitted light is captured by the same objective and is sent to the dichroic mirror (Amos and White, 2003). The reflected light is deviated by the mirror while the emitted fluorescent light passes through a confocal aperture to reduce the "out of focus" light. The focused light then passes through the emission filter and proceeds to the photomultiplier (Amos and White, 2003). The photomultiplier detects light from the specimen and the resultant development of an image on the computer (Amos and White, 2003). In order to generate an entire image, the single point is scanned in an X-Y manner as the laser focus is moved over the specimen (Choi *et al.*, 2013). The acquired images, which are stored on the computer, are ready for analysis using any conventional statistical computer software (Boruah and Neil, 2009).

It is better to use the laser scanning confocal microscope than the conventional light microscope because the images in the confocal microscope are detected by a computer instead

of an eye, so it is possible to detect more color differences when using the confocal (Boruah and Neil, 2009). In addition, fluorescent dyes, in most applications, have overlapping emission spectra (Zimmermann *et al.,* 2003). Hence, the emission signals cannot be separated completely into different detection channels resulting in cross talks. However, if the fluorescent dyes have distinct excitation spectra, the fluorescent dyes can be excited sequentially using one excitation wavelength at a time (Zimmermann *et al.,* 2003). This is possible with confocal systems that offer the multitracking feature (Paddock and Eliceiri, 2014). Therefore, confocal microscopy has less cross talks hence improves resolution (Choi *et al.*, 2013; Paddock and Eliceiri, 2014). The high resolution of a confocal microscope (Choi *et al.*, 2013) makes it easier to utilize double labeling to study the physical interaction of protein partners and co-localization (Paddock and Eliceiri, 2014). Additionally, one can use optical sectioning of the specimen without physical contact and perform 3-D reconstruction of specimen (Choi *et al.*, 2013; Paddock and Eliceiri, 2014). Therefore, confocal microscopy has become a powerful tool in life sciences (Paddock and Eliceiri, 2014).

8.2 10% Buffered formalin (2l)

200ml formalin

7g NaH_2PO_4 (ACE, Southdale, Gauteng, South Africa)

13g Na_2HPO_4 (ACE, Southdale, Gauteng, South Africa)

1800ml distilled water

8.3 Gelatin-coating solution

5g gelatin (ACE, Southdale, Gauteng, South Africa)

0.5g chromium potassium sulfate dodecahydrate ($CrK(SO_4)_2.12H_2O$ (ACE, Southdale, Gauteng, South Africa); mix in 1000ml distilled water

8.4 Phosphate buffered saline (PBS) pH 7.4

8g NaCl (ACE, Southdale, Gauteng, South Africa)

1.15g Na_2HPO_4 (ACE, Southdale, Gauteng, South Africa)

0.2g KCl (ACE, Southdale, Gauteng, South Africa)

0.2g KH_2PO_4 (ACE, Southdale, Gauteng, South Africa)

To 1000ml distilled water

8.5 Peroxidase quenching solution

30% H_2O_2 in methanol

8.6 Permeabilized buffer

0.1% Triton-X 100 (Sigma-Aldrich Co., St. Louis, MO, USA) in PBS (pH 7.4)

8.7 Blocking solution

5% normal goat serum (Sigma-Aldrich Co., St. Louis, MO, USA) in PBS (pH 7.4)

To make 20ml blocking solution, add 1ml of goat serum to 19ml of PBS (pH 7.4)

8.8 Rabbit polyclonal anti-Integrin β5 in blocking solution (1:100)

1µl Rabbit ant-Integrin β5 (Abcam, Cambridge, MA, USA)

99µl blocking solution

8.9 Mouse monoclonal anti-Vinculin in blocking solution (1:100)

1µl Mouse ant-Vinculin (Abcam, Cambridge, MA, USA)

99µl blocking solution

8.10 Mouse monoclonal anti-Paxillin in blocking solution (1:100)

1µl Mouse ant-Paxillin (Abcam, Cambridge, MA, USA)

99µl blocking solution

8.11 Rabbit monoclonal anti-FAK in blocking solution (1:100)

1µl Rabbit ant-FAK (Abcam, Cambridge, MA, USA)

99µl blocking solution

8.12 Goat F(ab') 2 polyclonal secondary antibody to Rabbit IgG (TRITC) pre-adsorbed in blocking solution (1:100)

1µl Goat ant-Rabbit IgG (TRITC) pre-adsorbed (Abcam, Cambridge, MA, USA)

99µl blocking solution

8.13 Goat F(ab') 2 polyclonal secondary antibody to Mouse IgG (FITC) pre-adsorbed in blocking solution (1:100)

1µl Goat ant-Mouse IgG (FITC) pre-adsorbed (Abcam, Cambridge, MA, USA)

99µl blocking solution

8.14 DAPI (4',6-diamidino-2-phenylindole)

DAPI binds to dsDNA; it is used to label nuclei. The maximum excitation for DAPI bound to dsDNA is 358nM and the maximum emission is 461nM.

1000X DAPI stock solution

Dissolve 0.2 mg DAPI in 1 ml dH_2O and store at 4°C in the dark

McIlvaine's buffer, pH 7.0

Stock solution A: 0.1 M citric acid, for 200 ml use 4.2 g

Stock solution B: 0.2 M Na2HPO4, for 800 ml use 22.7 g

Mix 2 parts of stock A and 8 parts of stock B to make McIlvaine's buffer, pH 7.0

DAPI staining solution (600 nM DAPI)

10 ml McIlvaine's buffer, pH 7.0

10 ml 1000X DAPI stock

After sections were incubated with the secondary antibody followed by three PBS washes for 5 minutes, sections were counterstained with DAPI to label nuclei (300µl on each section) for 3minutes, washed three times with PBS for 5minutes; then, coverslips were mounted with a Fluoromount and examined for nuclei staining under the Zeiss LSM 780 confocal microscope (Carl Zeiss, Jena, Germany).

9 APPENDIX D: REAL TIME QUANTITATIVE POLYMERASE CHAIN REACTION (qPCR)

9.1 The principle of qPCR and the rationale for using it in the study

Polymerase chain reaction (PCR) is a technique that allows exponential amplification and detection of short sequences of DNA within a longer double stranded DNA template (Wilhelm and Pingoud, 2003; Ding and Cantor, 2004; Wang and Kaltenboeck, 2005). The technique uses a pair of primers that are complementary to a defined sequence on each of the two strands of the DNA (Hoebeeck *et al.*, 2005). These primers are extended by DNA polymerases so that copies are made of designated sequences leading to exponential amplification (Arya *et al.*, 2005; Wang and Kaltenboeck, 2005). The real-time qPCR technique collects data throughout the PCR process as it occurs, thus amplifying and detecting DNA sequences using fluorescent dyes that correlate PCR product concentration to fluorescence intensity (Wong and Medrano, 2005). Therefore, the qPCR technique enables sensitive and specific quantification of the initial target sequence amounts and PCR products accumulated during the amplification cycle (Ding and Cantor, 2004; Wang and Kaltenboeck, 2005).

In this study, the qPCR was performed to quantify gene expression of the focal adhesion proteins vinculin, integrin β5, paxillin and focal adhesion kinase (FAK) in the uterine epithelial cells from day 1 and day 6 pregnant rats of all treatment regimes.

9.2 RNA extraction method

About 30mg of uterine epithelial tissue from each animal of day 1 and 6 of pregnant rats was isolated from each uterine horn as described previously (Kaneko *et al.*, 2008; 2009). The uterine horn was cut open longitudinally. The surface luminal epithelial tissue was removed using sterile surgical blades and was incubated in liquid nitrogen where it was ground using a mortar and pestle. The tissue powder was immediately transferred into a 1.5ml microcentrifuge tube (Whitehead Scientific) containing 300µl of lysis buffer (50mM Tris-HCl (pH7.5) supplemented with β-mercaptoethanol (added 20µl of 14.3M β-mercaptoethanol to each 1ml volume of lysis buffer). The mixture was vortexed for 10 seconds and then 600µl of diluted proteinase K (10µl of proteinase K diluted in 590µl of TE buffer (10mM Tris HCl, pH 8.0, 1mM EDTA) was added and incubated at 15-25°C for 10 minutes and centrifuged for 10 minutes at ≥12000 x g (Thermo Scientific Inc., 2011). The supernatant was transferred into a new RNase-free microcentrifuge tube to which 450µl of ethanol (99.9%) was added and mixed by pipetting. The lysate was transferred to the GeneJET RNA purification column inserted in a collection tube and centrifuged for 1min at ≥12000 x g. The GeneJET RNA purification column was placed into a new 2ml collection tube to which 700µl of wash buffer 1 was added and centrifuged for 1minute at ≥12000 x g. The GeneJET RNA purification column was placed back to which 600µl of wash buffer 2 (supplemented with 63% ethanol) was added and centrifuged for 1minute at ≥12000 x g. Then 250µl of wash buffer 2 was added to the GeneJET RNA purification column and centrifuged for 2 minutes at ≥12000 x g. In order to elude RNA, the GeneJET RNA purification column was transferred to a sterile 1.5ml RNase-free microcentrifuge tube to which 100µl of nuclease-free water was added and centrifuged for 1minute at ≥12000 x g (Thermo Scientific Inc., 2011).

9.3 Complimentary DNA (cDNA) synthesis

The standard cDNA synthesis protocol was used similar to the one used by the supplier of the high capacity cDNA reverse transcription kit (Thermo Fisher Scientific Inc., 2011). A 2X reverse transcription master mix (20µl per reaction) was prepared on ice as shown in Table 5.1.

Table 9.1: Components of master mix for cDNA synthesis

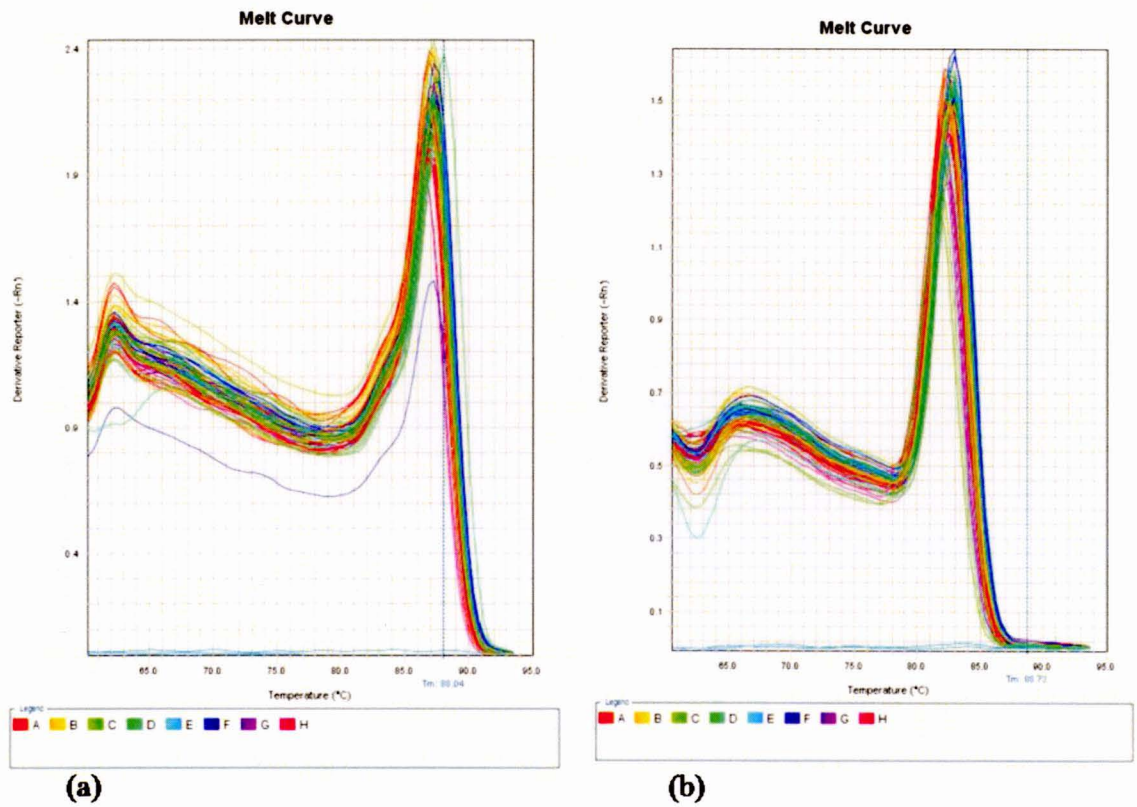
Component	Volume/reaction (µl)	
	With multiscribe reverse transcriptase (+RT)	Without multiscribe reverse transcriptase (-RT)
10X RT Buffer	2.0	2.0
25X dNTP mix (100mM)	0.8	0.8
10X RT Random Primers	2.0	2.0
Multiscribe Reverse Transcriptase	1.0	1.0 (Nuclease-free water)
RNase inhibitor	1.0	1.0
Nuclease-free water	3.2	4.2
Total per reaction	10.0	10.0

In order to get the recommended 20µl in each reaction tube, 10µl of the master mix was added with 10µl from each clean RNA sample (500ng/10µl). Reaction tubes in both +RT and –RT groups were prepared in duplicates, which were run by a Thermocycler Gene Amp PCR System 2400 (Applied Biosystems) to make cDNA. Before each run, the thermal cycler conditions were programmed as recommended by the supplier of the high capacity cDNA reverse transcriptase kit (Thermo Fisher Scientific Inc., 2011) as shown in Table 5.2.

Table 9.2: cDNA synthesis thermocycling conditions

Variable	Step 1	Step 2	Step3	Step4
Temperature (^{o}C)	25	37	85	4
Time	10 minutes	120 minutes	5 minutes	∞

9.4 Melt curves of the PCR products



(a) (b)

Figure 9.1: Vinculin and integrin β5 melt curves. (a) Melt curve of vinculin PCR product. The melting temperature of vinculin PCR product is 88.04^{0}C. (b) Melt curve of integrin β5 PCR product. The melting temperature of integrin β5 is 88.73^{0}C.

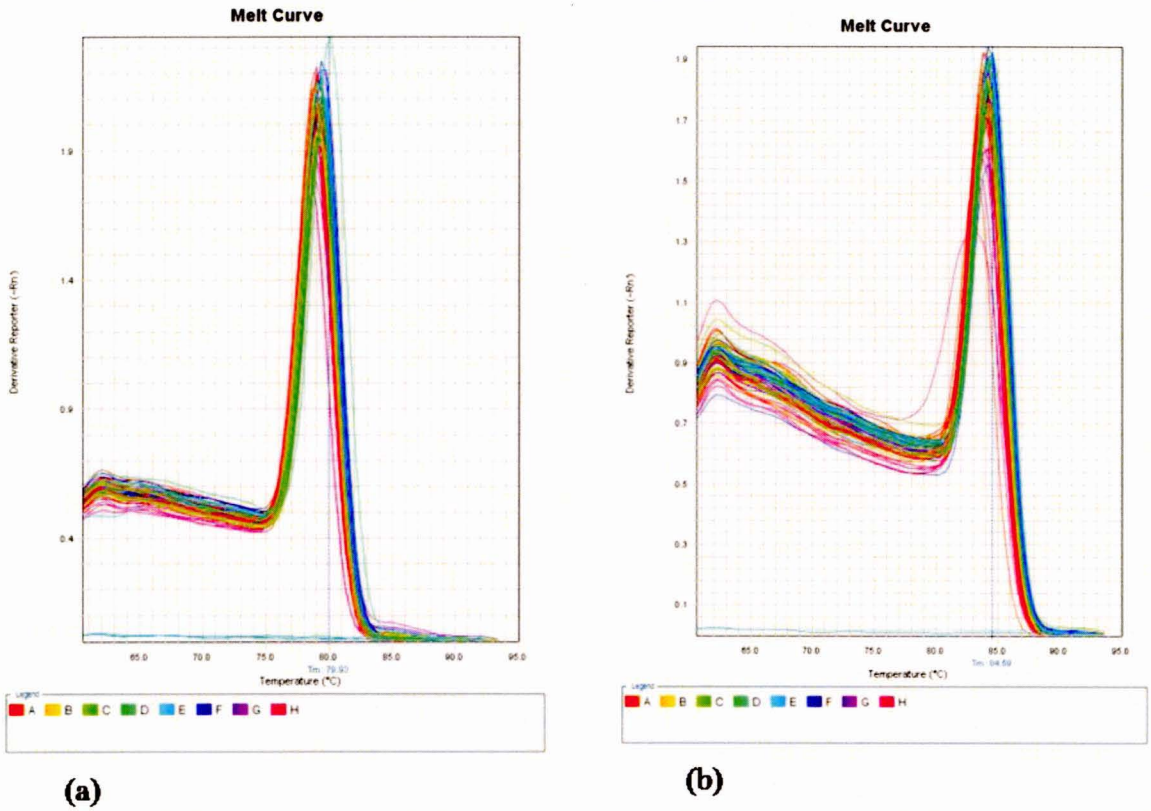


Figure 9.2: FAK and paxillin melt curves. (a) Melt curve of FAK PCR product. The melting temperature of FAK PCR product is 79.93^{0}C. (b) Melt curve of paxillin PCR product. The melting temperature of paxillin PCR product is 84.59^{0}C.

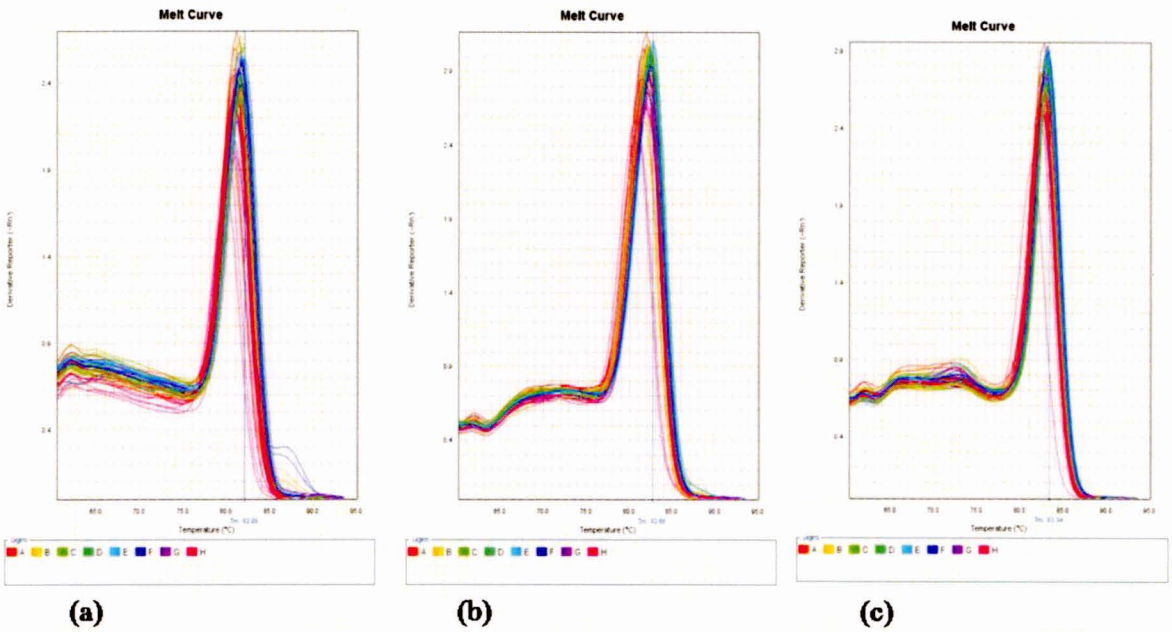


Figure 9.3: Melt curves of reference genes. (a) Melt curve of β-actin PCR product. The melting temperature of β-actin PCR product is 82.09^0C. (b) Melt curve of 18Sr PCR product. The melting temperature of 18Sr PCR product is 82.66^0C. (c) Melt curve of LdhA PCR product. The melting temperature of LdhA PCR product is 83.34^0C.

9.5 Gel electrophoresis of genes of interest and reference genes

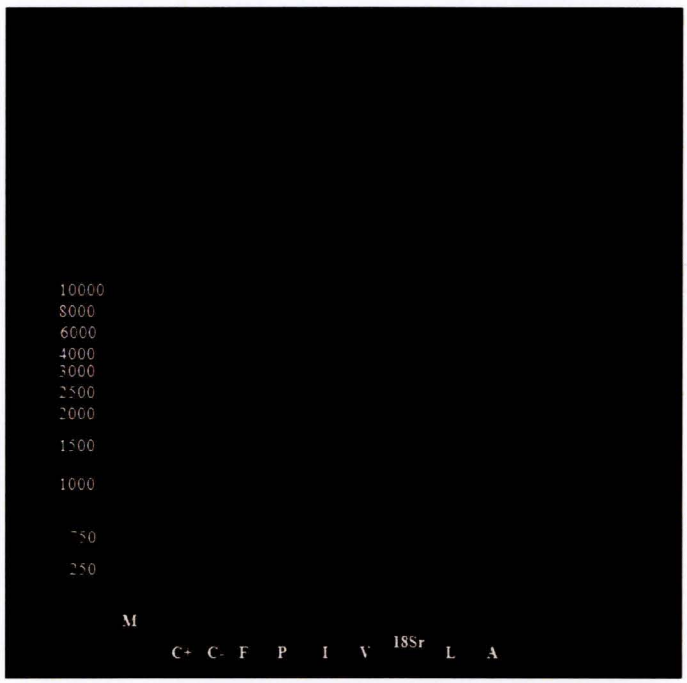


Figure 9.4: Gel electrophoresis of genes of interest and reference genes. (M) Molecular weight ladder. It is a 1kb DNA ladder, SM number 0313 Fermentas, Lot number 00037642. The range of the ladder is 250 to 10,000 base pairs (bp). The following are the molecular weight of each of the gene products: (V) vinculin = 139 bp, (P) paxillin = 112 bp, (I) integrin β5 = 97 bp, (F) FAK = 86 bp, 18Sr = 204 bp, (L) LdhA = 108 bp, (A) β-actin = 74 bp. C+ and C– are controls.

9.6 Comparative C_T Method ($2^{-\Delta\Delta CT}$ Method) for calculating fold change in gene expression

The comparative C_T method ($2^{-\Delta\Delta CT}$ method) was used to determine the gene expression fold change relative to the control following drug treatment regimes (Schmittgen and Livak, 2008). The mean C_T values and standard deviations were used in the $\Delta\Delta C_T$ calculations. In this study, each sample type was run in triplicate. Each sample C_T mean was calculated and standard deviations were calculated for each mean C_T value. The following steps were followed:

Step 1: Calculated the mean C_T and standard deviation values of the replicate sample results.

Step 2: Calculated the ΔC_T value.

The ΔC_T value was calculated by:

$$\Delta C_T = C_{T\ target} - C_{T\ reference}$$

Step 3: Calculated the standard deviation of the ΔC_T value.

The standard deviation of the ΔC_T was calculated from the standard deviations of the target and reference values using the formula:

$s = (s_1 2 + s_2 2)^{½}$; where $X^{½}$ is the square root of X and s = standard deviation.

Step 4: Calculated the $\Delta\Delta C_T$ value.

The $\Delta\Delta C_T$ was calculated by:

$\Delta\Delta C_T = \Delta C_T$ test sample – ΔC_T calibrator sample

Step 5: Calculated the standard deviation of the $\Delta\Delta C_T$ value.

The calculation of $\Delta\Delta C_T$ involves subtraction of the ΔC_T calibrator value. This is subtraction of an arbitrary constant, so the standard deviation of the $\Delta\Delta C_T$ value is the same as the standard deviation of the ΔC_T value.

Step 6: Incorporated the standard deviation of the $\Delta\Delta C_T$ values into the fold-difference.

Fold-differences were calculated using the $\Delta\Delta C_T$ method and expressed as a range, which is a result of incorporating the standard deviation of the $\Delta\Delta C_T$ value into the fold-difference calculation.

10 APPENDIX E: REAGENTS/CHEMICALS AND DRUGS

Table 10.1: Chemicals used in the study and their suppliers

Absolute ethanol	Sigma-Aldrich Co., St. Louis, MO, USA
Agarose	Sigma-Aldrich Co., St. Louis, MO, USA
Chloroform	Sigma-Aldrich Co., St. Louis, MO, USA
4',6-diamidino-2-phenylindole (DAPI)	Sigma-Aldrich Co., St. Louis, MO, USA
Ethidium bromide	Sigma-Aldrich Co., St. Louis, MO, USA
Methanol	Sigma-Aldrich Co., St. Louis, MO, USA
Proteinase K	Thermo Scientific Inc., Pretoria, Gauteng, South Africa
Sodium hydrogen phosphate	Merck KGaA, Darmstadt, Germany
Triton-X 100	Sigma-Aldrich Co., St. Louis, MO, USA
Xylene	Sigma-Aldrich Co., St. Louis, MO, USA
Anastrozole	Sigma-Aldrich Co., St. Louis, MO, USA
Chlomiphene citrate	Sigma-Aldrich Co., St. Louis, MO, USA
Pontamine sky blue	BDH Chemical Supplies, Poole, England, UK
Gluteraldehyde	SPI-Chem, West Chester, PA, USA
Osmium tetroxide	SPI-Chem, West Chester, PA, USA
Thiosemicarbazide	SPI-Chem, West Chester, PA, USA
Hexamethyldisilazane (HMDS)	SPI-Chem, West Chester, PA, USA
Formalin	ACE, Southdale, Gauteng, South Africa
Normal goat serum	Sigma-Aldrich Co., St. Louis, MO, USA
Hydrogen peroxide	Sigma-Aldrich Co., St. Louis, MO, USA
Methanol	Sigma-Aldrich Co., St. Louis, MO, USA
Tris-ethylenediamine tetraacetic acid (EDTA)	Sigma-Aldrich Co., St. Louis, MO, USA
Diethyl pyrocarbonate (DEPC)	Sigma-Aldrich Co., St. Louis, MO, USA

Ethidium brodium	Sigma-Aldrich Co., St. Louis, MO, USA
Sodium chloride	Sigma-Aldrich Co., St. Louis, MO, USA
Toludine blue	Sigma-Aldrich Co., St. Louis, MO, USA
Anaket-Chanazine	Centaur Labs, Bryanston, Gauteng, South Africa
Euthapent solution	Centaur Labs, Bryanston, Gauteng, South Africa
Gelatin	Sigma-Aldrich Co., St. Louis, MO, USA
Acid alcohol	Sigma-Aldrich Co., St. Louis, MO, USA

11 APPENDIX F: EQUIPMENT AND KITS USED

Table 11.1: Equipment and manufacturers

Equipment and kits	Manufacturer
Automatic tissue processor (Shandon Citadel 1000 Carousel type)	Thermo Fisher Scientific, Pittsburgh, USA
Axioskop 2 Plus with Axio Cam HRc	Carl Zeiss, Jena, Germany
BioRAD Gel Doc XR system	BioRAD, Segrate, Milan, Italy
Dry block heater HB2	Hagar Designs, Pinelands, South Africa
Emitech K950X coater	Quorum Technologies Ltd, Ashford, Kent, UK
Eppendorf 5415D microfuge	Eppendorf, Cambridge, UK
Gemini Zeiss Ultra Plus	Carl Zeiss, Jena, Germany
GeneAmp PCR system 2400	Applied Biosystems, Norwalk, CT, USA
NanoDrop ND 1000	NanoDrop Technologies, Wilmington DE, USA
Leica 2035 Biocut microtome	Leica, Nussloch, Germany
7500 real-time PCR thermocycler	Applied Biosystems, Foster City, CA, USA
SEM FEI NOVA 600 Nanolab (EDS)	FEI Company, Hillsboro, OR, USA
Zeiss LSM 780 confocal microscope	Carl Zeiss, Jena, Germany
cDNA reverse transcription kit	Thermo Scientific Inc., Pretoria, Gauteng, South Africa
GeneJET RNA purification kit	Thermo Scientific Inc., Pretoria, Gauteng, South Africa
QuantiFast SYBR Green PCR kit	Thermo Scientific Inc., Pretoria, Gauteng, South Africa
Light microscope (for vaginal smears)	Carl Zeiss, Jena, Germany
Dissecting microscope	Carl Zeiss, Jena, Germany

12 APPENDIX G: STATISTICAL ANALYSES

12.1 STATISTICAL ANALYSIS FOR THE DOSE RESPONSE STUDY

Table 12.1: A summary of the analysis of variance using a one way ANOVA test to determine changes in the implantation means between various treatment regimes.

Source		Df	Sum of squares	Mean square	F-Ratio	P-value
Implantation sites	Group	6	323.08571	53.8476	15.9790	< 0.0001 *
	Error	28	88.80000	3.1714		
	C. Total	34	411.88571			

Table 12.2: A summary of comparisons of means of implantation sites using the Tukey-Kramer Absolute (Difference) HSD tests for treatment regimes at the 5 % level of significance.

	15mg/kg	CC	25mg/kg	10mg/kg	1mg/kg	Untreated	Saline
Mean ± SE	16.6± 0.8	11.6 ± 0.8	10.6 ± 0.8	8.4 ± 0.8	7.8 ± 0.8	7.8 ± 0.8	7.4 ± 0.8
15mg/kg	-3.518	1.482	2.482	4.682	5.398	5.282	5.682
CC	1.482	-3.518	-2.518	-0.318	0.398	0.282	0.682
25mg/kg	2.482	-2.518	-3.518	-1.318	-0.602	-0.718	-0.318
10mg/kg	4.682	-0.318	-1.318	-3.518	-2.802	-2.918	-2.518
1mg/kg	5.398	0.398	-0.602	-2.802	-3.212	-3.335	-2.935
Untreated	5.282	0.282	-0.718	-2.918	-3.335	-3.518	-3.118
Saline	5.682	0.682	-0.318	-2.518	-2.935	-3.118	-3.518

Note: Positive values show pairs of means that are significantly different.

Table 12.3: Means and standard deviations of implantation sites

Level	Number	Mean	Std Dev	Std Err Mean	Lower 95%	Upper 95%
10mg/kg	5	8.4000	1.14018	0.5099	6.984	9.816
15mg/kg	5	16.6000	3.97492	1.7776	11.664	21.536
1mg/kg	5	7.8333	0.98319	0.4014	6.802	8.865
25mg/kg	5	10.6000	1.14018	0.5099	9.184	12.016
CC	5	11.6000	0.89443	0.4000	10.489	12.711
Saline	5	7.4000	1.14018	0.5099	5.984	8.816
Untreated	5	7.8000	0.83666	0.3742	6.761	8.839

Table 12.4: The analysis of means using a Tukey-Kramer post hoc test in order to compare the number of implantation sites between treatment groups.

Level				Mean
15mg/kg	A			16.6
CC		B		11.6
25mg/kg		B	C	10.6
10mg/kg		B	C	8.40
1mg/kg			C	7.80
untreated			C	7.80
Saline			C	7.40

Levels not connected by same letter are significantly different.

12.2 STATISTICAL ANALYSES FOR SCANNING ELECTRON MICROSCOPY

12.2.1 Microvilli density

Table 12.5: A one way ANOVA summary of fit of microvilli density

R square	0.494591
Adj R square	0.462502
Root Mean Square Error	0.508135
Mean of Response	1.814815
Observations (or Sum Wgts)	135

Table 12.6: Analysis of variance of microvilli density

Source	DF	Sum of Squares	Mean Square	F Ratio	Prob > F
Rats	8	31.837037	3.97963	15.4129	<.0001*
Error	126	32.533333	0.25820		
C. Total	134	64.370370			

Table 12.7: Microvilli density means and standard deviations

Level	Number	Mean	Std Dev	Std Err Mean	Lower 95%	Upper 95%
1A	15	2.46667	0.516398	0.13333	2.1807	2.7526
1CC	15	2.46667	0.516398	0.13333	2.1807	2.7526
1U	15	2.53333	0.516398	0.13333	2.2474	2.8193
6A IP	15	1.33333	0.487950	0.12599	1.0631	1.6036
6A NP	15	1.53333	0.516398	0.13333	1.2474	1.8193
6CC IP	15	1.40000	0.507093	0.13093	1.1192	1.6808
6CC NP	15	1.66667	0.487950	0.12599	1.3964	1.9369
6U IP	15	1.40000	0.507093	0.13093	1.1192	1.6808
6U NP	15	1.53333	0.516398	0.13333	1.2474	1.8193

Table 12.8: The analysis of means using a Tukey-Kramer post hoc test in order to assess the changes in microvilli density between treatment groups.

Level		Mean
1U	A	2.5333333
1A	A	2.4666667
1CC	A	2.4666667
6CC NP	B	1.6666667
6A NP	B	1.5333333
6U NP	B	1.5333333
6CC IP	B	1.4000000
6U IP	B	1.4000000
6A IP	B	1.3333333

Levels not connected by same letter are significantly different.

12.2.2 Microvilli length

Table 12.9: A one way ANOVA summary of fit of microvilli length

R square	0.908512
Adj R square	0.902703
Root Mean Square Error	0.281718
Mean of Response	1.681481
Observations (or Sum Wgts)	135

Table 12.10: Analysis of variance of microvilli length

Source	DF	Sum of Squares	Mean Square	F Ratio	Prob > F
Rats	8	99.30370	12.4130	156.4033	<.0001*
Error	126	10.00000	0.0794		
C. Total	134	109.30370			

Table 12.11: Means and standard deviations of microvilli length

Level	Number	Mean	Std Dev	Std Err Mean	Lower 95%	Upper 95%
1A	15	2.93333	0.258199	0.06667	2.7903	3.0763
1CC	15	2.86667	0.351866	0.09085	2.6718	3.0615
1U	15	2.86667	0.351866	0.09085	2.6718	3.0615
6A IP	15	1.00000	0.000000	0.00000	1.0000	1.0000
6A NP	15	1.00000	0.000000	0.00000	1.0000	1.0000
6CC IP	15	1.13333	0.351866	0.09085	0.9385	1.3282
6CC NP	15	1.26667	0.457738	0.11819	1.0132	1.5202
6U IP	15	1.00000	0.000000	0.00000	1.0000	1.0000
6U NP	15	1.06667	0.258199	0.06667	0.9237	1.2097

Table 12.12: The analysis of means using a Tukey-Kramer post hoc test in order to assess the changes in microvilli length between treatment groups.

Level		Mean
1A	A	2.9333333
1CC	A	2.8666667
1U	A	2.8666667
6CC NP	B	1.2666667
6CC IP	B	1.1333333
6U NP	B	1.0666667
6A IP	B	1.0000000
6A NP	B	1.0000000
6U IP	B	1.0000000

Levels not connected by same letter are significantly different.

12.2.3 Microvilli surface beads

Table 12.13: A one way ANOVA summary of fit of microvilli surface beads

R square	0.392254
Adj R square	0.353667
Root Mean Square Error	0.599824
Mean of Response	0.592593
Observations (or Sum Wgts)	135

Table 12.14: Analysis of variance of microvilli surface beads

Source	DF	Sum of Squares	Mean Square	F Ratio	Prob > F
Rats	8	29.259259	3.65741	10.1654	<.0001*
Error	126	45.333333	0.35979		
C. Total	134	74.592593			

Table 12. 15: Means and standard deviations of microvilli surface beads

Level	Number	Mean	Std Dev	Std Err Mean	Lower 95%	Upper 95%
1A	15	1.33333	0.816497	0.21082	0.8812	1.7855
1CC	15	1.13333	0.833809	0.21529	0.6716	1.5951
1U	15	1.26667	0.798809	0.20625	0.8243	1.7090
6A IP	15	0.20000	0.414039	0.10690	-0.0293	0.4293
6A NP	15	0.26667	0.457738	0.11819	0.0132	0.5202
6CC IP	15	0.26667	0.457738	0.11819	0.0132	0.5202
6CC NP	15	0.33333	0.487950	0.12599	0.0631	0.6036
6U IP	15	0.20000	0.414039	0.10690	-0.0293	0.4293
6U NP	15	0.33333	0.487950	0.12599	0.0631	0.6036

Table 12.16: The analysis of means using a Tukey-Kramer post hoc test in order to assess the changes in microvilli surface beads between treatment groups.

Level		Mean
1A	A	1.3333333
1U	A	1.2666667
1CC	A	1.1333333
6CC NP	B	0.3333333
6U NP	B	0.3333333
6A NP	B	0.2666667
6CC IP	B	0.2666667
6A IP	B	0.2000000
6U IP	B	0.2000000

Levels not connected by same letter are significantly different.

12.2.4 Large surface protrusions

Table 12.17: A one way ANOVA summary of fit of large surface protrusions

R square	0.626049
Adj R square	0.602306
Root Mean Square Error	0.331742
Mean of Response	0.57037
Observations (or Sum Wgts)	135

Table 12.18: Analysis of variance of large surface protrusions

Source	DF	Sum of Squares	Mean Square	F Ratio	Prob > F
Rats	8	23.214815	2.90185	26.3678	<.0001*
Error	126	13.866667	0.11005		
C. Total	134	37.081481			

Table 12.19: Means and standard deviations of large surface protrusions

Level	Number	Mean	Std Dev	Std Err Mean	Lower 95%	Upper 95%
1A	15	0.00000	0.000000	0.00000	0.00000	0.0000
1CC	15	0.00000	0.000000	0.00000	0.00000	0.0000
1U	15	0.00000	0.000000	0.00000	0.00000	0.0000
6A IP	15	1.06667	0.258199	0.06667	0.92368	1.2097
6A NP	15	0.93333	0.457738	0.11819	0.67985	1.1868
6CC IP	15	0.80000	0.414039	0.10690	0.57071	1.0293
6CC NP	15	0.73333	0.457738	0.11819	0.47985	0.9868
6U IP	15	0.86667	0.351866	0.09085	0.67181	1.0615
6U NP	15	0.73333	0.457738	0.11819	0.47985	0.9868

Table 12.20: The analysis of means using a Tukey-Kramer post hoc test in order to assess the changes in large surface protrusions between treatment groups.

Level		Mean
6A IP	A	1.0666667
6A NP	A	0.9333333
6U IP	A	0.8666667
6CC IP	A	0.8000000
6CC NP	A	0.7333333
6U NP	A	0.7333333
1A	B	0.0000000
1CC	B	0.0000000
1U	B	0.0000000

Levels not connected by same letter are significantly different.

12.2.5 Uterine surface folding

Table 12.21: A one way ANOVA summary of fit of uterine surface folding

R square	0.432983
Adj R square	0.396982
Root Mean Square Error	0.464621
Mean of Response	1.614815
Observations (or Sum Wgts)	135

Table 12.22: Analysis of variance of uterine surface folding

Source	DF	Sum of Squares	Mean Square	F Ratio	Prob > F
Rats	8	20.770370	2.59630	12.0270	<.0001*
Error	126	27.200000	0.21587		
C. Total	134	47.970370			

Table 12.23: Means and standard deviations of uterine surface folding

Level	Number	Mean	Std Dev	Std Err Mean	Lower 95%	Upper 95%
1A	15	2.13333	0.516398	0.13333	1.8474	2.4193
1CC	15	2.13333	0.351866	0.09085	1.9385	2.3282
1U	15	2.06667	0.593617	0.15327	1.7379	2.3954
6A IP	15	1.13333	0.351866	0.09085	0.9385	1.3282
6A NP	15	1.53333	0.516398	0.13333	1.2474	1.8193
6CC IP	15	1.13333	0.351866	0.09085	0.9385	1.3282
6CC NP	15	1.60000	0.507093	0.13093	1.3192	1.8808
6U IP	15	1.20000	0.414039	0.10690	0.9707	1.4293
6U NP	15	1.60000	0.507093	0.13093	1.3192	1.8808

Table 12.24: The analysis of means using a Tukey-Kramer post hoc test in order to assess the changes in uterine surface folding between treatment groups.

Level				Mean
1A	A			2.1333333
1CC	A			2.1333333
1U	A	B		2.0666667
6CC NP	A	B	C	1.6000000
6U NP	A	B	C	1.6000000
6A NP		B	C	1.5333333
6U IP			C	1.2000000
6A IP			C	1.1333333
6CC IP			C	1.1333333

Levels not connected by same letter are significantly different.

12.2.6 Surface glycocalyx

Table 12.25: A one way ANOVA summary of fit of surface glycocalyx

R square	0.287097
Adj R square	0.241833
Root Mean Square Error	0.483593
Mean of Response	0.777778
Observations (or Sum Wgts)	135

Table 12.26: Analysis of variance of surface glycocalyx

Source	DF	Sum of Squares	Mean Square	F Ratio	Prob > F
Rats	8	11.866667	1.48333	6.3428	<.0001*
Error	126	29.466667	0.23386		
C. Total	134	41.333333			

Table 12.27: Means and standard deviations of surface glycocalyx

Level	Number	Mean	Std Dev	Std Err Mean	Lower 95%	Upper 95%
1A	15	1.13333	0.516398	0.13333	0.84736	1.4193
1CC	15	1.20000	0.414039	0.10690	0.97071	1.4293
1U	15	1.20000	0.414039	0.10690	0.97071	1.4293
6A IP	15	0.80000	0.414039	0.10690	0.57071	1.0293
6A NP	15	0.60000	0.507093	0.13093	0.31918	0.8808
6CC IP	15	0.53333	0.516398	0.13333	0.24736	0.8193
6CC NP	15	0.53333	0.516398	0.13333	0.24736	0.8193
6U IP	15	0.46667	0.516398	0.13333	0.18070	0.7526
6U NP	15	0.53333	0.516398	0.13333	0.24736	0.8193

Table 12.28: The analysis of means using a Tukey-Kramer post hoc test in order to assess the changes in surface glycocalyx between treatment groups.

Level				Mean
1CC	A			1.2000000
1U	A			1.2000000
1A	A	B		1.1333333
6A IP	A	B	C	0.8000000
6A NP		B	C	0.6000000
6CC IP			C	0.5333333
6CC NP			C	0.5333333
6U NP			C	0.5333333
6U IP			C	0.4666667

Levels not connected by same letter are significantly different.

12.2.7 Membrane pores

Table 12.29: A one way ANOVA summary of fit of membrane pores

Rsquare	0.653076
Adj Rsquare	0.631049
Root Mean Square Error	0.331742
Mean of Response	0.614815
Observations (or Sum Wgts)	135

Table 12.30: Analysis of variance of membrane pores

Source	DF	Sum of Squares	Mean Square	F Ratio	Prob > F
Rats	8	26.103704	3.26296	29.6490	<.0001*
Error	126	13.866667	0.11005		
C. Total	134	39.970370			

Table 12.31: Means and standard deviations of membrane pores

Level	Number	Mean	Std Dev	Std Err Mean	Lower 95%	Upper 95%
1A	15	0.00000	0.000000	0.00000	0.00000	0.0000
1CC	15	0.00000	0.000000	0.00000	0.00000	0.0000
1U	15	0.00000	0.000000	0.00000	0.00000	0.0000
6A IP	15	1.06667	0.457738	0.11819	0.81318	1.3202
6A NP	15	0.86667	0.351866	0.09085	0.67181	1.0615
6CC IP	15	0.93333	0.457738	0.11819	0.67985	1.1868
6CC NP	15	0.80000	0.414039	0.10690	0.57071	1.0293
6U IP	15	0.93333	0.258199	0.06667	0.79035	1.0763
6U NP	15	0.93333	0.457738	0.11819	0.67985	1.1868

Table 12.32: The analysis of means using a Tukey-Kramer post hoc test in order to assess the changes in membrane pores between treatment groups.

Level		Mean
6A IP	A	1.0666667
6CC IP	A	0.9333333
6U IP	A	0.9333333
6U NP	A	0.9333333
6A NP	A	0.8666667
6CC NP	A	0.8000000
1A	B	0.0000000
1CC	B	0.0000000
1U	B	0.0000000

Levels not connected by same letter are significantly different.

12.2.8 Small secretions

Table 12.33: A one way ANOVA summary of fit of small secretions

R square	0.302778
Adj R square	0.25851
Root Mean Square Error	0.515372
Mean of Response	1
Observations (or Sum Wgts)	135

Table 12.34: Analysis of variance of small secretions

Source	DF	Sum of Squares	Mean Square	F Ratio	Prob > F
Rats	8	14.533333	1.81667	6.8396	<.0001*
Error	126	33.466667	0.26561		
C. Total	134	48.000000			

Table 12.35: Means and standard deviations of small secretions

Level	Number	Mean	Std Dev	Std Err Mean	Lower 95%	Upper 95%
1A	15	1.53333	0.639940	0.16523	1.1789	1.8877
1CC	15	1.33333	0.723747	0.18687	0.9325	1.7341
1U	15	1.46667	0.516398	0.13333	1.1807	1.7526
6A IP	15	0.86667	0.351866	0.09085	0.6718	1.0615
6A NP	15	0.93333	0.258199	0.06667	0.7903	1.0763
6CC IP	15	0.80000	0.414039	0.10690	0.5707	1.0293
6CC NP	15	0.66667	0.487950	0.12599	0.3964	0.9369
6U IP	15	0.73333	0.593617	0.15327	0.4046	1.0621
6U NP	15	0.66667	0.487950	0.12599	0.3964	0.9369

Table 12.36: The analysis of means using a Tukey-Kramer post hoc test in order to assess the changes in small secretions between treatment groups.

Level					Mean
1A	A				1.5333333
1U	A	B			1.4666667
1CC	A	B	C		1.3333333
6A NP		B	C	D	0.9333333
6A IP			C	D	0.8666667
6CC IP			C	D	0.8000000
6U IP				D	0.7333333
6CC NP				D	0.6666667
6U NP				D	0.6666667

Levels not connected by same letter are significantly different.

12.2.9 Epithelial gland openings

Table 12.37: A one way ANOVA summary of fit of epithelial gland openings

R square	0.237934
Adj R square	0.189549
Root Mean Square Error	0.460044
Mean of Response	0.992593
Observations (or Sum Wgts)	135

Table 12.38: Analysis of variance of epithelial gland openings

Source	DF	Sum of Squares	Mean Square	F Ratio	Prob > F
Rats	8	8.325926	1.04074	4.9175	<.0001*
Error	126	26.666667	0.21164		
C. Total	134	34.992593			

Table 12.39: Means and standard deviations of epithelial gland openings

Level	Number	Mean	Std Dev	Std Err	Lower 95%	Upper 95%
1A	15	1.40000	0.507093	0.13093	1.1192	1.6808
1CC	15	1.33333	0.723747	0.18687	0.9325	1.7341
1U	15	1.26667	0.457738	0.11819	1.0132	1.5202
6A IP	15	0.80000	0.414039	0.10690	0.5707	1.0293
6A NP	15	0.93333	0.258199	0.06667	0.7903	1.0763
6CC IP	15	0.86667	0.351866	0.09085	0.6718	1.0615
6CC NP	15	0.80000	0.414039	0.10690	0.5707	1.0293
6U IP	15	0.80000	0.414039	0.10690	0.5707	1.0293
6U NP	15	0.73333	0.457738	0.11819	0.4798	0.9868

Table 12.40: The analysis of means using a Tukey-Kramer post hoc test in order to assess the changes in epithelial gland openings between treatment groups.

Level					Mean
1A	A				1.4000000
1CC	A	B			1.3333333
1U	A	B	C		1.2666667
6A NP	A	B	C	D	0.9333333
6CC IP		B	C	D	0.8666667
6A IP			C	D	0.8000000
6CC NP			C	D	0.8000000
6U IP			C	D	0.8000000
6U NP				D	0.7333333

Levels not connected by same letter are significantly different.

12.2.10 Cell apices

Table 12.41: A one way ANOVA summary of fit of cell apices

R square	0.368217
Adj R square	0.328104
Root Mean Square Error	0.415315
Mean of Response	1.4
Observations (or Sum Wgts)	135

Table 12.42: Analysis of variance of cell apices

Source	DF	Sum of Squares	Mean Square	F Ratio	Prob > F
Rats	8	12.666667	1.58333	9.1794	<.0001*
Error	126	21.733333	0.17249		
C. Total	134	34.400000			

Table 12.43: Means and standard deviations of cell apices

Level	Number	Mean	Std Dev	Std Err Mean	Lower 95%	Upper 95%
1A	15	1.06667	0.258199	0.06667	0.9237	1.2097
1CC	15	1.06667	0.258199	0.06667	0.9237	1.2097
1U	15	1.13333	0.351866	0.09085	0.9385	1.3282
6A IP	15	1.93333	0.457738	0.11819	1.6798	2.1868
6A NP	15	1.60000	0.507093	0.13093	1.3192	1.8808
6CC IP	15	1.33333	0.487950	0.12599	1.0631	1.6036
6CC NP	15	1.13333	0.351866	0.09085	0.9385	1.3282
6U IP	15	1.73333	0.457738	0.11819	1.4798	1.9868
6U NP	15	1.60000	0.507093	0.13093	1.3192	1.8808

Table 12.44: The analysis of means using a Tukey-Kramer post hoc test in order to assess the changes in cell apices between treatment groups.

Level					Mean
6A IP	A				1.9333333
6U IP	A	B			1.7333333
6A NP	A	B	C		1.6000000
6U NP	A	B	C		1.6000000
6CC IP		B	C	D	1.3333333
1U			C	D	1.1333333
6CC NP			C	D	1.1333333
1A				D	1.0666667
1CC				D	1.0666667

Levels not connected by same letter are significantly different.

12.2.11 Cell borbers

Table 12.45: A one way ANOVA summary of fit of cell borders

Rsquare	0.164525
Adj Rsquare	0.111479
Root Mean Square Error	0.486864
Mean of Response	2.096296
Observations (or Sum Wgts)	135

Table 12.46: Analysis of variance of cell borders

Source	DF	Sum of Squares	Mean Square	F Ratio	Prob > F
Rats	8	5.881481	0.735185	3.1016	0.0031*
Error	126	29.866667	0.237037		
C. Total	134	35.748148			

Table 12.47: Means and standard deviations of cell borders

Level	Number	Mean	Std Dev	Std Err Mean	Lower 95%	Upper 95%
1A	15	1.93333	0.457738	0.11819	1.6798	2.1868
1CC	15	2.00000	0.534522	0.13801	1.7040	2.2960
1U	15	2.00000	0.377964	0.09759	1.7907	2.2093
6A IP	15	1.93333	0.457738	0.11819	1.6798	2.1868
6A NP	15	2.00000	0.534522	0.13801	1.7040	2.2960
6CC IP	15	2.40000	0.507093	0.13093	2.1192	2.6808
6CC NP	15	2.53333	0.516398	0.13333	2.2474	2.8193
6U IP	15	1.93333	0.593617	0.15327	1.6046	2.2621
6U NP	15	2.13333	0.351866	0.09085	1.9385	2.3282

Table 12.48: The analysis of means using a Tukey-Kramer post hoc test in order to assess the changes in cell borders between treatment groups.

Level		Mean
6CC NP	A	2.5333333
6CC IP	A B	2.4000000
6U NP	A B	2.1333333
1CC	A B	2.0000000
1U	A B	2.0000000
6A NP	A B	2.0000000
1A	B	1.9333333
6A IP	B	1.9333333
6U IP	B	1.9333333

Levels not connected by same letter are significantly different.

12.3 STATISTICAL ANALYSES FOR IMMUNOFLUORESCENCE

12.3.1 Vinculin protein expression in uterine epithelial cells of day 1 and day 6 pregnant rats

Table 12.49: A one way ANOVA summary of fit of vinculin protein expression

R square	0.412845
Adj R square	0.375566
Root Mean Square Error	0.690832
Mean of Response	1.837037
Observations (or Sum Wgts)	135

Table 12.50: A summary of the analysis of variance using a one way ANOVA test to determine the expression of vinculin in the luminal uterine epithelial cells at day and day 6 of pregnancy in rats.

Source		df	Sum of squares	Mean square	F-Ratio	P-value
Vinculin expression	Group	8	42.28148	5.28519	11.0743	< 0.0001*
	Error	126	60.13333	0.47725		
	C. Total	134	102.41481			

Table 12.51: Means and standard deviations of vinculin protein expression

Level	Number	Mean	Std Dev	Std Err Mean	Lower 95%	Upper 95%
1A	15	1.60000	0.736788	0.19024	1.1920	2.0080
1CC	15	1.40000	0.632456	0.16330	1.0498	1.7502
1U	15	1.46667	0.639940	0.16523	1.1123	1.8211
6A IP	15	2.93333	0.258199	0.06667	2.7903	3.0763
6A NP	15	2.20000	0.861892	0.22254	1.7227	2.6773
6CC IP	15	1.26667	0.593617	0.15327	0.9379	1.5954
6CC NP	15	1.20000	0.560612	0.14475	0.8895	1.5105
6U IP	15	2.40000	0.828079	0.21381	1.9414	2.8586
6U NP	15	2.06667	0.883715	0.22817	1.5773	2.5561

Table 12.52: The analysis of means using a Tukey-Kramer post hoc test in order to compare the expression levels of vinculin between treatment groups.

Level						Mean
6A IP	A					2.9333333
6U IP	A	B				2.4000000
6A NP	A	B	C			2.2000000
6U NP		B	C	D		2.0666667
1A			C	D	E	1.6000000
1U			C	D	E	1.4666667
1CC				D	E	1.4000000
6CC IP					E	1.2666667
6CC NP					E	1.2000000

Levels not connected by same letter are significantly different.

12.3.2 Integrin β5 protein expression in uterine epithelial cells of day 1 and day 6 pregnant rats

Table 12.53: A one way ANOVA summary of fit of integrin β5 protein expression

R square	0.358614
Adj R square	0.317891
Root Mean Square Error	0.679246
Mean of Response	1.651852
Observations (or Sum Wgts)	135

Table 12.54: A summary of the analysis of variance using a one way ANOVA test to determine the expression of integrin β5 in the luminal uterine epithelial cells at day and day 6 of pregnancy in rats.

Source		df	Sum of squares	Mean square	F-Ratio	P-value
Integrin β5 expression	Group	8	32.503704	4.06296	8.8062	< 0.0001*
	Error	126	58.133333	0.46138		
	C. Total	134	90.637037			

Table 12.55: Means and standard deviations of integrin β5 protein expression

Level	Number	Mean	Std Dev	Std Err Mean	Lower 95%	Upper 95%
1A	15	1.53333	0.743223	0.19190	1.1217	1.9449
1CC	15	1.26667	0.457738	0.11819	1.0132	1.5202
1U	15	1.40000	0.632456	0.16330	1.0498	1.7502
6A IP	15	2.66667	0.617213	0.15936	2.3249	3.0085
6A NP	15	2.00000	0.845154	0.21822	1.5320	2.4680
6CC IP	15	1.13333	0.351866	0.09085	0.9385	1.3282
6CC NP	15	1.06667	0.258199	0.06667	0.9237	1.2097
6U IP	15	2.06667	0.961150	0.24817	1.5344	2.5989
6U NP	15	1.73333	0.883715	0.22817	1.2439	2.2227

Table 12.56: The analysis of means using a Tukey-Kramer post hoc test in order to compare the expression levels of integrin β5 between treatment groups.

Level					Mean
6A IP	A				2.6666667
6U IP	A	B			2.0666667
6A NP	A	B	C		2.0000000
6U NP		B	C	D	1.7333333
1A		B	C	D	1.5333333
1U		B	C	D	1.4000000
1CC			C	D	1.2666667
6CC IP				D	1.1333333
6CC NP				D	1.0666667

Levels not connected by same letter are significantly different.

12.3.3 Paxillin protein expression in uterine epithelial cells of day 1 and day 6 pregnant rats

Table 12.57: A one way ANOVA summary of fit of paxillin protein expression

R square	0.41648
Adj R square	0.379431
Root Mean Square Error	0.655461
Mean of Response	1.785185
Observations (or Sum Wgts)	135

Table 12.58: A summary of the analysis of variance using a one way ANOVA test to determine the expression of paxillin in the luminal uterine epithelial cells at day and day 6 of pregnancy in rats.

Source		df	Sum of squares	Mean square	F-Ratio	P-value
Paxillin expression	Group	8	38.637037	4.82963	11.2414	< 0.0001*
	Error	126	54.133333	0.42963		
	C. Total	134	92.770370			

Table 12.59: Means and standard deviations of paxillin protein expression

Level	Number	Mean	Std Dev	Std Err Mean	Lower 95%	Upper 95%
1A	15	1.53333	0.743223	0.19190	1.1217	1.9449
1CC	15	1.46667	0.639940	0.16523	1.1123	1.8211
1U	15	1.46667	0.639940	0.16523	1.1123	1.8211
6A IP	15	2.66667	0.617213	0.15936	2.3249	3.0085
6A NP	15	1.93333	0.798809	0.20625	1.4910	2.3757
6CC IP	15	1.20000	0.414039	0.10690	0.9707	1.4293
6CC NP	15	1.13333	0.351866	0.09085	0.9385	1.3282
6U IP	15	2.60000	0.736788	0.19024	2.1920	3.0080
6U NP	15	2.06667	0.798809	0.20625	1.6243	2.5090

Table 12.60: The analysis of means using a Tukey-Kramer post hoc test in order to compare the expression levels of paxillin between treatment groups.

Level					Mean
6A IP	A				2.6666667
6U IP	A				2.6000000
6U NP	A	B			2.0666667
6A NP	A	B	C		1.9333333
1A		B	C	D	1.5333333
1CC		B	C	D	1.4666667
1U		B	C	D	1.4666667
6CC IP			C	D	1.2000000
6CC NP				D	1.1333333

Levels not connected by same letter are significantly different.

12.3.4 FAK protein expression in uterine epithelial cells of day 1 and day 6 pregnant rats

Table 12.61: A one way ANOVA summary of fit of FAK protein expression

Rsquare	0.262931
Adj Rsquare	0.216133
Root Mean Square Error	0.425385
Mean of Response	1.355556
Observations (or Sum Wgts)	135

Table 12.62: A summary of the analysis of variance using a one way ANOVA test to determine the expression of FAK in the luminal uterine epithelial cells at day and day 6 of pregnancy in rats.

Source		df	Sum of squares	Mean square	F-Ratio	P-value
Paxillin expression	Group	8	8.133333	1.01667	5.6184	< 0.0001 *
	Error	126	22.800000	0.18095		
	C. Total	134	30.933333			

Table 12.63: Means and standard deviations of FAK protein expression

Level	Number	Mean	Std Dev	Std Err Mean	Lower 95%	Upper 95%
1A	15	1.13333	0.351866	0.09085	0.9385	1.3282
1CC	15	1.06667	0.258199	0.06667	0.9237	1.2097
1U	15	1.20000	0.414039	0.10690	0.9707	1.4293
6A IP	15	1.80000	0.414039	0.10690	1.5707	2.0293
6A NP	15	1.53333	0.516398	0.13333	1.2474	1.8193
6CC IP	15	1.26667	0.457738	0.11819	1.0132	1.5202
6CC NP	15	1.13333	0.351866	0.09085	0.9385	1.3282
6U IP	15	1.66667	0.487950	0.12599	1.3964	1.9369
6U NP	15	1.40000	0.507093	0.13093	1.1192	1.6808

Table 12.64: The analysis of means using a Tukey-Kramer post hoc test in order to compare the expression levels of FAK between treatment groups.

Level				Mean
6A IP	A			1.8000000
6U IP	A	B		1.6666667
6A NP	A	B	C	1.5333333
6U NP	A	B	C	1.4000000
6CC IP		B	C	1.2666667
1U		B	C	1.2000000
1A			C	1.1333333
6CC NP			C	1.1333333
1CC			C	1.0666667

Levels not connected by same letter are significantly different.

12.3.5 Vinculin epithelial domain localization in uterine epithelial cells of day 1 and day 6 pregnant rats

Table 12.65: A one way ANOVA summary of fit of vinculin epithelial localization

R square	0.387164
Adj R square	0.348254
Root Mean Square Error	0.930381
Mean of Response	2.014815
Observations (or Sum Wgts)	135

Table 12.66: Analysis of variance of vinculin epithelial localization

Source	DF	Sum of Squares	Mean Square	F Ratio	Prob > F
Rat groups	8	68.90370	8.61296	9.9502	<.0001*
Error	126	109.06667	0.86561		
C. Total	134	177.97037			

Table 12.67: Means and standard deviations of vinculin epithelial localization

Level	Number	Mean	Std Dev	Std Err Mean	Lower 95%	Upper 95%
1A	15	1.26667	1.03280	0.26667	0.6947	1.8386
1CC	15	1.26667	1.03280	0.26667	0.6947	1.8386
1U	15	1.00000	0.00000	0.00000	1.0000	1.0000
6A IP	15	2.00000	0.00000	0.00000	2.0000	2.0000
6A NP	15	2.20000	0.77460	0.20000	1.7710	2.6290
6CC IP	15	3.00000	1.46385	0.37796	2.1893	3.8107
6CC NP	15	3.20000	1.52128	0.39279	2.3575	4.0425
6U IP	15	2.00000	0.00000	0.00000	2.0000	2.0000
6U NP	15	2.20000	0.77460	0.20000	1.7710	2.6290

Table 12.68: The analysis of means using a Tukey-Kramer post hoc test in order to compare the epithelial localization of vinculin between treatment groups.

Level					Mean
6CC NP	A				3.2000000
6CC IP	A	B			3.0000000
6A NP	A	B	C		2.2000000
6U NP	A	B	C		2.2000000
6A IP		B	C	D	2.0000000
6U IP		B	C	D	2.0000000
1A			C	D	1.2666667
1CC			C	D	1.2666667
1U				D	1.0000000

Levels not connected by same letter are significantly different.

12.3.6 Integrin β5 epithelial domain localization in uterine epithelial cells of day 1 and day 6 pregnant rats

Table 12.69: A one way ANOVA summary of fit of integrin β5 epithelial domain localization

R square	0.450009
Adj R square	0.415089
Root Mean Square Error	0.866178
Mean of Response	1.97037
Observations (or Sum Wgts)	135

Table 12.70: Analysis of variance of integrin β5 epithelial domain localization

Source	DF	Sum of Squares	Mean Square	F Ratio	Prob > F
Rat groups	8	77.34815	9.66852	12.8868	<.0001*
Error	126	94.53333	0.75026		
C. Total	134	171.88148			

Table 12.71: Means and standard deviations of integrin β5 epithelial domain localization

Level	Number	Mean	Std Dev	Std Err Mean	Lower 95%	Upper 95%
1A	15	1.00000	0.00000	0.00000	1.0000	1.0000
1CC	15	1.00000	0.00000	0.00000	1.0000	1.0000
1U	15	1.00000	0.00000	0.00000	1.0000	1.0000
6A IP	15	2.00000	0.00000	0.00000	2.0000	2.0000
6A NP	15	2.20000	0.77460	0.20000	1.7710	2.6290
6CC IP	15	2.80000	1.37321	0.35456	2.0395	3.5605
6CC NP	15	3.13333	1.59762	0.41250	2.2486	4.0181
6U IP	15	2.20000	0.77460	0.20000	1.7710	2.6290
6U NP	15	2.40000	1.05560	0.27255	1.8154	2.9846

Table 12.72: The analysis of means using a Tukey-Kramer post hoc test in order to compare the epithelial localization of integrin β5 between treatment groups.

Level				Mean
6CC NP	A			3.1333333
6CC IP	A	B		2.8000000
6U NP	A	B		2.4000000
6A NP	A	B		2.2000000
6U IP	A	B		2.2000000
6A IP		B		2.0000000
1A			C	1.0000000
1CC			C	1.0000000
1U			C	1.0000000

Levels not connected by same letter are significantly different.

12.3.7 Paxillin epithelial domain localization in uterine epithelial cells of day 1 and day 6 pregnant rats

Table 12.73: A one way ANOVA summary of fit of paxillin epithelial localization

R square	0.439109
Adj R square	0.403497
Root Mean Square Error	0.743935
Mean of Response	1.859259
Observations (or Sum Wgts)	135

Table 12.74: Analysis of Variance of paxillin epithelial localization

Source	DF	Sum of Squares	Mean Square	F Ratio	Prob > F
Rat groups	8	54.59259	6.82407	12.3303	<.0001*
Error	126	69.73333	0.55344		
C. Total	134	124.32593			

Table 12.75: Means and standard deviations of paxillin epithelial localization

Level	Number	Mean	Std Dev	Std Err Mean	Lower 95%	Upper 95%
1A	15	1.00000	0.00000	0.00000	1.0000	1.0000
1CC	15	1.00000	0.00000	0.00000	1.0000	1.0000
1U	15	1.00000	0.00000	0.00000	1.0000	1.0000
6A IP	15	2.00000	0.00000	0.00000	2.0000	2.0000
6A NP	15	2.20000	0.77460	0.20000	1.7710	2.6290
6CC IP	15	2.40000	1.05560	0.27255	1.8154	2.9846
6CC NP	15	2.73333	1.43759	0.37118	1.9372	3.5294
6U IP	15	2.20000	0.77460	0.20000	1.7710	2.6290
6U NP	15	2.20000	0.77460	0.20000	1.7710	2.6290

Table 12.76: The analysis of means using a Tukey-Kramer post hoc test in order to compare the epithelial localization of paxillin between treatment groups.

Level		Mean
6CC NP	A	2.7333333
6CC IP	A	2.4000000
6A NP	A	2.2000000
6U IP	A	2.2000000
6U NP	A	2.2000000
6A IP	A	2.0000000
1A	B	1.0000000
1CC	B	1.0000000
1U	B	1.0000000

Levels not connected by same letter are significantly different.

12.3.8 FAK epithelial domain localization in uterine epithelial cells of day 1 and day 6 pregnant rats

Table 12.77: A one way ANOVA summary of fit of FAK epithelial localization

Rsquare	0.492045
Adj Rsquare	0.459794
Root Mean Square Error	0.687761
Mean of Response	2.777778
Observations (or Sum Wgts)	135

Table 12.78: Analysis of variance of FAK epithelial localization

Source	DF	Sum of Squares	Mean Square	F Ratio	Prob > F
Rat groups	8	57.73333	7.21667	15.2567	<.0001*
Error	126	59.60000	0.47302		
C. Total	134	117.33333			

Table 12.79: Means and standard deviations of FAK epithelial localization

Level	Number	Mean	Std Dev	Std Err Mean	Lower 95%	Upper 95%
1A	15	3.60000	0.50709	0.13093	3.3192	3.8808
1CC	15	3.73333	0.45774	0.11819	3.4798	3.9868
1U	15	3.73333	0.45774	0.11819	3.4798	3.9868
6A IP	15	2.13333	0.35187	0.09085	1.9385	2.3282
6A NP	15	2.33333	0.81650	0.21082	1.8812	2.7855
6CC IP	15	2.40000	0.82808	0.21381	1.9414	2.8586
6CC NP	15	2.53333	1.12546	0.29059	1.9101	3.1566
6U IP	15	2.33333	0.81650	0.21082	1.8812	2.7855
6U NP	15	2.20000	0.41404	0.10690	1.9707	2.4293

Table 12.80: The analysis of means using a Tukey-Kramer post hoc test in order to compare the epithelial localization of FAK between treatment groups.

Level		Mean
1CC	A	3.7333333
1U	A	3.7333333
1A	A	3.6000000
6CC NP	B	2.5333333
6CC IP	B	2.4000000
6A NP	B	2.3333333
6U IP	B	2.3333333
6U NP	B	2.2000000
6A IP	B	2.1333333

Levels not connected by same letter are significantly different.

12.4 STATISTICAL ANALYSIS FOR REAL-TIME qPCR

12.4.1 Vinculin gene expression in uterine epithelial cells of day 1 and day 6 pregnant rats

Table 12.81: A one way ANOVA summary of fit of vinculin normalised relative quantities (NRQ)

R square	0.825863
Adj R square	0.74605
Root Mean Square Error	0.138589
Mean of Response	0.477297
Observations (or Sum Wgts)	36

Table 12.82: Analysis of variance of vinculin normalised relative quantities (NRQ)

Source	DF	Sum of Squares	Mean Square	F Ratio	Prob > F
Pregnant rat groups	11	2.1861829	0.198744	10.3475	<.0001*
Error	24	0.4609680	0.019207		
C. Total	35	2.6471509			

Table 12.83: Means and standard deviations of vinculin normalised relative quantities (NRQ)

Level	Number	Mean	Std Dev	Std Err Mean	Lower 95%	Upper 95%
D1 A	3	0.304614	0.115862	0.06689	0.0168	0.5924
D1 CC	3	0.164213	0.059540	0.03438	0.0163	0.3121
D1 S	3	0.293903	0.118592	0.06847	-0.0007	0.5885
D1 U	3	0.335966	0.218249	0.12601	-0.2062	0.8781
D6 IP A	3	0.870238	0.218300	0.12604	0.3280	1.4125
D6 IP CC	3	0.210596	0.058337	0.03368	0.0657	0.3555
D6 IP S	3	0.819855	0.116831	0.06745	0.5296	1.1101
D6 IP U	3	0.807074	0.108520	0.06265	0.5375	1.0767
D6 NP A	3	0.468189	0.033472	0.01932	0.3850	0.5513
D6 NP CC	3	0.233768	0.060713	0.03505	0.0829	0.3846
D6 NP S	3	0.634713	0.253554	0.14639	0.0048	1.2646
D6 NP U	3	0.584435	0.078980	0.04560	0.3882	0.7806

Table 12.84: The analysis of NRQ means using a Tukey-Kramer post hoc test in order to compare vinculin gene expression between treatment groups.

Level					Mean
D6 IP A	A				0.87023848
D6 IP S	A				0.81985495
D6 IP U	A				0.80707417
D6 NP S	A	B			0.63471281
D6 NP U	A	B	C		0.58443528
D6 NP A	A	B	C	D	0.46818891
D1 U		B	C	D	0.33596645
D1 A		B	C	D	0.30461398
D1 S		B	C	D	0.29390350
D6 NP CC		B	C	D	0.23376821
D6 IP CC			C	D	0.21059567
D1 CC				D	0.16421300

Levels not connected by same letter are significantly different.

12.4.2 Integrin β5 gene expression in uterine epithelial cells of day 1 and day 6 pregnant rats

Table 12.85: A one way ANOVA summary of fit of integrin β5 normalised relative quantities (NRQ)

Rsquare	0.930762
Adj Rsquare	0.899029
Root Mean Square Error	0.010695
Mean of Response	0.045975
Observations (or Sum Wgts)	36

Table 12.86: Analysis of variance of integrin β5 normalised relative quantities (NRQ)

Source	DF	Sum of Squares	Mean Square	F Ratio	Prob > F
Pregnant rat groups	11	0.03690226	0.003355	29.3302	<.0001*
Error	24	0.00274509	0.000114		
C. Total	35	0.03964735			

Table 12.87: Means and standard deviations of integrin β5 normalised relative quantities (NRQ)

Level	Number	Mean	Std Dev	Std Err Mean	Lower 95%	Upper 95%
D1 A	3	0.026700	0.004866	0.00281	0.0146	0.03879
D1 CC	3	0.019200	0.004513	0.00261	0.0080	0.03041
D1 S	3	0.025867	0.004726	0.00273	0.0141	0.03761
D1 U	3	0.024233	0.001002	0.00058	0.0217	0.02672
D6 IP A	3	0.118967	0.012941	0.00747	0.0868	0.15111
D6 IP CC	3	0.012967	0.012007	0.00693	-0.0169	0.04279
D6 IP S	3	0.076333	0.008203	0.00474	0.0560	0.09671
D6 IP U	3	0.088600	0.023569	0.01361	0.0301	0.14715
D6 NP A	3	0.052967	0.011194	0.00646	0.0252	0.08077
D6 NP CC	3	0.015000	0.002883	0.00166	0.0078	0.02216
D6 NP S	3	0.054667	0.007541	0.00435	0.0359	0.07340
D6 NP U	3	0.036200	0.013427	0.00775	0.0028	0.06955

Table 12.88: The analysis of NRQ means using a Tukey-Kramer post hoc test in order to compare integrin β5 gene expression between treatment groups.

Level						Mean
D6 IP A	A					0.11896667
D6 IP U	A	B				0.08860000
D6 IP S		B	C			0.07633333
D6 NP S			C	D		0.05466667
D6 NP A			C	D		0.05296667
D6 NP U				D	E	0.03620000
D1 A				D	E	0.02670000
D1 S				D	E	0.02586667
D1 U				D	E	0.02423333
D1 CC					E	0.01920000
D6 NP CC					E	0.01500000
D6 IP CC					E	0.01296667

Levels not connected by same letter are significantly different.

12.4.3 Paxillin gene expression in uterine epithelial cells of day 1 and day 6 pregnant rats

Table 12.89: A one way ANOVA summary of fit of paxillin normalised relative quantities (NRQ)

R square	0.990905
Adj R square	0.986737
Root Mean Square Error	0.088282
Mean of Response	1.650925
Observations (or Sum Wgts)	36

Table 12.90: Analysis of variance of paxillin normalised relative quantities (NRQ)

Source	DF	Sum of Squares	Mean Square	F Ratio	Prob > F
Pregnant rat groups	11	20.379697	1.85270	237.7172	<.0001*
Error	24	0.187049	0.00779		
C. Total	35	20.566746			

Table 12.91: Means and standard deviations of paxillin normalised relative quantities (NRQ)

Level	Number	Mean	Std Dev	Std Err Mean	Lower 95%	Upper 95%
D1 A	3	1.23047	0.024491	0.01414	1.1696	1.2913
D1 CC	3	0.96560	0.029152	0.01683	0.8932	1.0380
D1 S	3	1.09263	0.054213	0.03130	0.9580	1.2273
D1 U	3	1.11717	0.068265	0.03941	0.9476	1.2867
D6 IP A	3	3.10930	0.166500	0.09613	2.6957	3.5229
D6 IP CC	3	1.09873	0.061847	0.03571	0.9451	1.2524
D6 IP S	3	2.78030	0.063999	0.03695	2.6213	2.9393
D6 IP U	3	2.79900	0.095691	0.05525	2.5613	3.0367
D6 NP A	3	1.81570	0.166550	0.09616	1.4020	2.2294
D6 NP CC	3	1.08090	0.079849	0.04610	0.8825	1.2793
D6 NP S	3	1.40677	0.064707	0.03736	1.2460	1.5675
D6 NP U	3	1.31453	0.037069	0.02140	1.2224	1.4066

Table 12.92: The analysis of NRQ means using a Tukey-Kramer post hoc test in order to compare paxillin gene expression between treatment groups.

Level						Mean
D6 IP A	A					3.1093000
D6 IP U		B				2.7990000
D6 IP S		B				2.7803000
D6 NP A			C			1.8157000
D6 NP S				D		1.4067667
D6 NP U				D	E	1.3145333
D1 A				D	E	1.2304667
D1 U					E	F 1.1171667
D6 IP CC					E	F 1.0987333
D1 S					E	F 1.0926333
D6 NP CC					E	F 1.0809000
D1 CC						F 0.9656000

Levels not connected by same letter are significantly different.

12.4.4 FAK gene expression in uterine epithelial cells of day 1 and day 6 pregnant rats

Table 12.93: A one way ANOVA summary of fit of FAK normalised relative quantities (NRQ)

R square	0.955631
Adj R square	0.935296
Root Mean Square Error	0.029796
Mean of Response	0.364963
Observations (or Sum Wgts)	36

Table 12.94: Analysis of variance of FAK normalised relative quantities (NRQ)

Source	DF	Sum of Squares	Mean Square	F Ratio	Prob > F
Pregnant rat groups	11	0.45891122	0.041719	46.9928	<.0001*
Error	24	0.02130667	0.000888		
C. Total	35	0.48021789			

Table 12.95: Means and standard deviations of FAK normalised relative quantities (NRQ)

Level	Number	Mean	Std Dev	Std Err Mean	Lower 95%	Upper 95%
D1 A	3	0.253519	0.029661	0.01712	0.17984	0.32720
D1 CC	3	0.156476	0.004700	0.00271	0.14480	0.16815
D1 S	3	0.234347	0.042419	0.02449	0.12897	0.33972
D1 U	3	0.272200	0.005048	0.00291	0.25966	0.28474
D6 IP A	3	0.583060	0.013701	0.00791	0.54902	0.61710
D6 IP CC	3	0.415896	0.022938	0.01324	0.35891	0.47288
D6 IP S	3	0.447192	0.022418	0.01294	0.39150	0.50288
D6 IP U	3	0.440666	0.042103	0.02431	0.33608	0.54526
D6 NP A	3	0.441733	0.030955	0.01787	0.36484	0.51863
D6 NP CC	3	0.338848	0.026038	0.01503	0.27417	0.40353
D6 NP S	3	0.393843	0.039059	0.02255	0.29682	0.49087
D6 NP U	3	0.401779	0.042139	0.02433	0.29710	0.50646

Table 12.96: The analysis of NRQ means using a Tukey-Kramer post hoc test in order to compare FAK gene expression between treatment groups.

Level							Mean
D6 IP A	A						0.58305982
D6 IP S		B					0.44719177
D6 NP A		B					0.44173333
D6 IP U		B					0.44066614
D6 IP CC		B	C				0.41589617
D6 NP U		B	C				0.40177939
D6 NP S		B	C				0.39384308
D6 NP CC			C	D			0.33884788
D1 U				D	E		0.27220000
D1 A				D	E		0.25351900
D1 S					E	F	0.23434673
D1 CC						F	0.15647578

Levels not connected by same letter are significantly different.

13 APPENDIX H: NON-IMMUNE CONTROLS

13.1 Non immune controls for ant-Vinculin and anti-Integrin β5

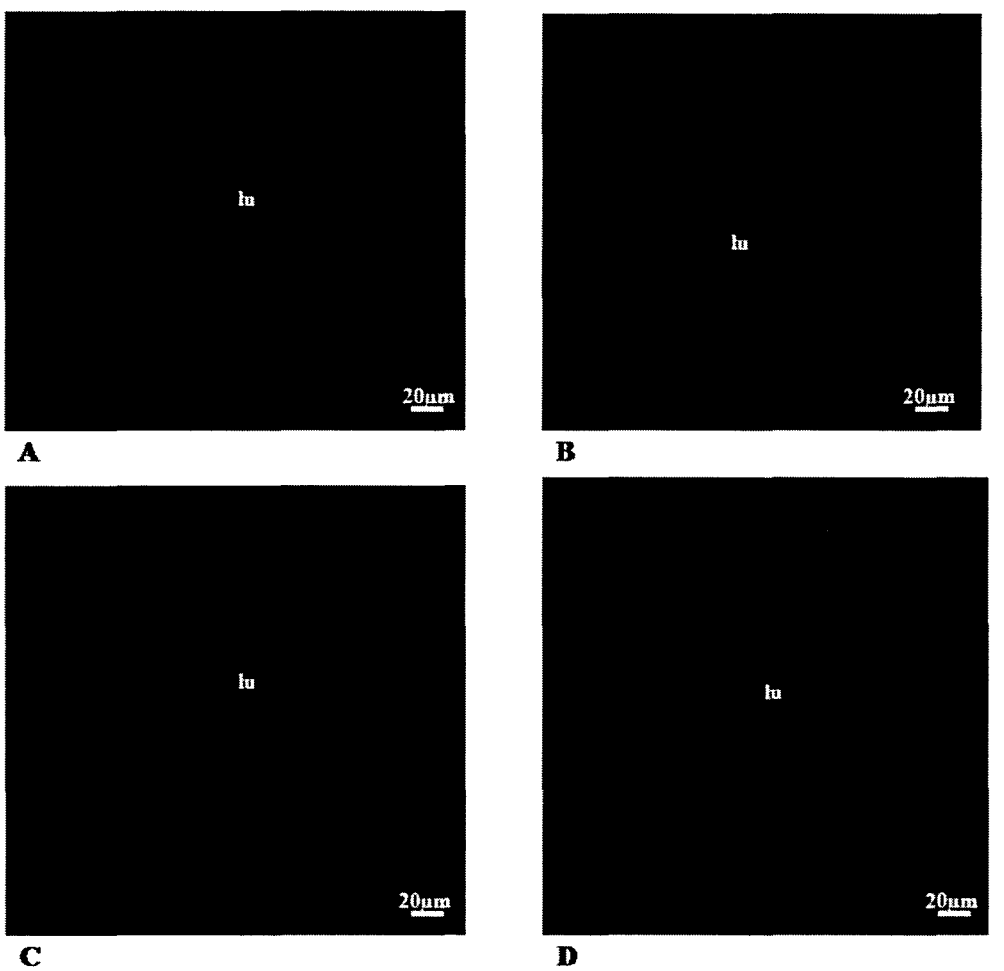


Figure 13.1: Non-immune control micrograph for vinculin and integrin β5. (A) Shows nuclei stained with DAPI (blue). (B) Non staining of secondary antibody for anti-Vinculin. (C) Non staining of secondary antibody for anti-integrin β5. (D) Merged micrograph of (A), (B) and (C).

13.2 Non-immune controls for anti-Paxillin and anti-FAK

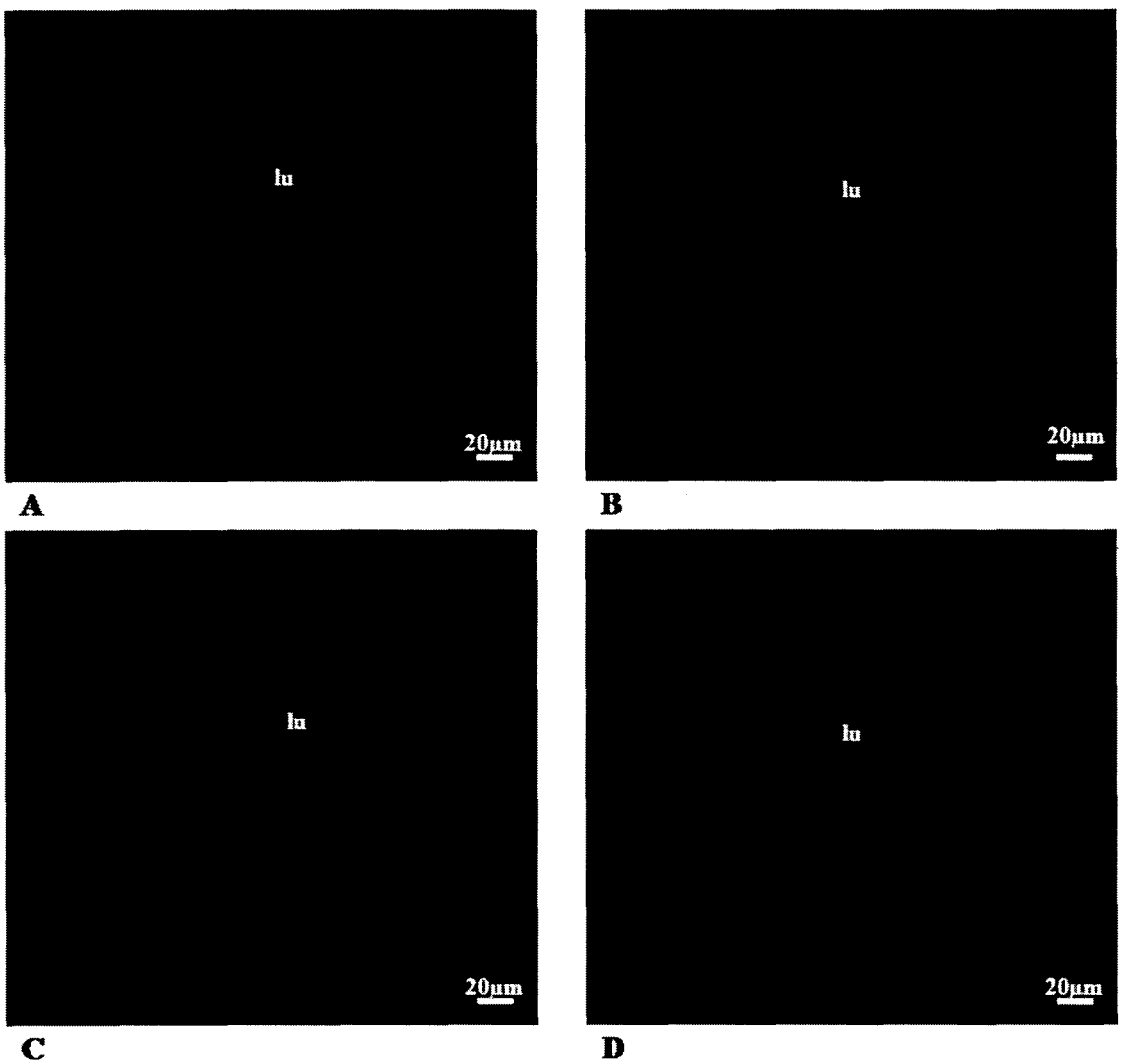


Figure 13.2: Non-immune control micrograph for paxillin and FAK. (A) Shows nuclei stained with DAPI (blue). (B) Non staining of secondary antibody for anti-Paxillin. (C) Non staining of secondary antibody for anti-FAK. (D) Merged micrograph of (A), (B) and (C).

14 APPENDIX I: ETHICS CLEARANCE CERTIFICATE

AESC3

STRICTLY CONFIDENTIAL

ANIMAL ETHICS SCREENING COMMITTEE (AESC)

CLEARANCE CERTIFICATE NO. 2012/11/03

APPLICANT: **Mr A Mwakikunga**

SCHOOL: **School of Anatomical Sciences**

PROJECT TITLE: Anastrozole when used as a superovulator, may alter key focal adhesion proteins associated with receptivity of uterine epithelial cells during implantation in the rat: a potential therapeutic clue in assisted reproductive technologies

Number and Species

57 Wistar 12-week old rats (52 females; 5 males)

Approval was given for to the use of animals for the project described above at an AESC meeting held on **27 March 2012**. This approval remains valid until **31 March 2014**.

The use of these animals is subject to AESC guidelines for the use and care of animals, is limited to the procedures described in the application form and to the following additional conditions:

Conditions:

- Provide detail on how vaginal smears will be done before experimentation is started.

Signed: _____ (Chairperson, AESC) Date: 4/5/12

I am satisfied that the persons listed in this application are competent to perform the procedures therein, in terms of Section 23 (1) (c) of the Veterinary and Para-Veterinary Professions Act (19 of 1982)

Signed: _____ (Registered Veterinarian) Date: 4/5/12

cc: Supervisor:
Director: CAS